

**Methods for carbon-11 and fluorine-18 labeling of peptides
as PET radiopharmaceuticals: direct labeling with
[¹¹C]methyl triflate on cysteine residues and [¹⁸F]fluoride on
the cationic silicon-based fluoride acceptor (SiFA) moiety.**

Joshua Chin

Department of Chemistry, McGill University, Montreal

August 2013

A thesis submitted to McGill University in partial fulfillment of the requirements of
the degree of Master of Science.

All rights reserved. This work may not be reproduced in whole or in part, by
photocopy or other means, without permission of the author.

© Joshua Chin 2013

Table of Contents	Page
Table of Contents	2
List of Tables	6
List of Figures	7
List of Abbreviations	10
Abstract	13
Résumé	15
Acknowledgements	17
Contributions of Authors	18
Preface	20
1. INTRODUCTION	22
1.1 Positron Emission Tomography (PET)	22
1.1.1 Fundamentals of PET	22
1.1.2 Spatial resolution in PET	24
1.1.3 Fluorine-18, carbon-11, and other PET radioisotopes	26
1.1.4 PET and [¹⁸ F]FDG in molecular imaging	30
1.2 Carbon-11 radiochemistry	32
1.2.1 Introduction	32
1.2.2 Carbon-11 production	33
1.2.3 Electrophilic carbon-11 building blocks	34
1.2.4 Other carbon-11 building blocks	37
1.3 Fluorine-18 radiochemistry	39
1.3.1 Introduction	39
1.3.2 Fluorine-18 production	40
1.3.3 Electrophilic [¹⁸ F]radiofluorination	41

1.3.4 Nucleophilic [^{18}F]radiofluorination	42
1.3.4.1 [^{18}F]Fluoride preparation and drying	42
1.3.4.2 Nucleophilic fluorine-18 radiochemistry	45
1.4 Radiolabeling of biomolecules	46
1.4.1 Introduction	46
1.4.2 Acylation	46
1.4.3 Chemoselective oxime ligation	48
1.4.4 Click Chemistry: Huisgen 1,3-dipolar cycloaddition	49
1.5 Novel labeling strategies	50
1.5.1 Introduction and early works	50
1.5.2 Boronic esters	52
1.5.3 Aluminum fluorides	53
1.5.4 Silicon fluorides	55
1.6 Current scope of research	59
1.6.1 Peptide labeling with carbon-11	60
1.6.2 Peptide labeling with fluorine-18	60
2. MANUSCRIPT	62
Manuscript title: <i>Direct one-step labeling of cysteine residues on peptides with</i>	
<i>[^{11}C]methyl triflate for the synthesis of PET radiopharmaceuticals.</i>	
2.1 Abstract	64
2.2 Introduction	65
2.3 Materials and methods	68
2.4 Results and discussion	77
2.5 Conclusion	91

3. Cationic SiFA compounds – RESULTS AND DISCUSSION	92
3.1 Introduction	92
3.2 Small-molecule synthesis	92
3.3 Peptide synthesis	102
3.4 Radiochemistry	107
3.5 Lipophilicity	109
3.6 Affinity determination by receptor autoradiography	117
3.7 Summary	118
4. Cationic SiFA compounds – EXPERIMENTAL SECTION	119
4.1 Regulatory notice	119
4.2 Materials	119
4.3 Instruments	120
4.4 Small-molecule synthesis	121
4.4.1 Synthesis of SiFA-benzyl-bromide	121
4.4.2 Synthesis of SiFA ⁺ -SH	125
4.4.3 Synthesis of SiFA ⁺ -CHO	128
4.4.4 Synthesis of SiFA ⁺ -MI	130
4.4.5 Synthesis of SiFA ⁺ -N ₃	132
4.4.6 Synthesis of SiFA ⁺ -C≡CH ₃	133
4.4.7 Synthesis of SiFA ⁺ -CO ₂ H	135
4.5 Peptide synthesis	138
4.5.1 Solid-Phase Peptide Synthesis (SPPS)	138
4.5.2 Chemiselective oxime ligation	144
4.5.3 Thiol-maleimide coupling	146
4.5.4 Huisgen 1,3-dipolar cycloaddition	148

4.6 Radiolabeling	151
4.6.1 Preparation of [¹⁸ F]F-/Kryptofix 2.2.2/K ⁺ complex	151
4.6.2 Radiosynthesis	152
4.6.3 Lipophilicity	152
5. SUMMMARY AND CONCLUSIONS	153
6. LITERATURE CITED	156
7. APPENDICES	177
7.1 Supplementary information (Manuscript)	177
7.2 Small-molecule characterization data	186
7.3 Peptide characterization data	234

List of Tables	Page
Table I: Positron-emitting isotopes of interest in PET imaging.	27
Table II: Physical properties of common radioisotopes used in PET.	28
Table III: Selected isotopes of carbon.	33
Table IV: Selected isotopes of fluorine.	39
Table V: Production routes for fluorine-18.	40
Table VI: HPLC elution methods for peptide analysis and purification.	70
Table VII: Measured logD _{7.4} and calculated ClogP values.	112

List of Figures	Page
Figure 1: Positron-electron annihilation.	23
Figure 2: PET from bench to bedside.	24
Figure 3: Positron range and acolinearity (non-linearity) of gamma rays.	25
Figure 4: Detector resolution.	26
Figure 5: L-DOPA and derived PET radiotracers.	28
Figure 6: Examples of fluorinated pharmaceuticals.	29
Figure 7: [^{18}F]Fluorodeoxyglucose ([^{18}F]FDG).	31
Figure 8: Carbon-11 building blocks derived from [^{11}C]CO ₂ or [^{11}C]CH ₄	34
Figure 9: Examples of [^{11}C]carboxylation reactions.	35
Figure 10: Examples of PET radiotracers produced via radiomethylation.	36
Figure 11: Other transformations with carbon-11.	37
Figure 12: Proposed mechanism of the [^{11}C]CO carbonylation reaction.	38
Figure 13: Examples of electrophilic radiofluorinations.	42
Figure 14: Production of anhydrous [^{18}F]K(K ₂₂₂)F.	44
Figure 15: Examples of nucleophilic radiofluorinations.	45
Figure 16: Original synthesis of no-carrier-added [^{18}F]SFB.	46
Figure 17: Select prosthetic groups for the radiofluorination of proteins.	47
Figure 18: 4-[^{18}F]Fluorobenzaldehyde as a prosthetic group.	48
Figure 19: Click chemistry.	50
Figure 20: Early attempts at heteroatom- ^{18}F radiochemistry.	51
Figure 21: Radiochemistry with alkylfluoroborates.	52
Figure 22: Radiochemistry with aluminum fluorides.	54
Figure 23: Radiochemistry with silicon fluorides.	55
Figure 24: Radiochemistry with SiFA.	57

Figure 25: SiFA compounds of reduced lipophilicity.	58
Figure 26: List of peptide structures.	71
Figure 27: Radiosynthesis of [^{11}C]GSMe (13): effect of solvent and base.	78
Figure 28: Nucleophilic sites on 1 and Cys-[Tyr ³ -octreotate] (9).	81
Figure 29: Radiosynthesis of [^{11}C] 2 : regioselectivity and effect of base.	83
Figure 30: Radiosynthesis of [^{11}C] 2 : effect of base.	86
Figure 31: Radiosynthesis of [^{11}C] 2 : effect of precursor quantity.	87
Figure 32: Radiosynthesis of [^{11}C]Cys(Me)-[Tyr ³ -octreotate] ([^{11}C] 10).	90
Figure 33: Structural analysis of SiFA.	93
Figure 34: A potential functionalization of SiFA <i>tert</i> -butyl groups.	93
Figure 35: Attempted sulfonylation of SiFA-aniline.	94
Figure 36: Structure of SiFAN ⁺ Br ⁻	95
Figure 37: Synthetic objective for cationic SiFA compounds.	95
Figure 38: Planned isolation scheme for quaternary ammonium salts.	96
Figure 39: Synthesis of SiFA-benzyl-bromide (3).	97
Figure 40: Synthesis of SiFA ⁺ -SH (6).	98
Figure 41: Thiol deprotection fails in the absence of a cationic quencher.	98
Figure 42: Synthesis of SiFA ⁺ -CHO (8).	99
Figure 43: Attempts at synthesis of SiFA ⁺ -CHO (8).	99
Figure 44: Synthesis of SiFA ⁺ -MI (10).	100
Figure 45: Synthesis of SiFA ⁺ -N ₃ (12).	101
Figure 46: Synthesis of SiFA ⁺ -C \equiv CH (13).	101
Figure 47: Synthesis of SiFA ⁺ -CO ₂ H (16).	101
Figure 48: Tyr ³ -octreotate (17) and site of modification.	103
Figure 49: Introduction of the SiFA moiety via SPPS.	104

Figure 50: Chemoselective oxime ligation.	105
Figure 51: Thiol-maleimide coupling reaction.	105
Figure 52: Click chemistry via comproportionation of Cu(0) and Cu(II).	106
Figure 53: Sample HPLC chromatogram for ¹⁸ F-labeling of peptide 26	108
Figure 54: Workup and isolation of radiolabeled cationic SiFA peptides.	109
Figure 55: Radiolabeled peptide isolation for shake-flask method.	111
Figure 56: Measured logD _{7.4} values for cationic SiFA-TATE peptides.	113
Figure 57: Virtual SiFA derivatives for ClogP calculations.	113
Figure 58: Sample HPLC radiochromatogram of partitioning phases.	114

List of Abbreviations

3-D	Three-dimensional
AO	Aminooxy
APF	4-Azidophenacyl fluoride
BBN	Bombesin
BEMP	2- <i>tert</i> -Butylimino-2-diethylamino-1,3-dimethylperhydro-1,3,2-diazaphosphorine
CNSC	Canadian Nuclear Safety Commission
CT	Computed tomography
DBU	1,8-Diazabicyclo[5.4.0]undec-7-ene
DIPEA	<i>N,N</i> -Diisopropylethylamine
DMF	<i>N,N</i> -Dimethylformamide
DMS	Dimethyl sulfate
DMSO	Dimethyl sulfoxide
ESI	Electrospray ionization
EtOH	Ethanol
FDG	Fluorodeoxyglucose
Fmoc	Fluorenylmethyloxycarbonyl
Gly-Sar	Glycylsarcosine
GSH	Glutathione
GSMe	<i>S</i> -methylglutathione
HBTU	<i>O</i> -(Benzotriazol-1-yl)- <i>N,N,N,N</i> -tetramethyluronium hexafluorophosphate

HPLC	High-performance liquid chromatography
HRMS	High-resolution mass spectrometry
IUPAC	International Union of Pure and Applied Chemistry
MALDI	Matrix-assisted laser desorption/ionization
MB-CHO	<i>p</i> -Methoxybenzaldehyde
mCi	Millicurie
MeCN	Acetonitrile
MEK	Methyl ethyl ketone
MeOTf	Methyl triflate; methyl trifluorosulfonate
MI	Maleimido
MMS	Methyl methanesulfonate
MRI	Magnetic resonance imaging
MS	Mass spectrometry
<i>ndc</i>	Non-decay-corrected
NMR	Nuclear magnetic resonance
NMSP	(3- <i>N</i> -Methyl)piperone
NOTA	1,4,7-Triazacyclononane-1,4,7-triacetic acid
NPFP	4-Nitrophenyl 2-fluoropropionate
PEG	Polyethylene glycol
PET	Positron emission tomography
PiB	Pittsburgh compound B
PMP	1-Methylpiperidin-4-yl propionate

PMT	Photomultiplier tube
QMA	Quaternary methyl ammonium
RCY	Radiochemical yield
RGD	Arg-Gly-Asp
SFB	<i>N</i> -succinimidyl 4-fluorobenzoate
SiFA	Silicon-based fluoride acceptor
SPECT	Single-photon emission computed tomography
SPPS	Solid-phase peptide synthesis
sst	Somatostatin
TATE	Tyr ³ -octreotate
TBS	<i>tert</i> -Butyldimethylsilyl
TFA	Trifluoroacetic acid
TIPS	Triisopropylsilane
TOF	Time-of-flight

Abstract

Radiolabeled peptides have emerged as an attractive platform for diagnostic and therapeutic oncology. However, the ^{11}C -radiolabeling of peptides for positron emission tomography (PET) has been poorly explored, owing to the relatively short half-life of carbon-11 ($t_{1/2} = 20.3$ min), and time-consuming multi-step radiochemical reactions. In addition, ^{18}F -radiolabeling via ^{18}F - ^{19}F isotopic exchange on the silicon-based fluoride acceptor (SiFA) platform has been hampered by the significant lipophilicity of the SiFA moiety.

Herein is described a novel method for the direct, one-step labeling of peptides at the side-chain of cysteine residues on peptides. A regioselective reaction at cysteine residues in the presence of competing amino acid side-chains is presented. Finally, the radiosynthesis of $[^{11}\text{C}]\text{Cys}(\text{Me})\text{-}[\text{Tyr}^3\text{-octreotate}]$ is undertaken as a demonstration of the applicability of the labeling method for peptides of biological interest. This octreotate derivative was obtained in non-decay-corrected radiochemical yields of $11 \pm 2\%$ ($n=3$) with a synthesis time of approx. 30 min.

The quaternary ammonium functional group has been introduced to mitigate the lipophilicity of the SiFA moiety. The design and synthesis of cationic SiFA building blocks bearing functional groups amenable to bioconjugation ($-\text{SH}$, $-\text{CHO}$, $-\text{maleimido}$, $-\text{N}_3$, $-\text{C}\equiv\text{CH}$, $-\text{CO}_2\text{H}$) are presented. These building blocks have been assessed for compatibility in bioconjugation reaction conditions. The

resulting cationic SiFA-Tyr³-octreotate conjugates applied to ¹⁸F-radiolabeling and lipophilicity assessment by the shake-flask method. These peptide conjugates exhibit reduced lipophilicities ($\log D_{7.4} = 0.43 - 2.19$). Conjugates containing a hydrophilic PEG linker present ($\log D_{7.4} = 0.43 - 0.92$) have particularly low lipophilicity as compared to noncationic SiFA-TATE ($\log D_{7.4} = 2.68$).

These results demonstrate the feasibility of labeling bioactive peptides with carbon-11 and fluorine-18 for use as PET radiotracers. These novel methods are characterized by facile one-step labeling conditions at room temperature under short reaction times, on the order of seconds or minutes.

Résumé

L'utilisation de peptides radiomarqués constitue une plateforme de recherche émergente pour le développement de nouveaux outils diagnostiques de même que de nouvelles thérapies en oncologie. Par contre, en raison de sa relative courte demi-vie ($t_{1/2} = 20.3$ min) et des réactions de radiochimie impliquant de multiples étapes lui étant associé, le marquage de peptides au carbone-11 pour l'imagerie de tomographie par émission de positons (TEP) demeure largement inexploré. Aussi, le marquage au fluor-18 par échange isotopique ^{19}F - ^{18}F suivant la méthodologie SiFA est limité par la lipophilicité marquée du fragment SiFA.

Nous décrivons ici une nouvelle méthode, directe et en une seule étape, permettant le marquage au carbone-11 sur la chaîne latérale de résidus cystéines au sein de peptides. La faisabilité de même que la régiosélectivité aux résidus cystéines en présence de chaînes latérales compétitives seront démontrées. Cette méthodologie est appliquée à la radiosynthèse du peptide d'intérêt biologique [^{11}C]Cys(Me)-[Tyr³-octreotate], lequel est obtenu dans un rendement de $11 \pm 2\%$ ($n=3$) (non-corrigé pour la désintégration) dans un délai d'approximativement 30 min.

De plus, l'incorporation de groupements fonctionnels du type ammoniums quaternaires est mise de l'avant comme solution afin d'atténuer la lipophilicité inhérente au fragment SiFA. Ainsi, nous décrivons le design et la synthèse de

fragments SiFA cationiques bioconjuguables (-SH, -CHO, -maleimido, -N₃, -C≡CH, -CO₂H). Qui plus est, la compatibilité de ces fragments a été évaluée dans des réactions de bioconjugaison, alors que les dérivés SiFA-Tyr³-octreotate obtenus, ont été radiomarké au fluor-18 et leur lipophilicité évalué par la méthode *shake-flask*. Ces peptides conjugués sont caractéristiques d'une lipophilicité réduite ($\log D_{7.4} = 0.43 - 2.19$), en particulier les dérivés contenant une chaîne PEG ($\log D_{7.4} = 0.43 - 0.92$), comparativement au SiFA-TATE neutre ($\log D_{7.4} = 2.68$).

Considérés dans leur ensemble, ces résultats démontrent la faisabilité des radiomarquages de peptides bioactifs avec des radioisotopes TEP tel que le carbone-11 et le fluor-18. De plus, ces nouvelles approches méthodologiques sont caractérisées par des conditions de radiomarquages favorables: réactions en une étape et à température ambiante de même des temps de réaction de l'ordre quelques secondes à quelques minutes.

Acknowledgements

I give my sincere thanks to all who have guided me throughout my journey of graduate studies over the past three years, culminating in the creation of this thesis.

Special thanks are due for my supervisors Dr. Ralf Schirmacher and Dr. R. Bruce Lennox, who have dedicated countless time and effort in providing direction and advice, and in helping me overcome the many hurdles of research. In addition, I would like to thank Dr. Esther Schirmacher and Dr. Alexey Kostikov for providing training and helpful discussions in peptide chemistry, organic chemistry, and radiochemistry.

All works presented herein would not have been possible without the assistance of the Cyclotron operators, notably Mr. Dean Jolly and Mrs. Miriam Kovacevic, who have worked beyond their responsibilities to accommodate for my rather fickle experiments.

I would like to thank my peers Dr. Radouane Koudih, Mr. Vadim Bernard-Gauthier, and Mrs. Sabrina Niedermoser for helpful discussions and for brightening the day in the darkest of times.

Last but not least, I would like to thank my parents, who have sacrificed everything to raise a child that fell in love with discovery and knowledge.

Contributions of Authors

The peer-reviewed manuscript entitled “Direct one-step labeling of cysteine residues on peptides with [^{11}C]methyl triflate for the synthesis of PET radiopharmaceuticals.”, presented in *Chapter 2 – Manuscript* of this thesis, was submitted to *Amino Acids* (Springer Science, Berlin) (May 2013) and was accepted for publication (July 2013). This study was performed in its entirety at the McConnell Brain Imaging Centre of the Montreal Neurological Institute, McGill University. All research planning and execution described herein was performed by the first author of the manuscript and author of the thesis, Joshua Chin, including peptide synthesis, radiochemistry, and writing of the manuscript draft. Matthew Vesnaver was an undergraduate research assistant under direct supervision of J.C. for solid-phase peptide synthesis. Vadim Bernard-Gauthier is acknowledged for helpful discussions with J.C. in project planning, particularly in radiochemistry. Erin Saucke-Lacelle is acknowledged for contributions towards research precluding and inspiring the current work, notably in the choice of decapeptide sequence. Dr. Björn Wängler and Dr. Carmen Wängler are acknowledged for project inspiration and contribution towards the peer-reviewed final submitted draft of the manuscript. Dr. Ralf Schirmacher is the thesis adviser for J.C., and all experimental work was performed in his laboratories.

All research planning and execution pertaining to cationic SiFA compounds described herein was performed by the author of the thesis, J.C.. Dr.

Alexey Kostikov and Dr. R.S. are acknowledged for providing project inspiration.

Dean Jolly and Miriam Kovacevic are acknowledged for cyclotron operations and production of carbon-11 and fluorine-18 radioisotopes. Dr. Esther Schirmacher, V.B.-G., Dr. Radouane Koudih, and Sabrina Niedermoser are acknowledged for helpful discussions.

Preface

The main goal of this research was to investigate novel methods for the incorporation of carbon-11 or fluorine-18 to bioactive peptides as PET radiotracers.

The first half of this thesis deals with the direct one-step labeling of cysteine residues on peptides with [^{11}C]methyl triflate. This has been accomplished by demonstrating the feasibility of radiolabeling with glutathione (GSH), a simple peptide, and by demonstrating regioselectivity using decapeptide Trp-Tyr-Trp-Ser-Arg-Cys-Lys-Trp-Thr-Gly. Finally, [^{11}C]Cys(Me)-[Tyr³-octreotate] was synthesized as a demonstration of applicability to peptides of biological interest. This work has been accepted for publication to Amino Acids (Springer Science, Berlin).

The remainder of the thesis addresses hydrophilicity optimization of the SiFA moiety for ^{18}F -labeling of peptides. This involves the design and synthesis of novel cationic SiFA building blocks, evaluation of their compatibility with peptides under a variety of bioconjugation methods, feasibility of one-step radiolabeling with anhydrous [^{18}F]fluoride, and finally, lipophilicity evaluation by the shake-flask method to determine contribution of these building block towards countering the high lipophilicity imparted by the SiFA species. This work is expressed in standard format under the following headings: Experimental Section

(Chapter 4), Results and Discussion (Chapter 3), and Appendices (Chapter 7), the latter of which contains all characterization data relevant to this study.

The Summary and Conclusions section (Chapter 5) attempts to reconcile both parts of the thesis into a unified vision. Briefly, both carbon-11 direct radiomethylation and fluorine-18 SiFA isotopic exchange methods are novel means to prepare bioactive peptides as PET radiotracers. This is a response to the current strong academic and medical interest in these peptides for diagnostic oncology and nuclear medicine.

Chapter 1: INTRODUCTION

1.1 Positron Emission Tomography (PET)

1.1.1 Fundamentals of PET

Positron emission tomography (PET) is a non-invasive nuclear medicine imaging technique that produces a three-dimensional (3-D) image or picture of functional processes in the body. This diagnostic technique is based on the detection of coincident gamma rays from electron-positron annihilation. The sum of these detected events is relayed into a mathematical algorithm to produce 3-D images of the tracer concentration in the process known as tomographic image reconstruction. Current clinical applications of PET lie in three important areas of clinical diagnosis and management: (1) cancer diagnosis and management, (2) cardiology and cardiac surgery, and (3) neurology and psychiatry^[1].

PET tracers consist of a positron-emitting radionuclide bound to a biologically active molecule, typically produced via automated synthesis from a cyclotron-manufactured radioisotope. These tracers are administered to subjects through inhalation or intravenous injection and concentrate in tissues of interest. Over time, the radionuclide undergoes positron emission (β^+ -decay), releasing a positron which travels a short distance in the tissue media before combining with a nearby electron to form a positronium hydrogen-like system, or anti-atom. The positronium, a bound electron-positron system analogous to the hydrogen atom

with a lifetime on the order of 10^{-10} sec^[2], readily annihilates to produce two anti-parallel 511 keV gamma ray photons (Figure 1).

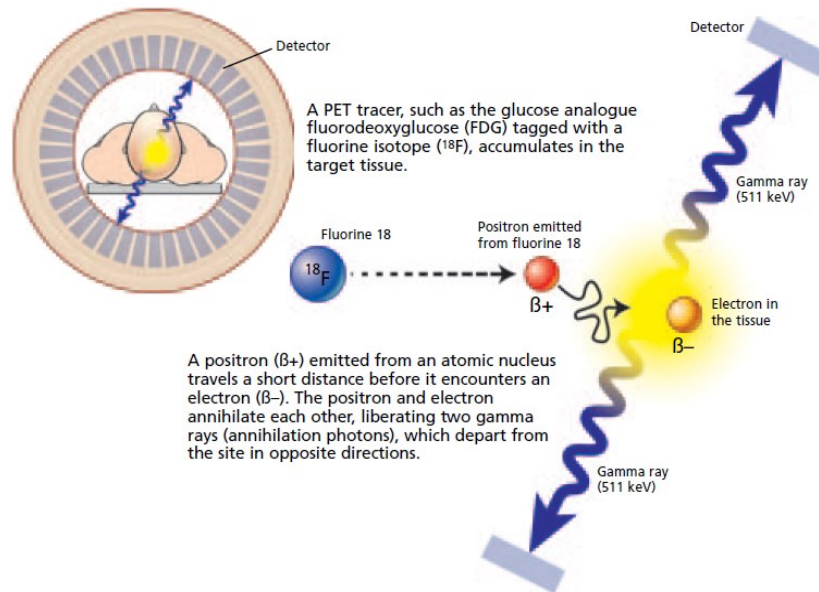


Figure 1: Positron-electron annihilation. Taken from literature^[3].

The coincident detection of pairs of gamma rays is achieved by a series of detectors arranged in a circular ring surrounding the subject. PET detectors consist of scintillation crystals, commonly either thallium-doped sodium iodide or bismuth germinate, which absorb 511 keV photons to generate a flash of light^[4]. Scintillation crystals are coupled to photomultiplier tubes (PMT), which convert the light input into an electronic signal that is recorded on computer as data for image reconstruction, providing the PET images as seen by clinicians (Figure 2).

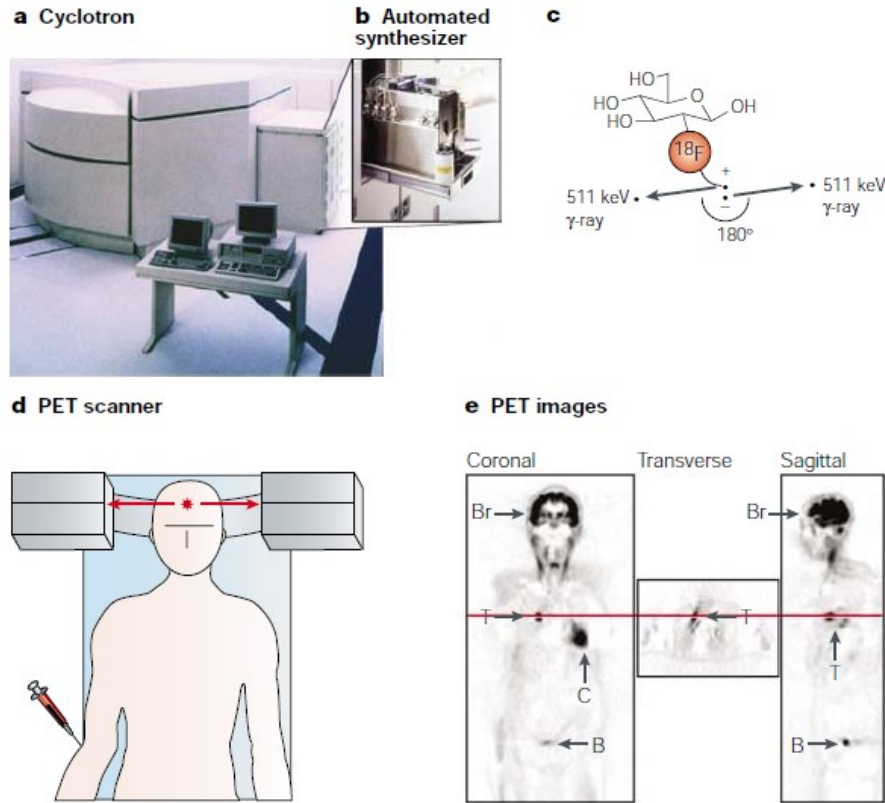


Figure 2: PET from bench to bedside. The many steps in the production of PET radiotracers and image acquisition. Taken from literature^[5].

1.1.2 Spatial resolution in PET

The spatial resolution of an image produced from a PET acquisition depends on three physical factors: (1) the positron range, (2) the positron acollinearity (gamma non-collinearity), and (3) the detector resolution^[6].

The positron range effect arises from the travel distance and direction of a positron following β^+ -decay and prior to the annihilation event. The travel distance depends on the kinetic energy contained in the positron from the β^+ -decay, which

dissipates upon travel by interaction with the medium. Higher positron energies will therefore result in greater average distances between decay and annihilation events (Figure 3a).

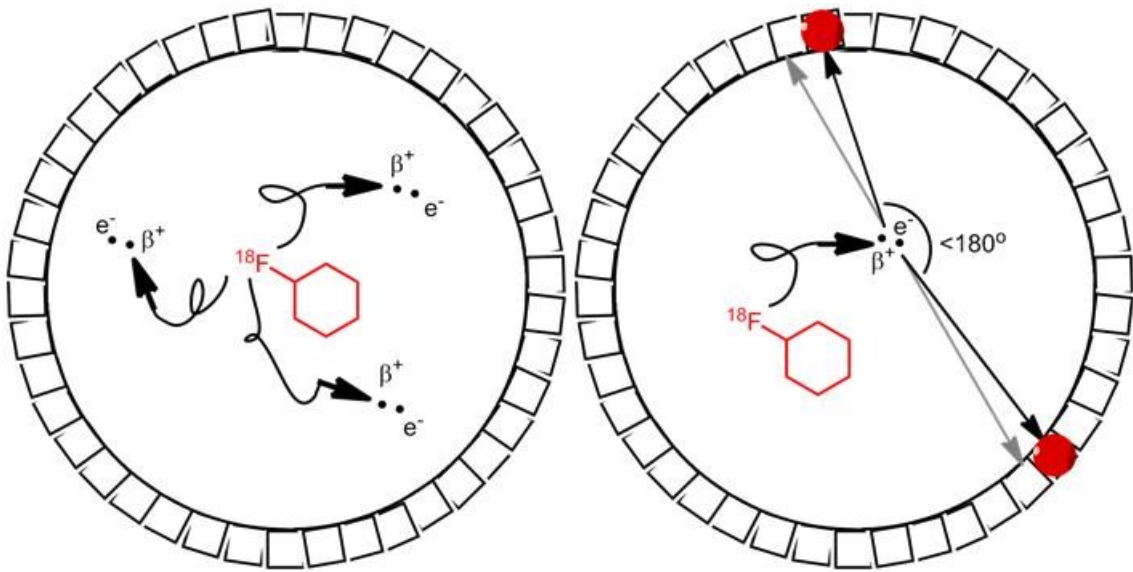


Figure 3: Positron range and acolinearity (non-linearity) of gamma rays.

Left: Positron range. Positron travel distance and direction introduces a distance between the decay and annihilation events. *Right:* Positron acolinearity. By conservation of momentum, annihilating particles in motion will generate gamma ray pairs deviating from the ideal 180° angle. Detector elements are not drawn to scale.

Ideally, a positron-electron annihilation event will generate two perfectly anti-parallel 511 keV gamma rays. However, acolinearity is observed if one or

both particles are not at rest, where the resulting pair of 511 keV gamma rays deviate from the ideal 180° angle due to conservation of momentum (Figure 3b).

The detector resolution is a technical limitation caused by the size of the detector element. Smaller detector pixels will improve spatial resolution (Figure 4).

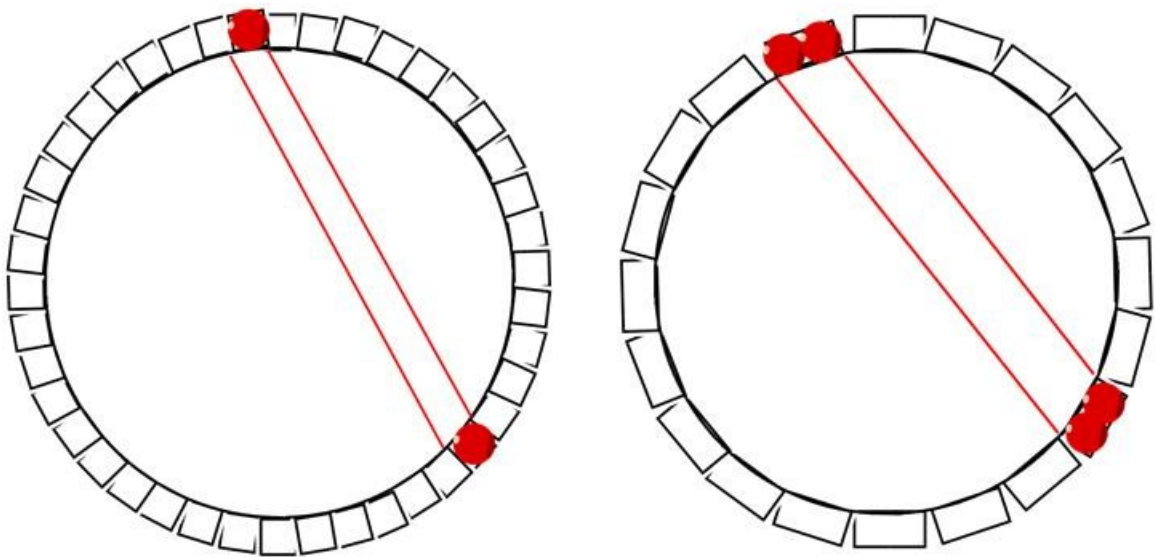


Figure 4: Detector resolution. Smaller detector elements (*left*) allow for a more precise localization of the annihilation event in comparison to larger detector elements (*right*).

1.1.3 Fluorine-18, Carbon-11, and other PET radioisotopes

Commonly used short-lived positron-emitting radionuclides produced by cyclotron (a circular particle accelerator) include the following: oxygen-15 (^{15}O), nitrogen-13 (^{13}N), carbon-11 (^{11}C), fluorine-18 (^{18}F), and copper-64 (^{64}Cu). Other

isotopes of potential interest in PET imaging are the generator-produced rubidium-82 (^{82}Rb), gallium-68 (^{68}Ga), and copper-62 (^{62}Cu), which are the decay products of long-lived parent nuclides^[7] (Table I).

Table I: Positron-emitting isotopes of interest in PET imaging. Taken from literature^[7].

	O-15	N-13	C-11	F-18	Rb-82	Ga-68	Cu-62
Half-life	2 min	11 min	20 min	110 min	75 s	68 min	9.7 min
Availability	On-site cyclotron	On-site cyclotron	On-site cyclotron	Cyclotron, regional distribution	Generator Sr-82/Rb-82	Generator Ge-68/Ga-68	Generator Zn-62/Cu-62

Oxygen-15, in the form of $^{15}\text{O}]\text{H}_2\text{O}$ is commonly used for quantification of regional blood flow in the brain^[8,9]. Nitrogen-13 is converted to $^{13}\text{N}]\text{NH}_3$ for use as myocardial blood flow imaging agent in PET^[10].

The applications for carbon-11 are wide-ranging, owing to a literature rich in the chemistry and radiochemistry of carbon. In addition, the presence of carbon in most pharmaceuticals and natural products allow for the radiosynthesis of tracers with identical pharmacological properties. However, this is counterbalanced by a short half-life ($t_{1/2} = 20$ min), limiting ^{11}C -radiochemistry to simple and rapid reactions such as methylation of alcohols and amines^[11].

Table II: Physical properties of common radioisotopes used in PET.

Isotope	Half-life (min)	Max. energy (MeV)	Range in water (mm)
^{18}F	109.7	0.653	2.39
^{11}C	20.4	0.96	4.11
^{13}N	9.96	1.19	5.39
^{15}O	2.07	1.72	8.2

Fluorine-18 shows favorable physical and chemical characteristics as a radionuclide of choice for the labeling of biologically-active molecules (Table II). ^{18}F is a particularly attractive radionuclide due to its relatively long half-life ($t_{1/2} = 109.7$ min) sufficient for greater scope and flexibility of synthetic labeling reactions compared to carbon-11. In addition, the low positron energy of ^{18}F (640 keV) allows the highest PET image resolution (2.39 mm) among all positron-emitting isotopes.

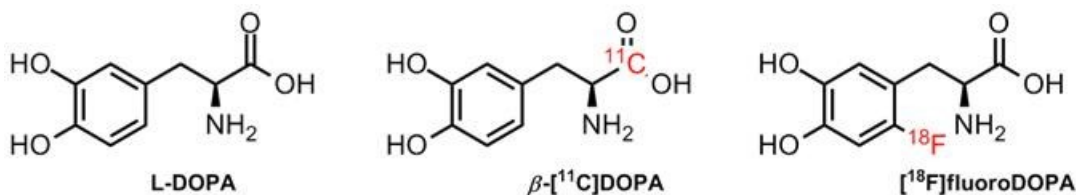


Figure 5: L-DOPA and derived PET radiotracers. Chemical structures of L-DOPA (dopamine precursor), isotopically-substituted β -[^{11}C]DOPA, and atomically substituted [^{18}F]fluoroDOPA.

Due to the scarcity of naturally-occurring organofluorines, radiofluorinated tracers are by necessity chemically different from the natural ligand. The advantage for carbon-11 radiolabelling is that, for example, the pharmacokinetic and pharmacodynamics properties of isotopically substituted β -[^{11}C]DOPA is not expected to differ from L-DOPA in the dopaminergic metabolic pathway^[12,13] (Figure 5). On the other hand, the atomic substitution in [^{18}F]fluoroDOPA could lead to differences in biodistribution and metabolic rates over L-DOPA^[14]. Fluorinated mimics must therefore take into account the physical properties of fluorine in tracer design. These include: (1) high electronegativity, (2) univalence (commonly, the substitution of C-H with C-F), (3) comparable electronic properties with oxygen (C-F bond length (1.42 Å) versus C-O bond length (1.43 Å)), and (4) improved metabolic stability by fluorinating metabolically labile sites in the target molecule^[15,16].

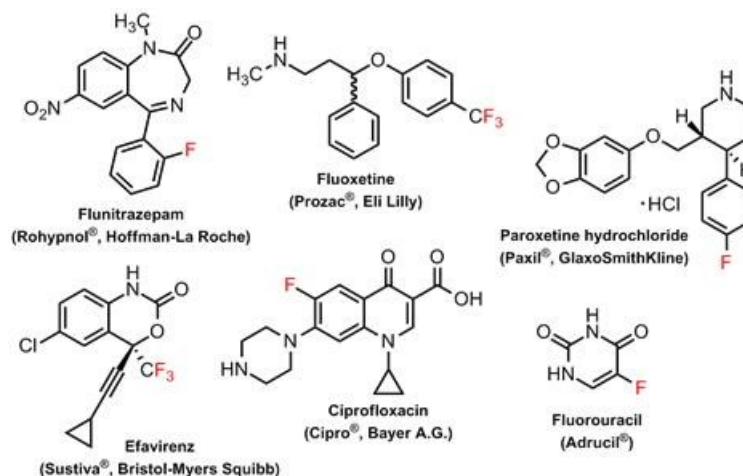


Figure 6: Examples of fluorinated pharmaceuticals.

Fluorine-18 PET has shown promise in conventional drug design as means to monitor *in vivo* drug distribution, as fluorinated pharmaceuticals are quite common in medicinal chemistry. PET is a particularly powerful technology when there is no easily measurable clinical pharmacodynamic marker, or when substantial time is required before an observable onset of therapy, as is the case for CNS and anticancer drugs^[17]. Classical examples of fluorine-containing pharmaceuticals include flunitrazepam (Rohypnol®, Hoffman-La Roche; benzodiazepine), fluoxetine (Prozac®, Eli Lilly; selective serotonin reuptake inhibitor), paroxetine hydrochloride (Paxil®, GlaxoSmithKline, selective serotonin reuptake inhibitor), efavirenz (Sustiva®, Bristol-Myers Squibb; non-nucleoside reverse transcriptase inhibitor), ciprofloxacin (Cipro®, Bayer A.G.; fluoroquinolone antibacterial), and fluorouracil (Adrucil®; thymidylate synthase inhibitor)^[18] and several other blockbuster drugs^[19], anticancer agents^[20], and fluorinated natural products^[21] (Figure 6).

1.1.4 PET and [¹⁸F]FDG in molecular imaging

As all disease states have a molecular or biological basis, PET, which uses radiolabeled molecules to image molecular interactions of biological process *in vivo*, is capable of early detection of disease without evidence of anatomical changes on computed tomography (CT) or magnetic resonance imaging (MRI).

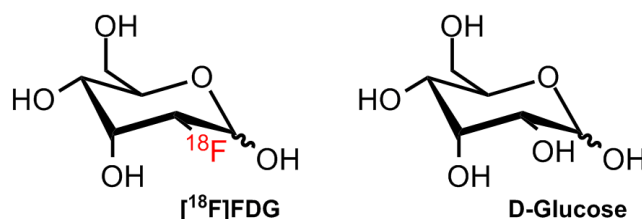


Figure 7: $[^{18}\text{F}]\text{Fluorodeoxyglucose}$ ($[^{18}\text{F}]\text{FDG}$). $[^{18}\text{F}]\text{FDG}$ is a radioanalogue of glucose substituted at the C-2 position.

$[^{18}\text{F}]\text{FDG}$ (Figure 7) has shown to be a valuable radiotracer for the molecular imaging of cancer, and the functions and dysfunctions of the brain and heart. $[^{18}\text{F}]\text{FDG}$ is a glucose analogue that undergoes facilitated transport and hexokinase-mediated phosphorylation *in vivo*. When phosphorylated, $[^{18}\text{F}]\text{FDG}$, unlike glucose, remains trapped in cells and is not rapidly metabolized, allowing the imaging of the rate of glucose uptake and glycolysis. $[^{18}\text{F}]\text{FDG}$ is used clinically for the early, presymptomatic diagnosis of Alzheimer's disease, for the detection of silent diseases such as Huntington's disease, and for assessing the metabolic viability of cardiac tissue in coronary heart disease patients^[22,23]. Clinical indications for FDG in oncology include differential diagnosis, preoperative staging of cancer, differentiation of scar and residual tissue, demonstration of suspected recurrences, follow-up of cancer therapy, and prognosis (assessment of cancer aggressiveness)^[24].

The emergence of the PET/CT combined scanner has led to powerful multimodality imaging owing to the simultaneous acquisition of both PET and CT

data from the same subject^[25]. Previously, image fusion of data from separate acquisitions was performed via software, but was largely limited to brain scans^[26]. PET/CT has allowed for the following: (1) comprehensive diagnostic anatomical and molecular whole-body survey in one session, (2) diagnostic information of higher accuracy, and (3) improved radiation treatment planning in oncology^[27].

1.2 Carbon-11 radiochemistry

1.2.1 Introduction

Carbon-11 is a short-lived radioisotope commonly used for the radiolabeling of PET tracers (Table III). The first recorded instances of carbon-11 production involved the bombardment of boron oxide (B_2O_3 ; natural abundance: 19.9% ^{10}B , 80.1% ^{11}B) targets by deuterons^[28] and protons^[29,30] in 1934 via the $^{10}B(d,n)^{11}C$ and $^{11}B(p,n)^{11}C$ reactions, respectively. Carbon-11 produced by these methods was later confirmed to be in the form of a gaseous mixture of $[^{11}C]$ carbon monoxide ($[^{11}C]CO$) and $[^{11}C]$ carbon dioxide ($[^{11}C]CO_2$)^[31]. The $^{14}N(p,\alpha)^{11}C$ reaction using N_2 gas, currently the route of production of greatest importance in PET, was first documented in 1939^[32].

Table III: Selected isotopes of carbon. Isotopes of carbon with half-lives on the order of seconds or greater are listed (β^+ : β^+ decay, β^- : β^- decay). Taken from literature^[33].

Nuclide	Z(p)	N(n)	Half-life	Decay mode
^{10}C	6	4	19.290 s	β^+ (100%)
^{11}C	6	5	20.39 min	β^+ (100%)
^{12}C	6	6	Stable	Stable
^{13}C	6	7	Stable	Stable
^{14}C	6	8	5.70×10^3 yr	β^- (100%)
^{15}C	6	9	2.449 s	β^- (100%)

Early examples of biochemical applications of carbon-11 include using $[^{11}\text{C}]\text{CO}_2$ as marker in processes such as photosynthesis^[34], and the study of $[^{11}\text{C}]\text{CO}$ metabolism in humans^[35]. The advent of medical cyclotrons, marked by the 1955 inauguration of the Medical Research Council Cyclotron Unit (MRC CU) at Hammersmith Hospital in London, UK^[36], focused research into the radiochemistry of carbon-11 and its medical applications.

1.2.2 Carbon-11 production

Presently, carbon-11 is widely produced from cyclotron in the form of $[^{11}\text{C}]\text{CO}_2$ or $[^{11}\text{C}]\text{methane}$ ($[^{11}\text{C}]\text{CH}_4$) *in situ* depending on the redox potential of the target. Proton bombardment of a N_2 gas target containing trace amounts of

O₂ (0.1-0.5%) affords carrier-free ¹¹C¹⁸O₂ whereas the presence of H₂ affords [¹¹C]hydrogen cyanide ([¹¹C]HCN) which is radiolytically converted to [¹¹C]CH₄ in situ^[37]. These two precursors are the starting point for the radiosynthesis of various carbon-11 building blocks (Figure 8).

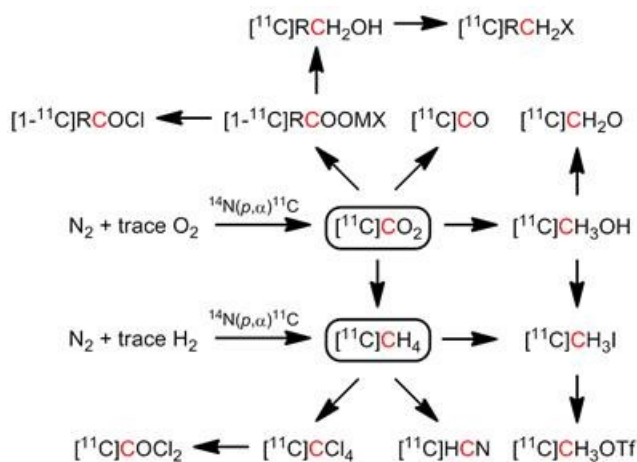


Figure 8: Carbon-11 building blocks derived from [¹¹C]CO₂ or [¹¹C]CH₄.

Adapted from literature^[38].

1.2.3 Electrophilic carbon-11 building blocks

Although [¹¹C]CO₂ can be directly incorporated into organic molecules, the poor electrophilicity of this building block necessitates highly reactive nucleophiles, such as methyl magnesium halides (i.e. Grignard reagents), as documented for the radiosynthesis of [1-¹¹C]acetate^[39,40] (Figure 9a). Recently, methods for [¹¹C]CO₂ fixation have been reported where cyclotron-produced [¹¹C]CO₂ was trapped by strong nitrogen bases (e.g. DBU^[41] or BEMP^[42]) and

converted to the corresponding isocyanate for the one-pot synthesis of ureas (symmetrical and unsymmetrical) and carbamates^[43] (Figure 9b).

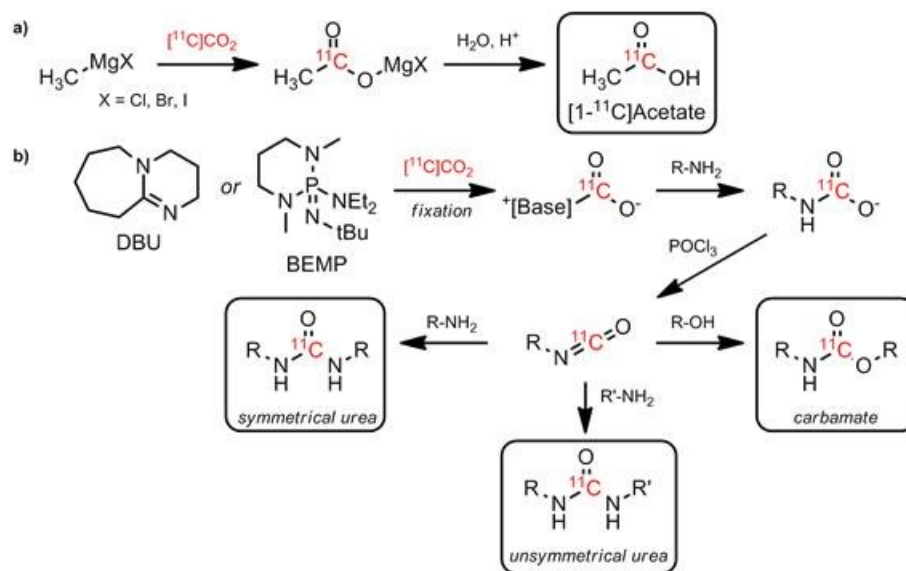


Figure 9: Examples of $[^{11}\text{C}]$ carboxylation reactions.

(a) Carboxylation via $[^{11}\text{C}]\text{CO}_2$. *(b)* $[^{11}\text{C}]\text{CO}_2$ fixation.

Carbon-11 in the form of $[^{11}\text{C}]\text{CH}_3\text{X}$, where X represents a good leaving group, can be used for the radiosynthesis of methyl ethers, methylamines, and methyl thioethers from their respective alcohol, amine, and thiol nucleophile precursors by simple $\text{S}_{\text{N}}2$ nucleophilic substitution. $[^{11}\text{C}]\text{Methyl iodide}$ ($[^{11}\text{C}]\text{CH}_3\text{I}$) is the most widespread radiomethylating agent, and can be produced from $[^{11}\text{C}]\text{CO}_2$ in two steps by reduction to $[^{11}\text{C}]\text{CH}_3\text{OH}$ via LiAlH_4 and subsequent treatment with hydroiodic acid under reflux conditions^[44]. Alternatively,

[^{11}C]methyl trifluoromethanesulfonate ([^{11}C]methyl triflate, [^{11}C]CH₃OTf), produced by treatment of [^{11}C]CH₃I with silver triflate at 175°C^[45], may be used as a stronger radiomethylating agent.

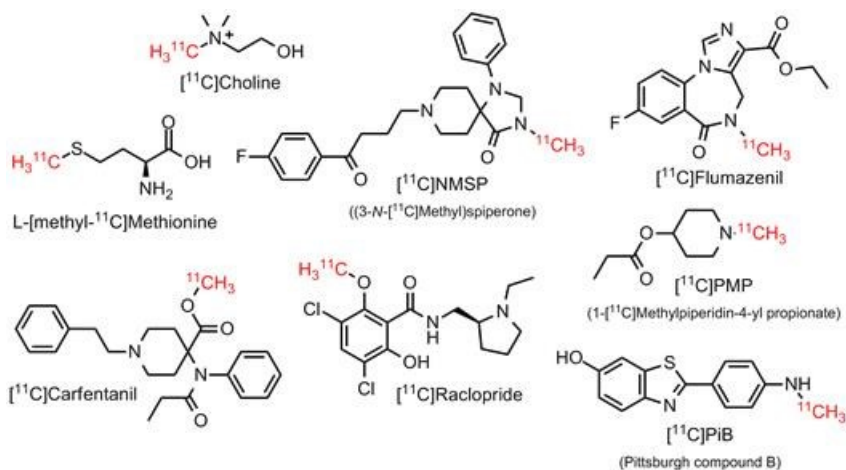


Figure 10: Examples of PET radiotracers produced via radiomethylation.

These transformations require [^{11}C]CH₃I or [^{11}C]CH₃OTf as starting material.

The methyl group is frequently encountered in biologically-active natural products and radiopharmaceuticals. It follows that radiomethylation of their respective desmethylated precursors provides a relatively facile means to monitor the *in vivo* behavior of these molecules. In particular, [^{11}C]CH₃I and [^{11}C]CH₃OTf has provided a simple radiosynthetic route for the production of PET radiotracers, including the following labeled natural products and pharmaceuticals: [^{11}C]methionine^[46], [^{11}C]choline^[47], [^{11}C]NMSP ((3-*N*-[^{11}C]methyl)spiperone)^[48], [^{11}C]flumazenil^[49], [^{11}C]carfentanil^[50], [^{11}C]raclopride^[51], [^{11}C]PMP (1-

[^{11}C]methylpiperidin-4-yl propionate)^[52,53], and [^{11}C]PiB (Pittsburgh compound B)^[54,55] (Figure 10).

1.2.4 Other carbon-11 building blocks

Nucleophilic carbon-11 building blocks may be employed to introduce the radioisotope to electrophile-bearing precursors. Examples include [^{11}C]methyllithium for the addition onto ketone functionalities^[56] and the reaction of [^{11}C]dimethylamine to benzyl and allyl bromides^[57] (Figure 11a,b). However, this strategy is not widely employed as these building blocks are produced from [^{11}C]CH₃I, necessitating more involved multistep radiosyntheses compared to electrophilic carbon-11 sources.

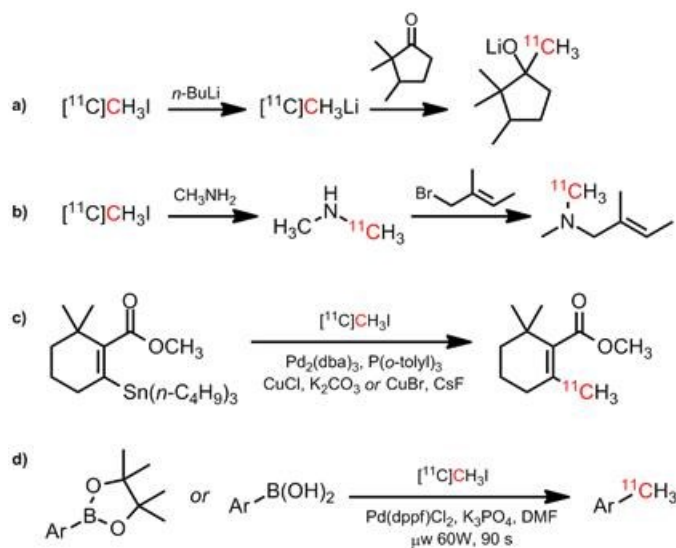


Figure 11: Other transformations with carbon-11.

Radiochemistry employing (*a,b*) nucleophilic carbon-11 sources and (*c,d*) palladium(0)-mediated cross-coupling reactions.

Recently, efforts have been undertaken to adapt palladium-mediated cross-coupling reactions towards carbon-11 radiochemistry, particularly with new $^{11}\text{C}_{\text{sp}3}$ - $^{12}\text{C}_{\text{sp}2}$ (vinyl or aryl) bond formation. More precisely, the $[^{11}\text{C}]\text{CH}_3\text{I}$ building block, readily available via existing production methods, can be coupled to organostannanes (Stille reaction)^[58] or to arylboronic acids or esters (Suzuki reaction)^[59] under palladium(0) catalysis (Figure 11c,d). These novel methodologies have expanded the library of potentially synthesizable PET tracers to include compounds bearing $[^{11}\text{C}]\text{CH}_3$ -C connectivities, as well as provide a more metabolically robust labeling site compared to $[^{11}\text{C}]\text{CH}_3$ -heteroatom tracers produced from traditional radiomethylation methods.

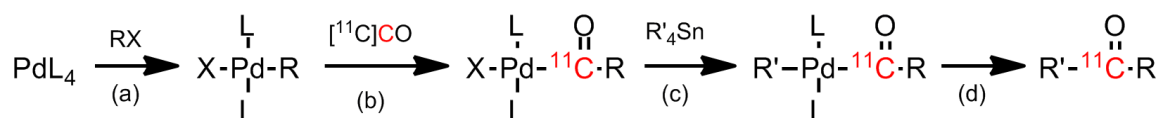


Figure 12: Proposed mechanism of the $[^{11}\text{C}]\text{CO}$ carbonylation reaction. The steps include: (a) oxidative addition, (b) $[^{11}\text{C}]\text{CO}$ insertion, (c) transmetallation, and (d) reductive elimination. Adapted from literature^[60].

Palladium(0) catalysis has also been employed in carbonylation reactions using $[^{11}\text{C}]\text{CO}$ for the synthesis of imides, ketones, amides, and acrylamides (Figure 12)^[60-62], although the generally poor solubility of $[^{11}\text{C}]\text{CO}$ in organic solvents presents a challenge towards its reactivity.

1.3 Fluorine-18 radiochemistry

1.3.1 Introduction

Table IV: Selected isotopes of fluorine. Isotopes of fluorine with half-lives on the order of seconds or greater are listed (β^+ : β^+ decay, β^- : β^- decay, β^-n : β^- delayed neutron emission). Taken from literature^[33].

Nuclide	Z(p)	N(n)	Half-life	Decay mode
^{17}F	9	8	64.49 s	β^+ (100%)
^{18}F	9	9	109.771 min	β^+ (100%)
^{19}F	9	10	Stable	Stable
^{20}F	9	11	11.163 s	β^- (100%)
^{21}F	9	12	4.158 s	β^- (100%)
^{22}F	9	13	4.23 s	β^- (89%), β^-n (<11%)
^{23}F	9	14	2.23 s	β^- (86%), β^-n (<14%)

First discovered by Snell in 1937^[63], fluorine-18 (^{18}F) is an artificial isotope of fluorine (Table IV) commonly employed as radioactive tracer of natural fluorine-19 (^{19}F) for chemical, biological, and medical studies^[64]. Although inorganic $[^{18}\text{F}]\text{F}^-$ has shown use as a bone scanning agent in PET imaging^[65], fluorine-18 is particularly attractive when chemically incorporated into organic molecules of biological and medical interest. Countless reviews have been produced detailing the radiochemistry of fluorine-18^[38,64,66-77].

1.3.2 Fluorine-18 production

Table V: Production routes for fluorine-18. Taken from literature^[78].

Nuclear reaction	Useful energy range (MeV)	Natural abundance (%)
$^{18}\text{O}(p, n)^{18}\text{F}$	14–4	0.2
$^{16}\text{O}(^3\text{He}, p)^{18}\text{F}$	15–1	99.7
$^{16}\text{O}(^3\text{He}, n)^{18}\text{Ne}: ^{18}\text{F}$	40–15	99.7
$^{16}\text{O}(\alpha, np)^{18}\text{F}$	40–20	99.7
$^{16}\text{O}(\alpha, 2n)^{18}\text{Ne}: ^{18}\text{F}$	52–10	99.7
$^{20}\text{Ne}(d, \alpha)^{18}\text{F}$	15–0	90.5
$^{20}\text{Ne}(p, 2pn)^{18}\text{F}$	40–30	90.5
$^{20}\text{Ne}(^3\text{He}, \alpha p)^{18}\text{F}$	40–10	90.5

Fluorine-18 is commonly produced by cyclotron (a circular particle accelerator) for radiopharmaceutical applications. The most common production route involves irradiation of an $[^{18}\text{O}]\text{H}_2\text{O}$ (^{18}O -enriched water; “ ^{18}O -heavy water”) liquid target with 20 MeV protons in an $^{18}\text{O}(p,n)^{18}\text{F}$ reaction to produce an aqueous solution of $[^{18}\text{F}]\text{fluoride}$ ($[^{18}\text{F}]\text{F}^-$)^[79]. Alternatively, irradiation of a ^{20}Ne gas target containing 0.1% cold F_2 carrier gas with deuterons is used to produce elemental fluorine ($[^{18}\text{F}]\text{F}_2$) in a $^{20}\text{Ne}(d,\alpha)^{18}\text{F}$ reaction^[80]. Other production methods exist, but have found limited adoption for routine radiosyntheses (Table V)^[78].

1.3.3 Electrophilic [^{18}F]radiofluorination

Electrophilic ^{18}F fluorinations, with the use of [^{18}F]F₂ or related electrophilic species, have historically played a role in the development of radiofluorinated tracers. An early synthesis of [^{18}F]FDG employed [^{18}F]acetyl hypofluorite ([^{18}F]AcOF), produced by passing the [^{18}F]F₂ target gas (from a $^{20}\text{Ne}(d,\alpha)^{18}\text{F}$ reaction) through a stainless steel tube packed with KOAc(HOAc)_{1.5}, to label D-glucal (Figure 13a)^[81].

Electrophilic fluorinations have gradually fallen out of favor for two reasons: (1) [^{18}F]F₂ suffers from low specific activity as its production requires an excess of cold fluorine carrier gas, and (2) electrophilic fluorinations are often non-regioselective, leading to the production of multiple products and undesirable by-products.

Recent developments in electrophilic radiofluorinations^[82] attempt to “tame” the reactivity of [^{18}F]F₂ by using [^{18}F]Selectfluor to cleanly label silyl enol ethers and electron-rich arylstannanes (Figure 13b), where multiple products would have been expected from conventional labeling methods^[83]. In addition, efforts to improve the specific activity of [^{18}F]F₂ have led to the development of [^{18}F]FCIO₃^[84] (Figure 13c) and more successfully, a [^{18}F]palladofluorine complex (Figure 13d)^[85] derived from no-carrier-added [^{18}F]fluoride ion as electrophilic fluorinating agents.

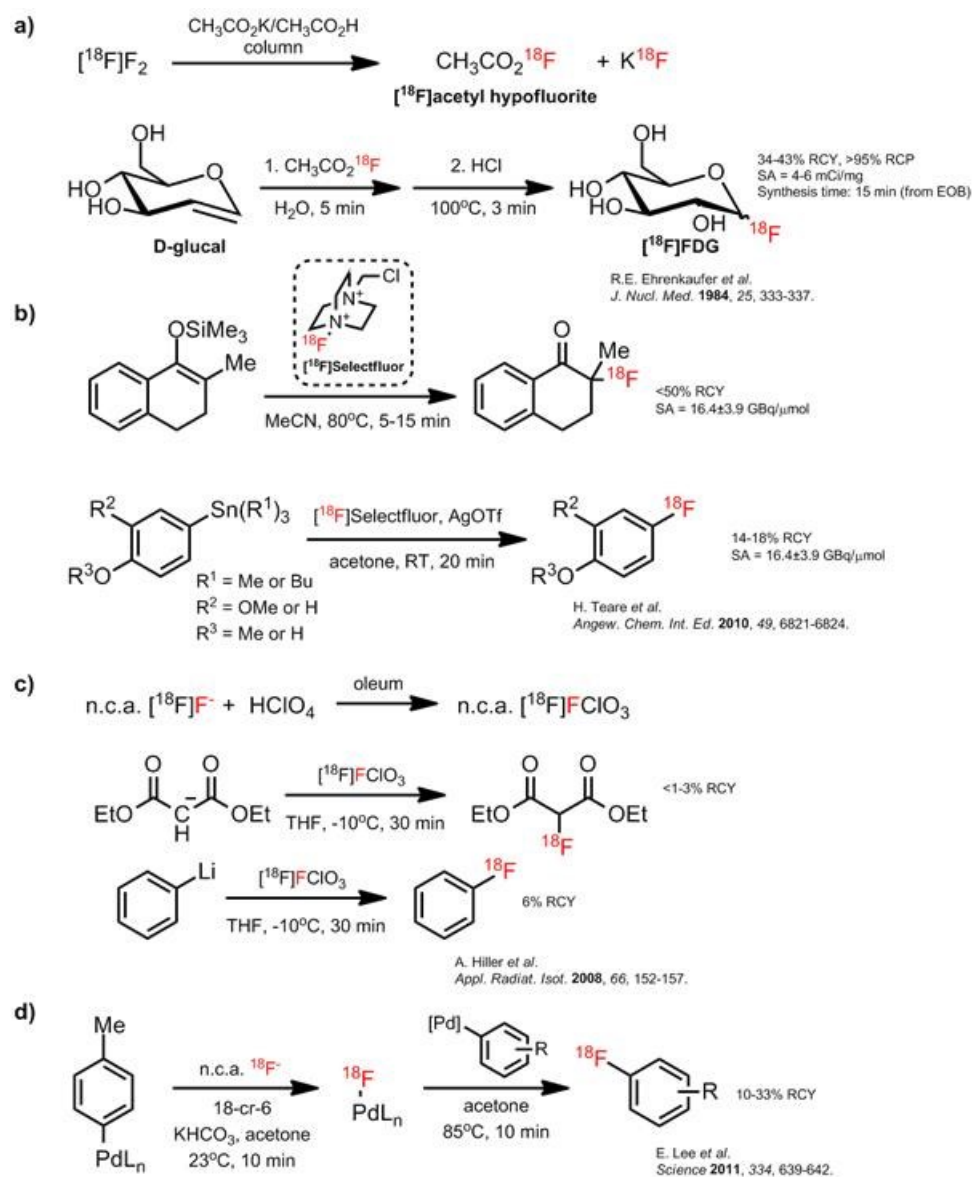


Figure 13: Examples of electrophilic radiofluorinations.

1.3.4 Nucleophilic [¹⁸F]radiofluorination

1.3.4.1 [¹⁸F]Fluoride preparation and drying

Due to high specific activities owing to a no-carrier-added (no non-radioactive or “cold” ¹⁹F added) method of [¹⁸F]fluoride ion production, and the

chemo/regioselectivity of nucleophilic reactions, nucleophilic radiofluorinations are the reactions of choice for the labeling of organic molecules. However, [^{18}F]fluoride ions are produced by the $^{18}\text{O}(\text{p},\text{n})^{18}\text{F}$ reaction as an aqueous solution in the [^{18}O]H $_2\text{O}$ target. The high heat of solution of the fluoride ion, caused by a small radius-to-charge ratio, makes the ion strongly solvated, thus highly inert and non-nucleophilic in the aqueous environment^[86]. In fact, synthetic chemistry using nucleophilic fluoride necessitates highly anhydrous conditions with minimal solvation to ensure a reactive “naked” fluoride ion. Therefore, a rigorous drying regimen is required to remove trace water that may interfere with conventional nucleophilic radiofluorinations.

The removal of the bulk of [^{18}O]H $_2\text{O}$ occurs by passing the solution of [^{18}F]F $^-$ through an activated anion-exchange cartridge (Figure 14). The retained [^{18}F]fluoride, along with a trace quantity of water, is subsequently eluted with a solution of Kryptofix[®] 2.2.2 and potassium carbonate in acetonitrile. Kryptofix[®] 2.2.2 (IUPAC name: 4,7,13,16,21,24-hexaoxa-1,10-diazabicyclo[8.8.8]hexacosane) is a cryptand that binds to potassium cations strongly and selectively ($\log K_a = 10.49$ ^[87]) serving a twofold purpose: (1) solubilisation of the [^{18}F]KF ion-pair in organic media (typically acetonitrile), and ensuring a high fluoride nucleophilicity in dipolar aprotic solvents^[88-90]. Potassium carbonate, or similar bases, are used to prevent the formation of [^{18}F]HF ($\text{p}K_a$

3.189^[91]). Hydrogen fluoride is a gas (bp 19.5°C^[91]) known to react with borosilicate glass, and is poorly nucleophilic.

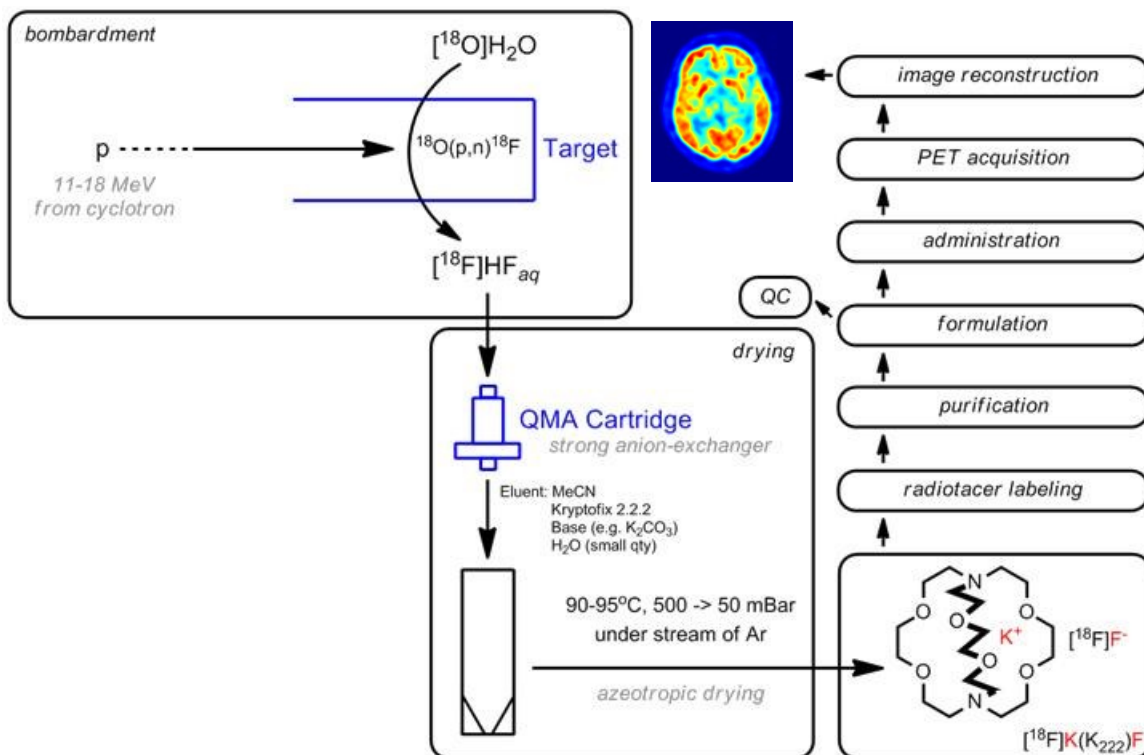


Figure 14: Production of anhydrous $[^{18}\text{F}]\text{K}(\text{K}_{222})\text{F}$. Early stages of nucleophilic radiofluorinations require a drying step to produce anhydrous $[^{18}\text{F}]\text{K}(\text{K}_{222})\text{F}$.

The trace water remaining in the eluent can be removed via azeotropic evaporation (acetonitrile/water azeotrope: bp 76°C, containing 16% H_2O ^[92]) *in vacuo* under a gentle stream of argon to afford $[^{18}\text{F}]\text{K}(\text{K}_{222})\text{F}$ that can be redissolved in the desired aprotic organic solvent. Typical solvents suitable for nucleophilic radiofluorinations include acetonitrile and dimethyl sulfoxide (DMSO).

1.3.4.2 Nucleophilic fluorine-18 radiochemistry

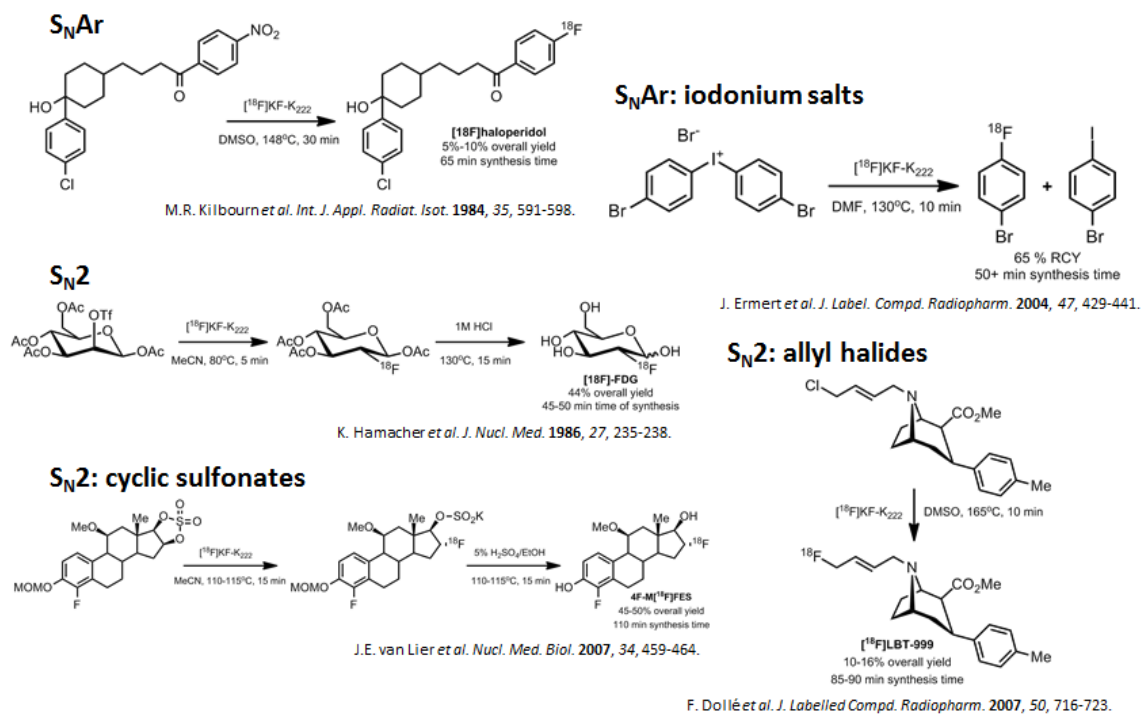


Figure 15: Examples of nucleophilic radiofluorinations.

Following drying, [¹⁸F]fluoride ions can be incorporated into organic molecules via nucleophilic substitution reactions. S_N2 radiofluorinations generally require electrophiles with excellent leaving groups, such as tosylates (e.g. [¹⁸F]FDG)^[89], allyl halides (e.g. [¹⁸F]LBT-999)^[93], cyclic sulfonates (e.g. 4F-M[¹⁸F]FES)^[94], and iodonium salts (e.g. [¹⁸F]*p*-bromofluorobenzene)^[95] (Figure 15). Nucleophilic aromatic substitutions (S_NAr) require electron-poor aromatic rings containing a trimethylamino or nitro leaving group (e.g. [¹⁸F]haloperidol)^[96].

1.4 Radiolabeling of biomolecules

1.4.1 Introduction

With increasing interest in the use of large biomolecules (oligonucleotides, peptides, and proteins) for the diagnosis and treatment of diseases, facile methods for ^{18}F labeling of these molecules are highly sought after. In particular, peptide-based radiopharmaceuticals have shown use in the imaging of thrombosis, tumors, and infection/inflammation^[97,98].

The high reaction temperatures typically required to introduce $^{18}\text{F}^-$ into tracer molecules are not compatible with these biomolecules and necessitate the use of secondary labeling precursors (prosthetic groups) and multistep procedures and purifications which increase the overall time of synthesis and reduce preparative yields of the desired radiotracer.

1.4.2 Acylation

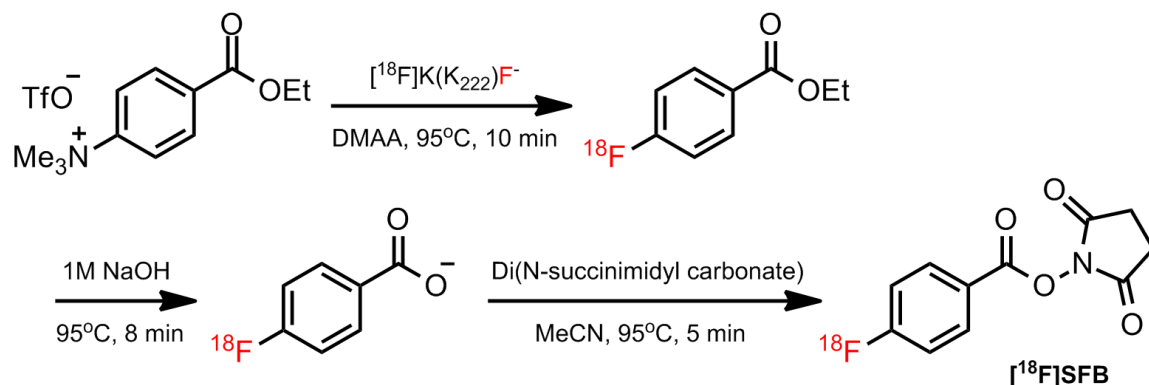


Figure 16: Original synthesis of no-carrier-added *N*-succinimidyl 4-

$[^{18}\text{F}]$ fluorobenzoate ($[^{18}\text{F}]\text{SFB}$). Taken from literature^[99].

The nucleophilic groups present in peptides and proteins: amino, carboxyl, hydroxyl, and thiol, suggest a radiolabeling strategy based on electrophilic prosthetic groups. A common labeling agent is *N*-succinimidyl 4- ^{18}F fluorobenzoate (^{18}F SFB), classically produced from the aryltrimethylammonium precursor in three radiochemical steps: (1) nucleophilic aromatic substitution with $^{18}\text{F}\text{F}^-$, (2) ester hydrolysis/deprotection, and (3) active ester formation (*N*-succinimidyl ester synthesis)^[99] (Figure 16). Alternative radiosynthetic routes have also been reported^[100,101]. ^{18}F SFB has shown use particularly in protein radiolabeling as this activated ester exhibits lower rates of hydrolysis compared to aliphatic equivalents, an important parameter for a successful ligation reaction under aqueous conditions necessitated by the protein. A comparison of ^{18}F SFB with the acylating prosthetic group 4-nitrophenyl 2- ^{18}F fluoropropionate (^{18}F NPFP), and the photochemical conjugate 4-azidophenacyl- ^{18}F fluoride (^{18}F APF) (Figure 17) has shown ^{18}F SFB as agent of choice for the labeling of monoclonal antibodies due to good conjugation yields and a high *in vivo* stability^[102]. In addition, ^{18}F SFB has found use in the labeling of chemotactic peptides^[103].

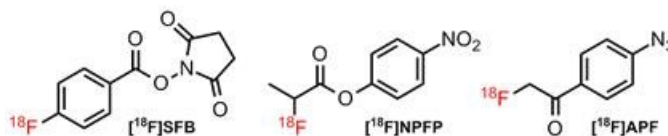


Figure 17: Select prosthetic groups for the radiofluorination of proteins.

1.4.3 Chemoselective oxime ligation

Oxime ligation, involving the coupling of an aldehyde to an aminooxy (hydroxyl amino) functionality to form an oxime, is a high efficient and selective reaction used for the synthesis of protein, peptide, carbohydrate, and oligonucleotide conjugates. 4-[^{18}F]fluorobenzaldehyde, produced in one step from the trimethylammonium precursor, has been shown to couple efficiently (60-80% labeling efficiencies) to fully-deprotected aminooxy-derivatized peptides in overall RCYs of 40% (end of bombardment)^[104] (Figure 18a). 4-[^{18}F]fluorobenzaldehyde has also found use in the synthesis of Cel-*S*-Dpr([^{18}F]FBOA)TOCA, a sugar-conjugated peptide, as the first tracer suitable for routine clinical applications in PET somatostatin receptor imaging^[105]. In addition, 4-[^{18}F]fluorobenzaldehyde has been adapted for the synthesis of hydrazones by coupling with hydrazine derivatives^[106] (Figure 18b).

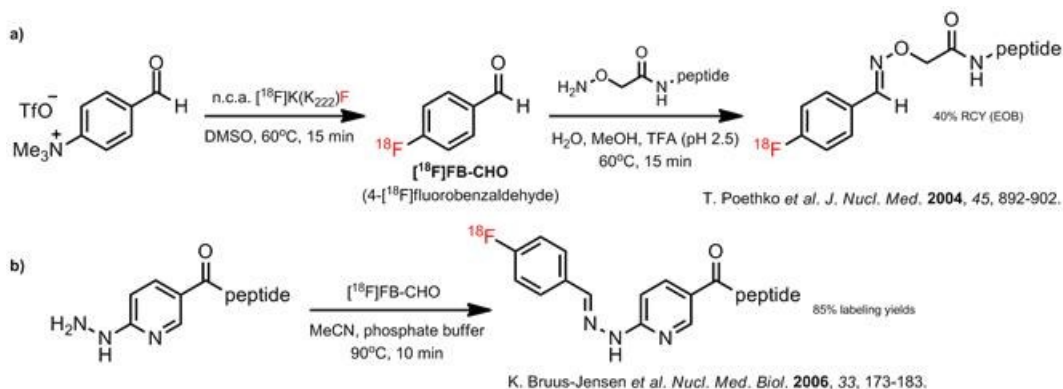


Figure 18: 4-[^{18}F]Fluorobenzaldehyde as a prosthetic group. Coupling of 4-[^{18}F]fluorobenzaldehyde onto aminooxy- and hydrazine-functionalized peptides.

1.4.4 Click Chemistry: Huisgen 1,3-dipolar cycloaddition

“Click chemistry” is a label for highly efficient reactions which meet the following requisites: modular, wide in scope, high-yielding, production of inoffensive byproducts, and stereospecific^[107]. The copper(I)-catalyzed Huisgen 1,3-dipolar cycloaddition between azides and alkynes has emerged as closest to the ideal “click” reaction, and the term “click reaction” is often used (albeit incorrectly) when referring to the Huisgen cycloaddition. This reaction has been adapted for the radiofluorination of peptides in a two-step approach from [¹⁸F]fluoroalkynes with azido-functionalized peptides^[108], and PEGylated [¹⁸F]fluoroazides with alkynyl-functionalized peptides^[109] (Figure 19a) . However, the cytotoxicity of copper has hampered efforts to bring these radiotracers to the clinic^[110,111]. Recently, catalyst-free 1,3-dipolar cycloadditions with strained cyclooctynes^[112,113] have shown promise as ligation strategy for prosthetic group radiolabeling, requiring no metal catalyst and no heating^[114]. This has led to the development of prosthetic groups for the facile ¹⁸F-labeling of peptides^[115,116] (Figure 19b) and small molecules^[117].

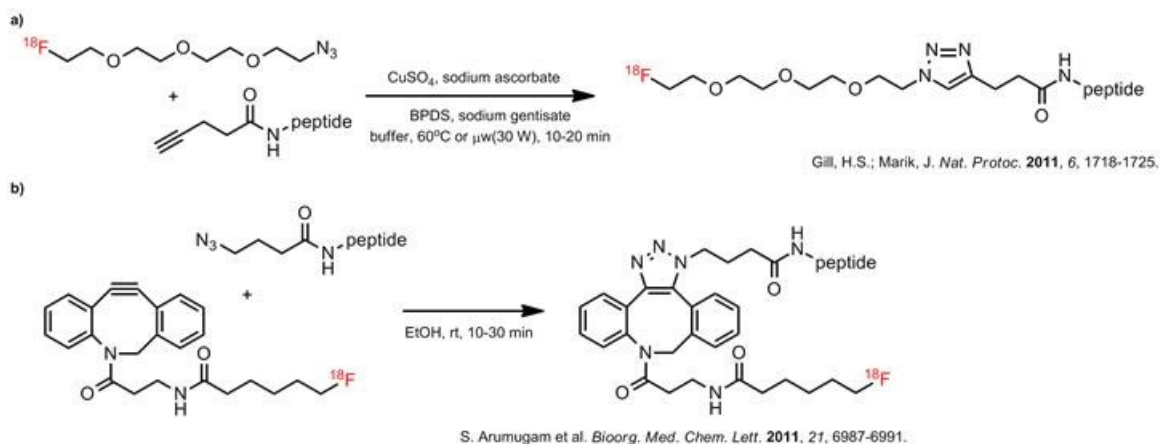


Figure 19: Click chemistry. (a) Copper(I)-catalyzed Huisgen 1,3-dipolar cycloaddition and (b) copper-free Huisgen 1,3-dipolar cycloaddition.

1.5 Novel labeling strategies

1.5.1 Introduction and early works

Several groups have reported nonconventional methods of ^{18}F and heteroatom (phosphorus, boron, aluminum, or silicon) bond formation as means for mild radiochemical incorporation of ^{18}F into molecules of biological interest.

Early attempts at heteroatom- ^{18}F fluorine labeling consist of reactions with phosphorodiamidic chlorides^[118] or chlorosilanes^[119]. P- ^{18}F bond formation has been demonstrated by the radiosynthesis of ^{18}F Dimefox (Figure 20a) from the chloride precursor, however no further developments has been reported. The synthesis of ^{18}F fluorotrimethylsilane from the chloride precursor has been reported (Figure 20b). However, administration to rats via inhalation has shown marked bone uptake of $^{18}\text{F}^-$, indicating rapid hydrolysis *in vivo*. More hindered Si-

^{18}F compounds have been suggested, which forms the basis of the silicon-based fluoride acceptor (SiFA) synthon.

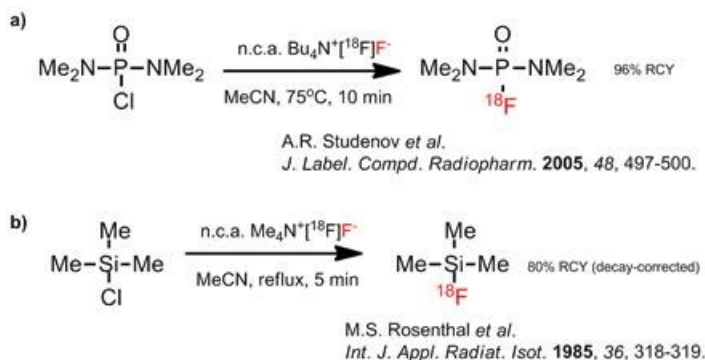


Figure 20: Early attempts at heteroatom- ^{18}F radiochemistry.

The very high Al-F, B-F, and Si-F bond strengths (bond energies: 159, 150, and 135 kcal/mol, respectively, compared with 83-85 kcal/mol for alkane C-C bond^[120,121]) has inspired research over the past decade to harness these fluorophilic heteroatoms for the fluorine-18 labeling of organic molecules.

1.5.2 Boronic esters

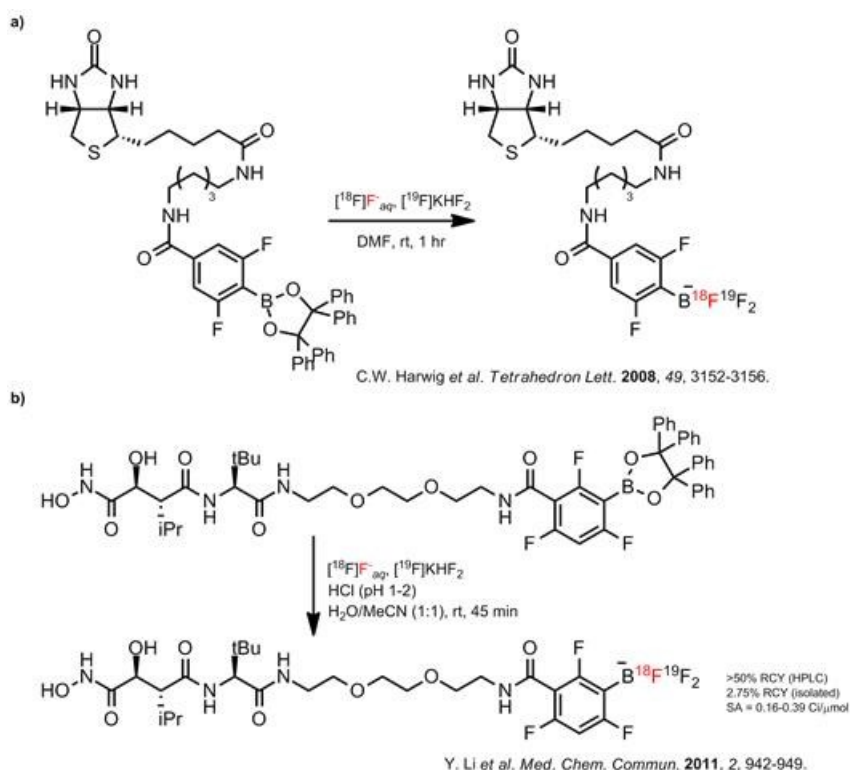


Figure 21: Radiochemistry with alkylfluoroborates.

Preliminary studies on alkylfluoroborates and alkylfluorosilicates by the Perrin group (University of British Columbia) have led to the development of [^{18}F]-labeled alkyltrifluoroborates from [^{18}F]fluoride ion under aqueous conditions at room temperature^[122] (Figure 21). These labeled boronic esters have shown remarkably high hydrolytic stability^[123,124], especially in the presence of an electron-withdrawing group bound to the aryl ring^[125]. *In vivo* studies in mice show rapid clearance of [^{18}F]alkylfluoroborates to the bladder with no detectable

defluorination and no observable bone deposition^[126]. This labeling system has been adapted for the synthesis of [¹⁸F]marimastat-alkyltrifluoroborate as a probe for *in vivo* PET imaging of cancer^[127], and work is currently under way for the development of a kit-like protocol for this radiotracer^[128]. However, due to the requirement for carrier fluoride in the radiolabeling step, specific activities are markedly low, which may potentially be remedied by emerging microreactor technologies^[129].

Recently, Perrin has reported high specific activities for ¹⁸F-labeled peptide bioconjugates from a cyclo-RGD-boronic ester precursor (12 Ci/μmol)^[130]. Moreover, favorable specific activities have also been reported for the novel ¹⁹F-¹⁸F isotopic exchange from a cyclo-RDG-BF₄⁻ precursor (555 GBq/μmol; 15 Ci/μmol)^[131]. Borimidines containing an alkynyl functionalities have also been successively employed for the one-pot two-step radiolabeling of cyclic RGD and bombesin (BBN) peptides via “click” chemistry^[132,133].

1.5.3 Aluminum fluorides

Goldenberg (Garden State Cancer Center, Belleville, NJ) and others have demonstrated the applicability of aluminum [¹⁸F]fluoride ([Al¹⁸F]²⁺) complexes for the one-pot, two-step labeling of peptides. [Al¹⁸F]²⁺ can be prepared easily from aluminum salts and aqueous [¹⁸F]fluoride ion. Initial studies have shown a dependence of radiolabeling yields and serum stability on the nature of the

chelate, with 1,4,7-triazacyclononane-1,4,7-triacetic acid (NOTA) possessing the most desirable properties among a series of chelates^[134,135] (Figure 22a). C-NETA was later developed as an improved NOTA-like chelate for high radiochemical yields (<85%)^[136] (Figure 22b). A one-step labeling protocol was later developed for the radiolabeling of heat-stable peptides^[137]. The $[Al^{18}F]^{2+}$ complexes have lately been used for the radiolabeling of small molecule nitroimidazoles as hypoxia imaging agents^[138] (Figure 22c). Recently, the $Al^{18}F$ method has been used in the labeling of antibody Fab' fragments^[139], and NOTA-conjugated peptide derivatives of bombesin (BBN)^[140] and octreotide^[141]. In addition, a lyophilized kit for rapid radiofluorination of peptides was reported^[142].

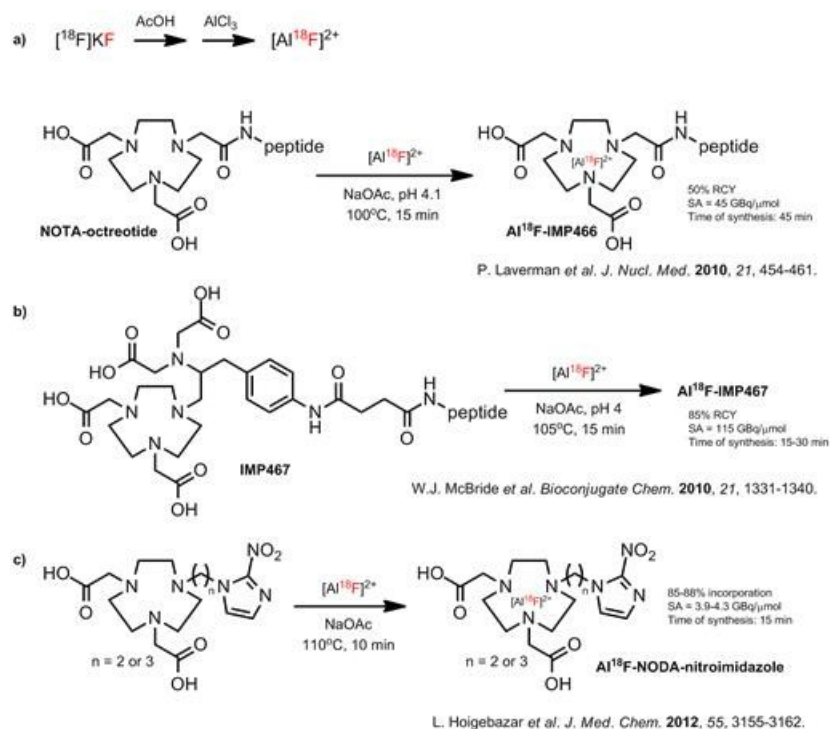


Figure 22: Radiochemistry with aluminum fluorides.

1.5.4 Silicon fluorides

Labeling via silicon- ^{18}F bond formation has been extensively pursued independently by the Ametamey (ETH-Zurich) and Jurkschat/Schirmacher/Wängler (Technische Universität Dortmund/McGill University/Ludwig-Maximilians-Universität München) groups. Ametamey has demonstrated the use of sterically-hindered silanols and silyl hydrides to produce ^{18}F fluorosilanes suitable for the one-step ^{18}F -radiolabeling of peptides^[143] (Figure 23a) with excellent hydrolytic stability ($t_{1/2}$ = 8h to 302 h in MeCN/buffer (2:1, pH 7) at room temperature)^[144]. However, *in vivo* studies of ^{18}F -labeled modified bombesin peptides reveal substantial hepatobiliary clearance, suggesting future work to reduce overall lipophilicity of these compounds^[145].

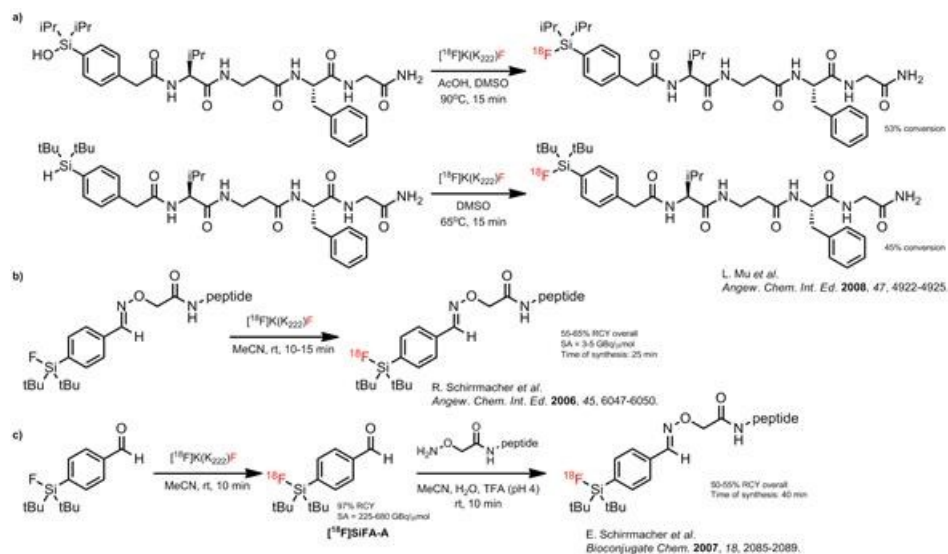


Figure 23: Radiochemistry with silicon fluorides.

(a) Silanols and silanes, and (b,c) silicon fluorides (SiFA).

Over the past decade, our group has developed hydrolytically stable *para*-functionalized aryl-di-*tert*-butylfluorosilanes, termed silicon-based fluoride acceptor (SiFA), that allow for rapid (~5 min) incorporation of $^{18}\text{F}^-$ by an efficient isotopic ^{19}F - ^{18}F exchange reaction at the silicon atom under ambient temperature for the one-step^[146] (Figure 23b) and two-step^[147] (Figure 23c) labeling of peptides from a SiFA-aldehyde (SiFA-A) moiety. The SiFA synthon has been further functionalized with a wide range of groups amenable for conjugation, including thiol, amine, maleimide, isocyanate, isothiocyanate, carboxylic acid, *N*-hydroysuccinimidyl ester, and perfluorophenyl ester^[148]. The SiFA moiety is characterized by high radiochemical yields and specific activities. In addition, work-up and purification of these [^{18}F]SiFA radiotracers involve a simple solid-phase extraction step without time-consuming high-performance liquid chromatography (HPLC), with the potential for ease of automation and development of kit-like labelling procedures obviating the need for highly skilled radiochemists.

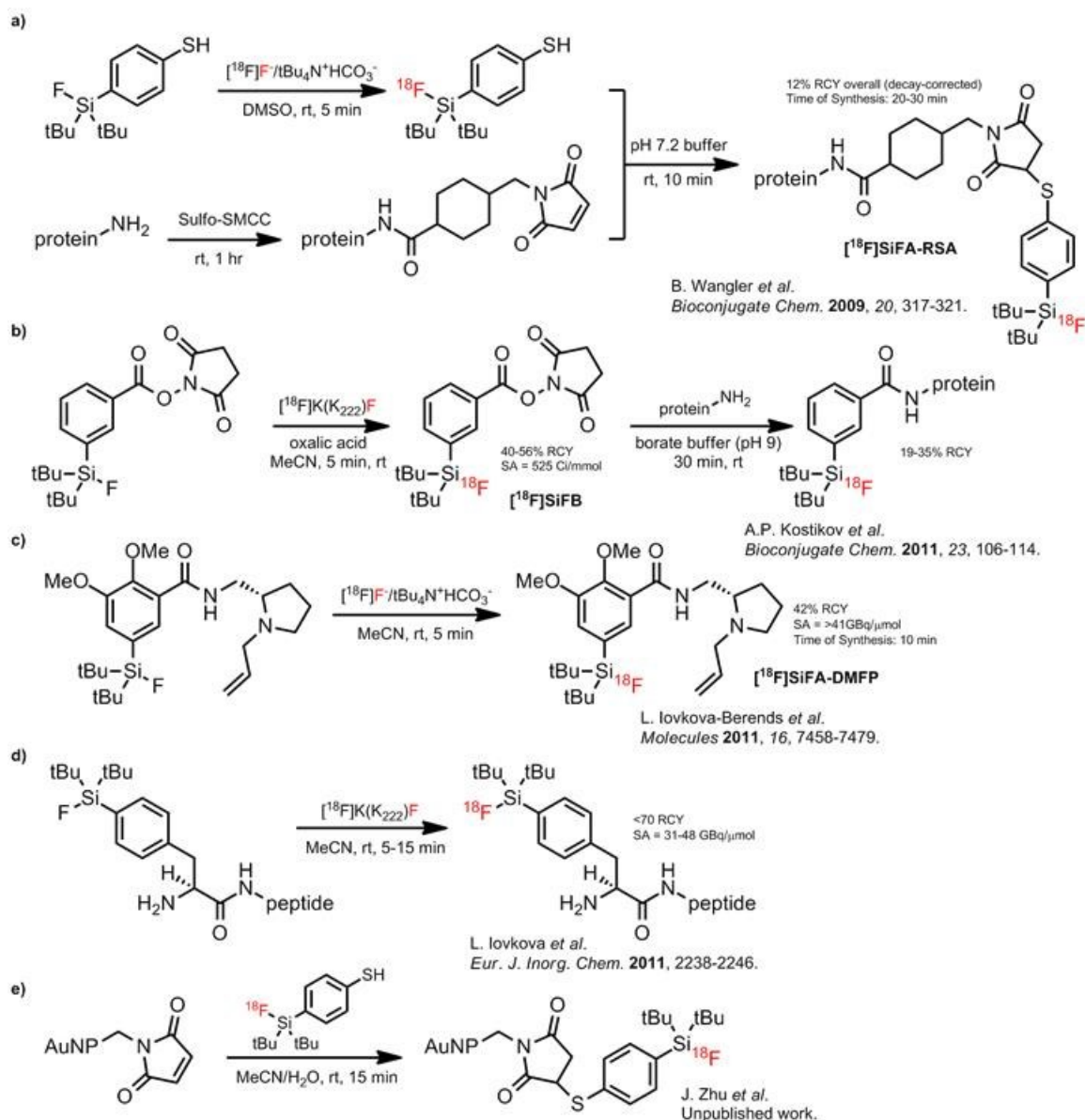


Figure 24: Radiochemistry with SiFA.

In particular, $[^{18}\text{F}]\text{SiFA}$ -thiol ($[^{18}\text{F}]\text{SiFA-SH}$), has found use in facile kit-like ^{18}F -labeling of maleimido-functionalized proteins in a two-step labeling^[149] (Figure 24a). $[^{18}\text{F}]\text{SiFA}$ labeling of unmodified proteins has also been achieved with *N*-succinimidyl 3-(di-*tert*-butyl $[^{18}\text{F}]\text{fluorosilyl}$)benzoate ($[^{18}\text{F}]\text{SiFB}$)^[150] (Figure 24b).

Despite its large size, the SiFA moiety has also been shown feasible for the ^{18}F -labeling of small molecule D_2 -receptor ligands^[151] (Figure 24c). Recently, the enantioselective synthesis of SiFA-modified phenylalanine has been reported feasible for solid-phase peptide synthesis^[152] (Figure 24d). Efforts are currently directed towards the two-step ^{18}F SiFA labeling of water-soluble maleimide-functionalized gold nanoparticles^[153,154] (Figure 24e).

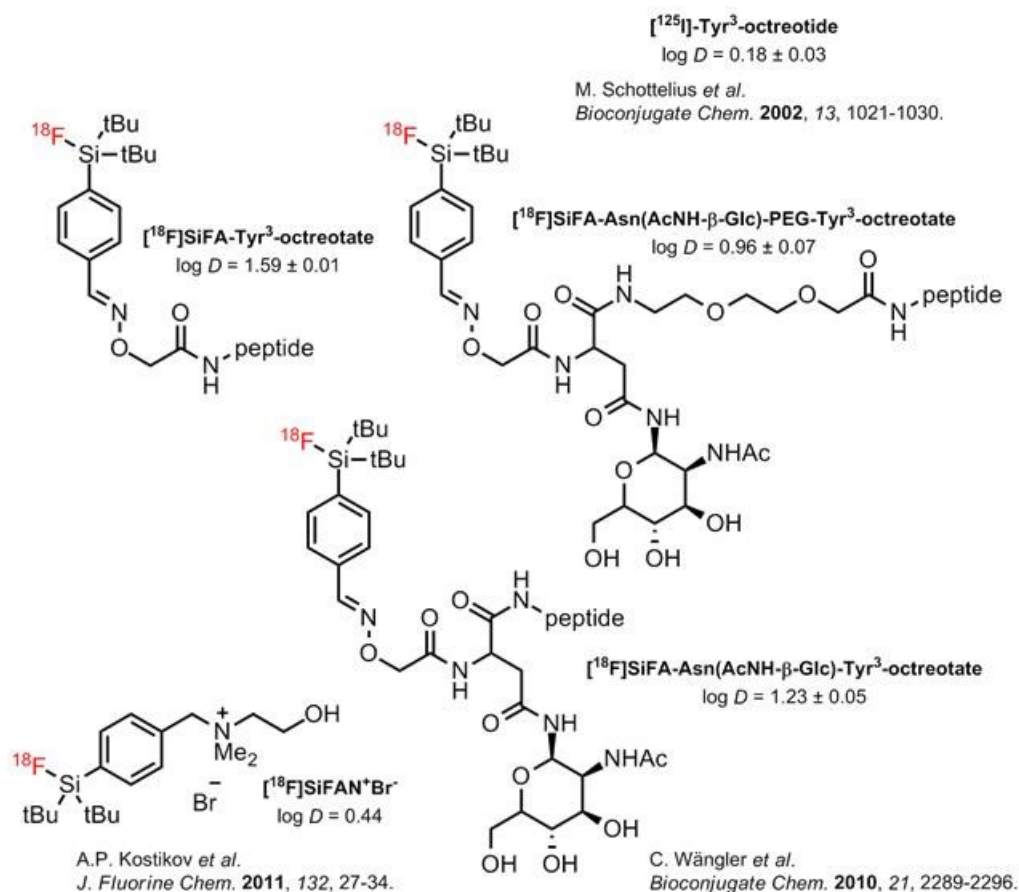


Figure 25: SiFA compounds of reduced lipophilicity.

[^{125}I]-Tyr³-octreotide is shown for comparison as a typical Tyr³-octreotide tracer^[155]. Tyr³-octreotide is an alcohol derivative of Tyr³-octreotate.

Initial applications of SiFA compounds for PET tumor imaging show high hepatic accumulation and nonspecific tissue binding due to the high lipophilicity imparted by the SiFA *tert*-butyl groups essential for hydrolytic stability. Recent investigation into the introduction of hydrophilic poly(ethylene glycol) (PEG) spacers and carbohydrates in the synthesis of SiFA-octreotate derivatives show a log P_{ow} value of 0.96, significantly lower than in the absence of these hydrophilic moieties (log P_{ow} = 1.59) (Figure 25)^[156]. In order to further reduce the lipophilicity of the SiFA synthon, the introduction of a chemical charge via the quaternary ammonium functional group has been considered. Preliminary studies into the proof-of-concept cationic SiFA molecule *N*-(4-(di-*tert*-butylfluorosilyl)benzyl)-2-hydroxy-*N,N*-dimethylethylammonium bromide (SiFA-N⁺Br⁻) show a moderately hydrophilic log P_{ow} value of 0.44^[157].

1.6 Current scope of research

The widespread use of peptides as PET radiotracers has been hampered by difficulties in the incorporation of carbon-11 or fluorine-18 into these complex molecules of interest without resorting to time-consuming multi-step syntheses or elaborate purification protocols.

1.6.1 Peptide labeling with carbon-11

In the case of carbon-11 labeling of peptides, there exist very few reported methodologies due to the short half-life of the isotope ($t_{1/2} = 20$ min). Herein, we propose a facile, one-step direct ^{11}C -methylation of cysteine residues in peptides using $[^{11}\text{C}]\text{MeOTf}$. Specifically, with the use of a variety of peptides, we demonstrate the feasibility of reaction, its regioselectivity towards cysteine residues, and a proof of applicability towards peptides of biological interest via the synthesis of $[^{11}\text{C}]\text{Cys}(\text{Me})\text{-}[\text{Tyr}^3\text{-octreotate}]$, a somatostatin analogue widely used in nuclear medicine.

1.6.2 Peptide labeling with fluorine-18

The SiFA platform remains attractive for the one- and two-step ^{18}F -labeling of peptides, but the high lipophilicity of the SiFA moiety remains a challenge in obtaining desirable pharmacokinetics in PET imaging. Having demonstrated that the high lipophilicity of the SiFA moiety can be compensated by applying hydrophilic moieties^[156], we propose the introduction of a cationic quaternary ammonium group onto SiFA molecules amenable towards bioconjugation as means to improve its hydrophilic profile. Furthermore, the design of these second-generation cationic SiFA synthons must meet the following considerations:

- a) Ease of synthesis: These synthons must be relatively straightforward to prepare, with minimal steps and manipulations. In addition, synthesis of these compounds from a common starting material is preferred.
- b) Ease of radiolabeling: As has been shown with reported SiFA compounds^[104-111,114,115], these cationic SiFA synthons must be labeled under comparable mild reaction conditions, ideally following with a cartridge-based purification and no preparative HPLC step.
- c) Large variety and versatility of functional groups: The functional groups appended to the SiFA synthons must be amenable to bioconjugation under standard reaction conditions.
- d) Suitability for peptide labeling: These SiFA synthons must be suitable for one-step peptide radiolabeling.
- e) Synthons of reduced lipophilicity: Cationic SiFA synthons must show a marked decrease in lipophilicity compared to non-cationic, first-generation synthons.

Chapter 2: MANUSCRIPT

“Direct one-step labeling of cysteine residues on peptides with [^{11}C]methyl triflate for the synthesis of PET radiopharmaceuticals.”

Submitted to *Amino Acids* (Springer), May 2013.

Accepted for publication, July 2013.

Supporting information to the manuscript is presented in *Chapter 7: Appendices – 7.1 Supplementary information*.

Chemical structure numbering exclusively presented in the text, figures, and tables of this chapter (Chapter 2) correspond to the numbering system as originally submitted to *Amino Acids*, and are not applicable as reference to any other chapter of this thesis.

Amino Acids (Manuscript)

Direct one-step labeling of cysteine residues on peptides with [^{11}C]methyl triflate for the synthesis of PET radiopharmaceuticals.

*Joshua Chin^{a,b}, Matthew Vesnaver^a, Vadim Bernard-Gauthier^{a,c}, Erin Saucke-Lacelle^a, Björn Wängler^d, Carmen Wängler^e, Ralf Schirmacher^{*a}*

^aMcConnell Brain Imaging Centre, Montreal Neurological Institute, McGill University, Montreal, Canada.

^bDepartment of Chemistry, McGill University, Montreal, Canada.

^cDepartment of Chemistry, Université de Montréal, Montreal, Canada.

^dMolecular Imaging & Radiopharmaceutical Chemistry, Department of Clinical Radiology and Nuclear Medicine, Medical Faculty Mannheim of Heidelberg University, Mannheim, Germany.

^eBiomedical Chemistry, Department of Clinical Radiology and Nuclear Medicine, Medical Faculty Mannheim of Heidelberg University, Mannheim, Germany.

* Corresponding author; e-mail address: ralf.schirmacher@mcgill.ca

2.1 Abstract

Radiolabeled peptides have emerged as an attractive platform for diagnostic and therapeutic oncology. However, the ^{11}C -radiolabeling of peptides for positron emission tomography (PET) has been poorly explored, owing to the relatively short half-life of carbon-11 ($t_{1/2} = 20.3$ min), and time-consuming multi-step radiochemical reactions. Existing methods have found limited use, and are not routinely encountered in the production of radiotracers. Herein, we propose a facile one-step direct ^{11}C -methylation of cysteine residues in peptides using $[^{11}\text{C}]$ methyl triflate under ambient temperatures (20°C) and short reaction times, on the order of seconds. Good regioselectivity of this method was demonstrated by HPLC in a simple peptide (glutathione; GSH) and a more complex test decapeptide (Trp-Tyr-Trp-Ser-Arg-Cys-Lys-Trp-Thr-Gly) bearing multiple nucleophilic sites. In addition, we extend this method towards the synthesis of $[^{11}\text{C}]\text{Cys}(\text{Me})$ -[Tyr³-octreotate] as demonstration of applicability for peptides of biological interest. This octreotate derivative was obtained in non-decay-corrected radiochemical yields of $11 \pm 2\%$ ($n=3$) with a synthesis time of approx. 30 min.

2.2 Introduction

Radiolabeled peptides have emerged as an attractive platform for diagnostic and therapeutic oncology. Advances in solid-phase peptide synthesis (SPPS) and well-established bioconjugation techniques have allowed for the ease of preparation, chemical modification, and radiolabeling of these compounds^[98,158]. In particular, small peptides (8-20 amino acids) show promise in nuclear imaging as they exhibit rapid pharmacokinetics, excellent tissue permeability, reduced immunogenicity, and good tumor targeting characteristics due to overexpressed peptide receptors in many cancers^[159,160]. To this date, ¹¹¹In-DTPA⁰-octreotide (¹¹¹In-OctreoScan, ¹¹¹In-pentetreotide) remains the first and most successful radiotracer for imaging somatostatin (SST) receptor-positive lesions in single-photon emission computed tomography (SPECT)^[161,162]. Due to inherently superior detection sensitivity and temporal resolution of the positron emission tomography (PET) modality^[163], various SST analogues labeled with positron-emitting copper-64 (⁶⁴Cu-CB-TE2A-Y³-TATE^[164]), fluorine-18 (Gluc/Cel-S-Dpr(¹⁸F)FBOA)TOCA^[105], Glu-Lys(¹⁸F)FP)-TOCA^[165], [¹⁸F]FP-Glu-TOCA^[166], SiFA-Asn(AcNH-β-Glc)-PEG-Tyr³-octreotate^[156,167], and ¹⁸F-AIF-NOTA-OC^[135]), and gallium-68 (⁶⁸Ga-DOTA-TOC^[168] and ⁶⁸Ga-DOTA-NOC^[169]) have been developed and are under preclinical or clinical evaluation.

Carbon-11 remains poorly explored in peptide labeling, owing to its relatively short half-life ($t_{1/2}$ = 20.3 min) and time-consuming, multi-step

radiochemical reactions generally associated with these complex biomolecules. The earliest reported synthesis of ^{11}C -labeled peptides was the labeling of methionine residues, specifically the tandem reductive deprotection and subsequent $[^{11}\text{C}]$ methyl iodide ($[^{11}\text{C}]\text{CH}_3\text{I}$) methylation of pentameric enkephalin peptides bearing benzyl-protected homocysteine residues^[170,171], and further adopted for synthesis of neuropeptide $[^{11}\text{C}]$ Substance P (RPKPQQFFGL $[^{11}\text{C}]\text{M}$)^[172]. However, this technique failed to see widespread adoption due to reaction conditions difficult to implement for routine production of radiotracers^[173]. Recently, *p*- $[^{11}\text{C}]$ methoxybenzaldehyde ($[^{11}\text{C}]\text{MB-CHO}$) derived from $[^{11}\text{C}]\text{CH}_3\text{I}$ has been developed as a prosthetic group for the chemoselective labeling of an aminooxyacetic acid-functionalized analogue of Tyr³-octreotate^[174]. However, this two-step labeling proceeds in an optimal synthesis time of 1 h, owing to the need for two radio-HPLC (high-performance liquid chromatography) purifications. Labeling using $[^{11}\text{C}]$ methyl trifluoromethylsulfonate ($[^{11}\text{C}]$ methyl triflate; $[^{11}\text{C}]\text{MeOTf}$) has been reported with the dipeptide glycylglycine ethyl ester on the amino-terminus as the first step towards the radiosynthesis of $[^{11}\text{C}]\text{Glycylsarcosine}$ (Gly-Sar) as PET tracer of peptide transporter PepT2^[175].

The direct, nonradioactive methylation of peptides and proteins has been previously reported using methyl sulfonates with high regioselectivity. Methyl *p*-nitrobenzenesulfonate (methyl nosylate) was used to selectively methylate the histidine-57 residue of α -chymotrypsin^[176] and cysteine residues of egg white

lysozyme and insulin B chain in the presence of lysine, histidine, methionine, tyrosine, and serine residues^[177]. Treatment of nuclear proteins with dimethyl sulfate (DMS) or methyl methanesulfonate (MMS) show methylation at cysteine and histidine residues^[178]. The methylation of metal-bound cysteinates on zinc finger peptides by DMS has also been reported^[179].

Herein we propose a facile, one-step direct ¹¹C-methylation of cysteine residues in peptides using [¹¹C]MeOTf. Specifically, we apply this method towards the labeling of a simple, commercially-available peptide (glutathione (GSH)) and a more complex decapeptide (Trp-Tyr-Trp-Ser-Arg-Cys-Lys-Trp-Thr-Gly) bearing multiple nucleophilic sites to demonstrate regioselectivity of radiomethylation. Furthermore, we extend this method towards the synthesis of [¹¹C]Cys(Me)-[Tyr³-octreotate] ([¹¹C]**10**) as demonstration of applicability towards peptides of biological interest.

2.3 Materials and methods

Regulatory notice

All manipulations involving radioactive materials have been performed in full accordance with Canadian Nuclear Safety Commission (CNSC) regulations.

Materials

Unless stated otherwise, commercially available chemical compounds were purchased from Sigma-Aldrich (Oakville, ON, Canada) in highest purity and used without further purification. Fmoc-protected resins and amino acids were purchased from NovaBiochem (Merck KGaA, Darmstadt, Germany) with the exception of Fmoc-Cys(Me)-OH, which was purchased from Bachem (Torrance, CA, USA), Fmoc-Arg(Pbf)-OH, which was purchased from GL Biochem (Shanghai, China), and Fmoc-Ser(Me)-OH and Fmoc-Thr(Me)-OH, which were purchased from Iris Biotech (Marktredwitz, Germany). Bulk solvents were rated HPLC grade or higher, and purchased from Fischer Scientific (Waltham, MA, USA). [^{11}C]CO₂ was prepared at the cyclotron unit of the McConnell Brain Imaging Centre, Montreal Neurological Institute. SepPak QMA and C-18 light cartridges were obtained from Waters Corporation (Milford, MA, USA).

Instruments

Semi-preparative HPLC was performed on an Agilent 1200 system (Agilent Technologies, Santa Clara, CA, USA; running on Agilent ChemStation software) equipped with a MZ semi-prep LiChrosorb column (RP-Select B 5 μ m, 250 x 10 mm; Merck, Germany) at a flow rate of 2 mL/min, and UV detection was performed at 230 nm and 254 nm. Analytical HPLC was performed on an Agilent 1200 system equipped with a Raytest Gabi Star radioactivity detector (Raytest Isotopenmessgeräte GmbH, Straubenhardt, Germany) and either a Chromolith Performance column (RP-18e, 100 x 4.6 mm; Merck, Germany) at a flow rate of 4.0 mL/min or an Aeris PEPTIDE column (XB-C18 3.6 μ m, 250 x 4.6 mm; Phenomenex, Torrance, CA, USA) at a flow rate of 0.8 mL/min, and UV detection was performed at 210 nm, 230 nm, and 254 nm. HPLC mobile phases consist of eluent A (0.1% TFA in MeCN) and eluent B (0.1% TFA in H₂O) filtered through a 0.45 μ m nylon membrane filter and degassed before use. Different HPLC methods were used depending on choice of peptide and column (Table VI). All samples for preparative and analytical HPLC were diluted with a minimum of 50% v/v eluent B prior to injection. Samples were injected via a model 7725i Rheodyne syringe loading sample injector fitted with a 2 mL loop (Rheodyne, Cotati, CA, USA). Gamma counting was performed using a CRC-25PET Dose Calibrator (Capintec, Ramsey, NJ, USA). Mass spectrometry of peptides was

performed using a Brucker Microflex LT MALDI-TOF MS (Brucker Daltonics, Billerica, MA, USA).

Table VI: HPLC elution methods for peptide analysis and purification.

Analytical and preparative HPLC elution methods used in the current study.

Method	Column	Flow (mL/min)	Gradient timeline (min)	Eluent A (%)	Eluent B (%)	Elution
A	LiChrosorb	2.0	0.00	25	75	Linear gradient
			40.00	100	0	Linear gradient
			45.00	25	75	Equilibration
B	LiChrosorb	2.0	0.00	0	100	Linear gradient
			30.00	100	0	Linear gradient
			35.00	0	100	Equilibration
C	Aeris PEPTIDE	0.8	0.00	0	100	Linear gradient
			5.00	15	85	Linear gradient
			15.00	20	80	Linear gradient
			17.50	100	0	Linear gradient
			20.00	100	0	Isocratic
			25.00	0	100	Equilibration
D	Chromolith Performance	4.0	0.00	0	100	Linear gradient
			10.00	100	0	Linear gradient
			12.00	0	100	Equilibration
E	Aeris PEPTIDE	0.8	0.00	0	100	Linear gradient
			5.00	25	75	Linear gradient
			15.00	35	65	Linear gradient
			17.50	100	0	Linear gradient
			20.00	100	0	Isocratic
			25.00	0	100	Equilibration

Peptide synthesis: General procedure for the synthesis of 1-12

Peptides **1-12** (Figure 26) were synthesized on solid support using standard Fmoc solid-phase peptide synthesis as described by Wellings and Atherton^[180] on a Fmoc-Thr(tBu)-Wang or a Fmoc-Gly-Wang resin (standard coupling: 4 equiv. amino acid, 4 equiv. HBTU, 4 equiv. DIPEA in DMF; Fmoc deprotection: 50% piperidine in DMF; disulfide cyclization: 4 equiv. TI(TFA)₃ in DMF). The peptides were cleaved from the resin and deprotected upon treatment with a solution of TFA/TIPS/H₂O (95:2.5:2.5, 2 mL) for 60 min, and then

precipitated from solution upon addition of excess diethyl ether. The crude solid was washed three times with excess diethyl ether, and purified by semi-preparative HPLC (1-8: Method A; 9-12: Method B) to afford the desired peptide as a white solid after lyophilisation with a purity of 95% or greater determined by quality control (HPLC Method E).

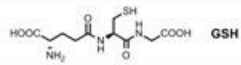
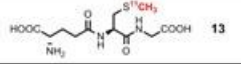
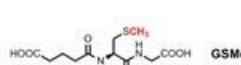
Precursor	 GSH	Trp-Tyr-Trp-Ser-Arg-Cys-Lys-Trp-Thr-Gly	1	Cys-D-Phe-Cys-Tyr-D-Trp-Lys-Thr-Cys-Thr	9
Product	 13	Trp-Tyr-Trp-Ser-Arg-Cys(¹³ CH ₃)-Lys-Trp-Thr-Gly	[¹³ C]2	Cys(¹³ CH ₃)-D-Phe-Cys-Tyr-D-Trp-Lys-Thr-Cys-Thr	[¹³ C]10
Nonradioactive standards	 GSMe	Trp-Tyr-Trp-Ser-Arg-Cys(Me)-Lys-Trp-Thr-Gly Trp-Tyr-Trp-Ser-Arg-Cys(Lys(Me))-Trp-Thr-Gly Trp-Tyr-Trp-Ser-Arg(Me)-Cys-Lys-Trp-Thr-Gly Trp-Tyr(Me)-Trp-Ser-Arg-Cys-Lys-Trp-Thr-Gly Trp(omega-NMe)-Trp-Trp-Ser-Arg-Cys-Lys-Trp-Thr-Gly Trp-Tyr-Trp-Ser-Arg-Cys-Lys-Trp-Thr(Me)-Gly Trp-Tyr-Trp-Ser(Me)-Arg-Cys-Lys-Trp-Thr-Gly	2 3 4 5 6 7 8	Cys(Me)-D-Phe-Cys-Tyr-D-Trp-Lys-Thr-Cys-Thr Cys-D-Phe-Cys-Tyr-D-Trp-Lys-Thr-Cys(Me)-Thr Cys-D-Phe-Cys(Me)-Tyr-D-Trp-Lys-Thr-Cys-Thr	10 11 12

Figure 26: List of peptide structures. List of peptidic precursors, radiolabeled products, and nonradioactive standards employed in this study.

Synthesis of Trp-Tyr-Trp-Ser-Arg-Cys-Lys-Trp-Thr-Gly (1). 32% yield.

$R_{t(\text{Method A})} = 7.6$ min. HRMS (MALDI-TOF, m/z) for $C_{66}H_{86}N_{17}O_{14}S^+ [M+H]^+$ (calc'd): 1372.55 (1372.63).

Synthesis of Trp-Tyr-Trp-Ser-Arg-Cys(Me)-Lys-Trp-Thr-Gly (2). 48% yield.

$R_{t(\text{Method A})} = 7.7$ min. $R_{t(\text{Method E})} = 18.9$ min. HRMS (MALDI-TOF, m/z) for $C_{67}H_{88}N_{17}O_{14}S^+ [M+H]^+$ (calc'd): 1386.71 (1386.64).

Synthesis of Trp-Tyr-Trp-Ser-Arg-Cys-Lys(Me)-Trp-Thr-Gly (3). 16% yield.

$R_{t(\text{Method A})} = 7.6$ min. $R_{t(\text{Method E})} = 18.4$ min. HRMS (MALDI-TOF, m/z) for $\text{C}_{67}\text{H}_{88}\text{N}_{17}\text{O}_{14}\text{S}^+ [\text{M}+\text{H}]^+$ (calc'd): 1386.68 (1386.64).

Synthesis of Trp-Tyr-Trp-Ser-Arg(Me)-Cys-Lys-Trp-Thr-Gly (4). 6% yield.

$R_{t(\text{Method A})} = 7.8$ min. $R_{t(\text{Method E})} = 18.4$ min. HRMS (MALDI-TOF, m/z) for $\text{C}_{67}\text{H}_{88}\text{N}_{17}\text{O}_{14}\text{S}^+ [\text{M}+\text{H}]^+$ (calc'd): 1386.81 (1386.64).

Synthesis of Trp-Tyr(Me)-Trp-Ser-Arg-Cys-Lys-Trp-Thr-Gly (5). 44% yield.

$R_{t(\text{Method A})} = 7.7$ min. $R_{t(\text{Method E})} = 22.7$ min. HRMS (MALDI-TOF, m/z) for $\text{C}_{67}\text{H}_{88}\text{N}_{17}\text{O}_{14}\text{S}^+ [\text{M}+\text{H}]^+$ (calc'd): 1386.74 (1386.64).

Synthesis of Trp(α -N-Me)-Tyr-Trp-Ser-Arg-Cys-Lys-Trp-Thr-Gly (6). 51% yield. $R_{t(\text{Method A})} = 7.6$ min. $R_{t(\text{Method E})} = 17.9$ min. HRMS (MALDI-TOF, m/z) for $\text{C}_{67}\text{H}_{88}\text{N}_{17}\text{O}_{14}\text{S}^+ [\text{M}+\text{H}]^+$ (calc'd): 1386.68 (1386.64).

Synthesis of Trp-Tyr-Trp-Ser-Arg-Cys-Lys-Trp-Thr(Me)-Gly (7). 33% yield.

$R_{t(\text{Method A})} = 7.8$ min. $R_{t(\text{Method E})} = 19.9$ min. HRMS (MALDI-TOF, m/z) for $\text{C}_{67}\text{H}_{88}\text{N}_{17}\text{O}_{14}\text{S}^+ [\text{M}+\text{H}]^+$ (calc'd): 1386.47 (1386.64).

Synthesis of Trp-Tyr-Trp-Ser(Me)-Arg-Cys-Lys-Trp-Thr-Gly (8). 26% yield.

$R_{t(\text{Method A})} = 7.7$ min. $R_{t(\text{Method E})} = 19.3$ min. HRMS (MALDI-TOF, m/z) for $\text{C}_{67}\text{H}_{88}\text{N}_{17}\text{O}_{14}\text{S}^+ [\text{M}+\text{H}]^+$ (calc'd): 1386.30 (1386.64).

Synthesis of Cys-[Tyr³-octreotate] (9). 23% yield. $R_{t(\text{Method B})} = 17.7$ min.

HRMS (MALDI-TOF, m/z) for $\text{C}_{52}\text{H}_{70}\text{N}_{11}\text{O}_{13}\text{S}_3^+ [\text{M}+\text{H}]^+$ (calc'd): 1152.46 (1152.43).

Synthesis of Cys(Me)-[Tyr³-octreotate] (10). 14% yield. $R_{t(\text{Method B})} = 17.9$ min. $R_{t(\text{Method E})} = 18.8$ min. HRMS (MALDI-TOF, m/z) for $\text{C}_{53}\text{H}_{72}\text{N}_{11}\text{O}_{13}\text{S}_3^+ [\text{M}+\text{H}]^+$ (calc'd): 1166.37 (1166.45).

Synthesis of Cys-[Cys(Me)², Tyr³, Cys(SH)⁷-octreotate] (11). 18% yield. $R_{t(\text{Method B})} = 18.3$ min. $R_{t(\text{Method E})} = 20.7$ min. HRMS (MALDI-TOF, m/z) for $\text{C}_{53}\text{H}_{74}\text{N}_{11}\text{O}_{13}\text{S}_3^+ [\text{M}+\text{H}]^+$ (calc'd): 1168.47 (1168.46).

Synthesis of Cys-[Cys(SH)², Tyr³, Cys(Me)⁷-octreotate] (12). 16% yield. $R_{t(\text{Method B})} = 18.1$ min. $R_{t(\text{Method E})} = 20.2$ min. HRMS (MALDI-TOF, m/z) for $\text{C}_{53}\text{H}_{74}\text{N}_{11}\text{O}_{13}\text{S}_3^+ [\text{M}+\text{H}]^+$ (calc'd): 1168.58 (1168.46).

Production of [¹¹C]methyl iodide

Carbon-11 was produced in the form of [¹¹C]CO₂ from a Cyclone® 18/9 cyclotron (IBA, Louvain-La-Neuve, Belgium) by irradiation of N₂ containing 0.5% O₂ using the $^{14}\text{N}(p,\alpha)^{11}\text{C}$ nuclear reaction with 18 MeV protons. [¹¹C]CH₃I was prepared by an automatic synthesis module (Mel Module, Scintomics, Fürstfeldbruck, Germany) via a series of reactions previously described by Marazano *et al.*^[44]. Briefly, [¹¹C]CO₂ was reduced via LiAlH₄ and subsequently converted to [¹¹C]CH₃I by treatment with hydroiodic acid under reflux conditions.

Production of [¹¹C]methyl triflate

[¹¹C]MeOTf was synthesized as previously reported by Jewett^[45]. Briefly, [¹¹C]MeOTf was generated by reaction of freshly produced [¹¹C]CH₃I with 50 mg of silver triflate (50 mg graphitized carbon solid support; glass column) in an online flow-through process at 175°C using a N₂ gas flow of 20 mL/min. The freshly produced [¹¹C]MeOTf in N₂ carrier gas was used immediately for subsequent radiomethylation reactions.

General procedure for the radiosynthesis of [¹¹C]GSMc (13)

To a freshly prepared solution of glutathione (300 µg, 0.98 µmol) and aqueous NaOH (9 µL, 0-4.0 M, 0-24 µmol, 0-24 eq) in DMSO (300 µL) was bubbled freshly produced [¹¹C]MeOTf (185 MBq – 1.11 GBq) in N₂ carrier gas at room temperature (20°C) for 20 s without stirring. The reaction was subsequently quenched with TFA (4.5 µL, 59 µmol) and analyzed by reverse-phase HPLC (Method C) for radiochemical yield determination.

General procedure for the radiosynthesis of Trp-Tyr-Trp-Ser-Arg-Cys(¹¹CH₃)-Lys-Trp-Thr-Gly ([¹¹C]2)

To a freshly prepared solution of **1** (300 µg, 0.22 µmol) and aqueous NaOH (2.1 µL, 0-4.0 M, 0-48 eq) in DMSO (300 µL) was bubbled freshly produced [¹¹C]MeOTf (185 MBq – 1.11 GBq) in N₂ carrier gas at room

temperature (20°C) for 20 s without stirring. The reaction was subsequently quenched with TFA (4.5 μ L, 59 μ mol) and analyzed by reverse-phase HPLC (Method D or E) for radiochemical yield determination and regioselectivity of methylation.

General procedure for the radiosynthesis of Cys($^{11}\text{CH}_3$)-[Tyr 3 -octreotate] ([^{11}C]10)

To a freshly prepared solution of **9** (500 μ g, 0.43 μ mol) and aqueous NaOH (7.2 μ L, 2.0 M, 40 eq) in DMSO (300 μ L) was bubbled freshly produced [^{11}C]MeOTf (370 MBq – 4.81 GBq) in N₂ carrier gas at room temperature (20°C) for 20 s without stirring. The reaction was subsequently quenched with TFA (4.5 μ L, 59 μ mol) and analyzed and/or purified by reverse-phase HPLC (Method D or E).

Preparative isolation of [^{11}C]10

The appropriate reverse-phase HPLC fraction corresponding to the desired radiolabeled peptide was added to sodium phosphate buffer (8 mL, 0.05 M, pH 7.4) and loaded on a Waters SepPak C-18 light cartridge (preconditioned by subsequent rinsing with ethanol (10 mL) and water (10 mL)). The trapped radiolabeled peptide was washed with water (5 mL), eluted from the cartridge with ethanol (300-500 μ L) and diluted with isotonic saline solution (3-5 mL). The overall synthesis time was 30 min with non-decay-corrected radiochemical yields

(RCYs) of $11 \pm 2\%$ ($n=3$). [^{11}C]**10** was isolated with a maximum radioactivity level of 41.8 MBq and a maximum specific activity of 96.3 MBq/ μmol starting from ca. 340 MBq of [^{11}C]MeOTf.

2.4 Results and discussion

*Radiosynthesis of [^{11}C]GSMe (**13**): effect of solvent and base*

In order to evaluate the feasibility of direct one-step ^{11}C -methylation of peptides, preliminary studies were conducted on GSH, a simple, inexpensive peptide whose nonradioactive side-chain methylated standard, *S*-methylglutathione (GSMe), was also available commercially. Radiolabeling was performed using the trifluoromethane sulfonate [^{11}C]MeOTf as methylating agent due to its well-documented route of production^[45] and availability as a routine intermediate in most PET cyclotron units for the synthesis of various radiopharmaceuticals. Reversed-phase HPLC (RP-HPLC) method development using an Aeris PEPTIDE column afforded Method C (Table VI) as a satisfactory eluent method for the separation of precursor glutathione (GSH, $R_t = 9.1$ min) and product *S*-methylglutathione (**13**, $R_t = 10.7$ min) (Figure 27).

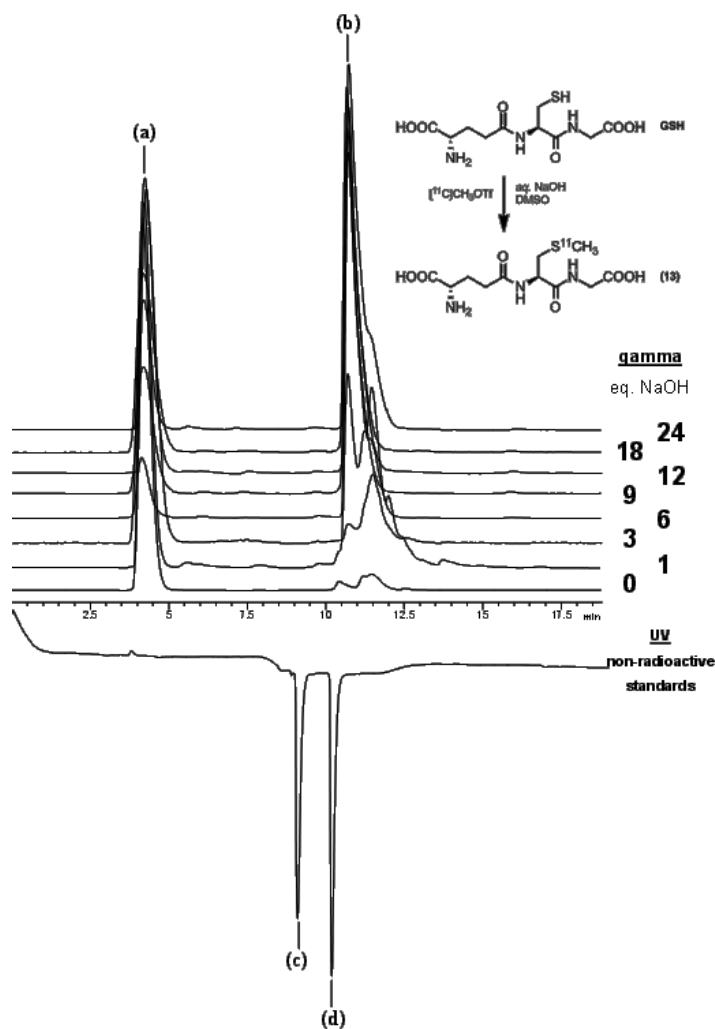


Figure 27: Radiosynthesis of $[^{11}\text{C}]\text{GSMe}$ (13): effect of solvent and base.

Above axis: Stacked radio-HPLC chromatograms (Method C) of the radiosynthesis of 13 under varying equivalents of NaOH. Reaction conditions: GSH (300 μg), 2.0 M NaOH (0-24 eq), DMSO (300 μL), $[^{11}\text{C}]\text{MeOTf}$ (185 MBq – 1.11 GBq), rt, 20 s. *Below axis:* HPLC chromatogram of GSH and GSMe (Method C). (a) $[^{11}\text{C}]\text{CH}_3\text{OH}$, $R_{\text{t(gamma)}} = 4.2$ min. (b) 13, $R_{\text{t(gamma)}} = 10.7$ min. (c) GSH, $R_{\text{t(210 nm)}} = 9.1$ min. (d) GSMe, $R_{\text{t(210 nm)}} = 10.2$ min. Detector delay $\Delta R_{\text{t}} \approx 0.58$ min at 0.8 mL/min.

Due to the individual setup of the radio-HPLC-UV in this study, there is a significant time delay between the integrated UV and discrete radioactivity detectors. As identification of radio-HPLC signals is commonly performed via coincident retention time with their respective nonradioactive carbon-12 standards, determination of this time delay is necessary. This flow-dependent time difference (ΔR_t) has been experimentally measured ($\Delta R_t \approx 0.58$ min at 0.8 mL/min; see *Chapter 7: Appendices – 7.1 Supplementary information*) and used throughout this study for the positive identification of radioactive products.

The labeling efficiency of [^{11}C]MeOTf towards GSH was evaluated in the presence of aqueous NaOH using the following three solvents: DMSO, methyl ethyl ketone (MEK), and acetonitrile (MeCN). Care was taken that all DMSO-containing peptide solutions were freshly prepared as DMSO-mediated oxidation of cysteine residues to cystine (disulfide bridge formation) has been documented to occur within hours^[181]. Reaction conditions using 18 equivalents of aqueous NaOH and DMSO as solvent (Figure 27) afforded appreciable radiochemical conversion of GSH to **13** ($65 \pm 4.5\%$ non-decay-corrected (*ndc*)), and was thereupon used as solvent of choice for optimization of other reaction parameters. Similar labeling conditions using MeCN afforded ca. 23% *ndc* radiochemical conversion. Interestingly, MEK, a solvent commonly employed in ^{11}C -radiomethylation reactions, afforded negligible yields of $<5\%$ *ndc*. Substitution of [^{11}C]MeOTf with [^{11}C]methyl iodide as radiomethylating agent

under the above labeling conditions provided no discernible yields of the desired labeled peptide.

When investigating the base-dependence of GSH labeling, at least 6 equivalents of aqueous NaOH were required for appreciable formation (75% *ndc* radiochemical conversion) of **13**. This slight excess of base, sufficient for the deprotonation of the two carboxylate and lone thiol moieties in GSH, resulted in a highly nucleophilic thiolate that rapidly reacted with [¹¹C]MeOTf, on the order of seconds to afford **13** as the major radiolabeled product. An excess of up to 24 equivalents of base does not appear to significantly alter the radiochemical yield (RCY) (Figure 27). Multiple minor peaks that appear in the radiochromatogram under lower equivalents of NaOH were not identified in the present study.

Synthesis of decapeptide 1 and its mono-methylated derivatives 2-8

In order to determine the regiospecificity of [¹¹C]MeOTf towards cysteine residues on peptides, a more complex decapeptide **1** containing various *N*-, *O*-, and *S*-nucleophilic amino acid side-chains (Figure 28) was synthesized by standard Fmoc solid-phase peptide synthesis (SPPS)^[180]. In addition, peptides **2-8** were synthesized as nonradioactive mono-methylated standards for HPLC analysis. These standards, which contain a single methylation group on the side-chain of the following residues: cysteine, lysine, arginine, tyrosine, threonine, and serine along with the *N*-terminal peptide backbone, were chosen as they could be

easily synthesized by SPPS standard protocols without additional steps. Following TFA cleavage from solid support, purification via semi-preparative HPLC, and lyophilization, peptides **1-8** were obtained in 6-51% yields (c.f. Materials and methods) with a purity of 95% or greater by quality control (HPLC Method E).

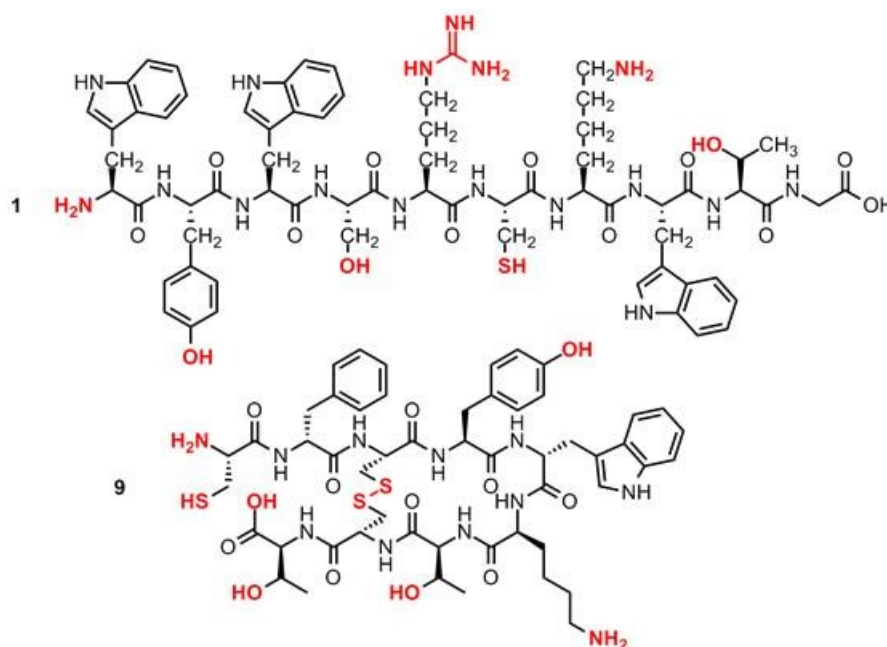


Figure 28: Nucleophilic sites on 1 and Cys-[Tyr³-octreotate] (9).

Above: Reactive sites (highlighted) on peptide **1** under investigation and amenable towards radiomethylation under neutral or basic conditions. *Below:* Potential reactive sites (highlighted) on peptide **9** amenable towards radiomethylation under neutral, basic, or reductive conditions.

Extensive RP-HPLC method development was required to provide an analytical separation of peptides **2-8** for the assessment of radiomethylation regioselectivity. As these peptides share an identical molecular mass and differ only in the site of attachment of the methyl group, initial efforts in method development using LiChrosorb- or Chromolith-based reversed-phase columns was unable to provide a satisfactory separation of these isomers. Only an Aeris PEPTIDE column (Method E) allowed an adequate separation of anticipated *S*-methylated product **2** from its isomers. Although this method was unable resolve peptides **3** and **4**, the separation of at least 0.5 min between peptide **2** and its isomers (Figure 29) proved sufficient for use in the subsequent radiosynthesis.

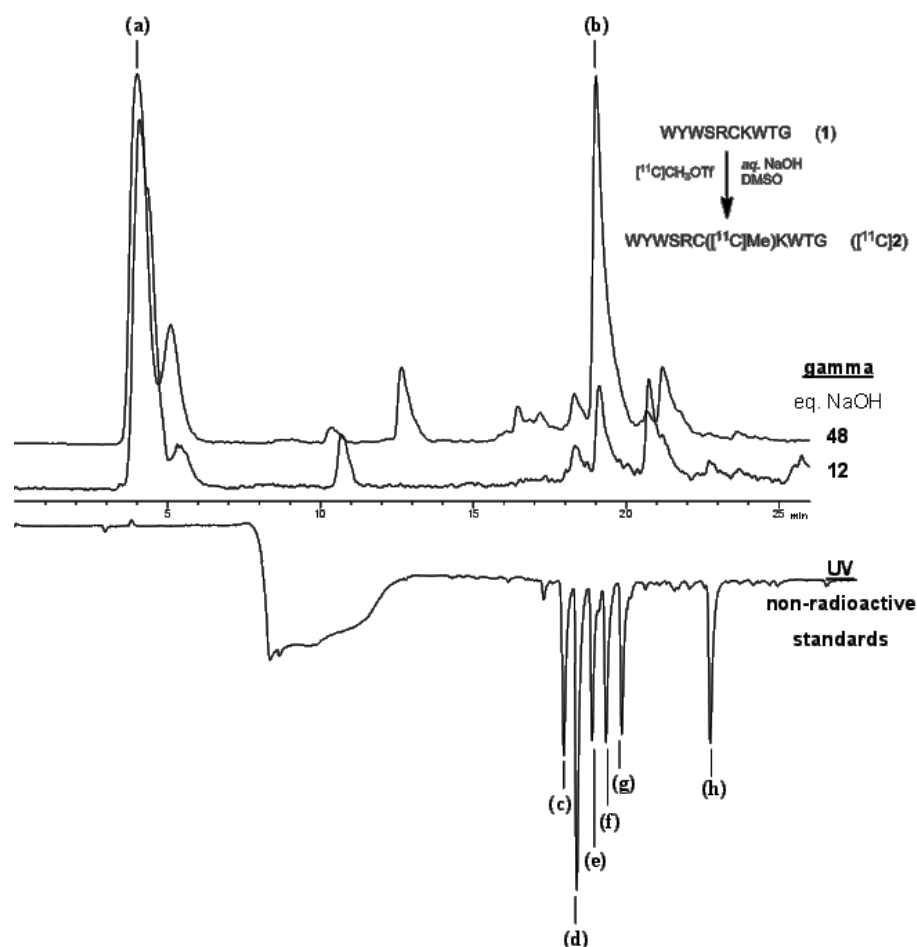


Figure 29: Radiosynthesis of $[^{11}\text{C}]\text{2}$: regioselectivity and effect of base.

Above axis: Stacked radio-HPLC chromatograms (Method E) of the radiosynthesis of $[^{11}\text{C}]\text{2}$ under varying equivalents of NaOH. Reaction conditions: **1** (300 μg), 2.0 M NaOH (12 or 48 eq), DMSO (300 μL), $[^{11}\text{C}]\text{MeOTf}$ (185 MBq – 1.11 GBq), rt, 20 s. *Below axis:* HPLC chromatogram of **2-8** (Method E). (a) $[^{11}\text{C}]\text{CH}_3\text{OH}$, $R_{\text{t(gamma)}} = 4.3$ min. (b) $[^{11}\text{C}]\text{2}$, $R_{\text{t(gamma)}} = 19.4$ min. (c) **6**, $R_{\text{t(210 nm)}} = 17.9$ min. (d) mixture of **3** and **4**, $R_{\text{t(210 nm)}} = 18.4$ min. (e) **2**, $R_{\text{t(210 nm)}} = 18.9$ min. (f) **8**, $R_{\text{t(210 nm)}} = 19.3$ min. (g) **7**, $R_{\text{t(210 nm)}} = 19.9$ min. (h) **5**, $R_{\text{t(210 nm)}} = 22.7$ min.

Detector delay $\Delta R_{\text{t}} \approx 0.58$ min at 0.8 mL/min.

Radiosynthesis of [¹¹C]2: regioselectivity and effect of base

Initial investigations into the base equivalent requirements in the [¹¹C]MeOTf labeling of hexa-protic peptide **1** proved difficult due to instability of this peptide sequence in the basic reaction conditions previously established for GSH labeling. As a result, major unidentified radioactive side-products were observed when pre-treating precursor **1** with any slight excess of NaOH over the course of minutes. In effect, yields of the desired radiopeptide were poor (<20% *ndc*) with long reaction times (>1 min) of the radiomethylating agent. Peptide radiomethylation using [¹¹C]MeOTf is a biphasic reaction which involves bubbling a gaseous mixture of [¹¹C]MeOTf in N₂ into the precursor solution. Efforts to minimize the decomposition of **1** and desired product [¹¹C]**2** include the following: (1) use of freshly-prepared and degassed peptide precursor solutions, (2) addition of aqueous NaOH in the desired quantities immediately prior to [¹¹C]MeOTf addition, (3) reduction in the time of [¹¹C]MeOTf/N₂ bubbling to 20 seconds, and (4) acidification via slight excess of TFA at the end of reaction to neutralize NaOH in solution. Efforts to replace aqueous NaOH with solid bases such as cesium carbonate (Cs₂CO₃) or freshly powdered NaOH have led to no successful labeling.

TFA was used as the choice of acid for quenching excess NaOH in the radiochemical reaction due to its lack of reactivity towards peptide **1**. Following TFA quench, composition of the crude radiomethylation reaction monitored via

radio-HPLC remains unchanged over the course of three hours (see *Chapter 7: Appendices – 7.1 Supplementary information*). The equivalents of acid added was also in lower quantities than reported elsewhere for DMSO/HCl-mediated oxidation of methionine to its sulfoxide^[182], a relevant concern due to a chemical similarity to the expected *S*-[¹¹C]methylcysteine residues of our current study.

Faced with the large volume of planned radiochemical reactions, analytical radio-HPLC acquisitions with long run times of 25 minutes (Method E), and the short half-life of carbon-11 ($t_{1/2} = 20.3$ min), RP-HPLC method development of a shorter acquisition run was necessary under the high-flow Chromolith Performance column (Method D), albeit at the cost of resolution between radiolabelled peptides. Nevertheless, all promising reaction conditions observed under Method D were further analyzed by Method E employing the better-resolving Aeris peptide column to fully assess regioselectivity.

Consistent with the radiosynthesis of **13**, appreciable incorporation yields for [¹¹C]**2** ($65 \pm 4.2\%$ *ndc*) were observed with at least 12 equivalents of NaOH (Figure 30) under Method D. However a closer analysis using Method E revealed inseparable, unidentified radioactive side-products that were diminished under 48 equivalents of base (Figure 29) with little effect on incorporation yields ($59 \pm 3.2\%$ *ndc*). The major radioactive HPLC peak under the latter conditions ($R_{t(\text{gamma})} = 19.4$ min) coincided with the retention time of the desired *S*-methylated product **2** ($R_{t(\text{gamma})} = 18.9$ min; detector delay $\Delta R_t \approx 0.58$ min), suggesting selective

methylation of the cysteine residues in the presence of other competing nucleophilic groups. Qualitatively, the amount of NaOH required appears high, which may suggest the presence of additional low molecular weight protic species, such as residual TFA, in the precursor sample. Radio-HPLC peaks adjacent to product **2** do not correspond to any available non-radioactive standards, therefore the percent selectivity towards cysteine (thiolate) radiomethylation cannot be determined in the current study.

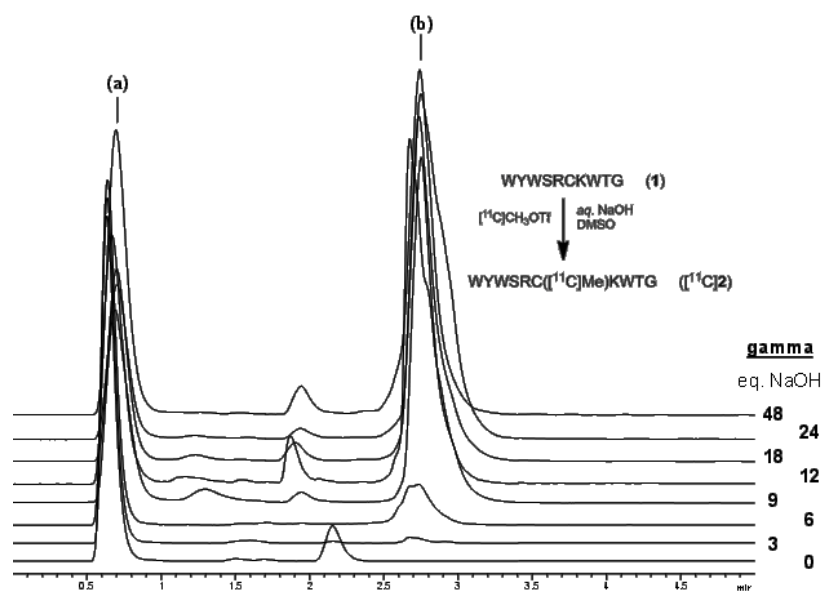


Figure 30: Radiosynthesis of $[^{11}\text{C}]\text{2}$: effect of base.

Stacked radio-HPLC chromatograms (Method D) of the radiosynthesis of $[^{11}\text{C}]\text{2}$ under varying equivalents of NaOH. Reaction conditions: **1** (300 μg), 2.0 M NaOH (0-48 eq), DMSO (300 μL), $[^{11}\text{C}]\text{MeOTf}$ (185 MBq – 1.11 GBq), rt, 20 s. (a) $[^{11}\text{C}]\text{CH}_3\text{OH}$, $R_{\text{t}(\text{gamma})} = 0.7$ min. (b) $[^{11}\text{C}]\text{2}$, $R_{\text{t}(\text{gamma})} = 2.8$ min.

Studies into lowering the quantity of peptide precursor **1** show a $64 \pm 3.5\%$ *ndc* radiochemical conversion to $[^{11}\text{C}]\mathbf{2}$ as a single radio-HPLC peak starting with 200 μg (0.15 μmol) of peptide **1** (Figure 31). Lower precursor quantities ($<200 \mu\text{g}$) show peak broadening suggesting the formation of multiple unidentified radiolabeled products.

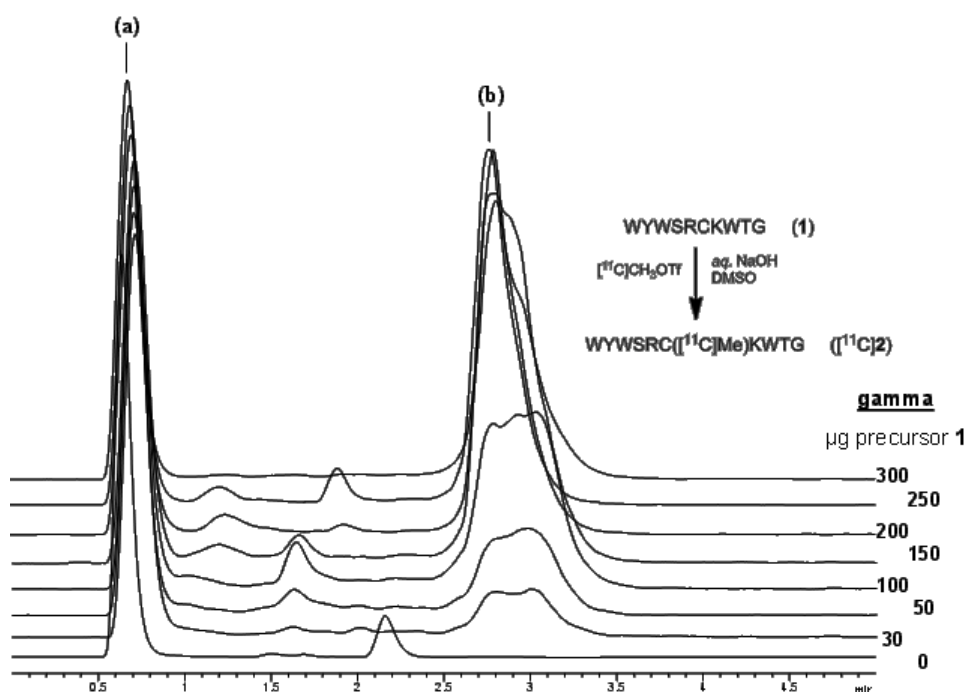


Figure 31: Radiosynthesis of $[^{11}\text{C}]\mathbf{2}$: effect of precursor quantity.

Stacked Radio-HPLC chromatograms (Method D) of the radiosynthesis of $[^{11}\text{C}]\mathbf{2}$ under varying amounts of peptide precursor **1**. Reaction conditions: **1** (0-300 μg), 2.0 M NaOH (48 eq), DMSO (300 μL), $[^{11}\text{C}]\text{MeOTf}$ (185 MBq – 1.11 GBq), rt, 20 s. (a) $[^{11}\text{C}]\text{CH}_3\text{OH}$, $R_{\text{t(gamma)}} = 0.7 \text{ min}$. (b) $[^{11}\text{C}]\mathbf{2}$, $R_{\text{t(gamma)}} = 2.8 \text{ min}$.

Synthesis of [^{11}C]Cys(Me)-[Tyr³-octreotate] (9) and its derivatives 10-12

Having determined the regioselectivity of [^{11}C]MeOTf radiomethylation towards cysteine residues, this labeling method was extended towards peptide **9**, an octreotate derivative containing an additional *N*-terminal cysteine residue. The choice for octreotate as model peptide in the current study is two-fold: (1) octreotate and octreotide (an octreotate derivative containing a reduced *C*-terminal threonine residue) are the most successful clinical imaging agents for visualization of somatostatin receptors on *ssr*-positive tumors and are currently widely studied as platform for various radioisotopes^[183-185], and (2) chemical modifications at the *N*-terminal end of octreotate do not significantly affect binding affinity of the tracer, but may allow for modulation of its pharmacokinetic properties^[186]. In particular, peptide **9** contains multiple functional groups that are nucleophilic under neutral or basic conditions (Figure 28). Peptide **9** was synthesized along with the nonradioactive standard **10** via SPPS as described above for peptides **1-8**. Of note, the *N*-terminal cysteine building block of **9** was appended following oxidative cyclization by thallium(III) trifluoroacetate to afford the desired oxidation state for the three cysteine residues of the peptide. Due to the cystine functionality of octreotate, derivatives **11** and **12** were synthesized as nonradioactive standards to verify for cystine reduction and subsequent *S*-methylation of these sites under radiolabeling reaction conditions. SPPS yields ranged from 14% to 23% following semi-preparative HPLC purification under

Method B. HPLC Method E proved sufficient to resolve peptides **9-12**, and was subsequently employed for analytical and preparative radio-HPLC in the radiosynthesis of [^{11}C]**10** (Figure 32).

*Preparative radiosynthesis of [^{11}C]**10***

Labeled octreotate derivative [^{11}C]**10** was synthesized upon treatment of penta-protic **9** with 40 equivalents of NaOH and [^{11}C]MeOTf. A ca. 52% *ndc* radiochemical conversion to the desired product was measured by analytical radio-HPLC without observable traces of [^{11}C]**11** or [^{11}C]**12** from reductive radiomethylation of cystine sites (Figure 32). Preparative workup involved injection of larger quantities (ca. 340 MBq) of the reaction medium to the same HPLC setup, collection of the fraction corresponding to the retention time of **10**, and immobilization of the radiolabeled peptide onto C-18 cartridge for removal of MeCN and TFA from HPLC eluent. Formulation of [^{11}C]**10** with ethanol (EtOH) and saline buffer afforded the final product in an overall synthesis time of 30 min and non-decay-corrected RCYs of $11 \pm 2\%$ ($n=3$). [^{11}C]**10** was isolated with a maximum radioactivity level of 41.8 MBq starting from ca. 340 MBq of [^{11}C]MeOTf. Specific activities (max. 96.3 MBq/ μmol) were unimpressive due to inability to separate starting precursor **9** ($R_{t(210\text{ nm})} = 18.0\text{ min}$) from [^{11}C]**10** ($R_{t(210\text{ nm})} = 18.8\text{ min}$) under the given HPLC method.

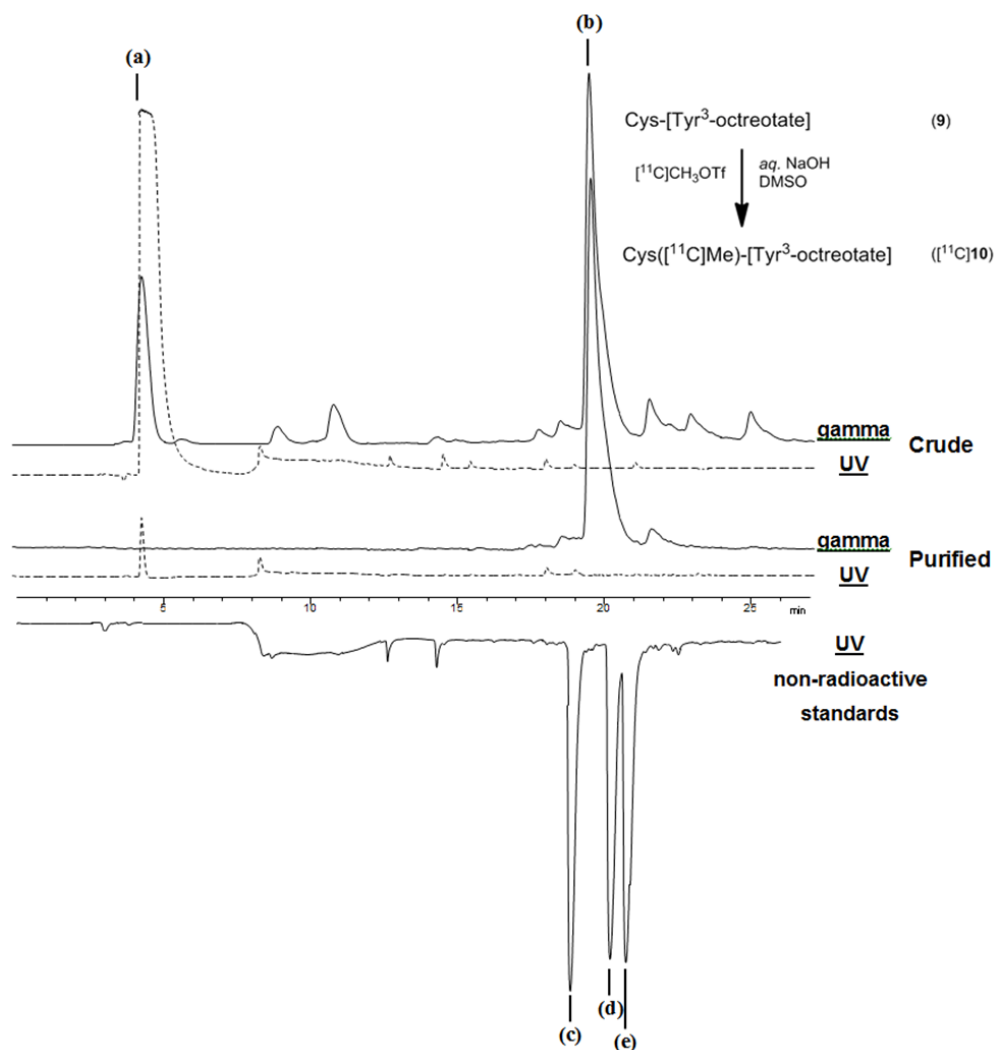


Figure 32: Radiosynthesis of $[^{11}\text{C}]\text{Cys}(\text{Me})\text{-[Tyr}^3\text{-octreotate]}$ ($[^{11}\text{C}]10$).

Above axis: HPLC radioactive and UV (210 nm) traces of the radiosynthesis of $[^{11}\text{C}]10$ (Method E). Reaction conditions: **9** (500 μg), 2.0 M NaOH (40 eq), DMSO (300 μL), $[^{11}\text{C}]\text{MeOTf}$ (370 MBq – 4.81 GBq), rt, 20 s. *Below axis:* HPLC chromatogram of **10-12** (Method E). (a) $[^{11}\text{C}]\text{CH}_3\text{OH}$, $R_{t(\text{gamma})} = 4.3$ min. (b) $[^{11}\text{C}]10$, $R_{t(\text{gamma})} = 19.4$ min. (c) **10**, $R_{t(210 \text{ nm})} = 18.8$ min. (d) **12**, $R_{t(210 \text{ nm})} = 20.2$ min. (e) **11**, $R_{t(210 \text{ nm})} = 20.7$ min. Detector delay $\Delta R_t \approx 0.58$ min at 0.8 mL/min.

2.5 Conclusion

We have successfully demonstrated the utility of [^{11}C]MeOTf towards the direct, one-step, and regioselective labeling of peptides at the side-chain of cysteine residues. In particular, the radiosyntheses of [^{11}C]GSMe (**13**) and Trp-Tyr-Trp-Ser-Arg-Cys([^{11}C]Me)-Lys-Trp-Thr-Gly ([^{11}C]2) were performed under ambient temperatures (20°C) and short reaction times, on the order of seconds. In addition, we extend this method towards the synthesis of [^{11}C]Cys(Me)-[Tyr³-octreotate] as demonstration of applicability for peptides of biological interest. This octreotate derivative was obtained in non-decay-corrected radiochemical yields of $11\pm 2\%$ ($n=3$) with a synthesis time of approx. 30 min. We are currently investigating solutions for addressing the following issues: (1) the stability of peptidic precursors and products under basic labeling conditions, (2) reduction of time of bubbling in the biphasic labeling reaction, e.g. via [^{11}C]MeOTf concentration, (3) reduction of the time of synthesis, especially in the radio-HPLC purification stage, (4) application of labeling method towards other peptides of oncological interest, such as bombesin, cholecystokinin/gastrin, neurotensin, and RGD (Arg-Gly-Asp)^[162], and finally, (5) the possibility of streamlining the radiochemical process via automation.

Chapter 3: Cationic SiFA compounds – RESULTS AND DISCUSSION

3.1 Introduction

The SiFA group (as described in *Chapter 1: Introduction – 1.5.4 Silicon fluorides*) show promise as alternative to existing ^{18}F -labeling strategies, particularly onto biomolecules such as peptides. However, poor pharmacokinetics of these compounds in PET studies demonstrate a need to address the lipophilic profile of the SiFA moiety^[156]. This chapter describes the design and synthesis of a new generation of hydrophilic SiFA building blocks that can be appended onto bioactive peptides. Detailed experimental procedures are described in *Chapter 4: Experimental Section*.

3.2 Small-molecule synthesis

Several functionalization routes have been considered for the synthesis of SiFA synthons (Figure 33) of reduced lipophilicity. Generally, the introduction of strongly polar functional groups, such as alcohols, amines, carboxylic acids, sulphonic acids, and phosphorus oxyacids will contribute to an increased hydrophilicity of an analogue^[187]. However their incorporation often demands the use of protecting groups and complex orthogonal deprotection strategies.

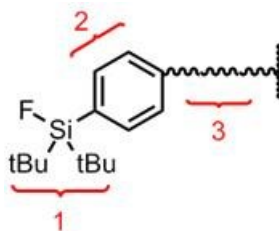


Figure 33: Structural analysis of SiFA.

A brief analysis of the SiFA synthon reveals three general sites of polar group incorporation: (1) the bulky *tert*-butyl groups, (2) the aryl ring, and (3) the linker region where the SiFA moiety is appended onto a target biomolecule (Figure 33). It is important to note the *tert*-butyl groups and aryl moiety are shown to be essential for *in vivo* hydrolytic stability of the SiFA synthon^[146], and therefore cannot be removed from the molecule.

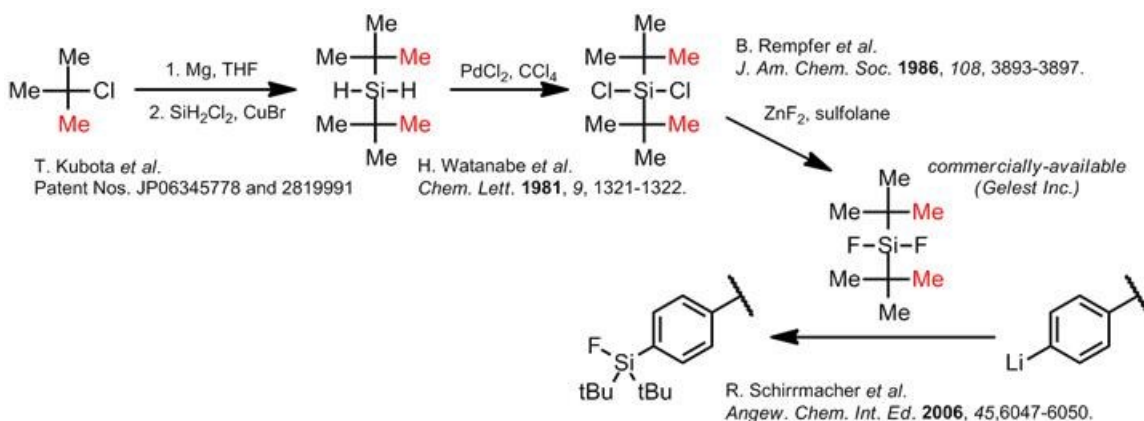


Figure 34: A potential functionalization of SiFA *tert*-butyl groups.

Highlighted is a potential site of chemical modification for the introduction of hydrophilic functional groups.

Functionalization of the *tert*-butyl groups was dismissed because the synthesis is anticipated to be highly involved. The di-*tert*-butyl silyl fluoride moiety ($\text{tBu}_2\text{SiF}\sim$) is incorporated at very early stages in the synthesis of SiFA building blocks from commercially-available di-*tert*-butylsilyldifluoride (tBu_2SiF_2) under harsh metalation/addition conditions with *tert*-butyllithium. Analogues of tBu_2SiF_2 bearing protected polar functionalities would have to be synthesized from tertiary alkyl chlorides (Figure 34). Briefly, the desired modified tertiary alkyl chloride is converted to the corresponding Grignard reagent and immediately added onto dichlorosilane in the appropriate stoichiometry (2:1) to afford a modified di-*tert*-butylsilane^[188]. Substitution of the thus formed silane to the silyl dichloride^[189] and then, the silyl fluoride^[190] affords an appropriate building block for SiFA moiety formation.

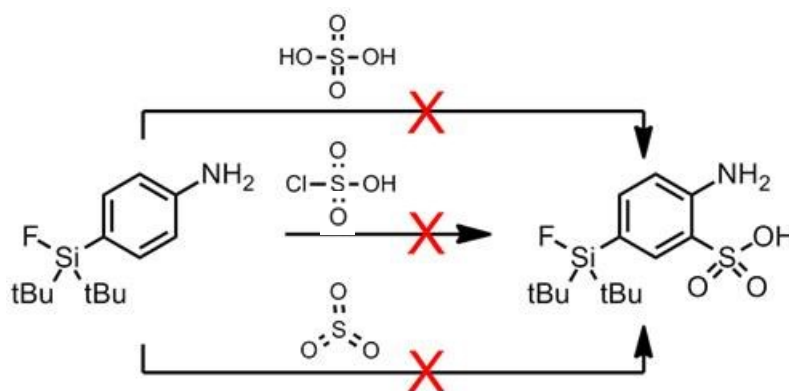


Figure 35: Attempted sulfonylation of SiFA-aniline.

Aryl ring modifications are chemically feasible approaches to the introduction of sulphonic acids, provided the aryl ring is sufficiently electron-rich (typically bearing a hydroxyl (-OH) or an amino (-NH₂) functional group). However, all efforts for the sulfonylation of SiFA-aniline^[106] (Figure 35) under classical sulfonylation conditions (e.g. sulfuric acid, chlorosulfonic acid, or sulfur trioxide) have led to product decomposition^[191]. Given these results, this approach was not explored further.

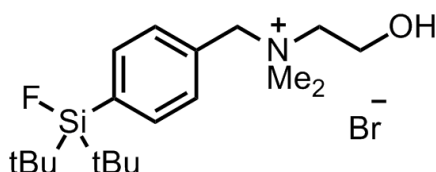


Figure 36: Structure of SiFAN⁺Br⁻.

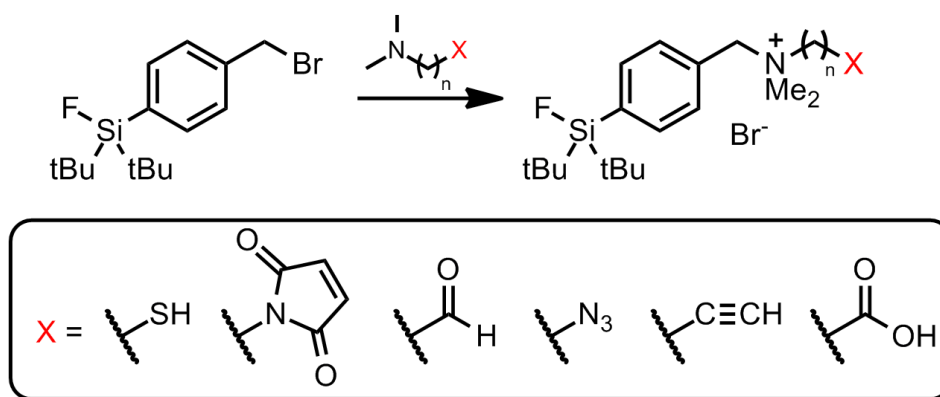
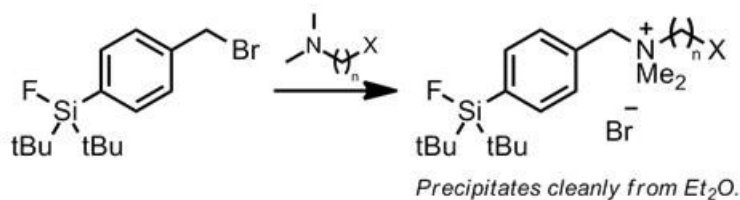


Figure 37: Synthetic objective for cationic SiFA compounds.

Modification on the SiFA linker region is a very attractive alternative as the desired polar functional groups can be introduced in the late stages of synthesis. Inspired by the hydrophilic properties of SiFAN⁺Br⁻ as a charged proof-of-principle SiFA molecule (Figure 36), and by the ease of synthesis of quaternary ammonium salts by simple quaternization of tertiary amines^[192], we report here the synthesis of charged SiFA compounds bearing functional groups amenable to bioconjugation. The functional groups under investigation include thiol and maleimide (thiol-maleimide coupling), aldehyde (aldehyde-aminooxy coupling), azide and alkyne (Huisgen 1,3-dipolar cycloaddition), and carboxylic acid (amide bond formation) (Figure 37).

a) Quaternization with unprotected tertiary amine.



b) Quaternization with protected tertiary amine.

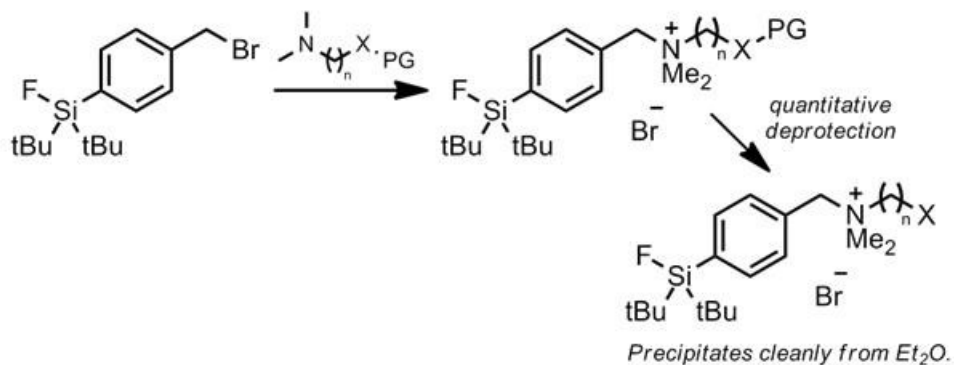


Figure 38: Planned isolation scheme for quaternary ammonium salts.

Due to the insolubility of quaternary ammonium salts in diethylether, these compounds can be isolated simply and cleanly from the crude quaternization reaction, as the alkyl halide and tertiary amine starting materials are generally soluble in the same medium. For reaction schemes involving an end-stage deprotection of a quaternary ammonium salt, the deprotection step must ensure quantitative conversion of the starting salt for a high purity of the desired final compound (Figure 38).

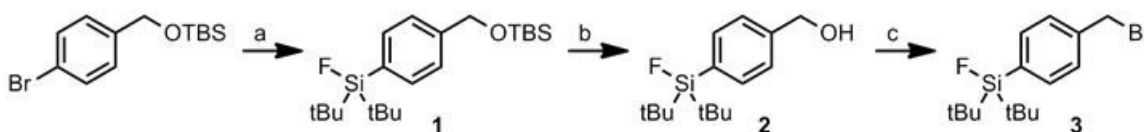


Figure 39: Synthesis of SiFA-benzyl-bromide (3). (a) 1. $t\text{BuLi}$, Et_2O , -78°C , 15 min; 2. $t\text{Bu}_2\text{SiF}_2$, Et_2O , $-70^\circ\text{C} \rightarrow \text{rt}$, overnight; (b) HCl , MeOH , rt , overnight, **76%** (2 steps); (c) CBr_4 , PPh_3 , CH_2Cl_2 , rt , overnight, **88%**.

Synthesis of benzyl bromide **3** has been previously described^[148,157], but we report here an improved synthetic protocol affording greater yields of **3** (Figure 39). Lithium-bromide exchange on TBS-protected 4-bromobenzyl alcohol with *tert*-butyllithium afforded the corresponding aryllithium *in situ* which was subsequently treated with $t\text{Bu}_2\text{SiF}_2$ to form SiFA compound **1**. We have demonstrated no significant order-of-addition effects between the aryllithium intermediate and $t\text{Bu}_2\text{SiF}_2$, obviating the reported need for anhydrous cannulation

techniques. **1** was subsequently deprotected by acid to afford alcohol **2**. Bromination of **2** afforded benzyl bromide **3** as a white solid in yields greater than previously reported (88% versus 80%)^[157]. Benzyl bromide **3** is the common starting material for quaternization reactions with tertiary amines to produce the desired quaternary ammonium salts.

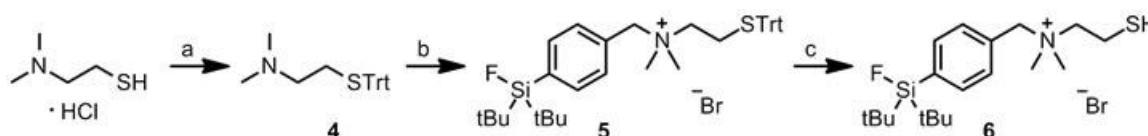


Figure 40: Synthesis of SiFA⁺-SH (6**).** (a) Ph₃CCl, CH₂Cl₂, DMF, rt, overnight, 86%; (b) **3**, Et₂O, 50°C, overnight, 65%; (c) TFA, Et₃SiH, CH₂Cl₂, rt, 4 hr, 56%.

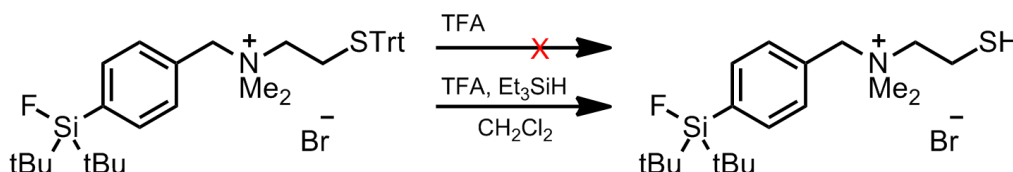


Figure 41: Thiol deprotection fails in the absence of a cationic quencher.

The synthesis of cationic SiFA⁺-SH (**6**) requires protection of the thiol functionality for proper regioselectivity during the quaternization step. 2-(dimethylamino)ethanethiol was *S*-tritylated with trityl chloride (triphenylmethylchloride) to afford tertiary amine **4** which was subsequently quaternized with benzyl bromide **3** to afford trityl-protected cationic SiFA **5**

(Figure 40). Classical deprotection by treatment with neat trifluoroacetic acid (TFA)^[193] resulted in no observable reaction (Figure 41). Instead, treatment of **5** with TFA and triethylsilane (a trityl cation scavenger) in dichloromethane cleanly afforded thiol **6**, isolated by precipitation in diethylether. Thiol deprotection was conducted under an atmosphere of argon to minimize undesired oxidation side-products.

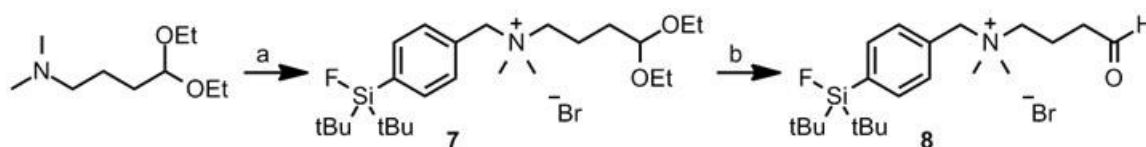


Figure 42: Synthesis of SiFA⁺-CHO (8**).** (a) **3**, CH₂Cl₂, rt, overnight, quantitative; (b) TFA, H₂O, rt, 30 min.

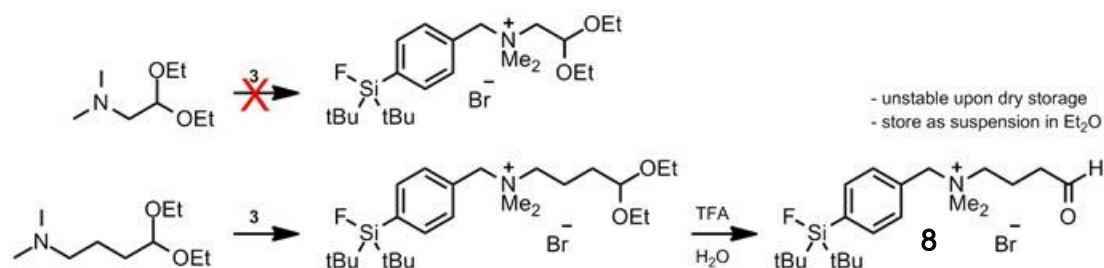


Figure 43: Attempts at synthesis of SiFA⁺-CHO (8**).**

The synthesis of cationic SiFA⁺-CHO (**8**) proceeded via the quaternization of benzyl bromide **3** with an acetal-protected tertiary amine (Figure 42). Two acetal-protected tertiary amines are commercially available: 2-

(dimethylamino)acetaldehyde diethyl acetal and 4-(dimethylamino)butanal diethyl acetal (Figure 43). Only the latter acetal provided the corresponding quaternary ammonium salt **7** as a stable, white solid. Classical deprotection of the acetal with TFA and water^[194] afforded the desired cationic aldehyde **8**. However, upon dry storage, **8** has been observed to rapidly decompose. Successful attempts at long-term storage (~6 months) of **8** involve storage as a suspension in diethylether at -20°C. Centrifugation of the stored suspension will afford **8** as a wet pellet that can be used immediately for chemoselective oxime synthesis.

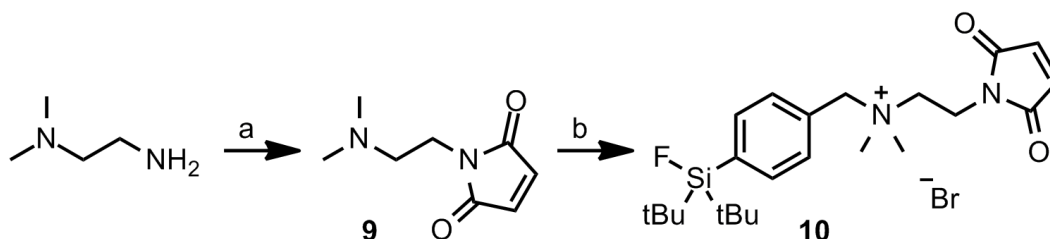


Figure 44: Synthesis of SiFA⁺-MI (10**).** (a) maleic anhydride, Na₂SO₄, PhMe, reflux, overnight, 20%; (b) **3**, CH₂Cl₂, rt, overnight, 66%.

Synthesis of cationic SiFA⁺-MI (**10**) proceeded via condensation of *N,N*-dimethylethylenediamine with maleic anhydride under dehydration conditions (anhydrous Na₂SO₄) and heating to afford maleimide **9** which was subsequently quaternized with **3** to afford the desired product (66% yield) (Figure 44).

Synthesis of cationic SiFA⁺-N₃ (**12**) proceeded via azide substitution of the nitrogen mustard 2-chloro-*N,N*-dimethylamine with sodium azide to afford azide **11** which was subsequently quaternized with **3** to afford the desired product (99% yield) (Figure 45).

Cationic SiFA⁺-C≡CH (**13**) was cleanly obtained from quaternization of *N,N*-dimethylprop-2-yn-1-amine with benzyl bromide **3** (96% yield) (Figure 46).

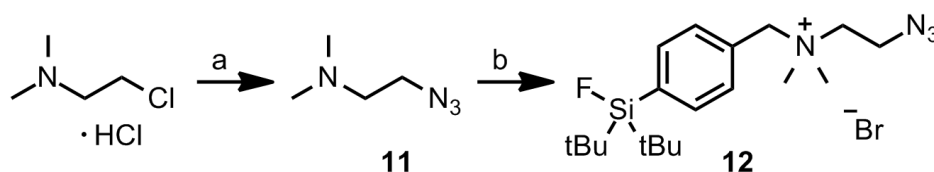


Figure 45: Synthesis of SiFA⁺-N₃ (12**).** (a) NaN₃, H₂O, 80°C, overnight, **63%**; (b) **3**, CH₂Cl₂, rt, overnight, **99%**.

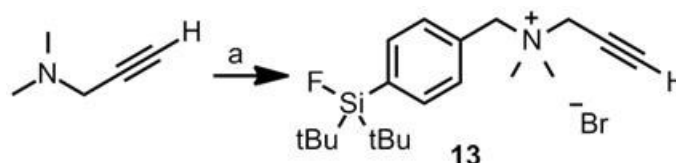


Figure 46: Synthesis of SiFA⁺-C≡CH (13**).** (a) **3**, CH₂Cl₂, rt, overnight, **96%**.

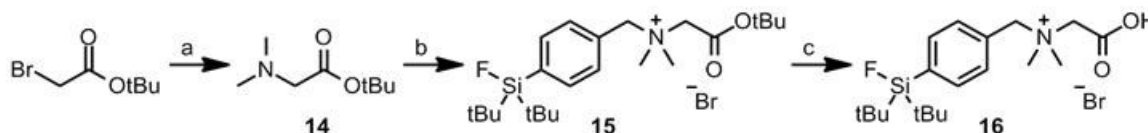


Figure 47: Synthesis of SiFA⁺-CO₂H (16**).** (a) Me₂NH, rt, overnight, **99%**; (b) CH₂Cl₂, rt, overnight, **85%**; (c) TFA, Et₃SiH, H₂O, rt, 4 hr, **86%**.

Tertiary amine **14** was synthesized from *tert*-butyl bromoacetate and *in situ* generated dimethylamine. Treatment of **14** with **3** afforded the *tert*-butyl ester **15** as the quaternized product which was subsequently deprotected under classical cleavage conditions with cation scavenger^[195] (TFA, H₂O, triisopropylsilane) to afford cationic SiFA⁺-CO₂H as the desired acid (**16**) (86% yield) (Figure 47).

3.3 Peptide synthesis

The choice for octreotate as a model peptide in the current study is two-fold: (1) octreotate and octreotide (an octreotate derivative with a reduced *C*-terminal threonine) are the most successful clinical imaging agents for visualization of somatostatin receptors on *ss**t*-positive tumors^[183-185], and (2) chemical modifications at the *N*-terminal of octreotate result in a low effect on the receptor affinity but allow for the modulation of its pharmacokinetic properties^[186] (Figure 48). The latter provides a labeling site highly tolerant of hydrophilic and lipophilic modifications, and is therefore ideal for the study of SiFA groups of variable lipophilicities. In addition, the nature and length of the *N*-terminal spacer does not compromise the binding affinity of modified octreotide, but its hydrophilicity and charge greatly impact its pharmacokinetic profile^[196].

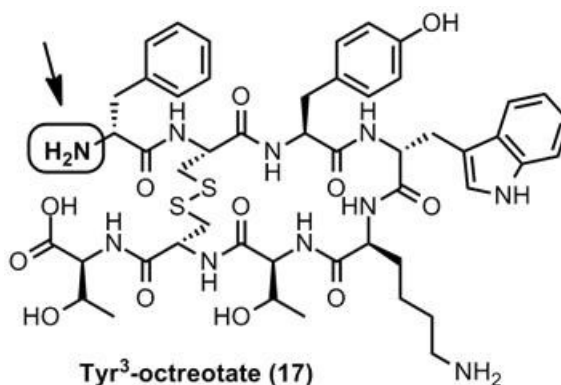


Figure 48: Tyr³-octreotate (17) and site of modification.

The synthesis of octreotate derivatives containing groups amenable for bioconjugation started with Tyr³-octreotate obtained from solid-phase peptide synthesis^[180] on a Fmoc-Thr(tBu)-Wang resin. The Tyr³-octreotate (TATE) standard (17)^[197] was subsequently cleaved from the resin and purified by reversed-phase HPLC. All other derivatives were further functionalized on resin prior to cleavage and purification. The aminooxy derivatives AO-TATE (18) and AO-PEG-TATE (19) were functionalized with aminooxyacetic acid with or without 8-amino-3,6-dioxaoctanoic acid as a polyethylene glycol (PEG) linker. Maleimide derivative MI-TATE (20) was functionalized with *N*-maleoyl- β -alanine. The alkyne derivatives HC \equiv C-TATE (21) and HC \equiv C-PEG-TATE (22) were synthesized from 5-hexynoic acid with or without 8-amino-3,6-dioxaoctanoic acid as a PEG linker. Azide-containing N₃-TATE (23) and N₃-PEG-TATE (24) were functionalized with 6-azidohexanoic acid with or without 8-amino-3,6-dioxaoctanoic acid as a PEG

linker. The above described peptide coupling reactions have reported yields of 20-45% (c.f. *Chapter 4: Experimental Section*).

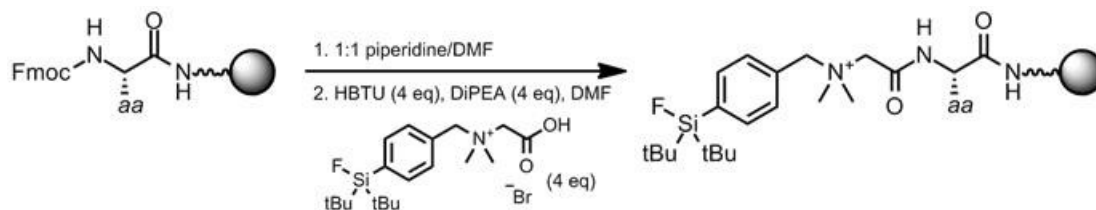


Figure 49: Introduction of the SiFA moiety via SPPS.

Direct peptide coupling of SiFA⁺-CO₂H (**16**) as a *N*-terminal cap onto resin-bound TATE cleanly afforded SiFA⁺-C(O)NH-TATE (**25**) in adequate yields (34% overall) using standard solid-phase peptide synthesis reaction conditions (Figure 49). However, the addition of a PEG₂ linker to form SiFA⁺-C(O)NH-PEG₂-TATE (**26**) afforded the desired peptide in poor yields (8%). These reactions show the feasibility of **16** in peptide synthesis on solid support, including tolerance to TFA cleavage conditions, but low yields reported in the synthesis of **26** may suggest a dependence of the yield on the nature of the amine-bearing reactant.

Chemoselective oxime ligation between aldehydes SiFA-A^[146,147] and SiFA⁺-CHO (**8**) under coupling conditions adapted from Poethko *et al.*^[104] and Wängler *et al.*^[156] afforded SiFA-TATE (**27**), SiFA⁺-aldehyde-AO-TATE (**28**), and SiFA⁺-aldehyde-AO-PEG-TATE (**29**) in good yields (48-64%) (Figure 50).

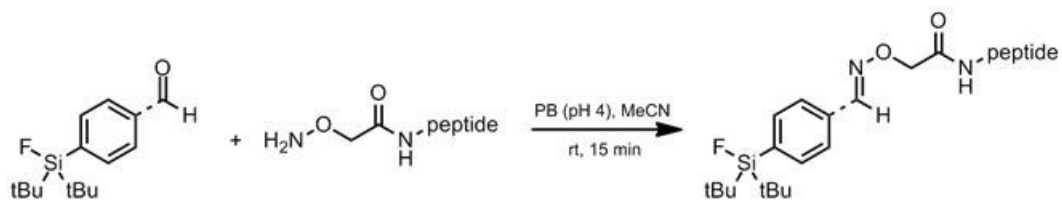


Figure 50: Chemoselective oxime ligation.

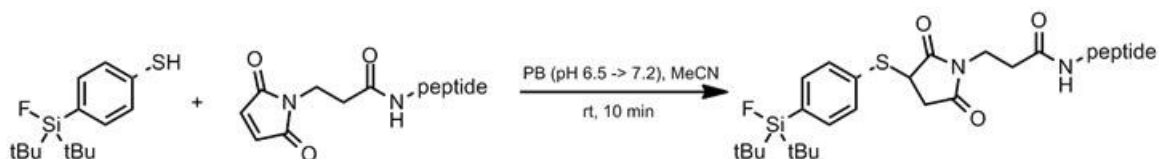


Figure 51: Thiol-maleimide coupling reaction.

Thiol-maleimide coupling between thiolated SiFA compounds (SiFA-SH^[149], SiFA⁺-SH (**6**)) and maleimide-containing MI-TATE (**20**) proceeded in good yields (43-85%) of **30** and **31**, respectively (Figure 51). The reactions were performed over a narrow pH range (6.5 – 7.5) to allow for the thiol maleimide selectivity. High pH values would promote an undesired amino-maleimide coupling while low pH values would catalyze maleimide hydrolysis^[198].

Due to the presence of a disulfide bridge in Tyr³-octreotate and its derivatives, appending SiFA building blocks via copper-catalyzed Huisgen 1,3-dipolar cycloadditions require non-reducing or very mild reducing conditions. Classically, Cu(I) as the active catalyst is produced by the *in situ* reduction of copper(II) salts with an excess of ascorbic acid as the stoichiometric reductant^[199]. The comproportionation of metallic copper and copper(II) salt has

been shown to generate Cu(I) at longer reaction times, and is suitable for reactions involving biomolecules^[200]. In addition, these conditions have been previously used in the conjugation of octreotate derivatives^[201,202]. During workup, soluble copper(II) salts can be removed with ease as the insoluble copper(II) sulfide. The ligation of azide-containing SiFA **12** and alkyne-functionalized peptides **21** and **22** afforded the desired **32** and **33**, respectively. Likewise, coupling of alkyne **13** with azidopeptides **23** and **24** afforded **34** and **35**, respectively. Yields for this class of reaction range from 19 to 25%. However, a significant quantity of hydrolyzed SiFA-peptide product (Si-F → Si-OH) has been observed during the purification step by HPLC, suggesting that the SiFA moiety may be somewhat hydrolytically unstable under the copper comproportionation reaction or workup conditions (Figure 52).

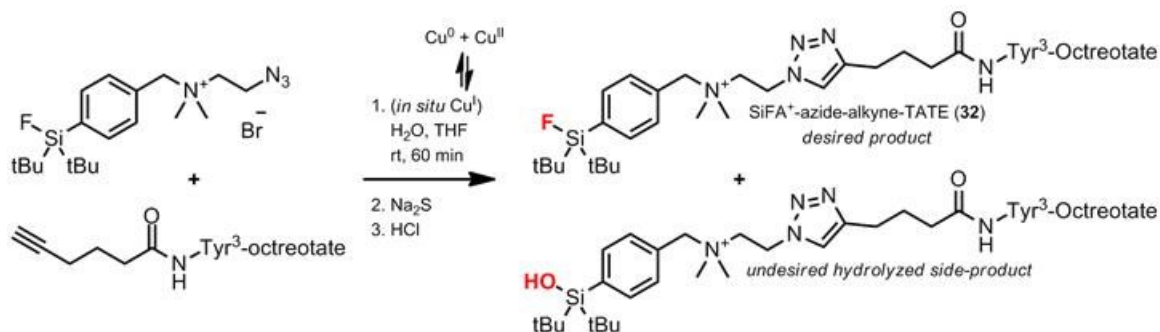


Figure 52: Click chemistry via comproportionation of Cu(0) and Cu(II).

Synthesis of SiFA⁺-azide-alkyne-TATE (**32**) as example, with formation of undesired side-product from hydrolysis.

3.4 Radiochemistry

The following peptides: SiFA⁺-C(O)NH-TATE (**25**), SiFA⁺-C(O)NH-PEG₂-TATE (**26**), SiFA-TATE (**27**), SiFA⁺-aldehyde-AO-TATE (**28**), SiFA⁺-aldehyde-AO-PEG-TATE (**29**), and SiFA⁺-thiol-MI-TATE (**31**) were brought forward for radiolabeling procedures. Due to the aforementioned synthetic yield issues in copper-catalyzed Huisgen 1,3-dipolar cycloaddition between functionalized SiFA and TATE fragments, the following peptides, SiFA⁺-azide-alkyne-TATE (**32**), SiFA⁺-azide-alkyne-PEG-TATE (**33**), SiFA⁺-alkyne-azide-TATE (**34**), and SiFA⁺-alkyne-azide-PEG-TATE (**35**) were not considered for further labeling or lipophilicity determination.

Treatment of SiFA-containing peptides with anhydrous [¹⁸F]fluoride was performed under conditions similar to those previously described by our group^[156]. Briefly, a dried solution of [¹⁸F]F⁻/Kryptofix 2.2.2/K⁺ complex in acetonitrile was added to a solution of the desired peptide. Although the reaction was left at 0°C for 5 min, the SiFA moiety was shown in small molecules to provide for ¹⁸F-¹⁹F exchange at temperatures as low as -20°C with completion of reaction in the order of seconds^[203]. A reaction temperature of 0°C was chosen to minimize potential side-reactions which may occur on the peptidic fragment at elevated temperatures. Even lower temperatures were not attempted due to anticipated condensation of atmospheric water into the reaction vial at sub-freezing temperatures, which would effectively halt the exchange reaction.

The completed reaction was verified by reversed-phase HPLC to confirm incorporation of [^{18}F]fluoride into the SiFA-functionalized peptides. In all cases, use of between 2.4 mCi and 13.8 mCi of starting [^{18}F]fluoride, provides incorporation yields exceeding 85% (Figure 53).

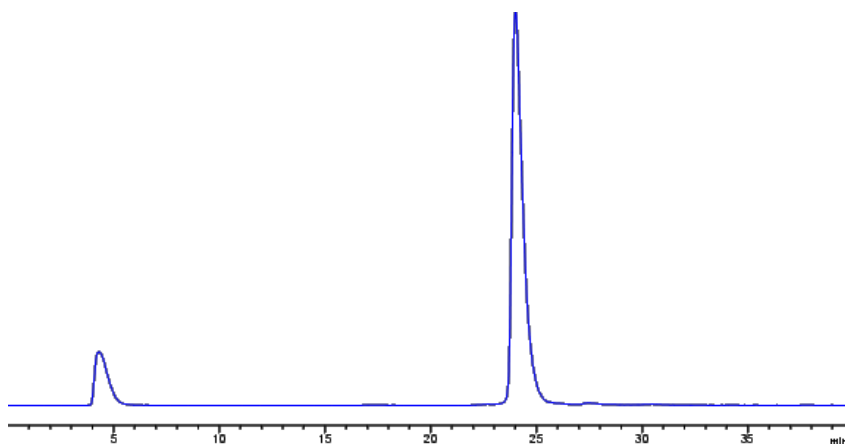


Figure 53: Sample HPLC chromatogram for ^{18}F -labeling of peptide 26.

Radiochemical conversion to [^{18}F]26 ($R_t = 24$ min) is approx. 86% with remainder as unreacted [^{18}F]fluoride ($R_t = 4$ min).

For peptide isolation and removal of MeCN, the completed reaction was quenched and loaded onto a cartridge containing C-18 material as the stationary phase, as previously described^[156] (Figure 54). The C-18 immobilized peptide was eluted with octanol and the peptide/octanol solution was subsequently used for lipophilicity determination by the shake-flask method. The choice of octanol as eluent is rather unusual, and is explained in the following section.

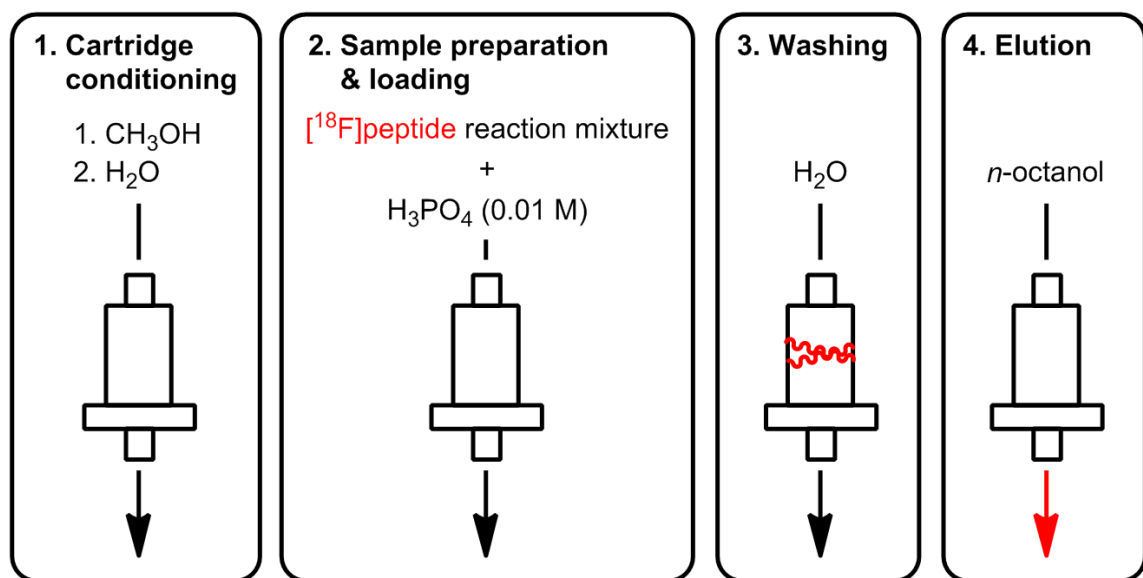


Figure 54: Workup and isolation of radiolabeled cationic SiFA peptides.

Localization of the radiolabeled peptide is highlighted.

3.5 Lipophilicity

Lipophilicity is a markedly important parameter in drug design. The correlation between lipophilicity and drug delivery^[204], particularly blood-brain barrier penetration, plays a crucial role in the development of molecular imaging agents for PET and SPECT (single-photon emission computed tomography^[205].

In recent years, attention has focused on the lipophilicity of peptides and their derivatives for biodistribution and metabolism assessment. In addition, better understanding of peptide lipophilicity may allow for improved methods for their chromatographic separation and purification^[206].

Lipophilicity is commonly expressed as $\log P_{ow}$, the logarithm of the *n*-octanol/water coefficient, and experimentally determined by the shake-flask method^[207]. As the name implies, the shake-flask method consists of partition of an analyte in a mixture of equal parts octanol and water, followed by measurement of ratio of analyte dissolved in octanol to water (octanol/water coefficient). For ionisable substances, the distribution coefficient $\log D_{(pH)}$ is a more useful value where the aqueous phase is buffered to a desired pH. This pH level is commonly set to 7.4, the physiological pH of blood serum, for analytes destined for biological studies.

For the current study, lipophilicity of SiFA-derivatized peptides was assessed at the level of ^{18}F -isotopically-radiolabeled peptides by gamma-counting. Due to its very low radio-detection limits, this method allows for $\log D_{7.4}$ determination from microgram-quantities of starting peptide, as opposed to milligram-quantities for classical measurement by spectrophotometry or physical isolation and weighing.

Due to the low quantities of starting $[^{18}\text{F}]$ fluoride in the ^{18}F - ^{19}F isotopic exchange on SiFA-derivatized peptides, isolation of the labeled peptide as described elsewhere^[156] by elution of the C-18 immobilized peptide with ethanol followed by aliquotization into an octanol/buffer partition was not deemed feasible. The quantity of radioactivity would fall short of the detection limit of available gamma-counters with aliquotization of this ethanol/ $[^{18}\text{F}]$ peptide fraction.

Concentration by evaporation of the ethanol was considered but not adopted due to the difficulty and increased times required for complete ethanol removal at ambient temperatures.

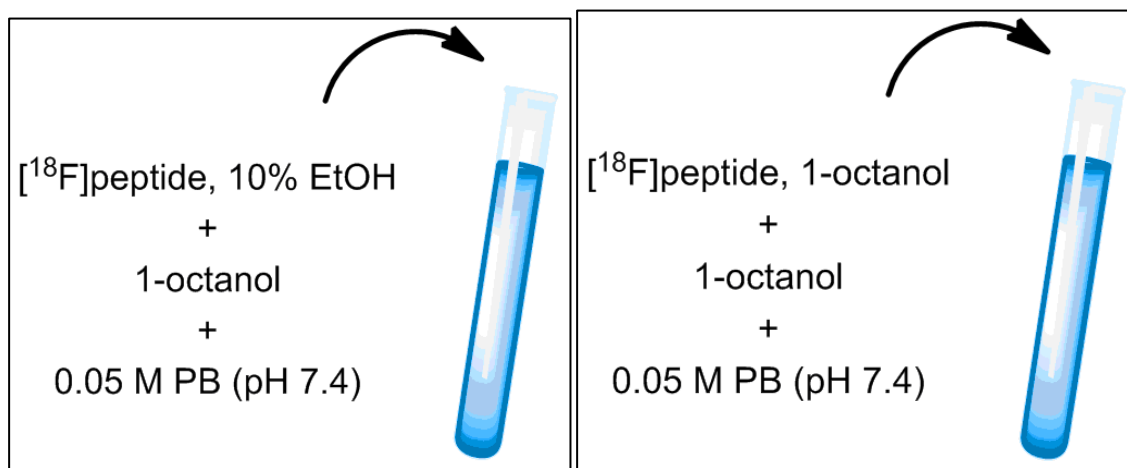


Figure 55: Radiolabeled peptide isolation for shake-flask method.

(*left*) Sample preparation by aliquotization of cartridge-eluted $[^{18}\text{F}]$ peptide/ethanol fraction. (*right*) $[^{18}\text{F}]$ peptide/octanol fraction by direct cartridge-elution with *n*-octanol for use directly in shake-flask method.

Another solution that was adopted was elution using 1-octanol as solvent (Figure 54). As lipophilicity determination by the shake-flask method classically employs this solvent as the organic phase, the resulting octanol/ $[^{18}\text{F}]$ peptide fraction can be used directly without further manipulation or modification (Figure 55). Despite experimentally low elution efficiencies (approx. 50% for all peptides examined) likely due to the high viscosity of octanol (viscosity $\eta(\text{OcOH}) = 6.24$

mPa·s^[208] at 303.15 K; η (EtOH) = 0.97 mPa·s^[209] at 303.15 K) (i.e. difficult passage of solvent through a small-bore cartridge and poor wetting of the C-18 solid-phase material with the given solvent), the amount of radioactivity in the isolated fraction was sufficient for at least one lipophilicity determination by shake-flask method per radiolabeling reaction.

Table VII: Measured logD_{7.4} and calculated ClogP values.

ClogP values were calculated from the corresponding cationic SiFA non-peptidic *N*-methanamide for qualitative comparison (see Figure 57).

Peptide	#	logD _{7.4} ⁽¹⁾	ClogP ⁽²⁾	$\Delta(\log D_{7.4} - \text{ClogP})$
SiFA ⁺ -C(O)NH-TATE	25	2.19 ± 0.15	0.20	1.99
SiFA ⁺ -C(O)NH-PEG ₂ -TATE	26	0.92 ± 0.13	N/A	N/A
SiFA-TATE	27	2.68 ± 0.16	3.47	-0.79
SiFA ⁺ -aldehyde-AO-TATE	28	1.20 ± 0.09	0.89	0.31
SiFA ⁺ -aldehyde-AO-PEG-TATE	29	0.43 ± 0.04	0.20	0.23
SiFA ⁺ -thiol-MI-TATE	31	1.33 ± 0.14	1.52	-0.19

⁽¹⁾ *n* = 3, values are mean ± SD.

⁽²⁾ ClogP values obtained from ChemBioDraw Ultra (PerkinElmer, Inc., Waltham, MA, USA).

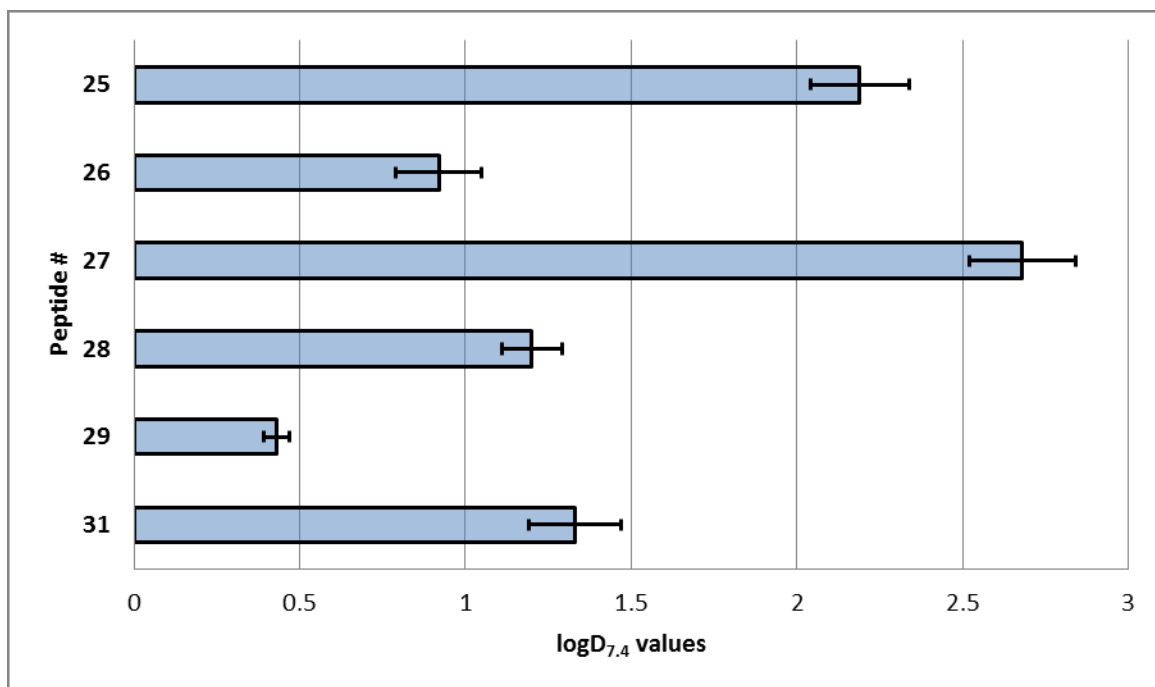


Figure 56: Measured logD_{7.4} values for cationic SiFA-TATE peptides.

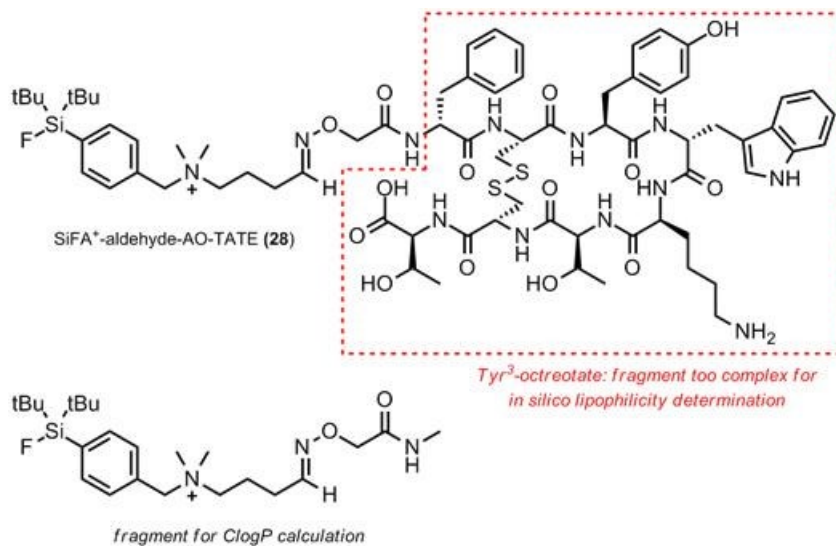


Figure 57: Virtual SiFA derivatives for ClogP calculations. (*top*) Structure of SiFA peptide (SiFA⁺-aldehyde-AO-TATE (28)) and (*bottom*) its corresponding *N*-methylamide virtual derivative for ClogP calculations (see Table VII).

The lipophilicity of all radiolabeled peptides studied herein was measured in triplicate from three independent radiolabeling reactions (Table VII, Figure 56). As added precaution, both phases were analyzed (post-partition) by HPLC to ensure no defluorination (hydrolysis) of the SiFA moiety as a result of the shake-flask method (Figure 58). As expected, all cationic SiFA-derivatized peptides displayed reduced lipophilicities compared to the first-generation SiFA-TATE (**27**). Interestingly, the measured $\log D_{7.4}$ values for **27** (2.68 ± 0.16) was markedly higher than previously reported (1.59 ± 0.01)^[156], although this does not invalidate the results obtained in the currently study. A plausible explanation of such an observation may be that trace levels of ethanol present in the previous shake-flask methodology (Figure 55), may underestimate lipophilicity by increasing solubilization of hydrophobic regions of the peptide analyte into the aqueous phase, although further study is needed to confirm such a hypothesis.

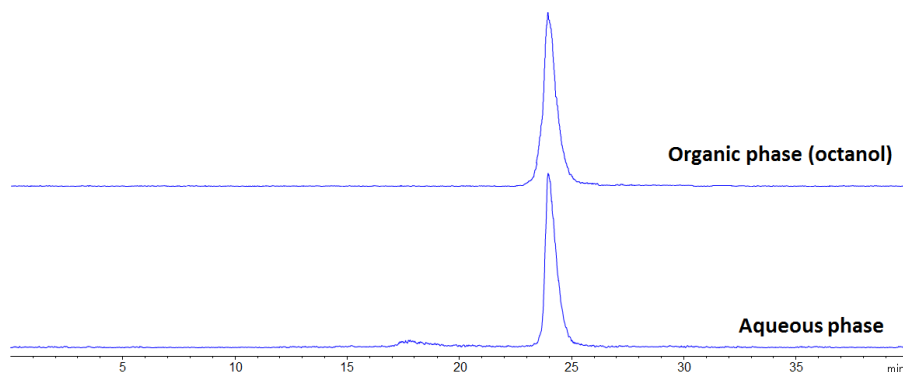


Figure 58: Sample HPLC radiochromatogram of partitioning phases.

The presence of [^{18}F]fluoride ($R_t = 4$ min) was not observed.

The estimation of lipophilicity by various *in silico* methodologies has also been considered. Classically, logP values of molecules can be computed via Rekker's^[210] or Leo's^[211] fragment-based systems^[212] although caution needs to be exercised when extending computational methods towards large molecules, particularly peptides. Peptides present the following additional challenges compared to small molecules, and these parameters are difficult to quantify: (1) solvent accessibility and hydrophobic collapse, (2) polar group interactions, (3) ionizable groups (e.g. zwitterions), (4) conformational effects, (5) intramolecular hydrogen-bonding, and (6) bound water molecules^[213]. Due to the lack of sufficient experimental logP values for peptides containing six or more amino acid residues, the above computational methods poorly extrapolate to this group of large molecules^[214]. In particular, the peptide of choice for the current study, Tyr³-octreotate, contains D-amino acids which introduce diastereomerism, likely affecting lipophilicity^[215,216], and not taken into account by peptide logP predictive systems. Many of the current programs (e.g. ALogP, QikProp, PLogP, XLogP, IALogP, LogKow, ACDLogP, MLogP) have shown poor predictive power for peptides greater than three amino acids in length^[217].

Despite these drawbacks, logP prediction software can be applied to the current collection of cationic SiFA peptides, as long as the peptidic portion of the molecule (octreotate) is removed and replaced by a non-peptidic fragment (e.g. a methyl group) (Figure 57). Although this exercise does not yield any useful

quantitative data, a qualitative comparison between different SiFA-derivatized peptides can be performed (Table VII). The predictive system used in the current exercise is ClogP^[218], a computer program based on Rekker's initial fragment-based method^[210]. Of note, no ClogP value could be calculated for peptide **26**, owing to a very long PEG linker region (ClogP values for higher molecular weight molecules are increasingly difficult to determine).

The difference between calculated LogD_{7.4} values for SiFA-TATE peptides and ClogP values for corresponding non-peptidic virtual equivalents is expressed in this study as $\Delta(\log D_{7.4} - \text{ClogP})$ (Table VII). This value occupies a narrow range between -0.79 and +0.31, suggesting that the theoretical hydrophilicity imparted by the specific SiFA group in question correlates well with the magnitude of lipophilicity of the overall molecule. However, this correlation does not agree with peptide **25**, which may be explained by its very short linker region between peptide and SiFA moiety. The proximity of the SiFA moiety to the peptide may create a hydrophobic pocket encompassing the cationic charge of the ammonium group, effectively removing its interaction with solvent (solvation). Therefore, SiFA⁺-CO₂H (**16**), the building block for the synthesis of SiFA⁺-C(O)NH-TATE (**25**), may not be ideally suitable for a reduction of lipophilicity.

3.6 Affinity determination by receptor autoradiography

Reubi *et al.* have developed a protocol for determination of somatostatin receptor binding affinity of octreotate derivatives^[219,220]. Briefly, cell membrane pellets isolated from CHO-K1 cells stably expressing human sst₁ and sst₅ receptors, and CCL39 cells stably expressing human sst₂, sst₃, and sst₄ receptors are treated with the universal somatostatin radioligand ¹²⁵I-[Leu⁸, D-Trp²², Tyr²⁵]-somatostatin 28 to saturate somatostatin receptors present on the membrane. The binding affinity of unlabelled analogues can be determined by treating the saturated receptors with varying concentrations of the desired cold peptide ranging from 0.1 to 1000 nM. The unlabeled universal somatostatin 28 was run in parallel as control experiment. IC₅₀ values for the peptides of interest are determined by a computer-assisted image processing system from the above experimental data.

At the time of the submission of this thesis, SiFA-labeled Tyr³-octreotate peptides have been submitted to Wängler and colleagues for determination of sst₁-sst₅ (somatostatin) receptor binding affinity by receptor autoradiography. This is to confirm that the presence of the SiFA moiety does not significantly alter the binding properties of octreotate.

3.7 Summary

The following second-generation cationic SiFA building blocks have been successfully synthesized here: SiFA⁺-SH (**6**), SiFA⁺-CHO (**8**), SiFA⁺-MI (**10**), SiFA⁺-N₃ (**12**), SiFA⁺-C≡CH (**13**), and SiFA⁺-CO₂H (**16**). In addition, several modified Tyr³-octreotate peptides (**18-24**) have been synthesized by SPPS to allow for bioconjugation with the above SiFA molecules, followed by further radiolabeling and lipophilicity determination. Overall, a general reduction of lipophilicity was achieved for the SiFA moiety via addition of a positively-charged quaternary ammonium group for the above radiolabeled peptides (**25, 26, 28, 29**, and **31**) compared to SiFA-TATE (**27**), which does not bear the ammonium group. In addition, the inclusion of a hydrophilic PEG linker greatly enhances the hydrophilicity of cationic SiFA peptides.

Chapter 4: Cationic SiFA compounds – EXPERIMENTAL SECTION

4.1 Regulatory notice

All manipulations involving radioactive materials have been performed in full accordance with Canadian Nuclear Safety Commission (CNSC) regulations.

4.2 Materials

Unless stated otherwise, commercially available chemical compounds were purchased from Sigma-Aldrich (Oakville, ON, Canada) in highest purity and used without further purification. ((4-bromobenzyl)oxy)(*tert*-butyl)dimethylsilane was prepared according to a literature procedure^[221]. Di-*tert*-butyldifluorosilane (99%) was purchased from Gelest (Morrisville, PA, USA). Fmoc-protected resins and amino acids, and 6-azidohexanoic acid were purchased from NovaBiochem (Merck KGaA, Darmstadt, Germany) with the exception of Fmoc-8-amino-3,6-dioxaoctanoic acid, which was purchased from Chem-Impex International (Wood Dale, IL, USA). 5-Hexynoic acid was purchased from Alfa Aesar (Ward Hill, MA, USA). Bulk solvents were rated HPLC grade or higher, and purchased from Fischer Scientific (Waltham, MA, USA). Highly enriched [¹⁸O]water (>97%) was purchased from Cambridge Isotope Laboratories (Andover, MA, USA). SepPak QMA and C-18 cartridges were obtained from Waters Corporation (Milford, MA,

USA). The purity of organic compounds prepared was determined by ^1H -NMR analysis.

4.3 Instruments

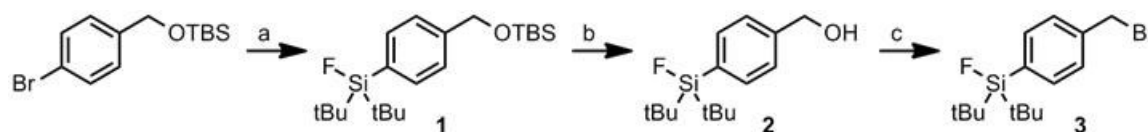
^1H -NMR and ^{13}C -NMR acquisitions were performed using a 300 MHz Varian Mercury (Agilent Technologies, Santa Clara, CA, USA) at the Nuclear Magnetic Resonance Facility, Department of Chemistry, McGill University, Montreal, Canada. High-resolution mass spectrometry (HRMS) was performed at the Centre regional de spectrométrie de masse, Department of Chemistry, Université de Montréal, Montreal, Canada.

Semi-preparative HPLC was performed on an Agilent 1200 system (Agilent Technologies, Santa Clara, CA, USA; running on Agilent ChemStation software) equipped with a MZ semi-prep LiChrosorb column (RP-Select B 5 μm , 250 x 10 mm; Merck, Germany) at a flow rate of 2 mL/min, and UV detection was performed at 230 nm and 254 nm. Analytical radio-HPLC was performed on an Agilent 1200 system equipped with a Raytest Gabi Star radioactivity detector (Raytest Isotopenmessgeräte GmbH, Straubenhardt, Germany) and a MZ-analytical LiChrosorb column (RP-Select B 5 μm , 250 x 4.6 mm) at a flow rate of 0.7 mL/min, and UV detection was performed at 210 nm, 230 nm, and 254 nm. HPLC mobile phases consist of eluent A (0.1% TFA in MeCN) and eluent B (0.1% TFA in H_2O) filtered through a 0.45 μm nylon membrane filter and

degassed before use. All samples for preparative and analytical HPLC were diluted with a minimum of 50% v/v eluent B prior to injection. Samples were injected via a model 7725i Rheodyne syringe loading sample injector fitted with a 2 mL loop (Rheodyne, Cotati, CA, USA). Gamma counting was performed using a CRC-25PET Dose Calibrator (Capintec, Ramsey, NJ, USA). Mass spectrometry of peptides was performed using a Bruker Microflex LT MALDI-TOF MS (Bruker Daltonics, Billerica, MA, USA).

4.4 Small-molecule synthesis

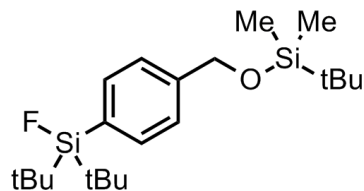
4.4.1 Synthesis of the common starting material SiFA-benzyl-bromide:



(a) 1. $t\text{BuLi}$, Et_2O , -78°C , 15 min; 2. $t\text{Bu}_2\text{SiF}_2$, Et_2O , $-70^\circ\text{C} \rightarrow \text{rt}$, overnight; (b) HCl , MeOH , rt , overnight, **76%** (2 steps); (c) CBr_4 , PPh_3 , CH_2Cl_2 , rt , overnight, **88%**.

4.4.1.1 Synthesis of di-*tert*-butyl(4-(((*tert*-

butyldimethylsilyl)oxy)methyl)phenyl)fluorosilane (1):



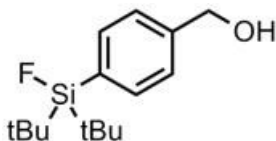
Adapted from Iovkova *et al.*^[148], with modifications. To a solution of ((4-bromobenzyl)oxy)(*tert*-butyl)dimethylsilane (5.00 g, 16.6 mmol) in anhydrous Et₂O (20 mL) was added dropwise over a period of 15 min a solution of *tert*-butyllithium in pentanes (1.7 M, 20.5 mL, 2.1 eq) at -78°C, and the formed solution was stirred at the same temperature for 15 min. To this solution was added dropwise over a period of 15 min a solution of di-*tert*-butyldifluorosilane (3.85 g, 21.4 mmol, 1.2 eq) in anhydrous Et₂O (10 mL) at -78°C, and the mixture was allowed to warm to room temperature overnight. The reaction was quenched by addition of saturated aqueous sodium chloride solution (100 mL), and the mixture was extracted with Et₂O (3 x 75 mL). The combined organic phase was dried (Na₂SO₄) and concentrated *in vacuo* to afford the crude product **1** as a pale-yellow liquid (6.35 g) that was carried forward without further purification.

¹H NMR (300 MHz, CDCl₃): δ 7.57 (d, 2H, *J* = 8.1 Hz), 7.34 (d, 2H, *J* = 7.8 Hz), 4.77 (s, 2H), 1.05 (d, 18H, *J*(¹H, ¹⁹F) = 1.2 Hz), 0.95 (s, 9H), 0.11 (s, 6H).

¹³C NMR (300 MHz, CDCl₃): δ 142.8, 133.9 (d, *J*(¹³C, ¹⁹F) = 5 Hz), 125.2 (d, *J*(¹³C, ¹⁹F) = 2 Hz), 64.9, 27.3 (d, *J*(¹³C, ¹⁹F) = 3 Hz), 26.0, 20.3 (d, *J*(¹³C, ¹⁹F) = 50 Hz), 18.4, -5.2.

HRMS (ESI, *m/z*) for C₂₁H₃₉FNaOSi₂ [M+Na]⁺ (calcd): 405.2418 (405.2421).

4.4.1.2 Synthesis of (4-(di-*tert*-butylfluorosilyl)phenyl)methanol (2):



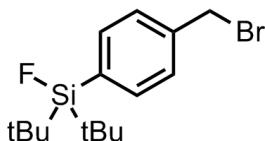
Adapted from Iovkova *et al.*^[148], with modifications. To a solution of crude **1** in MeOH (50 mL) was added dropwise concentrated aqueous hydrochloric acid solution (37 wt%, 0.5 mL) at 25°C, and the mixture was stirred at room temperature overnight. The solvent and the volatiles were then removed under reduced pressure. The residue was redissolved in Et₂O (100 mL) and the solution was washed with saturated aqueous sodium bicarbonate solution (50 mL). The aqueous phase was extracted with Et₂O (3 x 50 mL). The combined organic phase was washed with H₂O (50 mL), dried (Na₂SO₄) and concentrated *in vacuo*. The residue was purified by flash column chromatography on silica gel (9:1 to 7:1 hexanes/EtOAc) to afford **3** as a white solid (3.38 g, 76% over 2 steps).

¹H NMR (300 MHz, CDCl₃): δ 7.61 (d, 2H, *J* = 7.8 Hz), 7.38 (d, 2H, *J* = 7.8 Hz), 4.72 (d, 2H, *J* = 5.7 Hz), 1.75 (t, 1H, *J* = 5.9 Hz), 1.06 (d, 18H, *J*(¹H, ¹⁹F) = 1.2 Hz).

¹³C NMR (300 MHz, CDCl₃): δ 142.1, 134.2 (d, *J*(¹³C, ¹⁹F) = 17 Hz), 132.9 (d, *J*(¹³C, ¹⁹F) = 53 Hz), 126.1 (d, *J*(¹³C, ¹⁹F) = 4 Hz), 65.3, 27.3 (d, *J*(¹³C, ¹⁹F) = 4 Hz), 20.2 (d, *J*(¹³C, ¹⁹F) = 49 Hz).

HRMS (ESI, *m/z*) for C₁₅H₂₅FNaOSi [M+Na]⁺ (calcd): 291.1552 (291.1556).

4.4.1.3 Synthesis of (4-(bromomethyl)phenyl)di-*tert*-butylfluorosilane (3):

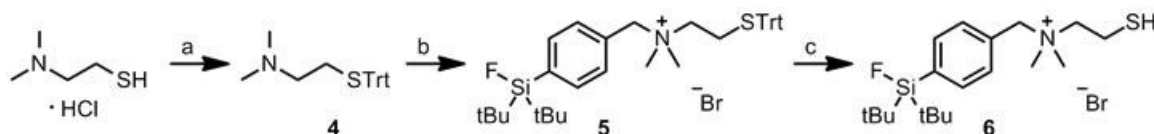


Adapted from Kostikov *et al.*^[157], with modifications. To a solution of **2** (1.34 g, 4.99 mmol) and carbon tetrabromide (1.82 g, 5.49 mmol, 1.1 eq) in anhydrous CH₂Cl₂ (50 mL) was added triphenylphosphine (1.44 g, 5.49 mmol, 1.1 eq) in small portions and the mixture stirred at room temperature overnight. The resulting colorless solution was concentrated *in vacuo*. To the residue was added anhydrous ether (50 mL) to precipitate triphenylphosphine oxide, and the resulting mixture was filtered. The filtrate was concentrated *in vacuo* and purified by flash column chromatography on silica gel (neat hexanes) to afford **3** as a colorless oil (1.45 g, 88%), which solidified on standing to a white solid.

¹H NMR (300 MHz, CDCl₃): δ 7.58 (d, 2H, *J* = 8.1 Hz), 7.40 (d, 2H, *J* = 8.1 Hz), 4.50 (s, 2H), 1.05 (d, 18H, *J*(¹H, ¹⁹F) = 0.9 Hz).

¹³C NMR (300 MHz, CDCl₃): δ 138.9, 134.4 (d, *J*(¹³C, ¹⁹F) = 17 Hz), 128.1, 33.3, 27.3 (d, *J*(¹³C, ¹⁹F) = 3 Hz), 20.3 (49 Hz).

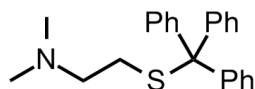
4.4.2 Synthesis of cationic SiFA⁺-SH:



(a) Ph_3CCl , CH_2Cl_2 , DMF, rt, overnight, **86%**; (b) **3**, Et_2O , 50°C , overnight, **65%**;

(c) TFA, Et_3SiH , CH_2Cl_2 , rt, 4 hr, **56%**.

4.4.2.1 Synthesis of *N,N*-dimethyl-2-(tritylthio)ethanamine (**4**):



To a solution of 2-(dimethylamino)ethanethiol hydrochloride (5.00 g, 35.3 mol) in anhydrous CH_2Cl_2 (15 mL) and anhydrous DMF (15 mL) was added trityl chloride (14.8 g, 52.9 mmol, 1.5 eq) in small portions and the mixture stirred at room temperature overnight. The solvents were removed under reduced pressure. The residue was dissolved in Et_2O (100 mL) and the solution was washed with 0.5 M aqueous NaOH solution (50 mL). The aqueous phase was extracted with Et_2O (3 x 20 mL). The combined organic phase was washed with H_2O (50 mL), dried (Na_2SO_4) and concentrated *in vacuo*. The residue was purified by flash column chromatography on silica gel (20:20:1 hexanes/ EtOAc / Et_3N) to afford **4** as a yellow solid (10.60 g, 86%).

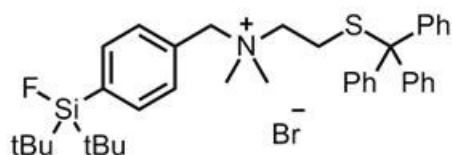
^1H NMR (300 MHz, CDCl_3): δ 7.45–7.41 (m, 6H), 7.32–7.17 (m, 9H), 2.27 (t, 2H, J = 4.8 Hz), 2.26 (t, 2H, J = 4.8 Hz), 2.09 (s, 6H).

^{13}C NMR (300 MHz, CDCl_3): δ 144.9, 129.6, 127.8, 126.5, 66.5, 58.2, 45.1, 30.0.

HRMS (ESI, m/z) for $\text{C}_{23}\text{H}_{26}\text{NS}$ $[\text{M}+\text{H}]^+$ (calcd): 348.1788 (348.1786).

4.4.2.2 Synthesis of *N*-(4-(di-*tert*-butylfluorosilyl)benzyl)-*N,N*-dimethyl-2-

(tritylthio)ethanaminium bromide (**5**):



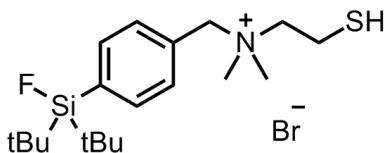
A solution of **3** (300 mg, 0.905 mmol) and **4** (415 mg, 1.19 mmol, 1.3 eq) in anhydrous Et_2O (7 mL) was stirred at 50°C overnight with formation of a white precipitate. The mixture was filtered, and the residue dried under a stream of argon to afford crude **5** as a white solid (403 mg, 65%) that was carried forward without further purification.

^1H NMR (300 MHz, CDCl_3): δ 7.62 (d, 2H, J = 7.8 Hz), 7.49 (d, 2H, J = 8.1 Hz), 7.38-7.33 (m, 6H), 7.29-7.17 (m, 9H), 4.84 (s, 2H), 2.99 (s, 6H), 2.99 (m, 2H), 2.67 (m, 2H), 1.04 (d, 18H, $J(^1\text{H}, ^{19}\text{F})$ = 0.6 Hz).

^{13}C NMR (300 MHz, CDCl_3): δ 143.6, 137.4 (d, $J(^{13}\text{C}, ^{19}\text{F})$ = 55 Hz), 134.7 (d, $J(^{13}\text{C}, ^{19}\text{F})$ = 17 Hz), 132.2, 129.5, 128.3, 128.0, 127.2, 68.0, 62.0, 51.7, 49.4, 27.2 (d, $J(^{13}\text{C}, ^{19}\text{F})$ = 12 Hz), 24.6, 20.2 (d, $J(^{13}\text{C}, ^{19}\text{F})$ = 48 Hz).

HRMS (ESI, m/z) for $\text{C}_{38}\text{H}_{49}\text{FNSSi}^+$ $[\text{M}]^+$ (calcd): 598.3333 (598.3334).

4.4.2.3 Synthesis of *N*-(4-(di-*tert*-butylfluorosilyl)benzyl)-2-mercapto-*N,N*-dimethylethanaminium bromide (6; SiFA⁺-SH):



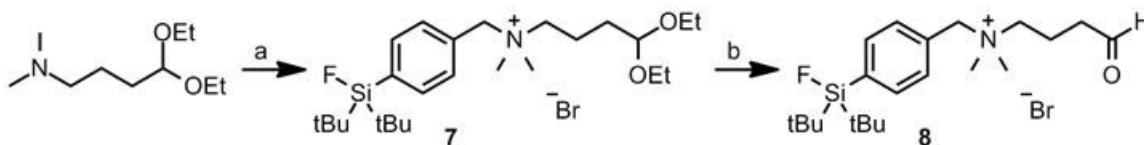
To a solution of **5** (140 mg, 0.206 mmol) in anhydrous CH₂Cl₂ (10 mL) was added trifluoroacetic acid (0.31 mL, 4.12 mmol, 20 eq) and triethylsilane (49.4 μL, 0.309 mmol, 1.5 eq) and the mixture stirred under an argon atmosphere at room temperature for 4 h. The solvent and reagents were removed under reduced pressure, and the residue was suspended in cold anhydrous Et₂O (5 mL). The mixture was filtered, and the residue dried under a stream of argon to afford crude **6** as a white solid (50.0 mg, 56%) that was carried forward without further purification.

¹H NMR (300 MHz, CDCl₃): δ 7.71 (d, 2H, *J* = 8.1 MHz), 7.67 (d, 2H, *J* = 8.4 Hz), 5.01 (s, 2H), 4.00 (m, 2H), 3.36 (s, 6H), 3.15 (m, 2H), 2.00 (br s, 1H), 1.04 (d, 18H, *J*(¹H, ¹⁹F) = 0.9 Hz).

¹³C NMR (300 MHz, CDCl₃): δ 137.7 (d, *J*(¹³C, ¹⁹F) = 56 Hz), 134.8 (d, *J*(¹³C, ¹⁹F) = 17 Hz), 132.2, 128.0, 67.8, 66.2, 50.0, 27.2, 20.2 (d, *J*(¹³C, ¹⁹F) = 48 Hz), 18.1.

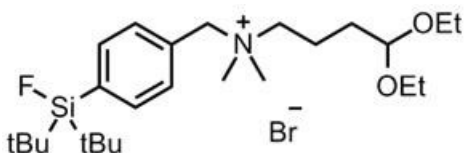
HRMS (ESI, *m/z*) for C₁₉H₃₅FNSSi⁺ [*M*⁺]⁺ (calcd): 356.2242 (356.2238).

4.4.3 Synthesis of cationic SiFA⁺-CHO:



(a) **3**, CH₂Cl₂, rt, overnight, quantitative; (b) TFA, H₂O, rt, 30 min.

4.4.3.1 Synthesis of *N*-(4-(di-*tert*-butylfluorosilyl)benzyl)-4,4-diethoxy-*N,N*-dimethylbutan-1-aminium bromide (**7**):



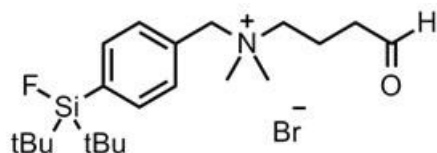
To a solution of **3** (100 mg, 0.302 mmol) in anhydrous CH₂Cl₂ (5 mL) was added 4-(dimethylamino)butanal diethyl acetal (57.1 mg, 0.302 mmol, 1 eq) and the mixture stirred at room temperature overnight. The resulting colorless solution was concentrated *in vacuo* to afford crude **7** as a white solid (quantitative yield) that was carried forward without further purification.

¹H NMR (300 MHz, CDCl₃): δ 7.68 (s, 4H), 5.02 (s, 2H), 4.52 (t, 1H, *J* = 4.7 Hz), 3.60 (m, 4H), 3.48 (m, 2H), 3.33 (s, 6H), 1.94 (m, 4H), 1.69 (dd, 2H, *J* = 11.2 Hz, 7.1 Hz), 1.16 (t, 6H, *J* = 7.1 Hz), 1.03 (d, 18H, *J*(¹H, ¹⁹F) = 0.6 Hz).

¹³C NMR (300 MHz, CDCl₃): δ 137.3 (d, *J*(¹³C, ¹⁹F) = 56 Hz), 134.6 (d, *J*(¹³C, ¹⁹F) = 18 Hz), 132.2, 128.3, 67.2, 63.3, 62.5, 49.8, 30.2, 27.2, 20.1 (d, *J*(¹³C, ¹⁹F) = 48 Hz), 17.4, 15.3.

HRMS (ESI, m/z) for $C_{25}H_{47}FNO_2Si^+$ [M^*] $^+$ (calcd): 4400.3369 (440.3355).

4.4.3.2 Synthesis of *N*-(4-(di-*tert*-butylfluorosilyl)benzyl)-*N,N*-dimethyl-4-oxobutan-1-aminium bromide (**8**; SiFA $^+$ -CHO):



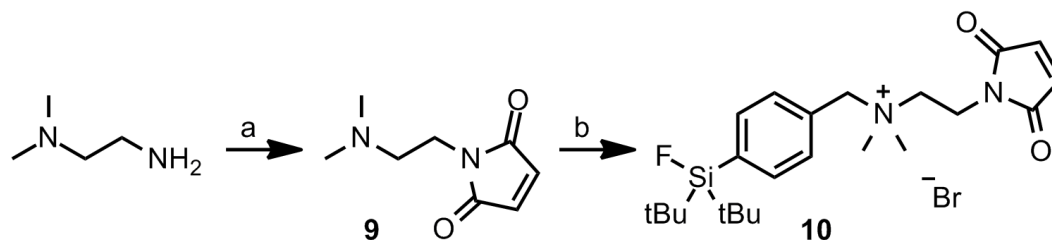
To crude **7** (10 mg) was added 95% TFA in H_2O (100 μ L) and the reaction was left to stand without stirring at room temperature for 30 min. The reaction was quenched with the addition of anhydrous Et_2O (1.5 mL) and cooled to minus 20 $^{\circ}C$ overnight with the appearance of a white precipitate. The resulting mixture was centrifuged (14,500 rpm, 5 min) and the supernatant removed to afford crude **8** as a white pellet that was used immediately for conjugation to amino-oxy derivatized peptides without further purification or drying.

1H NMR (300 MHz, $CDCl_3$): δ 9.79 (s, 1H), 7.74 (d, 2H, J = 8.1 Hz), 7.61 (d, 2H, J = 8.1 Hz), 4.81 (s, 2H), 3.73 (m, 2H), 3.23 (s, 6H), 2.80 (t, 2H, J = 6.5 Hz), 2.18 (m, 2H), 1.05 (d, 18H, $J(^1H, ^{19}F)$ = 48 Hz).

^{13}C NMR (300 MHz, $CDCl_3$): δ 200.0, 134.9 (d, 2H, J = 17 Hz), 132.0, 128.8, 127.7, 67.9, 65.0, 63.4, 49.8, 39.7, 27.2, 20.2 (d, 2H, J = 8.1 Hz), 15.5.

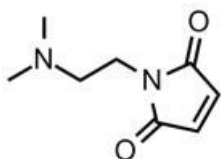
HRMS (ESI, m/z) for $C_{21}H_{37}FNOSi^+$ [M^*] $^+$ (calcd): 366.2632 (366.2623).

4.4.4 Synthesis of cationic SiFA⁺-MI:



(a) maleic anhydride, Na_2SO_4 , PhMe, reflux, overnight, **20%**; (b) **3**, CH_2Cl_2 , rt, overnight, **66%**.

4.4.4.1 Synthesis of 1-(2-(dimethylamino)ethyl)-1H-pyrrole-2,5-dione (**9**):



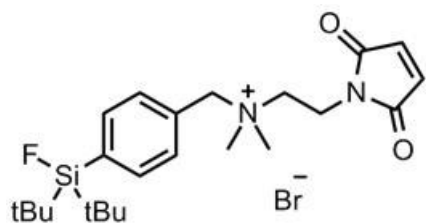
To a solution of *N,N*-dimethylethylenediamine (1.00 g, 11.9 mmol, 1 eq) and maleic anhydride (1.11 g, 11.9 mmol, 1 eq) in toluene (40 mL) was added anhydrous Na_2SO_4 (5 g) and stirred under reflux overnight. The solvents were removed under reduced pressure. The residue was dissolved in Et_2O (100 mL) and the solution was washed with 0.5 M aqueous NaOH solution (50 mL). The aqueous phase was extracted with Et_2O (3 x 20 mL). The combined organic phase was washed with H_2O (50 mL), dried (Na_2SO_4) and concentrated *in vacuo* to afford crude **9** as a red solid (370 mg, 20%) that was carried forward without further purification.

^1H NMR (300 MHz, CDCl_3): δ 6.68 (s, 2H), 3.62 (t, 2H, J = 6.6 Hz), 2.47 (t, 2H, J = 6.5 Hz), 2.24 (s, 6H).

^{13}C NMR (300 MHz, CDCl_3): δ 134.1, 57.0, 45.4, 35.8.

HRMS (ESI, m/z) for $\text{C}_8\text{H}_{13}\text{N}_2\text{O}_2$ $[\text{M}+\text{H}]^+$ (calcd): 169.0977 (169.0977).

4.4.4.2 Synthesis of *N*-(4-(di-*tert*-butylfluorosilyl)benzyl)-2-(2,5-dioxo-2,5-dihydro-1*H*-pyrrol-1-yl)-*N,N*-dimethylethanaminium bromide (10; SiFA⁺-MI):



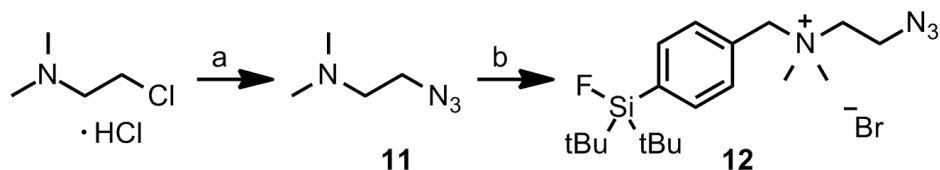
A solution of **3** (215 mg, 0.649 mmol) and crude **9** (109 mg, 0.649 mmol, 1 eq) in anhydrous CH_2Cl_2 (15 mL) was stirred at room temperature overnight. The solvent was removed under reduced pressure. Addition of Et_2O (15 mL) with formation of a white precipitate was followed by filtration to afford crude **10** as a white solid (231 mg, 66%) that was carried forward without further purification.

^1H NMR (300 MHz, CDCl_3): δ 7.75 (d, 2H, J = 8.1 Hz), 7.68 (d, 2H, J = 7.8 Hz), 6.76 (s, 2H), 5.12 (s, 2H), 4.18 (t, 2H, J = 6.0 Hz), 4.04 (t, 2H, J = 6.3 Hz), 3.43 (s, 6H), 1.02 (s, 18H).

^{13}C NMR (300 MHz, CDCl_3): δ 170.0, 137.5 (d, $J(^{13}\text{C}, ^{19}\text{F})$ = 55 Hz), 134.7 (d, $J(^{13}\text{C}, ^{19}\text{F})$ = 17 Hz), 134.6, 132.3, 128.0, 67.5, 61.3, 50.0, 32.2, 27.2, 20.1 (d, $J(^{13}\text{C}, ^{19}\text{F})$ = 48 Hz).

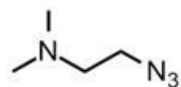
HRMS (ESI, m/z) for $C_{23}H_{36}FN_2O_2Si^+$ [M^*] $^+$ (calcd): 419.2530 (419.2525).

4.4.5 Synthesis of cationic SiFA $^+$ -N $_3$:



(a) NaN $_3$, H $_2$ O, 80°C, overnight, **63%**; (b) **3**, CH $_2$ Cl $_2$, rt, overnight, **99%**.

4.4.5.1 Synthesis of 2-azido-*N,N*-dimethylethanamine (11):



A solution of 2-chloro-*N,N*-dimethylamine hydrochloride (500 mg, 3.5 mmol) and NaN $_3$ (677 mg, 10.4 mmol, 3 eq) in H $_2$ O (20 mL) was stirred at 80°C overnight. To the reaction was added Et $_2$ O (40 mL) and NaOH (500 mg) and stirred vigorously for 30 min. The organic phase was washed with H $_2$ O (20 mL), dried (Na $_2$ SO $_4$) and concentrated in vacuo to afford crude **11** as a pale yellow oil (291 mg, 63%) that was carried forward without further purification.

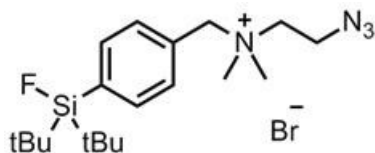
^1H NMR (300 MHz, CDCl $_3$): δ 3.35 (t, 2H, J = 6.3 Hz), 2.50 (t, 2H, J = 6.2 Hz), 2.27 (s, 6H).

^{13}C NMR (300 MHz, CDCl $_3$): δ 58.0, 49.0, 45.4.

HRMS (ESI, m/z) for $C_4H_{11}N_4$ [$M+H$] $^+$ (calcd): 115.0982 (115.0984).

4.4.5.2 Synthesis of 2-azido-*N*-(4-(di-*tert*-butylfluorosilyl)benzyl)-*N,N*-

dimethylethanaminium bromide (**12**; SiFA⁺-N₃):



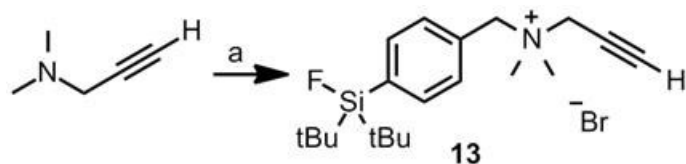
A solution of **3** (94.8 mg, 0.286 mmol) and **11** (42.4 mg, 0.372 mmol, 1.3 eq) in anhydrous CH₂Cl₂ (8 mL) was stirred at room temperature overnight. The solvent was removed under reduced pressure. Addition of Et₂O (8 mL) with formation of a white precipitate was followed by filtration to afford crude **12** as a white solid (127 mg, 99%) that was carried forward without further purification.

¹H NMR (300 MHz, CDCl₃): δ 7.72 (d, 2H, *J* = 8.4 Hz), 7.69 (d, 2H, *J* = 8.4 Hz), 5.13 (s, 2H), 4.16 (t, 2H, *J* = 5.3 Hz), 4.01 (t, 2H, *J* = 5.4 Hz), 3.40 (s, 6H), 1.03 (d, 18H, *J*(¹H, ¹⁹F) = 0.6 Hz).

¹³C NMR (300 MHz, CDCl₃): δ 137.6 (*J*(¹³C, ¹⁹F) = 56 Hz), 134.7 (*J*(¹³C, ¹⁹F) = 17 Hz), 132.4, 128.0, 68.5, 62.2, 50.5, 45.4, 27.2, 20.2 (*J*(¹³C, ¹⁹F) = 49 Hz).

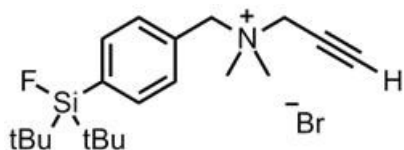
HRMS (ESI, *m/z*) for C₁₉H₃₄FN₄Si⁺ [*M*⁺] (calcd): 365.2539 (365.2531).

4.4.6 Synthesis of cationic SiFA⁺-C≡CH:



(a) **3**, CH₂Cl₂, rt, overnight, **96%**.

4.4.6.1 Synthesis of *N*-(4-(di-*tert*-butylfluorosilyl)benzyl)-*N,N*-dimethylprop-2-yn-1-aminium bromide (13; SiFA⁺-C≡CH):



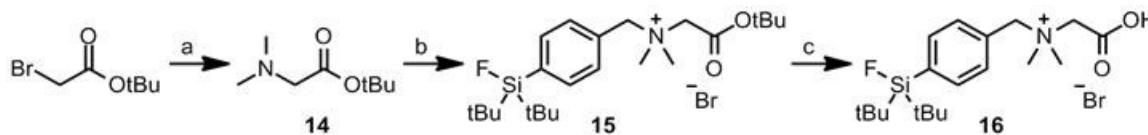
A solution of **3** (96.0 mg, 0.290 mmol) and *N,N*-dimethylprop-2-yn-1-amine (31.0 mg, 0.290 mmol, 1 eq) in anhydrous CH₂Cl₂ (8 mL) was stirred at room temperature overnight. The solvent was removed under reduced pressure. Addition of Et₂O (8 mL) with formation of a white precipitate was followed by filtration to afford crude **13** as a white solid (116 mg, 96%) that was carried forward without further purification.

¹H NMR (300 MHz, CDCl₃): δ 7.73 (d, 2H, *J* = 8.4 Hz), 7.70 (d, 2H, *J* = 8.4 Hz), 5.14 (s, 2H), 4.75 (s, 2H), 3.49 (s, 6H), 2.95 (t, 1H, *J* = 2.3 Hz), 1.03 (s, 18H).

¹³C NMR (300 MHz, CDCl₃): δ 134.8 (*J*(¹³C, ¹⁹F) = 17 Hz), 132.1, 128.0, 81.8, 71.8, 66.3, 53.6, 49.7, 27.2, 20.2 (d, *J*(¹³C, ¹⁹F) = 48 Hz).

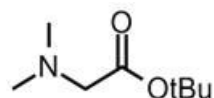
HRMS (ESI, *m/z*) for C₂₀H₃₃FNSi⁺ [*M*⁺]⁺ (calcd): 334.2366 (334.2361).

4.4.7 Synthesis of cationic SiFA⁺-CO₂H:



(a) Me₂NH, rt, overnight, **99%**; (b) CH₂Cl₂, rt, overnight, **85%**; (c) TFA, Et₃SiH, H₂O, rt, 4 hr, **86%**.

4.4.7.1 Synthesis of *tert*-butyl 2-(dimethylamino)acetate (**14**):



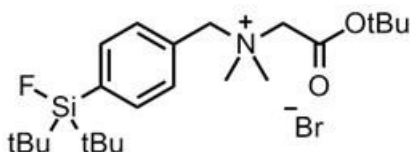
To a mixture of dimethylamine hydrochloride (10.1g, 124 mmol, 6.2 eq) in H₂O (20 mL) and Et₂O (80 mL) at 0°C was added K₂CO₃ (20 g) in small portions. The resulting mixture was stirred for 15 min at 0°C and the organic phase decanted into an oven-dried round bottom flask. To the solution was added *tert*-butyl bromoacetate (3.90 g, 20 mmol) and stirred at room temperature overnight with the formation of a white precipitate. The reaction was filtered, and the filtrate concentrated under reduced pressure to afford crude **14** as a colorless liquid (3.20 g, 99%) that was carried forward without further purification.

¹H NMR (300 MHz, CDCl₃): δ 3.04 (s, 2H), 2.32 (s, 6H), 1.45 (s, 9H).

¹³C NMR (300 MHz, CDCl₃): δ 169.9, 80.9, 61.2, 45.2, 28.1.

HRMS (ESI, m/z) for C₈H₁₈NO₂ [M+H]⁺ (calcd): 160.1332 (160.1332).

4.4.7.2 Synthesis of 2-(*tert*-butoxy)-*N*-(4-(di-*tert*-butylfluorosilyl)benzyl)-*N,N*-dimethyl-2-oxoethanaminium bromide (15):



A solution of **3** (861 mg, 2.62 mmol) and **14** (438 mg, 2.75 mmol, 1.05 eq) in anhydrous CH_2Cl_2 (30 mL) was stirred at room temperature overnight. The solvent was removed under reduced pressure. Addition of Et_2O (30 mL) with formation of a white precipitate was followed by filtration to afford crude **13** as a white solid (1.27 g, 85%) that was carried forward without further purification.

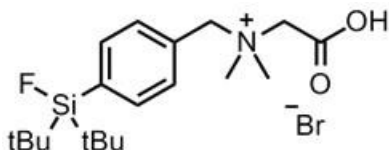
^1H NMR (300 MHz, CDCl_3): δ 7.69 (d, 2H, $J = 7.8$ Hz), 7.63 (d, 2H, $J = 7.8$ Hz), 5.26 (s, 2H), 4.59 (s, 2H), 3.59 (s, 6H), 1.49 (s, 9H), 1.03 (d, 18H, $J(^1\text{H}, ^{19}\text{F}) = 0.9$ Hz).

^{13}C NMR (300 MHz, CDCl_3): δ 163.8, 137.8 (d, $J(^{13}\text{C}, ^{19}\text{F}) = 58$ Hz), 134.8 (d, $J(^{13}\text{C}, ^{19}\text{F}) = 12$ Hz), 132.2, 128.1, 85.5, 67.2, 61.0, 50.5, 28.0, 27.2, 20.2 (d, $J(^{13}\text{C}, ^{19}\text{F}) = 48$ Hz).

HRMS (ESI, m/z) for $\text{C}_{23}\text{H}_{41}\text{FNO}_2\text{Si}^+ [\text{M}^+]^+$ (calcd): 410.2895 (410.2885).

4.4.7.3 Synthesis of 1-carboxy-*N*-(4-(di-*tert*-butylfluorosilyl)benzyl)-*N,N*-

dimethylmethanaminium bromide (**16**; SiFA⁺-CO₂H):



A solution of **15** (300 mg, 0.61 mmol) and triisopropylsilane (155 mg, 0.98 mmol, 1.6 eq) in H₂O (200 μ L) and TFA (7.6 mL) was stirred at room temperature for 4 hours. The solvent was removed under reduced pressure. Addition of Et₂O (30 mL) with formation of a white precipitate was followed by filtration to afford crude **14** as a white solid (230 mg, 86%) that was carried forward without further purification.

¹H NMR (300 MHz, DMSO-*d*₆): δ 7.71 (d, 2H, J = 8.1 Hz), 7.57 (d, 2H, J = 7.8 Hz), 4.75 (s, 2H), 4.26 (s, 2H), 3.19 (s, 6H), 1.03 (d, 18H, $J(^1\text{H}, ^{19}\text{F})$ = 0.6 Hz).

¹³C NMR (300 MHz, DMSO-*d*₆): δ 166.4, 135.4 (d, $J(^{13}\text{C}, ^{19}\text{F})$ = 54 Hz), 134.1, 132.1, 129.0, 67.0, 60.4, 50.1, 26.9, 19.7 (d, $J(^{13}\text{C}, ^{19}\text{F})$ = 49 Hz).

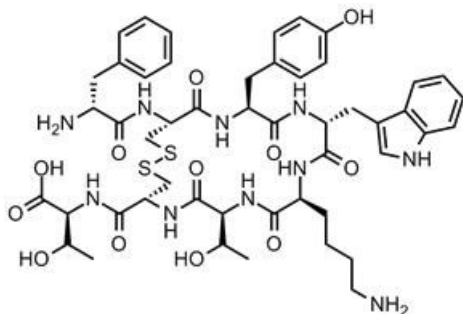
HRMS (ESI, *m/z*) for C₁₉H₃₃FNO₂Si⁺ [*M*⁺]⁺ (calcd): 354.2266 (354.2259).

4.5 Peptide synthesis

4.5.1 Solid-Phase Peptide Synthesis: *General procedure for the synthesis of Tyr³-octreotate (TATE) (17), AO-TATE (18), AO-PEG-TATE (19), MI-TATE (20), HC≡C-TATE (21), HC≡C-PEG-TATE (22), N₃-TATE (23), N₃-PEG-TATE (24), SiFA⁺-C(O)NH-TATE (25), and SiFA⁺-C(O)NH-PEG₂-TATE (26).*

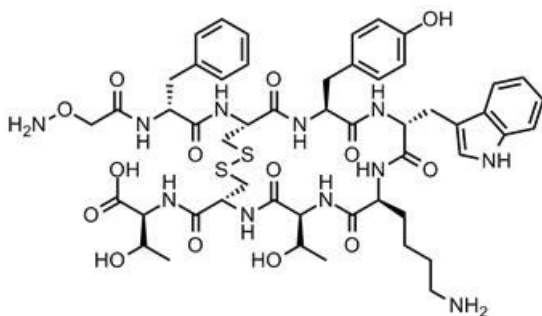
Tyr³-octreotate was synthesized on solid support using standard Fmoc solid-phase peptide synthesis as described by Wellings and Atherton^[180] on a Fmoc-Thr(tBu)-Wang resin (standard coupling: 4 equiv. amino acid, 4 equiv. HBTU, 4 equiv. DIPEA in DMF; Fmoc deprotection: 50% piperidine in DMF; disulfide cyclization: 4 equiv. Ti(TFA)₃ in DMF). Tyr³-octreotate derivatives were functionalized from Tyr³-octreotate on solid support with the appropriate Fmoc-protected (Fluorenylmethyloxycarbonyl-protected) amino acid or carboxylic acid building blocks under the above coupling conditions. The peptides were cleaved from the resin and deprotected upon treatment with a solution of TFA/TIPS/H₂O (95:2.5:2.5, 2 mL) for 60 min, and then precipitated from solution upon addition of excess diethyl ether. The crude solid was washed three times with excess diethyl ether, and purified by semi-preparative HPLC (0:100 eluent A/B to 100:0 eluent A/B in 30 min gradient) to afford the desired peptide as a white solid after lyophilisation.

4.5.1.1 Synthesis of Tyr³-octreotate (17; TATE):



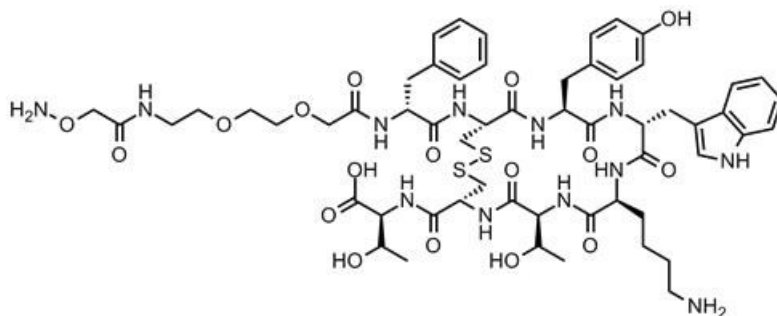
Tyr³-octreotate was synthesized on solid support using standard Fmoc solid-phase peptide synthesis as described above. 44% yield; $R_{t(\text{purification})} = 16.8$ min. HRMS (MALDI-TOF, m/z) for $C_{49}H_{65}N_{10}O_{12}S_2^+$ $[M+H]^+$ (calc'd): 1049.28 (1049.42). Characterization data is in agreement with literature values^[197].

4.5.1.2 Synthesis of AO-TATE (18):



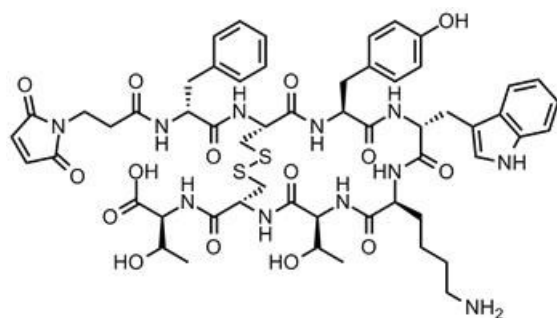
AO-TATE was synthesized using Fmoc solid-phase peptide synthesis from Tyr³-octreotate on solid support with aminooxyacetic acid as building block. 29% yield. $R_{t(\text{purification})} = 17.3$ min. HRMS (MALDI-TOF, m/z) for $C_{51}H_{68}N_{11}O_{14}S_2^+$ $[M+H]^+$ (calc'd): 1122.44 (1122.44). Characterization data is in agreement with literature values^[202].

4.5.1.3 Synthesis of AO-PEG-TATE (19):



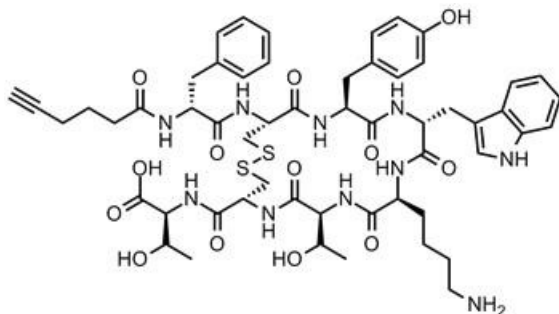
AO-PEG-TATE was synthesized using Fmoc solid-phase peptide synthesis from Tyr³-octreotate on solid support with Fmoc-8-amino-3,6-dioxaoctanoic acid and aminooxyacetic acid as building blocks. 24% yield. $R_{t(\text{purification})} = 17.7$ min. HRMS (MALDI-TOF, m/z) for $C_{57}H_{79}N_{12}O_{17}S_2^+$ $[M+H]^+$ (calc'd): 1267.11 (1267.51).

4.5.1.4 Synthesis of MI-TATE (20):



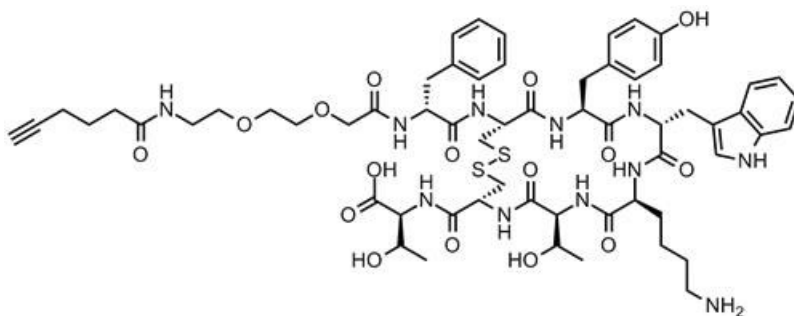
MI-TATE was synthesized using Fmoc solid-phase peptide synthesis from Tyr³-octreotate on solid support with N-maleoyl- β -alanine as building block. 25% yield; $R_{t(\text{purification})} = 20.6$ min. HRMS (MALDI-TOF, m/z) for $C_{56}H_{70}N_{11}O_{15}S_2^+$ $[M+H]^+$ (calc'd): 1200.55 (1200.45).

4.5.1.5 Synthesis of HC≡C-TATE (21):



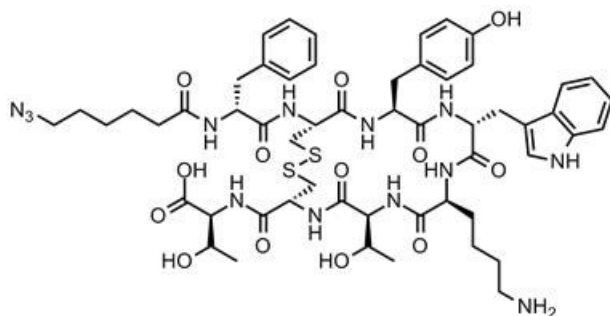
HC≡C-TATE was synthesized using Fmoc solid-phase peptide synthesis from Tyr³-octreotate on solid support with 5-hexynoic acid as building block. 44% yield. $R_{t(\text{purification})} = 20.5$ min. HRMS (MALDI-TOF, m/z) for $C_{55}H_{71}N_{10}O_{13}S_2^+$ $[M+H]^+$ (calc'd): 1143.75 (1143.46).

4.5.1.6 Synthesis of HC≡C-PEG-TATE (22):



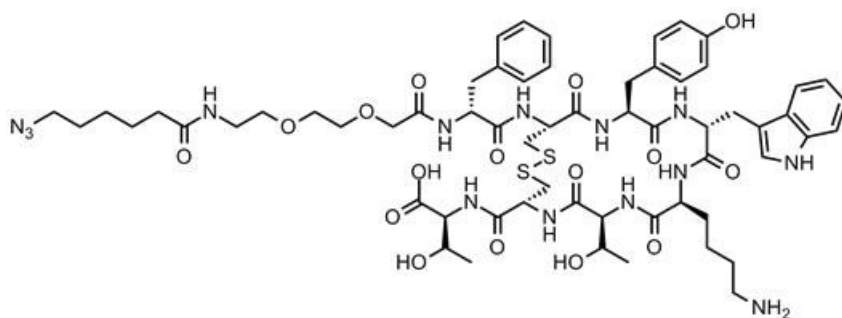
HC≡C-PEG-TATE was synthesized using Fmoc solid-phase peptide synthesis from Tyr³-octreotate on solid support with Fmoc-8-amino-3,6-dioxaoctanoic acid and 5-hexynoic acid as building blocks. 45% yield. $R_{t(\text{purification})} = 20.2$ min. HRMS (MALDI-TOF, m/z) for $C_{61}H_{82}N_{11}O_{16}S_2^+$ $[M+H]^+$ (calc'd): 1288.54 (1288.54).

4.5.1.7 Synthesis of N₃-TATE (23):



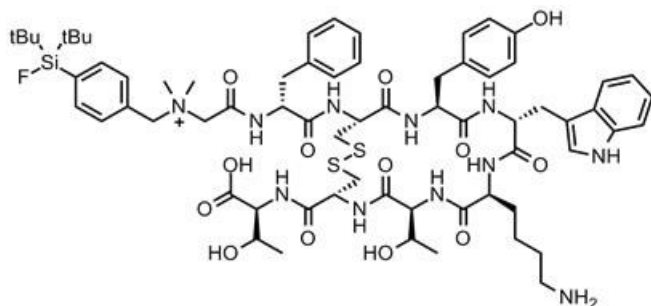
N₃-TATE was synthesized using Fmoc solid-phase peptide synthesis from Tyr³-octreotate on solid support with 6-azidohexanoic acid as building block. 20% yield. $R_{t(\text{purification})} = 21.3$ min. HRMS (MALDI-TOF, m/z) for $C_{55}H_{74}N_{13}O_{13}S_2^+$ $[M+H]^+$ (calc'd): 1188.46 (1188.50).

4.5.1.8 Synthesis of N₃-PEG-TATE (24):



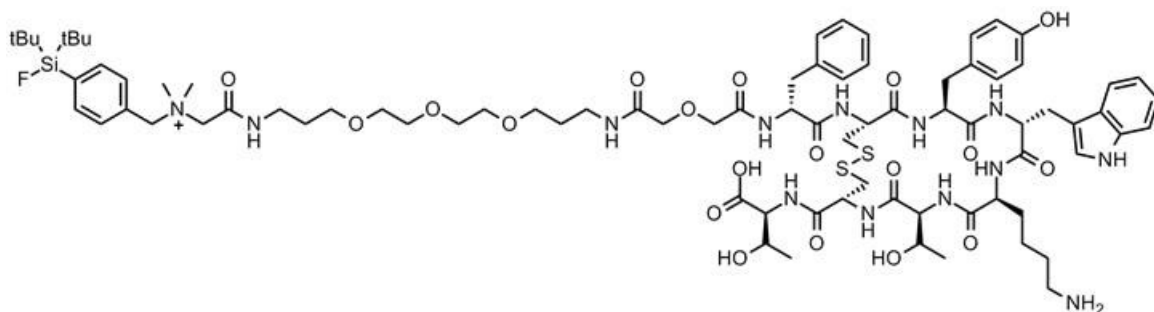
N₃-PEG-TATE was synthesized using Fmoc solid-phase peptide synthesis from Tyr³-octreotate on solid support with Fmoc-8-amino-3,6-dioxaoctanoic acid and 6-azidohexanoic acid as building blocks. 23% yield. $R_{t(\text{purification})} = 20.1$ min. HRMS (MALDI-TOF, m/z) for $C_{61}H_{85}N_{14}O_{16}S_2^+$ $[M+H]^+$ (calc'd): 1333.52 (1333.57).

4.5.1.9 Synthesis of SiFA⁺-C(O)NH-TATE (25):



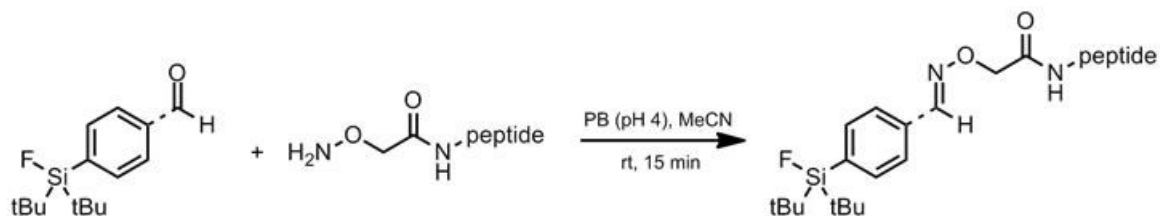
SiFA⁺-C(O)NH-TATE was synthesized using Fmoc solid-phase peptide synthesis from Tyr³-octreotate on solid support with SiFA⁺-CO₂H as building block. 34% yield. $R_{t(\text{purification})} = 23.1$ min. HRMS (MALDI-TOF, m/z) for C₆₈H₉₅FN₁₁O₁₃S₂Si⁺ [M]⁺ (calc'd): 1384.79 (1384.63).

4.5.1.10 Synthesis of SiFA⁺-C(O)NH-PEG₂-TATE (26):



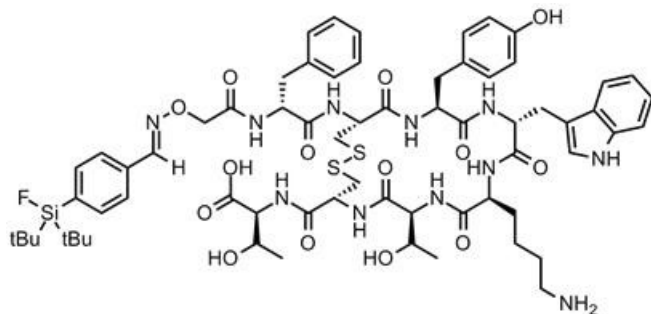
SiFA⁺-C(O)NH-PEG₂-TATE was synthesized using Fmoc solid-phase peptide synthesis from Tyr³-octreotate on solid support with Fmoc-NH-PEG₂-COOH (20 atoms) and SiFA⁺-CO₂H as building blocks. 8% yield. $R_{t(\text{purification})} = 23.0$ min. HRMS (MALDI-TOF, m/z) for C₈₂H₁₂₁FN₁₃O₁₉S₂Si⁺ [M]⁺ (calc'd): 1703.20 (1702.81).

4.5.2 Chemoselective oxime ligation: *General procedure for the synthesis of SiFA-TATE (27), SiFA⁺-aldehyde-AO-TATE (28), and SiFA⁺-aldehyde-AO-PEG-TATE (29).*



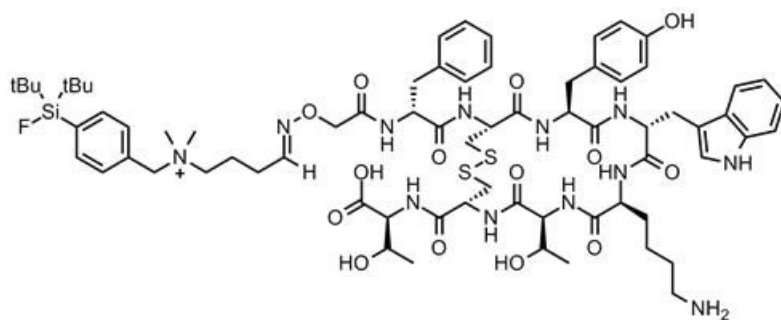
Synthesis via aldehyde-aminooxy condensation according to the following general procedure: a solution of the aminooxy-containing peptide (1.7-10.1 μmol) in phosphate buffer (200 μL , 0.25M, pH 4) and acetonitrile (200 μL) was added to a solution of the aldehyde-containing SiFA synthon (2.5-31.9 μmol ; 1.1-3.2 eq) in acetonitrile (100 μL) with subsequent addition of phosphate buffer (100 μL , 0.5M, pH 4). The reaction was left standing without stirring at room temperature for 15 min and purified by semi-preparative HPLC (0-100% MeCN + 0.1% TFA in 30 min gradient) to afford the desired peptide as a white solid after lyophilisation.

4.5.2.1 Synthesis of SiFA-TATE (27):



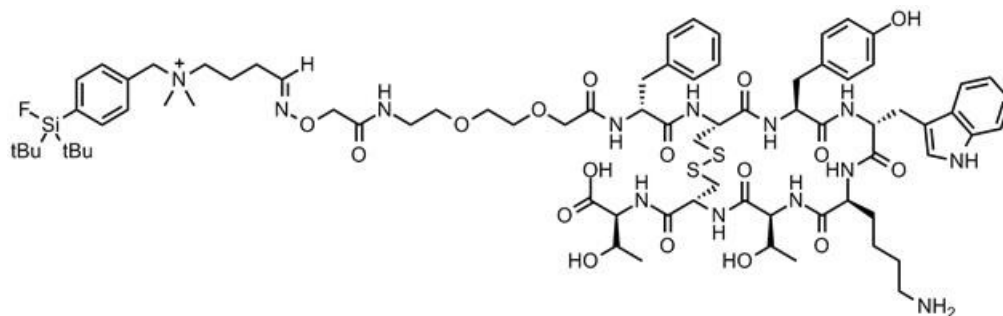
SiFA-TATE was synthesized via aldehyde-aminooxy condensation from SiFA-aldehyde (SiFA-A) and AO-TATE. 55% yield. $R_{t(\text{purification})} = 25.5$ min. HRMS (MALDI-TOF, m/z) for $C_{66}H_{89}FN_{11}O_{14}S_2Si^+$ $[M+H]^+$ (calc'd): 1370.61 (1370.58). Characterization data is in agreement with literature values^[105].

4.5.2.2 Synthesis of SiFA⁺-aldehyde-AO-TATE (28):



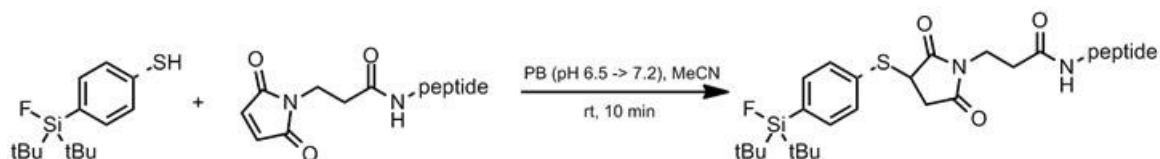
SiFA⁺-aldehyde-AO-TATE was synthesized via aldehyde-aminooxy condensation from SiFA⁺-aldehyde (SiFA⁺-CHO) and AO-TATE. 48% yield. $R_{t(\text{purification})} = 22.7$ min. HRMS (MALDI-TOF, m/z) for $C_{72}H_{102}FN_{12}O_{14}S_2Si^+$ $[M]^+$ (calc'd): 1469.71 (1469.68).

4.5.2.3 Synthesis of SiFA⁺-aldehyde-AO-PEG-TATE (29):



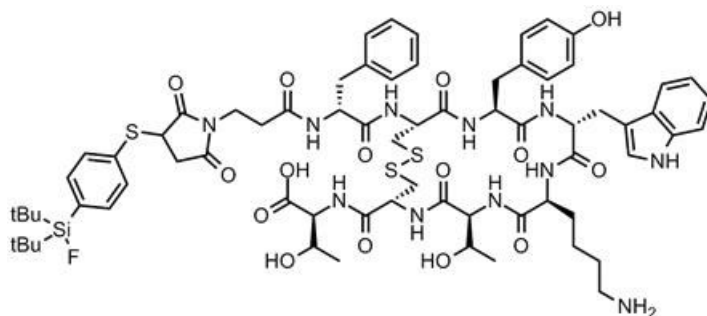
SiFA⁺-aldehyde-AO-PEG-TATE was synthesized via aldehyde-aminooxy condensation from SiFA⁺-aldehyde (SiFA⁺-CHO) and AO-PEG-TATE. 64% yield. $R_{t(\text{purification})} = 22.6$ min. HRMS (MALDI-TOF, m/z) for $C_{78}H_{113}FN_{13}O_{17}S_2Si^+$ $[M]^+$ (calc'd): 1615.00 (1614.76).

4.5.3 Thiol-maleimide coupling: *General procedure for the synthesis of SiFA-thiol-MI-TATE (30) and SiFA⁺-thiol-MI-TATE (31).*



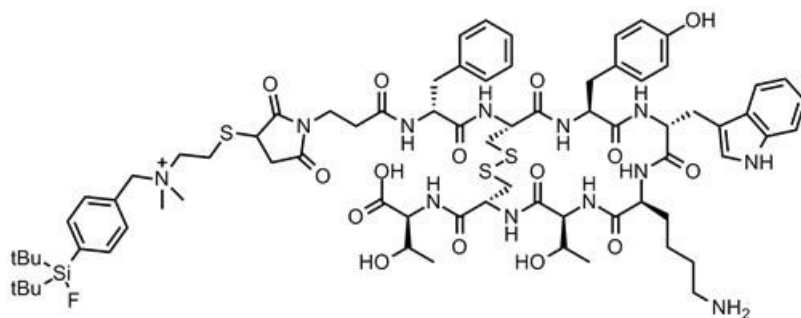
Synthesis via thiol-maleimide coupling according to the following general procedure: a solution of the maleimide-containing peptide (0.5-5.3 μmol) in phosphate buffer (200 μL , 0.1M, pH 6.5) and acetonitrile (200 μL) was added to a solution of the thiol-containing SiFA synthon (2.8-11.9 μmol ; 2.0-5.5 eq) in phosphate buffer (200 μL , 0.1M, pH 6.5) and acetonitrile (200 μL) with subsequent addition of phosphate buffer (200 μL , 0.5M, pH 7.2). The reaction was left standing without stirring at room temperature for 10 min and purified by semi-preparative HPLC (0-100% MeCN + 0.1% TFA in 30 min gradient) to afford the desired peptide as a white solid after lyophilisation.

4.5.3.1 Synthesis of SiFA-thiol-MI-TATE (30):



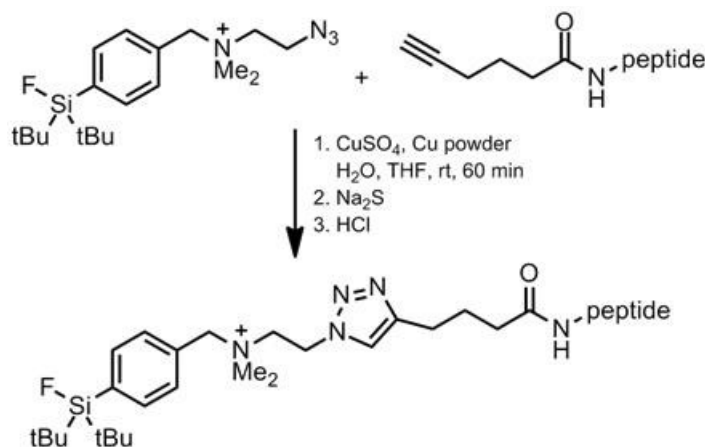
SiFA-thiol-MI-TATE was synthesized via thiol-maleimide coupling from SiFA-SH and MI-TATE. 43% yield. $R_{t(\text{purification})} = 26.2$ min. HRMS (MALDI-TOF, m/z) for $\text{C}_{70}\text{H}_{93}\text{FN}_{11}\text{O}_{15}\text{S}_3\text{Si}^+$ $[\text{M}+\text{H}]^+$ (calc'd): 1470.35 (1470.58).

4.5.3.2 Synthesis of SiFA⁺-thiol-MI-TATE (31):



SiFA⁺-thiol-MI-TATE was synthesized via thiol-maleimide coupling from SiFA⁺-SH and MI-TATE. 85% yield. $R_{t(\text{purification})} = 22.6$ min. HRMS (MALDI-TOF, m/z) for $\text{C}_{75}\text{H}_{104}\text{FN}_{12}\text{O}_{15}\text{S}_3\text{Si}^+$ $[\text{M}]^+$ (calc'd): 1555.68 (1555.67).

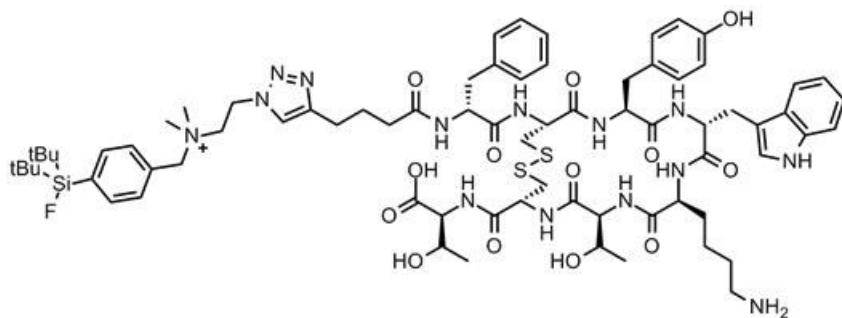
4.5.4 Huisgen 1,3-dipolar cycloaddition: *General procedure for the synthesis of SiFA⁺-azide-alkyne-TATE (32), SiFA⁺-azide-alkyne-PEG-TATE (33), SiFA⁺-alkyne-azide-TATE (34), and SiFA⁺-alkyne-azide-PEG-TATE (35).*



Synthesis via Huisgen 1,3-dipolar cycloaddition according to the following general procedure: a solution of the azide- or alkyne-containing peptide (1.6-4.4 μmol) in H₂O (375 μL) and THF (375 μL) was added to the complementary alkyne- or azide-containing SiFA synthon (3.1-6.3 μmol ; 1.2-2.0 eq), with subsequent addition of a CuSO₄ solution (110 μL , 0.1M, 11 μmol) and copper powder (10 mg). The reaction was left under mechanical shaker for 60 min, with subsequent removal of the solids by centrifugation (14,500 rpm, 5 min). Addition of a Na₂S solution (22 μmol , 4.8 mg Na₂S•9H₂O in 100 μL H₂O) to the supernatant resulted in the formation of a black precipitate that was removed by centrifugation (14,500 rpm, 5 min). The resulting supernatant was left to stand for 15 min without stirring, and subsequently treated with an aqueous HCl solution (100 μL , 2M) and

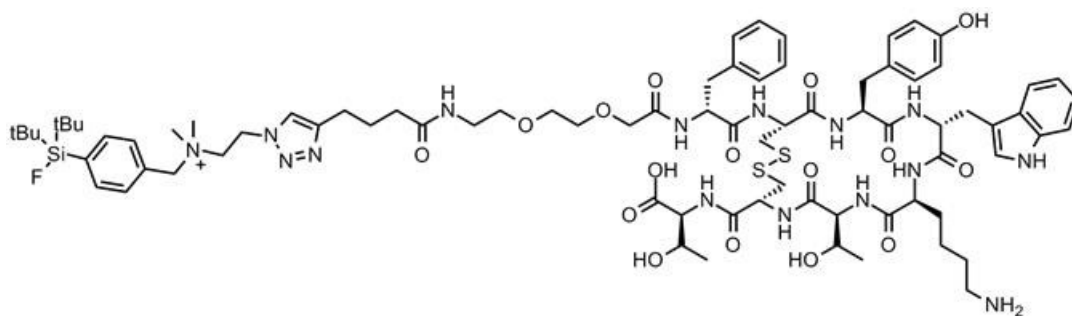
purified by semi-preparative HPLC (0-100% MeCN + 0.1% TFA in 30 min gradient) to afford the desired peptide as a white solid after lyophilisation.

4.5.4.1 Synthesis of SiFA⁺-azide-alkyne-TATE (32):



SiFA⁺-azide-alkyne-TATE was synthesized via azide-alkyne Huisgen cycloaddition from SiFA⁺-N₃ and alkyne-TATE. 25% yield. $R_{t(\text{purification})} = 23.2$ min. HRMS (MALDI-TOF, m/z) for C₇₄H₁₀₄FN₁₄O₁₃S₂Si⁺ [M]⁺ (calc'd): 1507.71 (1507.71).

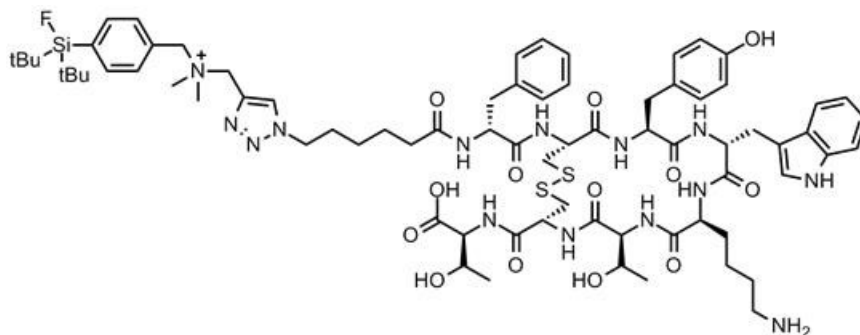
4.5.4.2 Synthesis of SiFA⁺-azide-alkyne-PEG-TATE (33):



SiFA⁺-azide-alkyne-PEG-TATE was synthesized via azide-alkyne Huisgen cycloaddition from SiFA⁺-N₃ and alkyne-PEG-TATE. 19% yield. $R_{t(\text{purification})} = 22.3$

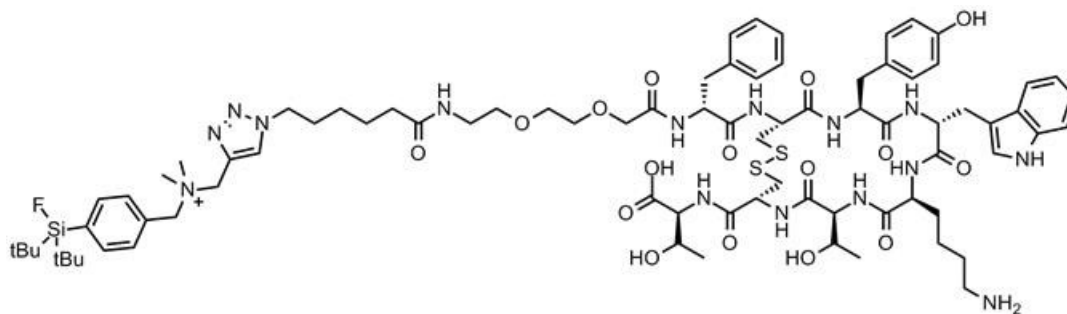
min. HRMS (MALDI-TOF, m/z) for $C_{80}H_{115}FN_{15}O_{16}S_2Si^+$ $[M]^+$ (calc'd): 1652.42 (1652.78).

4.5.4.3 Synthesis of SiFA⁺-alkyne-azide-TATE (34):



SiFA⁺-alkyne-azide-TATE was synthesized via alkyne-azide Huisgen cycloaddition from SiFA⁺-C≡CH and azide-TATE. 19% yield. $R_{t(\text{purification})}$ = 23.1 min. HRMS (MALDI-TOF, m/z) for $C_{75}H_{106}FN_{14}O_{13}S_2Si^+$ $[M]^+$ (calc'd): 1521.75 (1521.73).

4.5.4.4 Synthesis of SiFA⁺-alkyne-azide-PEG-TATE (35):



SiFA⁺-alkyne-azide-PEG-TATE was synthesized via alkyne-azide Huisgen cycloaddition from SiFA⁺-C≡CH and azide-PEG-TATE. 20% yield. $R_{t(\text{purification})}$ =

23.1 min. HRMS (MALDI-TOF, m/z) for $C_{81}H_{117}FN_{15}O_{16}S_2Si^+$ $[M]^+$ (calc'd): 1666.47 (1666.80).

4.6 Radiolabeling

4.6.1 Preparation of a stock solution containing $[^{18}F]F^-$ /Kryptofix 2.2.2/ K^+ complex for peptide labeling.

$[^{18}F]F^-$ was produced by a $^{18}O(p,n)^{18}F$ nuclear reaction on an enriched $[^{18}O]H_2O$ (purity >97%) target. The resulting aqueous $[^{18}F]F^-$ was loaded onto a Waters QMA ion exchange cartridge and eluted with a mixture of acetonitrile (1 mL), water (9 μ L), potassium oxalate solution (0.1 M, 9 μ L), and Kryptofix® 2.2.2 (3.3 mg). The solvents were removed by coevaporation to dryness under reduced pressure (600 mbar) using a stream of argon at 100°C for 5 min. The drying step was repeated twice with CH_3CN (1 mL, 5 min) and full vacuum (<10 mbar) was applied in the final drying step (3 min). The dried $[^{18}F]K(K_{222})F$ complex was dissolved in anhydrous CH_3CN (1 mL) and left to cool to room temperature on standing for use as stock solution in subsequent labeling reactions.

4.6.2 Radiosynthesis of SiFA⁺-C(O)NH-TATE (25), SiFA⁺-C(O)NH-PEG₂-TATE (26), SiFA-TATE (27), SiFA⁺-aldehyde-AO-TATE (28), SiFA⁺-aldehyde-AO-PEG-TATE (29), and SiFA⁺-thiol-MI-TATE (31).

The stock solution containing [¹⁸F]F-/Kryptofix 2.2.2/K⁺ complex (475 μ L; 2.4-13.8 mCi) was added to a solution of peptide in anhydrous CH₃CN (25 μ L of a 1 mmol/L stock solution). The mixture was left standing without stirring for 5 min at 0°C (ice bath). Completion of reaction was confirmed by analytical radio-HPLC (0:100 eluent A/B to 100:0 eluent A/B in 40 min gradient). Subsequently, the reaction mixture was added to aqueous H₃PO₄ (0.01 M, pH 4.7, 9 mL) and loaded onto a Waters SepPak C-18 light cartridge, pre-conditioned by elution/washing with methanol (5 mL) followed by water (10 mL). The trapped [¹⁸F]SiFA peptide was washed with water (5 mL) and gently eluted from the cartridge with wet 1-octanol (1 mL). Subsequent centrifugation at 14 000 rpm for 2 min and isolation of the organic phase afforded a solution of the labeled peptide in 1-octanol that was used for lipophilicity evaluation without further purification.

4.6.3 Lipophilicity

The above radiolabeled peptide solution in 1-octanol (750 μ L) was added to phosphate buffer (0.05 M, pH 7.4, 750 μ L), and the mixture was vigorously vortexed for 5 min. After subsequent centrifugation at 14 000 rpm for 5 min, an aliquot of 500 μ L was taken from each phase and measured in a gamma-counter.

Chapter 5: SUMMARY AND CONCLUSIONS

We have successfully demonstrated the utility of [^{11}C]MeOTf towards the direct, one-step, and regioselective labeling of peptides at the side-chain of cysteine residues. In particular, the radiosyntheses of [^{11}C]GSMe and Trp-Tyr-Trp-Ser-Arg-Cys([^{11}C]Me)-Lys-Trp-Thr-Gly were performed under ambient temperatures (20°C) and short reaction times, on the order of seconds. In addition, we extend this method towards the synthesis of [^{11}C]Cys(Me)-[Tyr³-octreotate] as a demonstration of its applicability to peptides of biological interest. This octreotate derivative was obtained in non-decay-corrected radiochemical yields of $11\pm 2\%$ ($n=3$) with a synthesis time of approx. 30 min.

The inclusion of a permanent cationic charge (quaternary ammonium functional group) onto the SiFA moiety has also provided for the development of a variety of building blocks: SiFA⁺-SH (**6**), SiFA⁺-CHO (**8**), SiFA⁺-MI (**10**), SiFA⁺-N₃ (**12**), SiFA⁺-C \equiv CH (**13**), and SiFA⁺-CO₂H (**16**). These were easily synthesized in one or two steps from the common precursor SiFA-Br (**3**). These building blocks contain functional groups amenable to peptide bioconjugation, and even for direct solid-phase peptide synthesis for SiFA⁺-CO₂H (**16**). The cationic SiFA building blocks were shown to be compatible with most bioconjugation reaction conditions, except for Huisgen 1,3-dipolar cycloaddition, where partial SiFA hydrolysis was observed. The cationic SiFA-peptide conjugates SiFA⁺-C(O)NH-

TATE (25), SiFA⁺-C(O)NH-PEG₂-TATE (26), SiFA⁺-aldehyde-AO-TATE (28), SiFA⁺-aldehyde-AO-PEG-TATE (29), and SiFA⁺-thiol-MI-TATE (31) along with the previously reported^[105] SiFA-TATE (27) were labeled in a one-step by treatment with anhydrous [¹⁸F]F-/Kryptofix 2.2.2/K⁺ complex at room temperature for 5 min.

Lipophilicity determination by shake-flask method revealed a decrease in lipophilicity for the above radiolabeled quaternary ammonium-containing conjugates (logD_{7.4} between 0.43 and 2.19) compared to uncharged [¹⁸F]27. In particular, peptides [¹⁸F]26 and [¹⁸F]29, bearing a hydrophilic PEG linker alongside the cationic SiFA moiety exhibit a significant reduction in lipophilicity (logD_{7.4} 0.92 and 0.43, respectively) whereas [¹⁸F]25, containing a very short linker region, was only modestly more hydrophilic than [¹⁸F]27 (logD_{7.4} 2.19 versus 2.68, respectively). This suggests that the combination of cationic SiFA moiety along with a long hydrophilic linker is a promising strategy to tune physicochemical properties, and hence, pharmacokinetic properties of the target tracer peptide. In fact, very recent investigations into the combination of the cationic SiFA moiety developed herein and carbohydrate/PEG linkers described previously^[156] on Tyr³-octreotate have shown greatly reduced lipophilicities (LogD_{7.4} ranging from -1.21 to -1.39), excellent plasma stabilities (>98% after 120 min at 37°C), and favorable *in vivo* mice PET scan images with hot spots in the kidneys, the bladder, and the target tumor^[222]. This validates the quaternary

ammonium functional group as an effective strategy, when combined with hydrophilic linkers, to reduce or eliminate undesirable nonspecific hepatic binding prevalent in previously published PET scan data on SiFA-peptide conjugates.

Overall, the labeling of peptides with [^{11}C]MeOTf (directly) and anhydrous [^{11}F]fluoride (via cationic SiFA moiety) has shown to proceed efficiently at room temperature and short reaction times, on the order of seconds or minutes. In particular, [^{18}F]labeling of cationic SiFA-peptide conjugates has produced peptides displaying improved hydrophilic profiles compared to first-generation (uncharged) conjugates. These developments present a response to the pressing need for facile radiolabeling methods in the production of peptidic PET radiopharmaceuticals, an important topic of current research. These simplified methodologies also can be translated to automated synthetic modules, essential for scaling-up starting radioactivity levels, and hence greater number of doses per synthetic run. We are currently investigating solutions for broadening the library of bioactive peptides amenable to these types of labeling to include bombesin, cholecystokinin/gastrin, neurotensin, and RGD (Arg-Gly-Asp), which are of great interest in diagnostic oncology.

Chapter 6: LITERATURE CITED

- (1) Bailey, D.L.; Townsend, D.W.; Valk, P.E.; Maisey, M.N. *Positron Emission Tomography: Basic Sciences*. – London: Springer-Verlag, **2005**.
- (2) Deutsch, M. *Phys. Rev.* **1951**, *82*, 455-456.
- (3) Bybel, B.; Brunken, R.C.; Shah, S.N.; Wu, G.; Turbner, E.; Neumann, D.R. *Clev. Clin. J. Med.* **2006**, *73*, 1075-1087.
- (4) Melcher, C.L. *J. Nucl. Med.* **2000**, *41*, 1051-1055.
- (5) Gambhir, S.S. *Nat. Rev. Cancer* **2002**, *2*, 683-693.
- (6) Levin, C.S. *Eur. J. Nucl. Med. Mol. Imaging* **2005**, *32*, S325-S345.
- (7) Muehllehner, G.M.; Karp, J.S. *Phys. Med. Biol.*, **2006**, *51*, R117-R137.
- (8) Frackowiak, R.S.J.; Lenzi, G.L.; Jones, T.; Heather, J.D. *J. Comput. Assist. Tomogr.* **1980**, *4*, 727-736. [
- (9) Huang, S.C.; Carson, R.E.; Hoffman, E.J.; Carson, J.; MacDonald, N.; Barrio, J.R.; Phelps, M.E. *J. Cereb. Blood Flow Metab.* **1983**, *3*, 141-153.
- (10) Schelbert, H.R.; Phelps, M.E.; Huang, S.C.; MacDonald, N.S.; Hansen, H.; Selin, C.; Kuhl, D.E. *Circulation* **1981**, *63*, 1259-1272.
- (11) Scott, P.J.H. *Angew. Chem. Int. Ed.* **2009**, *48*, 6001-6004.
- (12) Bjurling, P.; Antoni, G.; Watanabe, Y.; Långström, B. *Acta Chem. Scand.* **1990**, *44*, 178-182.
- (13) Bjurling, P.; Watanabe, Y.; Oka, S.; Nagasawa, T.; Yamada, H.; Långström, B. *Acta Chem. Scand.* **1990**, *44*, 183-188.

- (14) Popkov, A.; Blahutová, A.; Kaňová, M. *J. Label. Compd. Radiopharm.* **2007**, *50*, 528-529.
- (15) Böhm, H.J.; Banner, D.; Bendels, S.; Kansy, M.; Kuhn, B.; Müller, K.; Obst-Sander, U.; Stahl, M. *ChemBioChem* **2004**, *5*, 637-643.
- (16) Müller, K.; Faeh, C.; Diederich, F. *Science* **2007**, *317*, 1881-1886.
- (17) Burns, H.D.; Hamill, T.G.; Eng, W.-S.; Francis, B.; Fioravanti, C.; Gibson, R.E. *Curr. Opin. Chem. Biol.* **1999**, *3*, 388-394.
- (18) Nicolaou, K.C.; Montagnon, T. *Molecules that Changed the World.* – Weinheim, Germany: Wiley-VCH, **2008**.
- (19) O'Hagan, D. *J. Fluorine Chem.* **2010**, *131*, 1071-1081.
- (20) Isanbor, C.; O'Hagan, D. *J. Fluorine Chem.* **2006**, *127*, 303-319.
- (21) Bégué, J.-P.; Bonnet-Delphon, D. *J. Fluorine Chem.* **2006**, *127*, 992-1012.
- (22) Phelps, M.E. *J. Nucl. Med.* **2000**, *41*, 661-681.
- (23) Phelps, M.E. *Proc. Natl. Acad. Sci. USA* **2000**, *97*, 9226-9233.
- (24) Rigo, P.; Paulus, P.; Kaschten, B.J.; Hustinx, R.; Bury, T.; Jerusalem, G.; Benoit, T.; Foidart-Willems, J. *Eur. J. Nucl. Med.* **1996**, *23*, 1641-1674.
- (25) Beyer, T.; Townsend, D.W.; Brun, T.; Kinahan, P.E.; Charron, M.; Roddy, R.; Jerin, J.; Young, J.; Byars, L.; Nutt, R. *J. Nucl. Med.* **2000**, *41*, 1369-1379.
- (26) Townsend, D.W.; Cherry, S.R. *Eur. Radiol.* **2001**, *11*, 1968-1974.

- (27) Weber, W.A.; Grosu, A.L.; Czernin, J. *Nat. Clin. Pract. Oncol.* **2008**, *5*, 160-170.
- (28) Lauritsen, C.C.; Crane, H.R.; Harper, W.W. *Science*, **1934**, *79*, 234-235.
- (29) Crane, H.R.; Lauritsen, C.C. *Phys. Rev.* **1934**, *45*, 430-432.
- (30) Crane, H.R.; Lauritsen, C.C. *Phys. Rev.* **1934**, *45*, 497-498.
- (31) Yost, D.M.; Ridenour, L.N.; Shinohara, K. *J. Chem. Phys.* **1935**, *3*, 133-136.
- (32) Barkas, W.H. *Phys. Rev.* **1939**, *56*, 287.
- (33) Audi, G.; Bersillon, O.; Blachot, J.; Wapstra, A.H. *Nucl. Phys. A* **2003**, *729*, 3-128.
- (34) Ruben, S.; Hassid, W.Z.; Kamen, M.D. *J. Am. Chem. Soc.* **1939**, *61*, 661-663.
- (35) Tobias, C.A.; Lawrence, J.H.; Roughton, F.J.W.; Root, W.S.; Gregersen, M.I. *Am. J. Physiol.* **1945**, *145*, 253-263.
- (36) Brady, F.; Clark, J.C.; Luthra, S.K. *J. Label. Compd. Radiopharm.* **2007**, *50*, 903-926.
- (37) Christman, D.R.; Finn, R.D.; Karlstrom, K.I.; Wolf, A.P. *Int. J. Appl. Radiat. Isot.* **1975**, *26*, 435-442.
- (38) Miller, P.W.; Long, N.J.; Vilar, R.; Gee, A.D. *Angew. Chem. Int. Ed.* **2008**, *47*, 8998-9033.
- (39) Buchanan, J.M.; Hastings, A.B.; Nesbitt, F.B. *J. Biol. Chem.* **1943**, *150*, 413-425.

- (40) Pike, V.W.; Eakins, M.N.; Allan, R.M.; Selwyn, A.P. *Int. J. Appl. Radiat. Isot.* **1982**, *33*, 505-512.
- (41) Hooker, J.M.; Reibel, A.T.; Hill, S.M.; Schueller, M.J.; Fowler, J.S. *Angew. Chem. Int. Ed.* **2009**, *48*, 3482-3485.
- (42) Wilson, A.A.; Garcia, A.; Houle, S.; Vasdev, N. *Org. Biomol. Chem.* **2010**, *8*, 428-432.
- (43) Rotstein, B.H.; Liang, S.H.; Holland, J.P.; Collier, T.L.; Hooker, J.M.; Wilson, A.A.; Vasdev, N. *Chem. Commun.* **2013**, *49*, 5621-5629.
- (44) Marazano, C.; Maziere, M.; Berger, G.; Comar, D. *Int. J. Appl. Radiat. Isot.* **1977**, *28*, 49-52.
- (45) Jewett, D.M. *Appl. Radiat. Isot.* **1992**, *43*, 1383-1385.
- (46) Långström, B.; Lundqvist, H. *Int. J. Appl. Radiat. Isot.* **1976**, *27*, 357-363.
- (47) Friedland, R.P.; Mathis, C.A.; Budinger, T.F.; Moyer, B.R.; Rosen, M. *J. Nucl. Med.* **1983**, *24*, 812-815.
- (48) Burns, H.D.; Dannals, R.F.; Långström, B.; Ravert, H.T.; Zemyan, S.E.; Duelfer, T.; Wong, D.F.; Frost, J.J.; Kuhar, M.J.; Wagner, H.N. *J. Nucl. Med.* **1984**, *25*, 222-1227.
- (49) Maziere, M.; Hantraye, P.; Prenant, C.; Sastre, J.; Comar, D. *Int. J. Appl. Radiat. Isot.* **1984**, *35*, 973-976.
- (50) Dannals, R.F.; Ravert, H.T.; Frost, J.J.; Wilson, A.A.; Burns, H.D.; Wagner, Jr., H.N. *Int. J. Appl. Radiat. Isot.* **1985**, *36*, 303-306.

- (51) Farde, L.; Ehrin, E.; Eriksson, L.; Greitz, T.; Hall, H.; Hedström, C.-G.; Litton, J.-E.; Sedvall, G. *Proc. Natl. Acad. Sci.* **1985**, *82*, 3863-3867.
- (52) Kilbourn, M.R.; Snyder, S.E.; Sherman, P.S.; Kuhl, D.E. *Synapse* **1996**, *22*, 123-131.
- (53) Snyder, S.E.; Tluczek, L.; Jewett, D.M.; Nguyen, T.B.; Kuhl, D.E.; Kilbourn, M.R. *Nucl. Med. Biol.* **1998**, *25*, 751-754.
- (54) Mathis, C.A.; Wang, Y.; Holt, D.P.; Huang, G.-F.; Debnath, M.L.; Klunk, W.E. *J. Med. Chem.* **2003**, *46*, 2740-2754.
- (55) Klunk, W.E.; Engler, H.; Nordberg, A.; Wang, Y.; Blomqvist, G.; Holt, D.P.; Bergström, M.; Savitcheva, I.; Huang, G.-F.; Estrada, S.; Ausén, B.; Debnath, M.L.; Barletta, J.; Price, J.C.; Sandell, J.; Lopresti, B.J.; Wall, A.; Koivisto, P.; Antoni, G.; Mathis, C.A.; Långström, B. *Ann. Neurol.* **2004**, *55*, 306-319.
- (56) Reiffers, S.; Vaalburg, W.; Wiegman, T.; Wynberg, H.; Woldring, M.G. *Int. J. Appl. Radiat. Isot.* **1980**, *31*, 535-539.
- (57) Jacobson, O.; Mishani, E. *Appl. Radiat. Isot.* **2008**, *66*, 188-193.
- (58) Hosoya, T.; Sumi, K.; Doi, H.; Wakao, M.; Suzuki, M. *Org. Biomol. Chem.* **2006**, *4*, 410-415.
- (59) Hostetler, E.D.; Terry, G.E.; Burns, H.D. *J. Label. Compd. Radiopharm.* **2005**, *48*, 629-634.
- (60) Lidström, P.; Kihlberg, T.; Långström, B. *J. Chem. Soc., Perkin Trans. 1* **1997**, 2701-2706.

- (61) Karimi, F.; Barletta, J.; Långström, B. *Eur. J. Org. Chem.* **2005**, 2374-2378.
- (62) Eriksson, J.; Åberg, O.; Långström, B. *Eur. J. Org. Chem.* **2007**, 455-461.
- (63) Snell, A.H. *Phys. Rev.* **1937**, *51*, 143.
- (64) De Kleijn, J.P. *J. Fluorine Chem.* **1977**, *10*, 31-350.
- (65) Hawkins, R.A.; Choi, Y.; Huang, S.-C.; Hoh, C.K.; Dahlbom, M.; Schiepers, C.; Satyamurthy, N.; Barrio, J.R.; Phelps, M.E. *J. Nucl. Med.* **1992**, *33*, 633-642.
- (66) Schirmacher, R.; Wängler, C.; Schirmacher, E. *Mini-Rev. Org. Chem.* **1997**, *4*, 317-329.
- (67) Fowler, J.S.; Wolf, A.P. *Acc. Chem. Res.* **1997**, *30*, 181-188.
- (68) Bolton, R. *J. Label. Compd. Radiopharm.* **2002**, *45*, 485-528.
- (69) Elsinga, P.H. *Methods* **2002**, *27*, 208-217.
- (70) Lasne, M.-C.; Perrio, C.; Rouden, J.; Barré, L.; Roeda, D.; Dolle, F.; Crouzel, C. *Top. Curr. Chem.* **2002**, *222*, 201-258.
- (71) Glaser, M.; Luthra, S.K.; Brady, F. *Intl. J. Oncol.* **2003**, *22*, 253-267.
- (72) Adam, M.J.; Wilbur, D.S. *Chem. Soc. Rev.* **2005**, *34*, 153-163.
- (73) Le Bars, D. *J. Fluorine Chem.* **2006**, *127*, 1488-1493.
- (74) Miller, P.W.; Long, N.J.; Vilar, R.; Gee, A.D. *Angew. Chem. Int. Ed.* **2008**, *47*, 8998-9033.
- (75) Cai, L.; Lu, S.; Pike, V.W. *Eur. J. Org. Chem.* **2008**, 2853-2873.

- (76) Ametamey, S.M.; Honer, M.; Schubiger, P.A. *Chem. Rev.* **2008**, *108*, 1501-1516.
- (77) Alauddin, M.M. *Am. J. Nucl. Med. Mol. Imaging* **2012**, *2*, 55-76.
- (78) *Cyclotron produced radionuclides: physical characteristics and production methods*. – Vienna: International Atomic Energy Agency, **2009**.
- (79) Ruth, T.J.; Wolf, A.P. *Radiochim. Acta* **1979**, *26*, 21-24.
- (80) Casella, V.; Ido, T.; Wolf, A.P.; Fowler, J.S.; MacGregor, R.R.; Ruth, T.J. *J. Nucl. Med.* **1980**, *21*, 750-757.
- (81) Ehrenkaufer, R.E.; Potocki, J.F.; Jewitt, D.M. *J. Nucl. Med.* **1984**, *25*, 333-337.
- (82) Scott, P.J.H.; Littich, P. *Angew. Chem. Int. Ed.* **2012**, *51*, 1106-1109.
- (83) Teare, H.; Robins, E.G.; Kirjavainen, A.; Forsback, S.; Sandford, G.; Solin, O.; Luthra, S.K.; Gouverneur, V. *Angew. Chem. Int. Ed.* **2010**, *122*, 6973.
- (84) Hiller, A.; Fischer, C.; Jordanova, A.; Patt, J.T.; Steinbach, J. *Appl. Radiat. Isot.* **2008**, *66*, 152-157.
- (85) Lee, E.; Kamlet, A.S.; Powers, D.C.; Neumann, C.N.; Boursalian, G.B.; Furuya, T.; Choi, D.C.; Hooker, J.M.; Ritter, T. *Science* **2011**, *334*, 639.
- (86) Burgess, M.A. *Metal Ions in Solution*. – New York: John Wiley & Sons, **1978**.
- (87) Izatt, R.M.; Pawlak, K.; Bradshaw, J.S.; Bruening, R.L.; *Chem. Rev.* **1991**, *91*, 1721-2085.

- (88) Coenen, H.H.; Klatte, B.; Knöchel, A.; Schüller, M.; Stöcklin, G. *J. Labelled Compd. Radiopharm.* **1986**, *23*, 455-466.
- (89) Hamacher, K.; Coenen, H.H.; Stöcklin, G. *J. Nucl. Med.* **1986**, *27*, 235-238.
- (90) Jewitt, D.M.; Toorongian, S.A.; Mulholland, G.K.; Watkins, L.; Kilbourn, M.R. *Appl. Radiat. Isot.* **1988**, *39*, 1109-1111.
- (91) *The Merck Index*, 14th ed. "Hydrogen Fluoride", can be found under <https://themerckindex.cambridgesoft.com>, **2012**.
- (92) *The Merck Index*, 14th ed. "Acetonitrile", can be found under <https://themerckindex.cambridgesoft.com>, **2012**.
- (93) Dollé, F.; Helfenbein, J.; Hinnen, F.; Mavel, S.; Mincheva, Z.; Saba, W.; Schöllhorn-Peyronneau, M.-A.; Valette, H.; Garreau, L.; Chalon, S.; Halldin, C.; Madelmont, J.-C.; Deloye, J.-B.; Bottlaender, M.; Le Gaillard, J.; Guilloteau, D.; Emond, P. *J. Label. Compd. Radiopharm.* **2007**, *50*, 716-723.
- (94) Ahmed, N.; Langlois, R.; Rodrigue, S.; Bénard, F.; van Lier, J.E. *Nucl. Med. Biol.* **2007**, *34*, 459-464.
- (95) Ermert, J.; Hocke, C.; Ludwig, T.; Gail, R.; Coenen, H.H. *J. Label. Compd, Radiopharm.* **2004**, *47*, 429-441.
- (96) Kilbourn, M.R.; Welch, M.J.; Dence, C.S.; Tewson, T.J.; Saji, H.; Maeda, M. *Int. J. Appl. Radiat. Isot.* **1984**, *35*, 591-598.
- (97) Okarvi, S.M. *Eur. J. Nucl. Med.* **2001**, *28*, 929-938.
- (98) Okarvi, S.M. *Med. Res. Rev.* **2004**, *24*, 357-397.

- (99) Guhlke, S.; Coenen, H.H.; Stöcklin, G. *Appl. Radiat. Isot.* **1994**, *45*, 715-727.
- (100) Vaidyanathan, G.; Zalutsky, M.R. *Nat. Protoc.* **2006**, *1*, 1655-1661.
- (101) Scott, P.J.H.; Shao, X. *J. Label. Compd. Radiopharm.* **2010**, *53*, 586-591.
- (102) Wester H.-J.; Hamacher, K.; Stöcklin, G. *Nucl. Med. Biol.* **1996**, *23*, 365-372.
- (103) Vaidyanathan, G.; Zalutsky, M.R. *Nucl. Med. Biol.* **1995**, *22*, 759-764.
- (104) Poethko, T.; Schottelius, M.; Thumshirn, G.; Hersel, U.; Herz, M.; Henriksen, G.; Kessler, H.; Schwaiger, M.; Wester, H.-J. *J. Nucl. Med.* **2004**, *45*, 892-902.
- (105) Schottelius, M.; Poethko, T.; Herz, M.; Reubi, J.-C.; Kessler, H.; Schwaiger, M.; Wester, H.-J. *Clin. Cancer Res.* **2004**, *10*, 3593-3606.
- (106) Bruus-Jensen, K.; Poethko, T.; Schottelius, M.; Hauser, A.; Schwaiger, M.; Wester, H.-J. *Nucl. Med. Biol.* **2006**, *33*, 173-183.
- (107) Kolb, H.C.; Finn, M.G.; Sharpless, K.B. *Angew. Chem. Int. Ed.* **2001**, *40*, 2004-2021.
- (108) Marik, J.; Sutcliffe, J.L. *Tetrahedron Lett.* **2006**, *47*, 6681-6684.
- (109) Gill, H.S.; Marik, J. *Nat. Protoc.* **2011**, *6*, 1718-1725.
- (110) Brewer, G.J. *Clin. Neurophysiol.* **2010**, *121*, 459-460.
- (111) Ala, A.; Walker, A.P.; Ashkan, K.; Dooley, J.S.; Schilsky, M.L. *Lancet* **2007**, *369*, 397-408.

- (112) Debets, M.F.; van Berkel, S.S.; Schoffelen, S.; Rutjes, F.P.J.T.; van Hest, J.C.M.; van Delft, F.L. *Chem. Commun.* **2010**, *46*, 97.
- (113) Kuzmin, A.; Poloukhine, A.; Wolfert, M.A.; Popik, V.V. *Bioconjugate Chem.* **2010**, *21*, 2076.
- (114) Evans, H.L.; Slade, R.L.; Carroll, L.; Smith, G.; Nguyen, Q.-D.; Iddon, L.; Kamaly, N.; Stöckmann, H.; Leeper, F.J.; Aboagye, E.O.; Spivey, A.C. *Chem. Commun.* **2012**, *48*, 991-993.
- (115) Arumugam, S.; Chin, J.; Schirmacher, R.; Popik, V.V.; Kostikov, A.P. *Bioorg. Med. Chem. Lett.* **2011**, *21*, 6987-6991.
- (116) Campbell-Verduyn, L.S.; Mirfeizi, L.; Schoonen, A.K.; Dierckx, R.A.; Elsinga, P.H.; Feringa, B.L. *Angew. Chem. Int. Ed.* **2011**, *50*, 11117-11120.
- (117) Bouvet, V.; Wuest, M.; Wuest, F. *Org. Biomol. Chem.* **2011**, *9*, 7393-7399.
- (118) Studenov, A.R.; Adam, M.J.; Wilson, J.S.; Ruth, T.J. *J. Label. Compd. Radiopharm.* **2005**, *48*, 497-500.
- (119) Rosenthal, M.S.; Bosch, A.L.; Nickles, R.J.; Gatley, S.J. *Int. J. Appl. Radiat. Isot.* **1985**, *36*, 318-319.
- (120) Sanderson, R.T. *Chemical Bonds and Bond Energy*. – New York: Academic Press, **1976**.
- (121) Darwent, B. deB. *Bond Dissociation Energies in Simple Molecules*. – Washington, D.C.: NSRDS-NBS, **1970**.

- (122) Ting, R.; Adam, M.J.; Ruth, T.J.; Perrin, D.M. *J. Am. Chem. Soc.* **2005**, *127*, 13094-13095.
- (123) Harwig, C.W.; Ting, R.; Adam, M.J.; Ruth, T.J.; Perrin, D.M. *Tetrahedron Lett.* **2008**, *49*, 3152-3156.
- (124) Ting, R.; Lo, J.; Adam, M.J.; Ruth, T.J.; Perrin, D.M. *J. Fluorine Chem.* **2008**, *129*, 349-358.
- (125) Ting, R.; Harwig, C.W.; Lo, J.; Li, Y.; Adam, M.J.; Ruth, T.J.; Perrin, D.M. *J. Org. Chem.* **2008**, *73*, 4662-4670.
- (126) Ting, R.; Harwig, C.; auf dem Keller, U.; McCormick, S.; Austin, P.; Overall, C.M.; Adam, M.J.; Ruth, T.J.; Perrin, D.M. *J. Am. Chem. Soc.* **2008**, *130*, 12045-12055.
- (127) auf dem Keller, U.; Bellac, C.L.; Li, Y.; Lou, Y.; Lange, P.F.; Ting, R.; Harwig, C.; Kappelhoff, R.; Dedhar, S.; Adam, M.J.; Ruth, T.J.; Bénard, F.; Perrin, D.M.; Overall, C.M. *Cancer Res.* **2010**, *70*, 7562-7569.
- (128) Li, Y.; Ting, R.; Harwig, C.W.; auf dem Keller, U.; Bellac, C.L.; Lange, P.F.; Inkster, J.A.H.; Schaffer, P.; Adam, M.J.; Ruth, T.J.; Overall, C.M.; Perrin, D.M. *MedChemComm* **2011**, *2*, 942-949.
- (129) Elizarov, A.M.; van Dam, R.M.; Shin, Y.S.; Kolb, H.C.; Padgett, H.C.; Stout, D.; Shu, J.; Huang, J.; Daridon, A.; Heath, J.R. *J. Nucl. Med.* **2010**, *51*, 282-287.
- (130) Liu, Z.; Li, Y.; Lozada, J.; Schaffer, P.; Adam, M.J.; Ruth, T.J.; Perrin, D.M. *Angew. Chem. Int. Ed.* **2013**, *52*, 2303-2307.

- (131) Liu, Z.; Li, Y.; Lozada, J.; Pan, J.; Lin, K.-S.; Schaffer, P.; Perrin, D.M. *J. Label. Compd. Radiopharm.* **2012**, *55*, 491-496.
- (132) Li, Y.; Guo, J.; Tang, S.; Lang, L.; Chen, X.; Perrin, D.M. *Am. J. Nucl. Med. Mol. Imaging* **2013**, *3*, 44-56.
- (133) Li, Y.; Liu, Z.; Harwig, C.W.; Pourghiasian, M.; Lau, J.; Lin, K.-S.; Schaffer, P.; Benard, F.; Perrin, D.M. *Am. J. Med. Mol. Imaging* **2013**, *3*, 57-70.
- (134) McBride, W.J.; Sharkey, R.M.; Karacay, H.; D'Souza, C.A.; Rossi, E.A.; Laverman, P.; Chang, C.-H.; Boerman, O.C.; Goldenberg, D.M. *J. Nucl. Med.* **2009**, *50*, 991-998.
- (135) Laverman, P.; McBride, W.J.; Sharkey, R.M.; Eek, A.; Joosten, L.; Oyen, W.J.G.; Goldenberg, D.M.; Boerman, O.C. *J. Nucl. Med.* **2010**, *51*, 454-461.
- (136) McBride, W.J.; D'Souza, C.A.; Sharkey, R.M.; Karacay, H.; Rossi, E.A.; Chang, C.-H.; Goldenberg, D.M. *Bioconjugate Chem.* **2010**, *21*, 1331-1340.
- (137) D'Souza, C.A.; McBride, W.J.; Sharkey, R.M.; Todaro, L.J.; Goldenberg, D.M. *Bioconjugate Chem.* **2011**, *22*, 1793-1803.
- (138) Hoigebazar, L.; Jeong, J.M.; Lee, J.-Y.; Shetty, D.; Yang, B.Y.; Lee, Y.-S.; Lee, D.S.; Chung, J.-K.; Lee, M.C. *J. Med. Chem.* **2012**, *55*, 3155-3162.
- (139) McBride, W.J.; D'Souza, C.A.; Sharkey, R.M.; Goldenberg, D.M. *Appl. Radiat. Isot.* **2012**, *70*, 200-204.

- (140) Dijkgraaf, I.; Franssen, G.M.; McBride, W.J.; D'Souza, C.A.; Laverman, P.; Smith, C.J.; Goldenberg, D.M.; Oyen, W.J.G.; Boerman, O.C. *J. Nucl. Med.* **2012**, *53*, 947-952.
- (141) Laverman, P.; D'Souza, C.A.; Eek, A.; McBride, W.J.; Sharkey, R.M.; Oyen, W.J.G.; Goldenberg, D.M.; Boerman, O.C. *Tumor Biol.* **2012**, *33*, 427-434.
- (142) McBride, W.J.; D'Souza, C.A.; Karacay, H.; Sharkey, R.M.; Goldenberg, D.M. *Bioconjugate Chem.* **2012**, *23*, 538-547.
- (143) Mu, L.; Höhne, A.; Schubiger, P.A.; Ametamey, S.M.; Graham, K.; Cyr, J.E.; Dinkelborg, L.; Stellfeld, T.; Srinivasan, A.; Voightmann, U.; Klar, U. *Angew. Chem. Int. Ed.* **2008**, *47*, 4922-4925.
- (144) Höhne, A.; Yu, Lian.; Mu, L.; Reiher, M.; Voightmann, U.; Klar, U.; Graham, K.; Schubiger, P.A.; Ametamey, S.M. **2009**, *15*, 3736-3743.
- (145) Höhne, A.; Mu, L.; Honer, M.; Schubiger, P.A.; Ametamey, S.M.; Graham, K.; Stellfeld, T.; Borkowski, S.; Berndorff, D.; Klar, U.; Voightmann, U.; Cyr, J.E.; Friebe, M.; Dinkelborg, L.; Srinivasan, A. *Bioconjugate Chem.* **2008**, *19*, 1871-1879.
- (146) Schirmacher, R.; Bradtmöller, G.; Schirmacher, E.; Thews, O.; Tillmanns, J.; Seissmeier, T.; Buchholz, H.G.; Bartenstein, P.; Wängler, B.; Niemeyer, C.M.; Jurkschat, K. *Angew. Chem. Int. Ed.* **2006**, *45*, 6047-6050.
- (147) Schirmacher, E.; Wängler, B.; Cypryk, M.; Bradtmöler, G.; Schäfer, M.; Eisenhut, M.; Jurkschat, K.; Schirmacher, R. *Bioconjugate Chem.* **2007**, *18*, 2085-2089.

- (148) Iovkova, L.; Wängler, B.; Schirmacher, E.; Schirmacher, R.; Quandt, G.; Boening, G.; Schürmann, M.; Jurkschat, K. *Chem. Eur. J.* **2009**, *15*, 2140-2147.
- (149) Wängler, B.; Quandt, G.; Iovkova, L.; Schirmacher, E.; Wängler, C.; Boening, G.; Hacker, M.; Schmoeckel, M.; Jurkschat, K.; Bartenstein, P.; Schirmacher, R. *Bioconjugate Chem.* **2009**, *20*, 317-321.
- (150) Kostikov, A.P.; Chin, J.; Orchowski, K.; Niedermoser, S.; Kovacevic, M.M.; Aliaga, A.; Jurkschat, K.; Wängler, B.; Wängler, C.; Wester, H.-J.; Schirmacher, R. *Bioconjugate Chem.* **2012**, *23*, 106-114.
- (151) Iovkova-Berends, L.; Wängler, C.; Zöller, T.; Höfner, G.; Wanner, K.T.; Rensch, C.; Bartenstein, P.; Kostikov, A.; Schirmacher, R.; Jurkschat, K.; Wängler, B. *Molecules* **2011**, *16*, 7458-7479.
- (152) Iovkova, L.; Könning, D.; Wängler, B.; Schirmacher, R.; Schoof, S.; Arndt, H.-D.; Jurkschat, K. *Eur. J. Inorg. Chem.* **2011**, 2238-2246.
- (153) Zhu, J.; Waengler, C.; Lennox, R.B.; Schirmacher, R. *Langmuir* **2012**, *28*, 5508-5512.
- (154) Zhu, J. Unpublished work.
- (155) Schottelius, M.; Wester, H.-J.; Reubi, J.C.; Senekowitsch-Schmidtke, R.; Schwaiger, M. *Bioconjugate Chem.* **2002**, *13*, 1021-1030.
- (156) Wängler, C.; Waser, B.; Alke, A.; Iovkova, L.; Buchholz, H.-G.; Niedermoser, S.; Jurkschat, K.; Fottner, C.; Bartenstein, P.; Schirmacher, R.; Reubi, J.-C.; Wester, H.-J.; Wängler, B. *Bioconjugate Chem.* **2010**, *21*, 2289-2296.

- (157) Kostikov, A.P.; Iovkova, L.; Chin, J.; Schirmacher, E.; Wängler, B.; Wängler, C.; Jurkschat, K.; Cosa, G.; Schirmacher, R. *J. Fluorine Chem.* **2011**, *132*, 27-34.
- (158) Ambrosini, V.; Fani, M.; Fanti, S.; Forrer, F.; Maecke, H.R. *J. Nucl. Med.* **2011**, *52*, 42S-55S.
- (159) Weiner, R.E.; Thakur, M.L. *Semin. Nucl. Med.* **2001**, *31*, 296-311.
- (160) Reubi, J.-C. *Endocr. Rev.* **2003**, *24*, 389-427.
- (161) Rufini, V.; Calcagni, M.L.; Baum, R.P. *Semin. Nucl. Med.* **2006**, *36*, 228-247.
- (162) Fani, M.; Maecke, H.R.; Okarvi, S.M. *Theranostics* **2012**, *2*, 481-501.
- (163) Rahmim, A.; Zaidi, H. *Nucl. Med. Comm.* **2008**, *29*, 193-207.
- (164) Sprague, J.E.; Peng, Y.; Sun, X.; Weisman, G.R.; Wong, E.H.; Achilefu, S.; Anderson, C.J. *Clin. Cancer Res.* **2004**, *10*, 8674-8682.
- (165) Meisetschläger, G.; Poethko, T.; Stahl, A.; Wolf, I.; Scheidhauer, K.; Schottelius, M.; Herz, M.; Wester, H.-J.; Schwaiger, M. *J. Nucl. Med.* **2006**, *47*, 566-573.
- (166) Wester, H.-J.; Schottelius, M.; Scheidhauer, K.; Meisetschläger, G.; Herz, M.; Rau, F.C.; Reubi, J.-C.; Schwaiger, M. *Eur. J. Nucl. Med. Mol. Imaging* **2003**, *30*, 117-122.

- (167) Wängler, C.; Niedermoser, S.; Chin, J.; Orchowski, K.; Schirmacher, E.; Jurkschat, K.; Iovkova-Berends, L.; Kostikov, A.P.; Schirmacher, R.; Wängler, B. *Nat. Protoc.* **2012**, *7*, 1946-1955.
- (168) Koukouraki, S.; Strauss, L.G.; Georgoulas, V.; Schuhmacher, J.; Haberkorn, U.; Karkavitsas, N.; Dimitrakopoulou-Strauss, A. *Eur. J. Nucl. Med. Mol. Imaging* **2006**, *33*, 460-466.
- (169) Wild, D.; Mäcke, H.R.; Waser, B.; Reubi, J.-C.; Ginj, M.; Rasch, H.; Müller-Brand, J.; Hofmann, M. *Eur. J. Nucl. Med. Mol. Imaging* **2005**, *32*, 724.
- (170) Långström, B.; Sjöberg, S.; Ragnarsson, U. *J. Label. Compd. Radiopharm.* **1981**, *18*, 479-487.
- (171) Hartvig, P.; Någren, K.; Lundberg, P.O.; Muhr, C.; Terenius, L.; Lundqvist, H.; Lärksfors, L.; Långström, B. *Regul. Pept.* **1986**, *16*, 1-13.
- (172) Franzén, H.M.; Ragnarsson, U.; Någren, K.; Långström, B. *J. Chem. Soc. Perkin Trans. I* **1987**, 2241-2247.
- (173) Lundqvist, H.; Tolmachev, V. *Biopolymers (Pept. Sci.)* **2002**, *66*, 381-392.
- (174) Henriksen, G.; Schottelius, M.; Poethko, T.; Hauser, A.; Wolf, I.; Schwaiger, M.; Wester, H.-J. *Eur. J. Nucl. Med. Mol. Imaging* **2004**, *31*, 1653-1657.

- (175) Nabulsi, N.B.; Smith, D.E.; Kilbourn, M.R. *Bioorg. Med. Chem.* **2005**, *13*, 2993-3001.
- (176) Nakagawa, Y.; Bender, M.L. *J. Am. Chem. Soc.* **1969**, *91*, 1566-1567.
- (177) Heinrikson, R.L. *Biochem. Biophys. Res. Commun.* **1970**, *41*, 967-972.
- (178) Boffa, L.C.; Bolognesi, C. *Carcinogenesis* **1985**, *6*, 1399-1401.
- (179) Roehm, P.C.; Berg, J.M. *J. Am. Chem. Soc.* **1998**, *120*, 13083-13087.
- (180) Wellings, D.A.; Atherton, E. *Methods Enzymol.* **1997**, *289*, 44.
- (181) Tam, J.P.; Wu, C.-R.; Liu, W.; Zhang, J.-W. *J. Am. Chem. Soc.* **1991**, *113*, 6657-6662.
- (182) Savige, W.E.; Fontana, A. *Int. J. Peptide Protein Res.* **1980**, *15*, 285-297.
- (183) Bauer, W.; Briner, U.; Doepfner, W.; Haller, R.; Huguenin, R.; Marbach, P.; Petcher, T.J.; Pless, J. *Life Sci.* **1982**, *31*, 1133-1140.
- (184) De Jong, M.; Valkema, R.; Jamar, F.; Kvols, L.K.; Kwekkeboom, D.J.; Breeman, W.A.; Bakker, W.H.; Smith, C.; Pauwels, S.; Krenning, E.P. *Semin. Nucl. Med.* **2002**, *32*, 133-140.
- (185) Decristoforo, C.; Maina, T.; Nock, B.; Gabriel, M.; Cordopatis, P.; Moncayo, R. *Eur. J. Nucl. Med. Mol. Imaging* **2003**, *30*, 1211-1219.
- (186) Wang, Q.; Graham, K.; Schauer, T.; Fietz, T.; Mohammed, A.; Liu, X.; Hoffend, J.; Haberkorn, U.; Eisenhut, M.; Mier, W. *Nucl. Med. Biol.* **2004**, *31*, 21-30.

- (187) Thomas, G. *Medicinal Chemistry, 2nd ed.* – West Sussex, England: John Wiley & Sons, **2007**.
- (188) Kubota, T.; Yamamoto, A.; Endo, M. (Shin Etsu Chem. Co. Ltd.)
Production of di-*t*-butylsilane. Japanese patent JP06345778, 1994.
- (189) Watanabe, H.; Ohkawa, T.; Muraoka, T.; Nagai, Y. *Chem. Lett.* **1981**, *10*, 1321-1322.
- (190) Rempfer, B.; Oberhammer, H.; Auner, N. *J. Am. Chem. Soc.* **1986**, *108*, 3893-3897.
- (191) Chin, J. Unpublished work.
- (192) Jones, R.A. *Quaternary Ammonium Salts: Their Use in Phase-Transfer Catalysts.* – London: Academic Press, **2001**.
- (193) Lee, H.B.; Pattarawarapan, M.; Roy, S.; Burgess, K. *Chem. Commun.* **2003**, 1674.
- (194) Ellison, R.A.; Lukenbach, E.R.; Chiu, C.-W. *Tetrahedron Lett.* **1975**, *16*, 499.
- (195) Mehta, A.; Jaouhari, R.; Benson, T.J.; Douglas, K.T. *Tetrahedron Lett.* **1992**, *33*, 5441.
- (196) Antunes, P.; Ginja, M.; Walter, M.A.; Chen, J.; Reubi, J.C.; Maecke, H.R. *Bioconjugate Chem.* **2007**, *18*, 84-92.
- (197) Bigott-Hennkens, H.M.; Junnotula, S.; Ma, L.; Gallazzi, F.; Lewis, M.R.; Jurisson, S.S. *J. Med. Chem.* **2008**, *51*, 1223-1230.

- (198) Hermanson, G.T. *Bioconjugate Techniques*, 2nd ed. – London: Academic Press, **2008**.
- (199) Rostovtsev, V.V.; Green, L.G.; Fokin, V.V.; Sharpless, K.B. *Angew. Chem. Int. Ed.* **2002**, *41*, 2596-2599.
- (200) Bock, V.D.; Hiemstra, H.; van Maarseveen, J.H. *Eur. J. Org. Chem.* **2006**, 51-68.
- (201) Knör, S.; Modlinger, A.; Poethko, T.; Schottelius, M.; Wester, H.-J.; Kessler, H. *Chem. Eur. J.* **2007**, *13*, 6082-6090.
- (202) Wängler, C.; Schäfer, M.; Schirmacher, R.; Bartenstein, P.; Wängler, B. *Bioorg. Med. Chem.* **2011**, *19*, 3964-3874.
- (203) Chin, J. Unpublished work.
- (204) Benson, H.A.E.; Namjoshi, S. *J. Pharm. Sci.* **2008**, *97*, 3591-3610.
- (205) Waterhouse, R.N. *Mol. Imaging Biol.* **2003**, *5*, 376-389.
- (206) Michel, M.; Bączek, T.; Studzińska, S.; Bodzioch, K.; Jonsson, T.; Kaliszan, R.; Buszewski, B. *J. Chromatogr. A* **2007**, *1175*, 49-54.
- (207) *OECD Guidelines for the Testing of Chemicals – Partition Coefficient (n-Octanol/Water), pH-Metric Method for Ionisable Substances.* **2009**.
- (208) Ye, C.W.; Li, J. *Russ. J. Phys. Chem. A* **2012**, *86*, 1515-1521.
- (209) *The Landolt-Börnstein Database.* – Berlin: Springer, **2013**.
- (210) Nys, G.G.; Rekker, R.F. *Chem. Ther.* **1974**, *9*, 361-374.

- (211) Leo, A. *Rational approaches to the design of bioactive compounds*. – Amsterdam: Elsevier, **1991**.
- (212) Sarkar, A.; Kellogg, G.E. *Curr. Top. Med. Chem.* **2010**, *10*, 67-83.
- (213) El Tayar, N.; Karajiannis, H.; van de Waterbeemd, H. *Amino Acids* **1995**, *8*, 125-139.
- (214) Vallat, P.; Gaillard, P.; Carrupt, P.-A.; Tsai, R.-S.; Testa, B. *Helv. Chim. Acta* **1995**, *78*, 471-485.
- (215) Tsai, R.-S.; Carrupt, P.-A.; Testa, B.; El Tayar, N.; Grunewald, G.L.; Casy, A.F. *J. Chem. Res. (M)* **1993**, 1901.
- (216) Evans, S.E.; Gaides, A.; Gall, M. *Pharmacol. Biochem. Behavior* **1991**, *40*, 1033.
- (217) Thompson, S.J.; Hattotuagama, C.K.; Holliday, J.D.; Flower, D.R. *Bioinformation* **2006**, *1*, 237-241.
- (218) Chou, J.; Hoekman, D. *Perspect. in Drug Discov. & Design* **2000**, *18*, 19.
- (219) Reubi, J.C.; Schär, J.-C.; Waser, B.; Wenger, S.; Heppeler, A.; Schmitt, J.S.; Mäcke, H.R. *Eur. J. Nucl. Med.* **2000**, *27*, 273-282.
- (220) Cescato, R.; Erchegyi, J.; Waser, B.; Piccard, V.; Maecke, H.R.; Rivier, J.E.; Reubi, J.C. *J. Med. Chem.* **2008**, *51*, 4030-4037.
- (221) Sessler, J.L.; Wang, B.; Harriman, A. *J. Am. Chem. Soc.* **1995**, *117*, 704-714.

(222) Niedermoser, S.; Wängler, C.; Chin, J.; Kostikov, A.; Bartenstein, P.; Jugold, M.; Schirmacher, E.; Schirmacher, R.; Wängler, B. (2013) Chemical and biological evaluation of new hydrophilic [^{18}F]-SiFA-derivatized somatostatin-analogues. Oral presentation at: SNMMI 2013. Society of Nuclear Medicine and Molecular Imaging 2013 Annual Meeting; 2013 June 8-12; Vancouver Convention Centre, Vancouver, Canada.

Chapter 7: APPENDICES

7.1 Supplementary information (Manuscript)

Supporting information to *Chapter 2: Manuscript*.

Amino Acids (Supplementary Information)

Direct one-step labeling of cysteine residues on peptides with [^{11}C]methyl triflate for the synthesis of PET radiopharmaceuticals.

Joshua Chin^{a,b}, Matthew Vesnaver^a, Vadim Bernard-Gauthier^{a,c}, Erin Saucke-Lacelle^a, Björn Wängler^d, Carmen Wängler^e, Ralf Schirmacher^{,a}*

^aMcConnell Brain Imaging Centre, Montreal Neurological Institute, McGill University, Montreal, Canada.

^bDepartment of Chemistry, McGill University, Montreal, Canada.

^cDepartment of Chemistry, Université de Montréal, Montreal, Canada.

^dMolecular Imaging & Radiopharmaceutical Chemistry, Department of Clinical Radiology and Nuclear Medicine, Medical Faculty Mannheim of Heidelberg University, Mannheim, Germany.

^eBiomedical Chemistry, Department of Clinical Radiology and Nuclear Medicine, Medical Faculty Mannheim of Heidelberg University, Mannheim, Germany.

* Corresponding author; e-mail address: ralf.schirmacher@mcgill.ca

Delay time calibration between UV and radioactivity detectors

The discrete Raytest Gabi Star radioactivity detector associated with the Agilent 1200 system (HPLC) functions by measuring radioactivity levels of the HPLC line output from the integrated UV/vis detector. Therefore, a measureable time delay between UV and radioactivity detectors is anticipated, and expected to depend solely on the flow of eluent (controllable by the HPLC pump module).

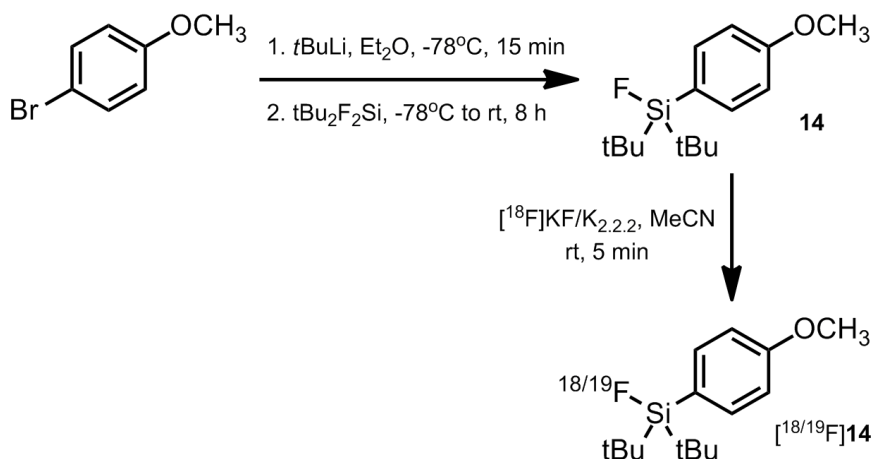


Figure S1. Synthesis of **14** and radiosynthesis of [^{18/19}F]**14** via isotopic exchange.

In order to experimentally measure this time delay accurately, the ideal analyte needed should be detectable under both detection systems at the levels injected. In particular, the SiFA (silicon-fluoride acceptor) compound **14** was chosen which, when treated with anhydrous [¹⁸F]fluoride, would afford a mixture of [¹⁸F]**14** and [¹⁹F]**14** by isotopic exchange typical for this class of compound (Figure S1)^[S1]. These isotopic equivalents can be assumed to possess identical

physical properties, therefore inseparable under the given HPLC conditions (as isotopic effects of atoms heavier than the hydrogen-deuterium series are negligible).

Synthesis of di-tert-butylfluoro(4-methoxyphenyl)silane (14).

Adapted from Iovkova *et al.*^[S2], with modifications. To a solution of 1-bromo-4-methoxybenzene (1.00 g, 5.4 mmol) in anhydrous Et₂O (20 mL) was added dropwise over a period of 15 min a solution of *tert*-butyllithium in pentanes (1.7 M, 6.6 mL, 2.1 eq) at -78°C, and the formed solution was stirred at the same temperature for 15 min. To this solution was added dropwise over a period of 15 min a solution of di-*tert*-butyldifluorosilane (1.16 g, 6.4 mmol, 1.2 eq) in anhydrous Et₂O (10 mL) at -78°C, and the mixture was allowed to warm to room temperature overnight. The reaction was quenched by addition of saturated aqueous sodium chloride solution (100 mL), and the mixture was extracted with Et₂O (3 x 75 mL). The combined organic phase was dried (Na₂SO₄), concentrated *in vacuo*, and purified by flash column chromatography on silica gel (neat hexanes) to afford **14** as a colorless oil (1.42 g, 70%), which solidified on standing to a white solid. ¹H NMR (300 MHz, CDCl₃): δ 7.53 (d, 2H, *J* = 8.7 Hz), 6.93 (d, 2H, *J* = 8.7 Hz), 3.83 (s, 3H), 1.05 (d, 18H, *J*(¹H, ¹⁹F) = 1.2 Hz). ¹³C NMR (300 MHz, CDCl₃): δ 180.7, 135.4 (d, *J*(¹³C, ¹⁹F) = 17 Hz), 124.4 (d, *J*(¹³C, ¹⁹F) =

54 Hz), 113.4, 54.9, 27.4 (d, $J(^{13}\text{C}, ^{19}\text{F}) = 4$ Hz), 20.3 (d, $J(^{13}\text{C}, ^{19}\text{F}) = 50$ Hz).

HRMS (ESI, m/z) for $\text{C}_{15}\text{H}_{26}\text{FOSi}$ $[\text{M}+\text{H}]^+$ (calcd): 269.1731 (269.1732).

Preparation of a stock solution containing the $[\text{}^{18}\text{F}]\text{F}^-/\text{Kryptofix 2.2.2}/\text{K}^+$ complex

$[\text{}^{18}\text{F}]\text{F}^-$ was produced by a $^{18}\text{O}(p,n)^{18}\text{F}$ nuclear reaction on an enriched $[\text{}^{18}\text{O}]\text{H}_2\text{O}$ (purity 98.5%) target. The resulting aqueous $[\text{}^{18}\text{F}]\text{F}^-$ was loaded onto a Waters QMA ion exchange cartridge and eluted with a mixture of acetonitrile (2 mL), water (30 μL), potassium oxalate solution (0.5 M, 30 μL), and Kryptofix[®] 2.2.2 (10.5 mg). The solvents were removed by coevaporation to dryness under reduced pressure (600 mbar) using a stream of argon at 100°C for 5 min. The drying step was repeated twice with CH_3CN (1 mL, 5 min) and full vacuum (<10 mbar) was applied in the final drying step (3 min). The dried $[\text{}^{18}\text{F}]\text{F}^-/\text{Kryptofix 2.2.2}/\text{K}^+$ complex was dissolved in anhydrous CH_3CN (2 mL) and left to cool to room temperature on standing for use as stock solution in subsequent labeling reactions.

Radiosynthesis of $[\text{}^{18}/^{19}\text{F}]\textbf{14}$

The stock solution containing $[\text{}^{18}\text{F}]\text{F}^-/\text{Kryptofix 2.2.2}/\text{K}^+$ complex (5 μL) was added to a solution of **14** in anhydrous CH_3CN (1 μL of a 0.5 mg/ μL stock solution) and further diluted with 20 μL MeCN. The reaction mixture was left

standing at room temperature for 5 min and immediately injected into the radio-HPLC for detector time delay calibration.

HPLC UV and radioactivity detector flow-dependent time delay determination

Time delay calibration was performed on the Agilent 1200 system equipped with a Raytest Gabi Star radioactivity detector and a Chromolith Performance column (RP-18e, 100 x 4.6 mm; Merck, Germany) at flow rates between 0.5 mL/min and 4.5 mL/min. UV detection was performed at 210 nm, 230 nm, and 254 nm. HPLC mobile phases consist of eluent A (0.1% TFA in MeCN) and eluent B (0.1% TFA in H₂O) filtered through a 0.45 µm nylon membrane filter and degassed before use. Method F (Table S1) was employed as gradient profile for the elution of [^{18/19}F]14. All samples for preparative and analytical HPLC were diluted with a minimum of 50% v/v eluent B prior to injection. Samples were injected via a model 7725i Rheodyne syringe loading sample injector fitted with a 2 mL loop (Rheodyne, Cotati, CA, USA).

Table S1. HPLC elution method F used in the current study.

Method	Column	Flow (mL/min)	Gradient timeline (min)	Eluent A (%)	Eluent B (%)	Elution
F	Chromolith Performance	0.5-4.5	0.00	50	50	Linear gradient
			5.00	100	0	Linear gradient
			20.00	100	0	Isocratic
			25.00	50	50	Equilibration

The UV and radioactivity elution profiles of [$^{18/19}\text{F}$]**14** was experimentally determined over a range of HPLC flow rates (Table S2). A flow-time delay calibration curve was subsequently constructed (Figure S2), and employed throughout the current study for identification of radiolabeled peptides.

Table S2. Retention times of [$^{18/19}\text{F}$]**14** over a range of HPLC flow rates.

Flow (mL/min)	$R_{t(\text{UV})}$ (min)	$R_{t(\gamma)}$ (min)	ΔR_t (min)
0.5	12.04	12.96	0.92
0.6	10.21	10.97	0.76
0.7	8.93	9.59	0.66
0.8	7.97	8.55	0.58
0.9	7.20	7.73	0.53
1.0	6.59	7.07	0.48
1.5	4.73	5.08	0.35
2.0	3.78	4.05	0.27
2.5	3.13	3.37	0.24
3.0	2.72	2.93	0.21
3.5	2.39	2.58	0.19
4.0	2.14	2.32	0.18
4.5	1.93	2.09	0.16

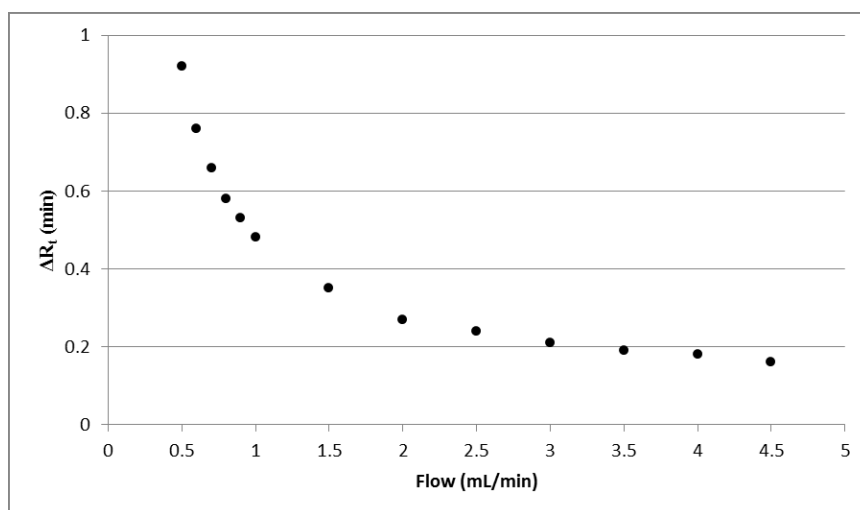


Figure S2. Flow-time delay calibration curve between UV/vis and radioactivity detectors of the Agilent 1200 system (HPLC).

Effect of TFA quench over time in the radiosynthesis of (^{11}C)2

In order to limit degradation of peptide under basic conditions required for radiomethylation, a slight excess of TFA was added to the reaction mixture immediately following bubbling of ^{11}C MeOTf to neutralize residual NaOH. Once quenched, the radio-HPLC profile of the reaction mixture remains unchanged up to 3 hours (Figure S3).

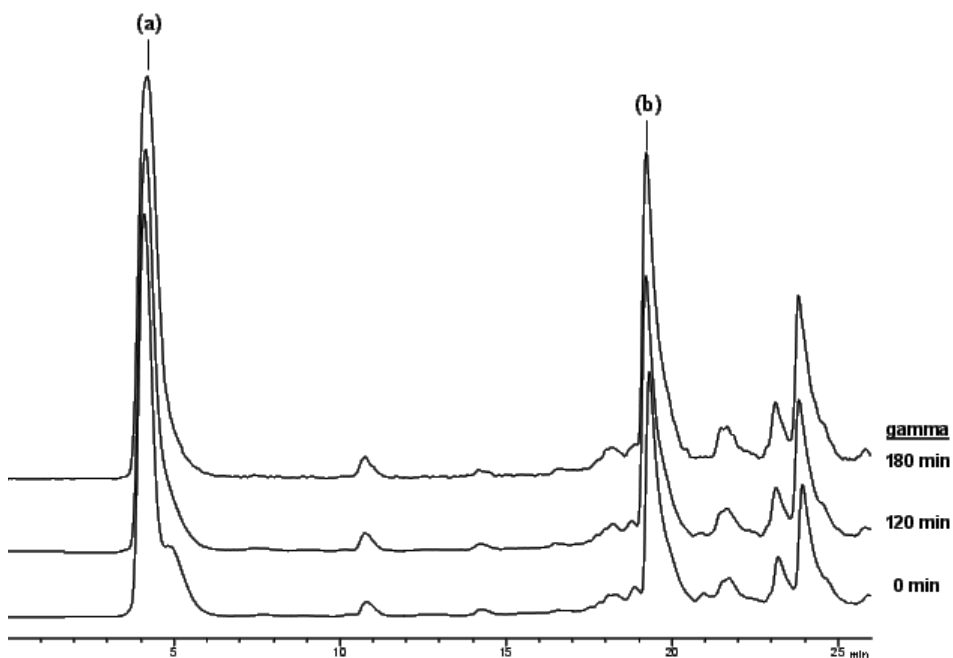


Figure S3. Radio-HPLC profile of crude reaction (expt. 24) over 3 hours following TFA quench. (a) ^{11}C CH₃OH, $R_{t(\text{gamma})} = 4.3$ min. (b) ^{11}C 2, $R_{t(\text{gamma})} = 19.4$ m.

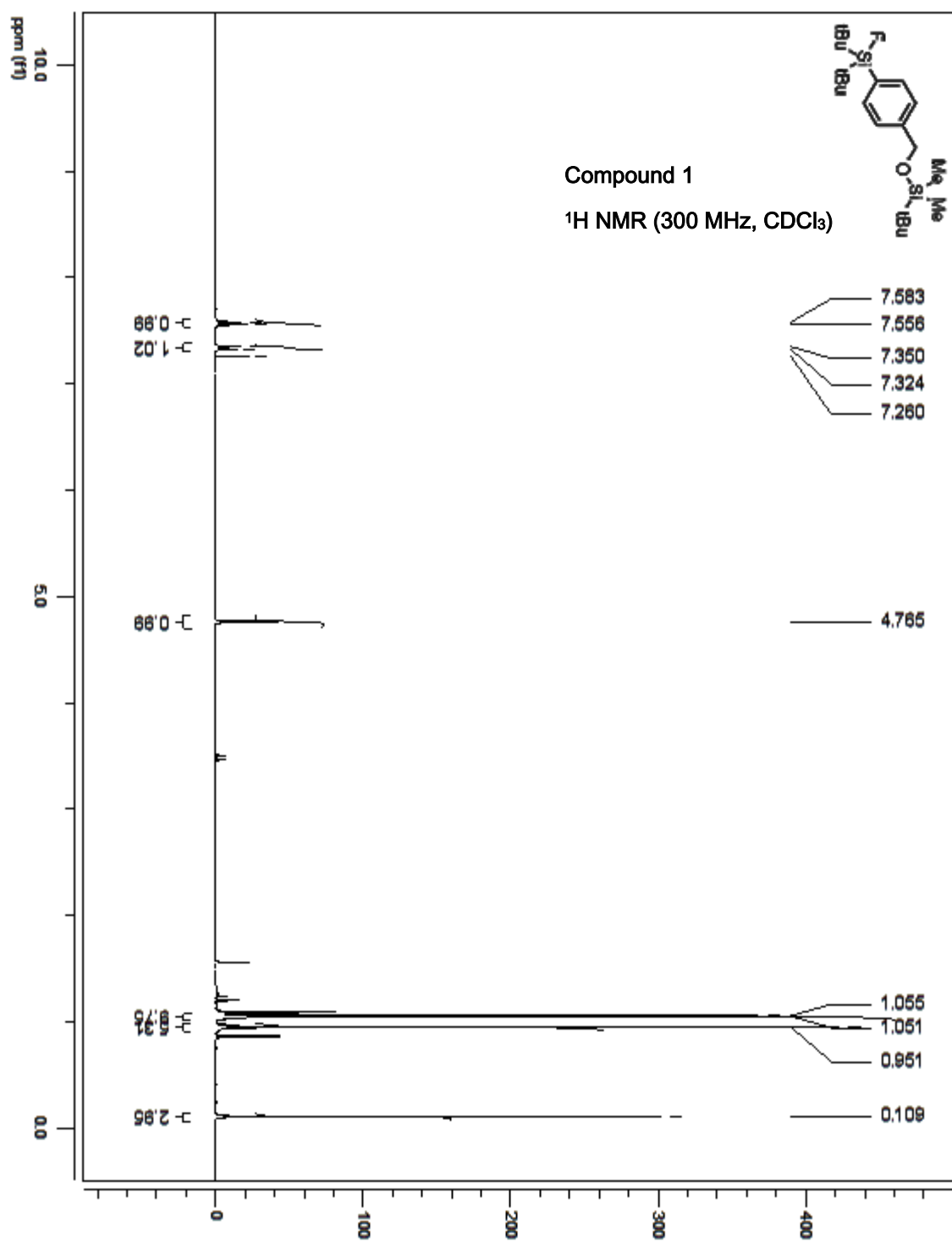
References

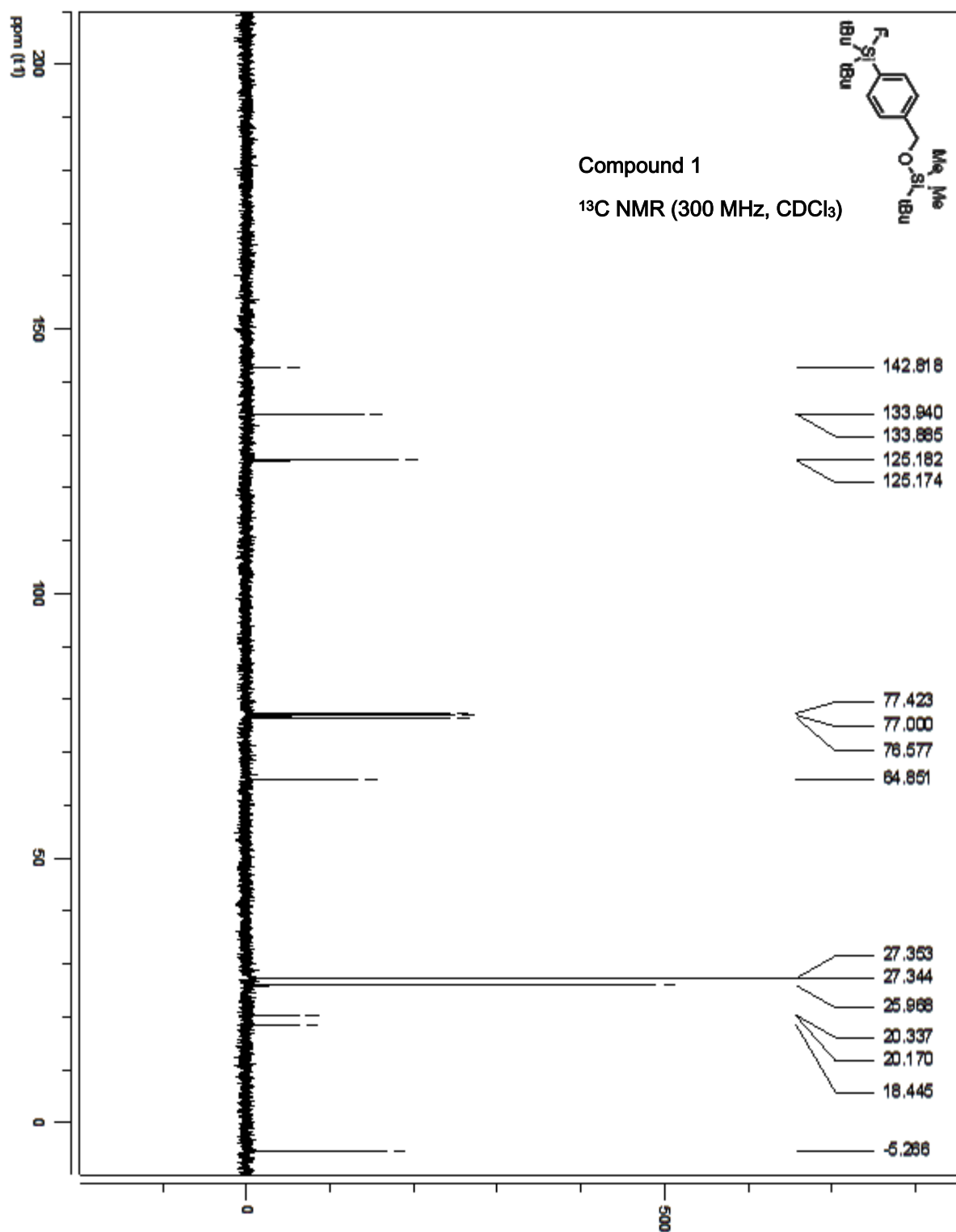
- (S1) Schirmacher, R.; Bradtmöller, G.; Schirmacher, E.; Thews, O.; Tillmanns, J.; Seissmeier, T.; Buchholz, H.G.; Bartenstein, P.; Wängler, B.; Niemeyer, C.M.; Jurkschat, K. *Angew. Chem. Int. Ed.* **2006**, *45*, 6047-6050.
- (S2) Iovkova, L.; Wängler, B.; Schirmacher, E.; Schirmacher, R.; Quandt, G.; Boening, G.; Schürmann, M.; Jurkschat, K. *Chem. Eur. J.* **2009**, *15*, 2140-2147.

7.2 Small-molecule characterization data

^1H -NMR and ^{13}C -NMR acquisitions were performed using a 300 MHz Varian Mercury at the Nuclear Magnetic Resonance Facility, Department of Chemistry, McGill University, Montreal, Canada. The purity of organic compounds prepared was determined by ^1H -NMR analysis.

High-resolution mass spectrometry (HRMS) was performed at the Centre regional de spectrométrie de masse, Department of Chemistry, Université de Montréal, Montreal, Canada.

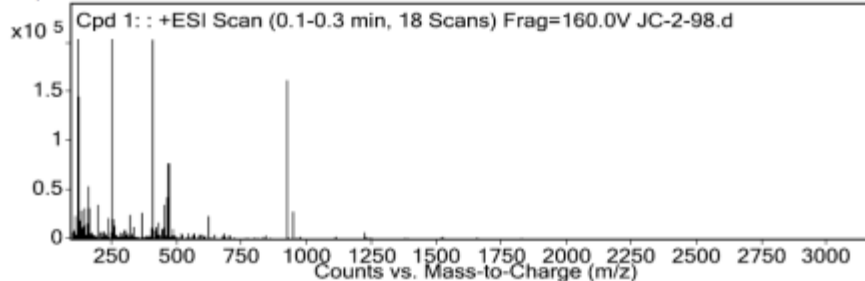




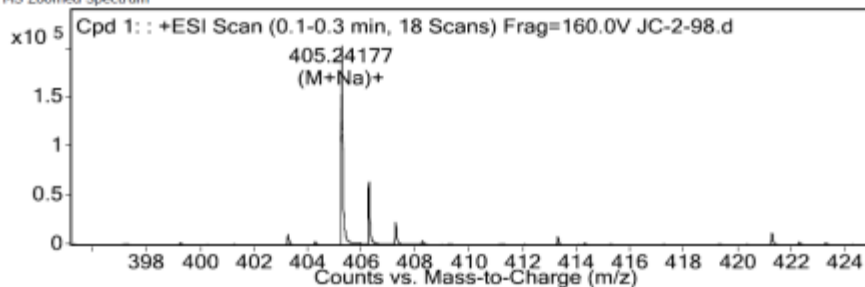
Rapport d'analyse

Data File JC-2-98.d
Sample Type Sample
Analysis Date 5/8/2012 1:29:17 PM
Acq Method ESI_POS_DLm
Comment
Sample Name JC-2-98
Position P1-D5
User Name Marie-Christine
DA Method ESI_POS_DLm

MS Spectrum

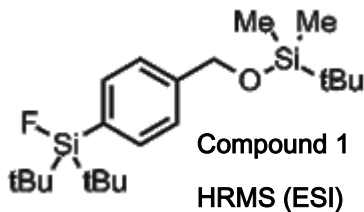


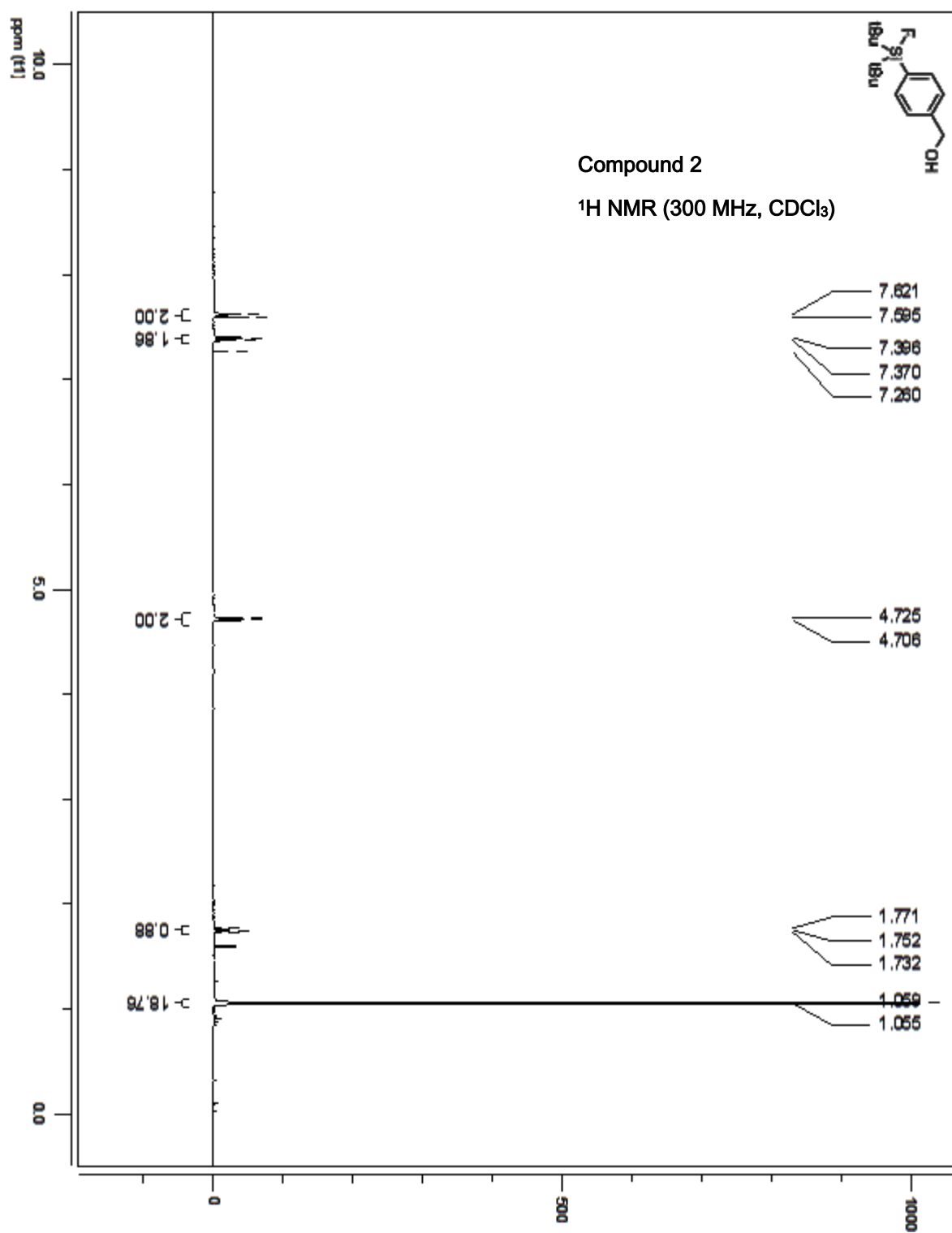
MS Zoomed Spectrum

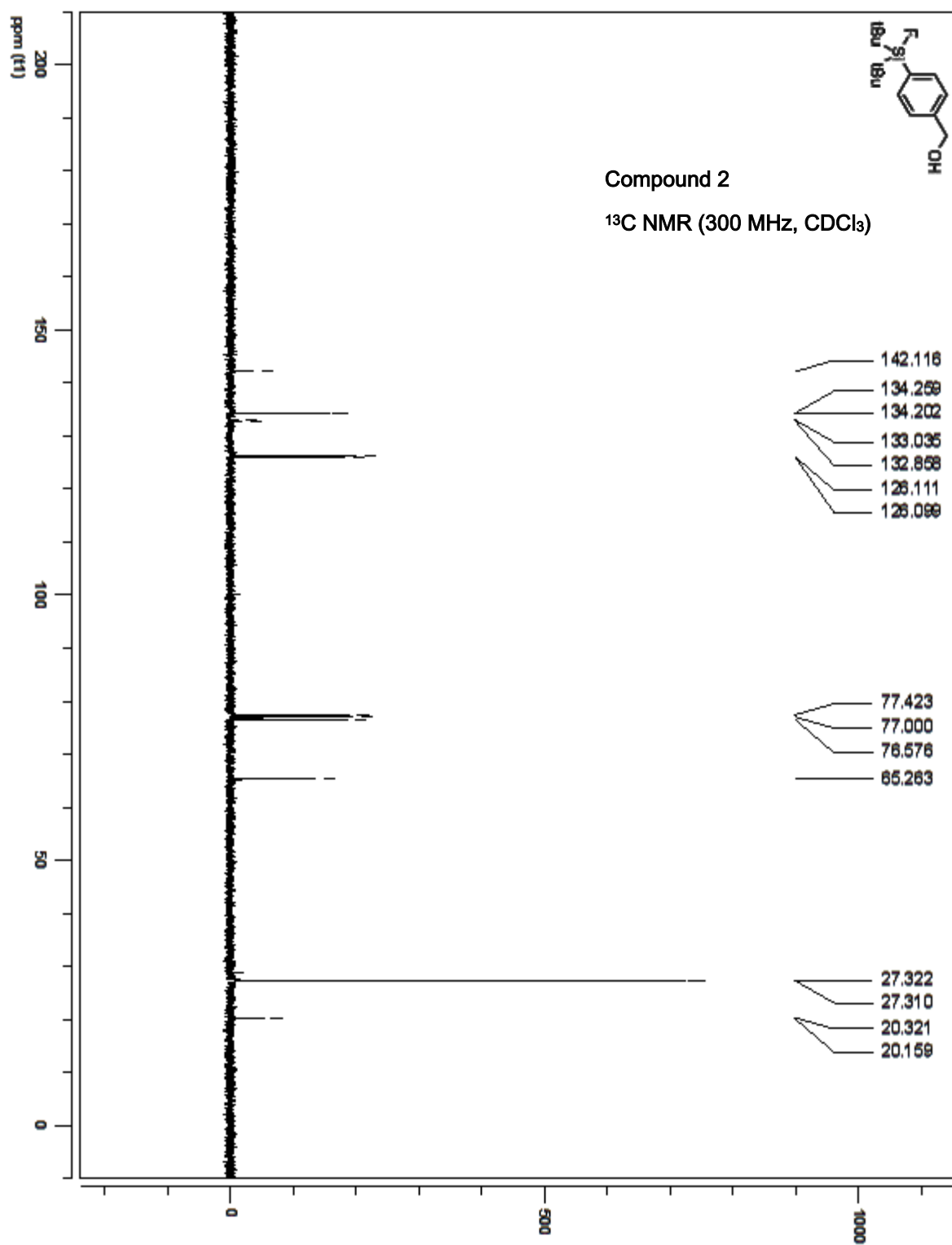


MS Spectrum Peak List

Ion	Ion Formula	Abund	Expe. m/z	Calc. m/z	Diff(ppm)
(M+Na)+	C ₂₁ H ₃₉ FN ₂ OSi ₂	202835.9	405.24177	405.24157	-0.49



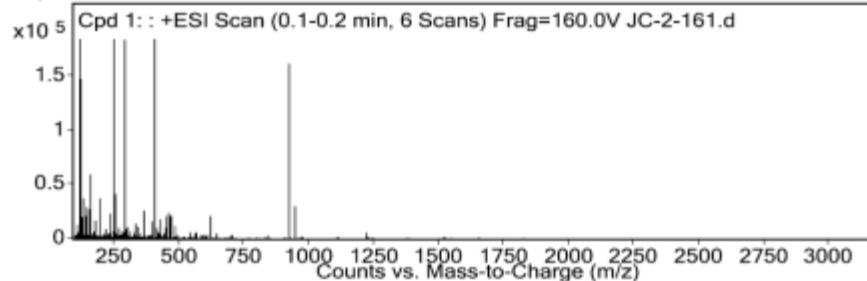




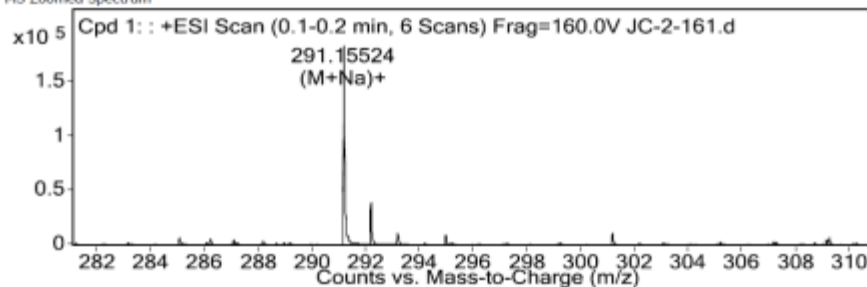
Rapport d'analyse

Data File	JC-2-161.d	Sample Name	JC-2-161
Sample Type	Sample	Position	P1-D6
Analysis Date	5/8/2012 1:31:20 PM	User Name	Marie-Christine
Acq Method	ESI_POS_DLM	DA Method	ESI_POS_DLM
Comment			

MS Spectrum

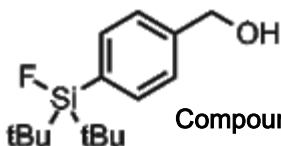


MS Zoomed Spectrum



MS Spectrum Peak List

Ion	Ion Formula	Abund	Expe. m/z	Calc. m/z	Diff(ppm)
(M+Na)+	C15H25FNaOSi	190681.3	291.15524	291.15509	0.52

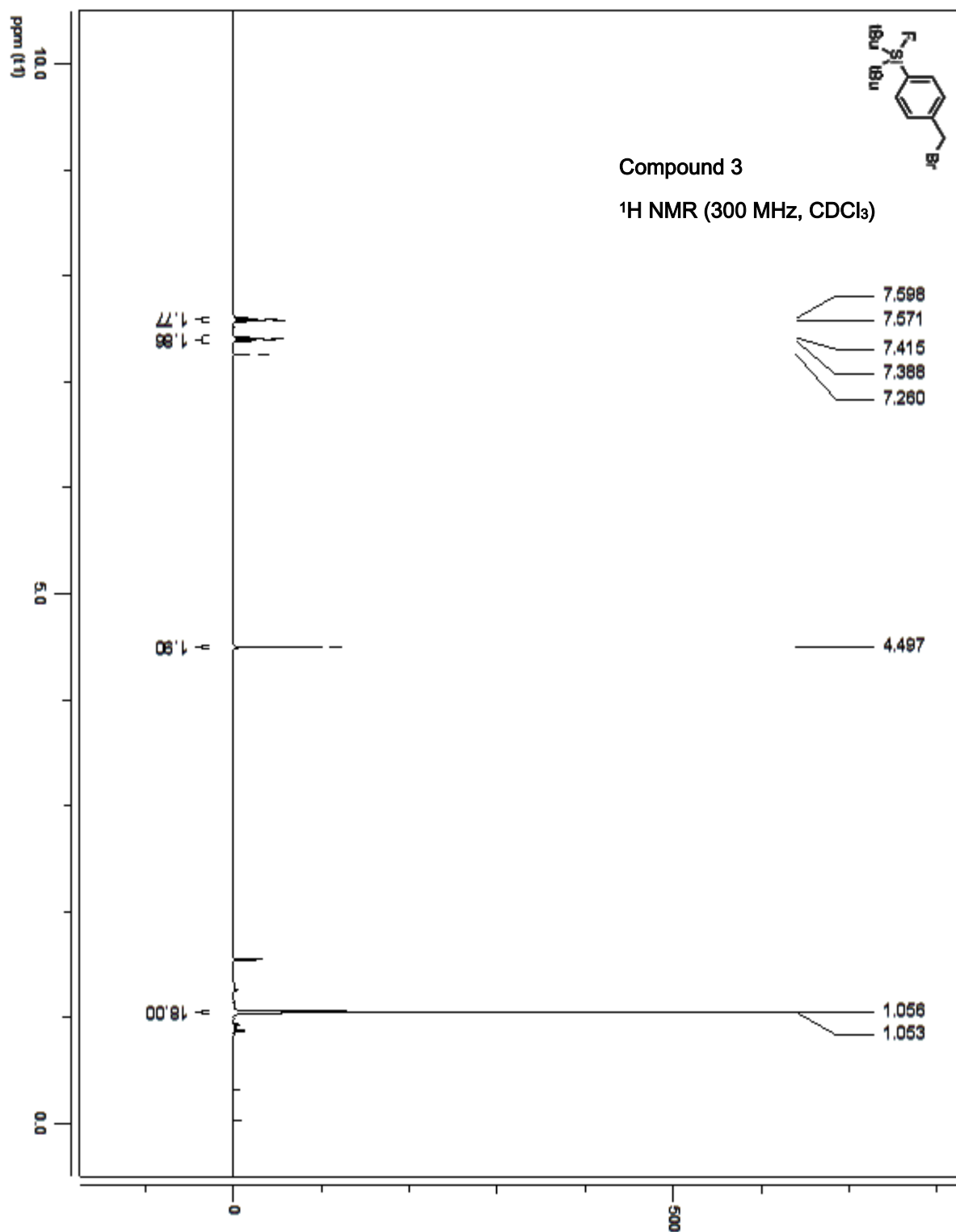


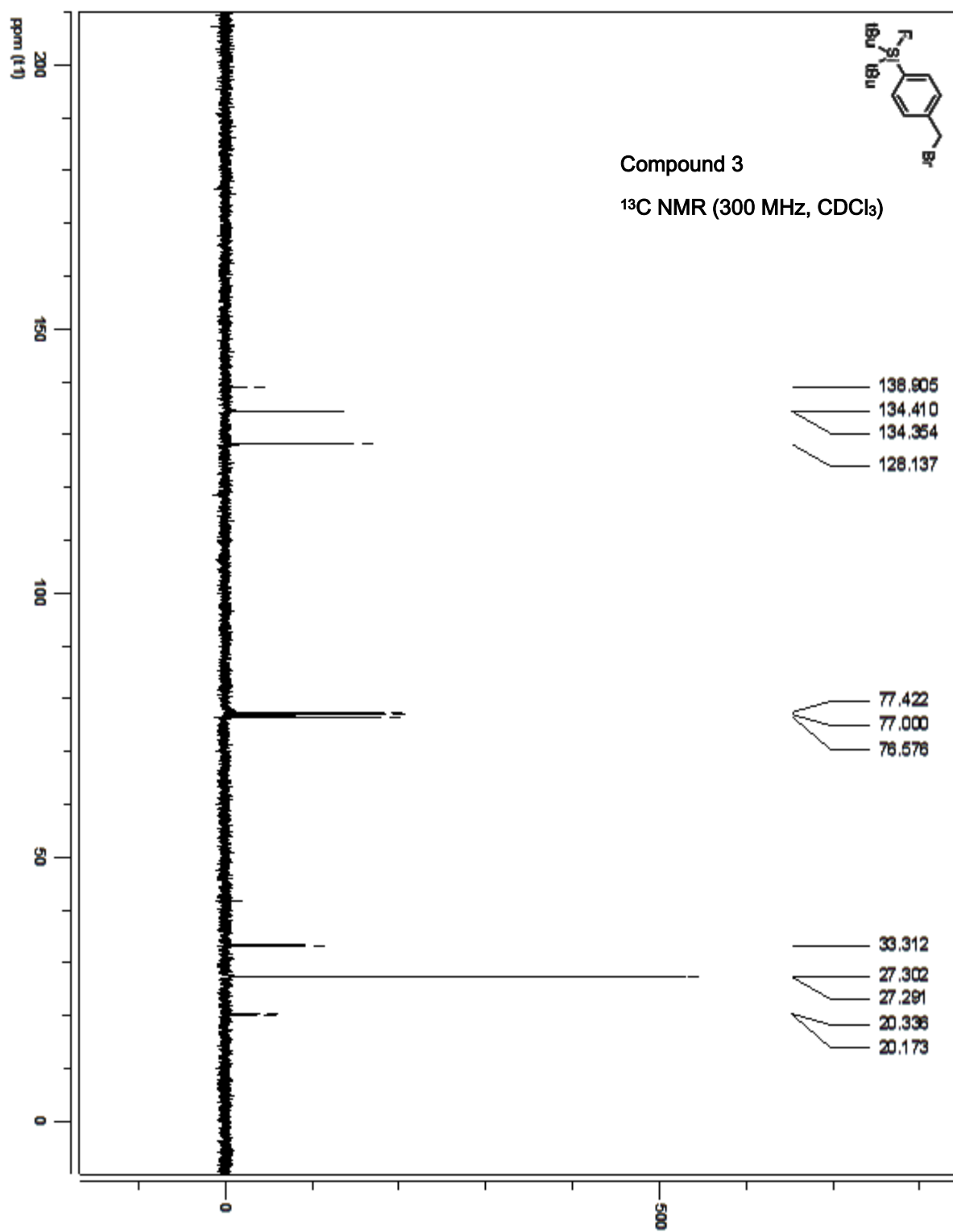
HRMS (ESI)

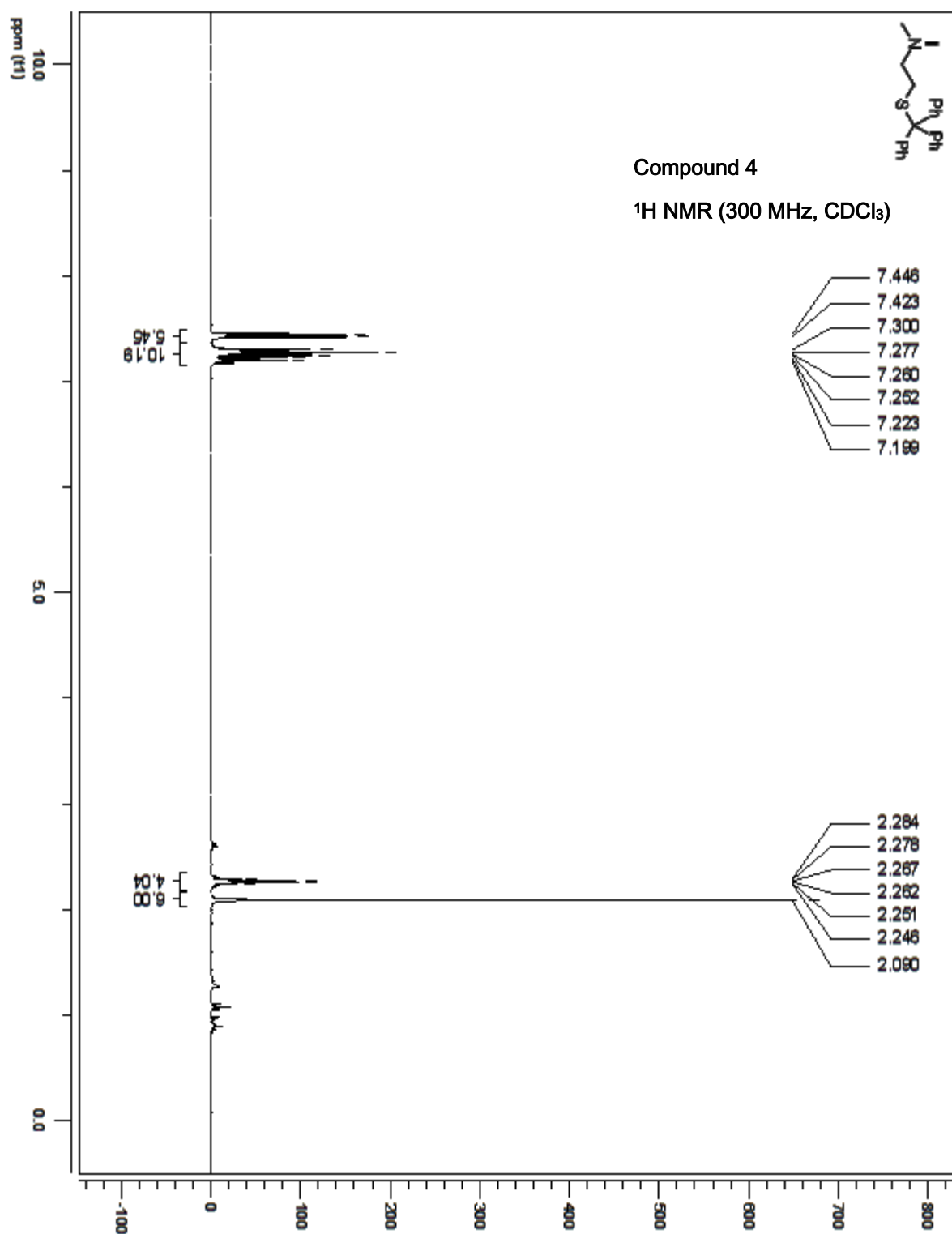


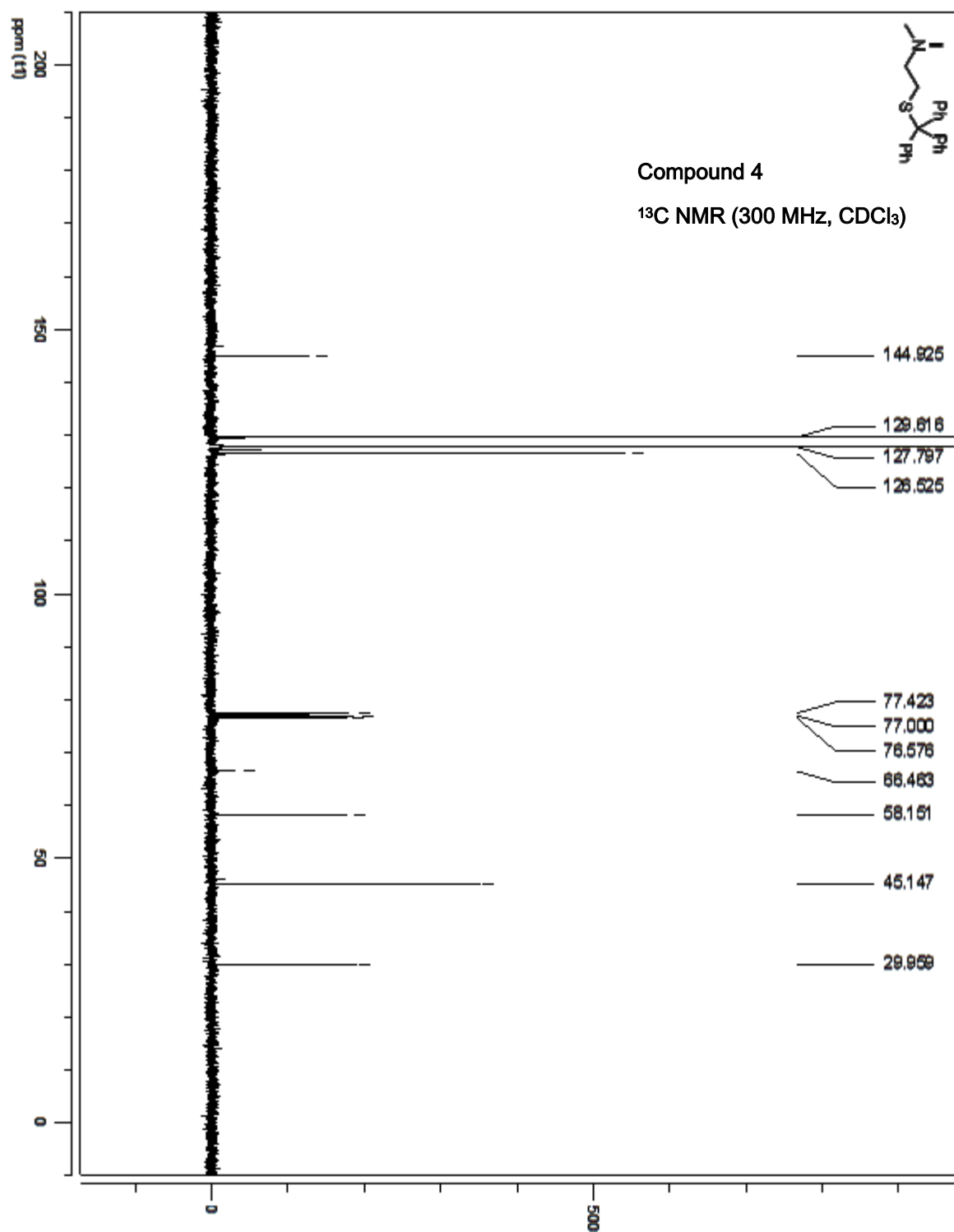
Centre Regional de Spectrometrie de Masse
Universite de Montreal

Page 1 of 1





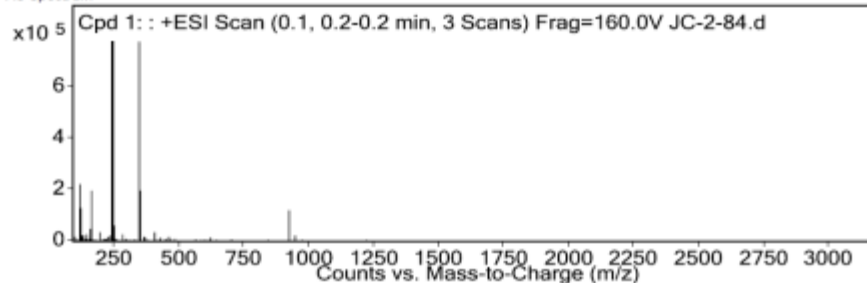




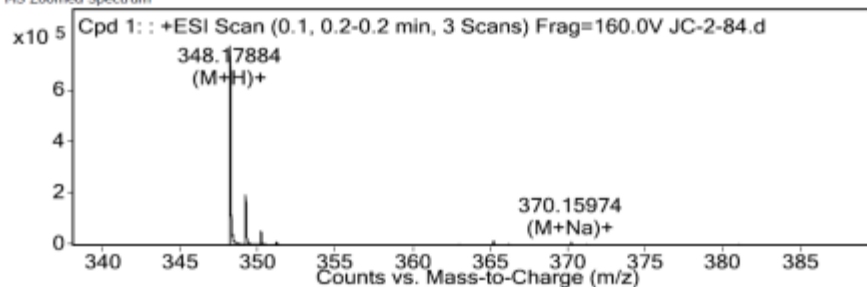
Rapport d'analyse

Data File JC-2-84.d
Sample Type Sample
Analysis Date 5/8/2012 1:35:03 PM
Acq Method ESI_POS_DLM
Comment
Sample Name JC-2-84
Position P1-D6
User Name Marie-Christine
DA Method ESI_POS_DLM

MS Spectrum

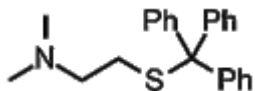


MS Zoomed Spectrum



MS Spectrum Peak List

Ion	Ion Formula	Abund	Expe. m/z	Calc. m/z	Diff(ppm)
(M+H)+	C23H26NS	774330	348.17884	348.17805	2.27
(M+Na)+	C23H25NNaS	11612.9	370.15974	370.15999	-0.68

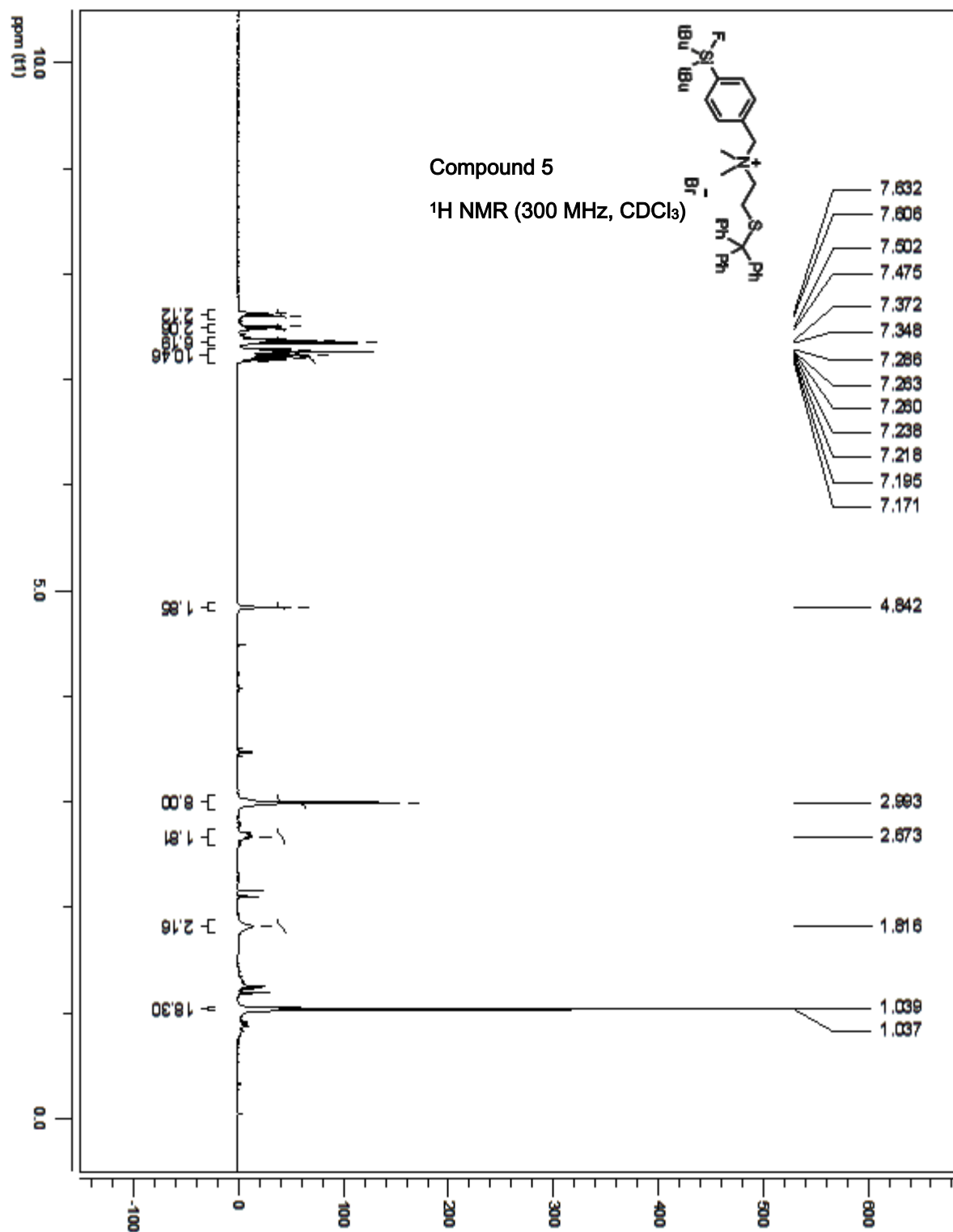


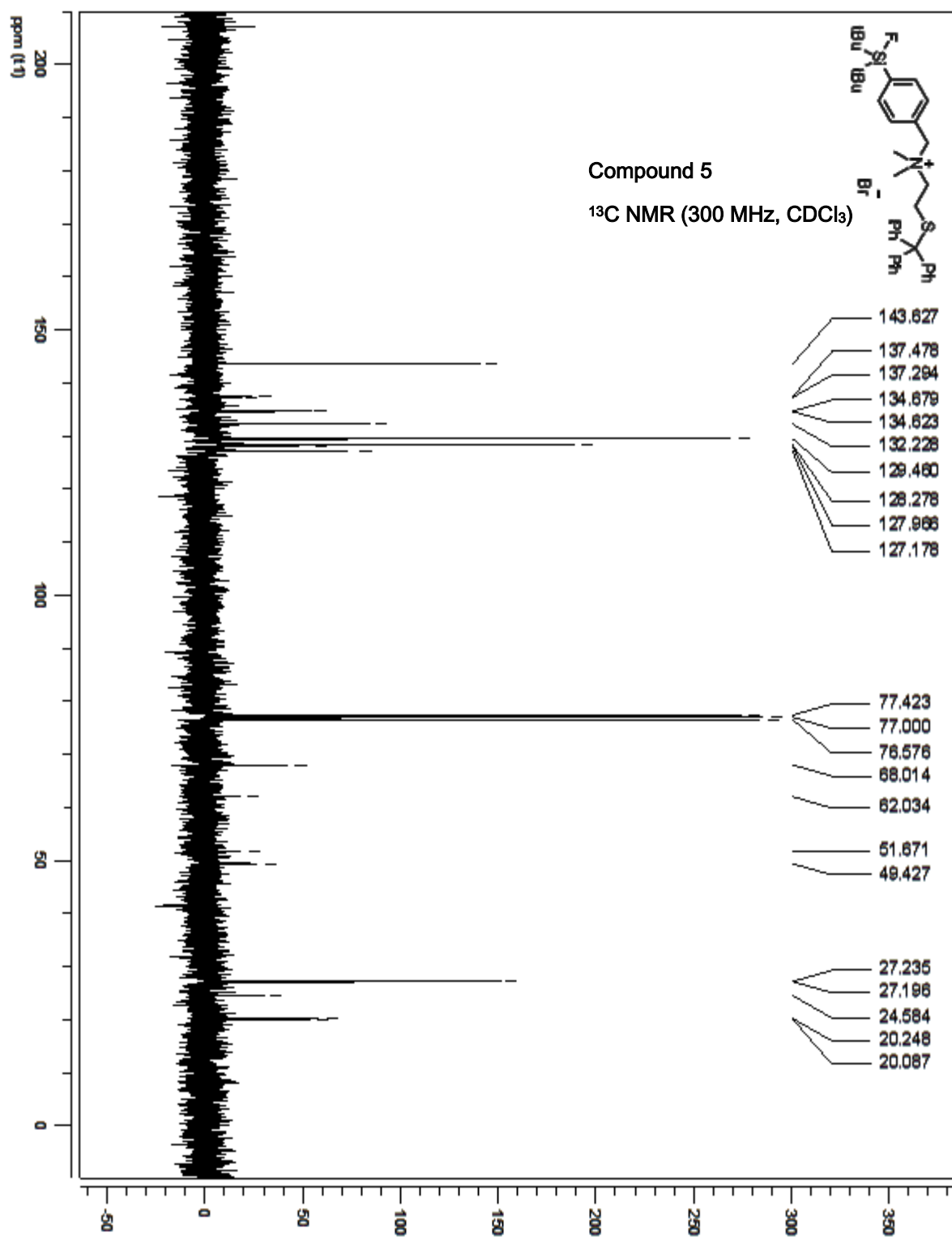
Compound 4

HRMS (ESI)



Centre Regional de Spectrometrie de Masse
Universite de Montreal





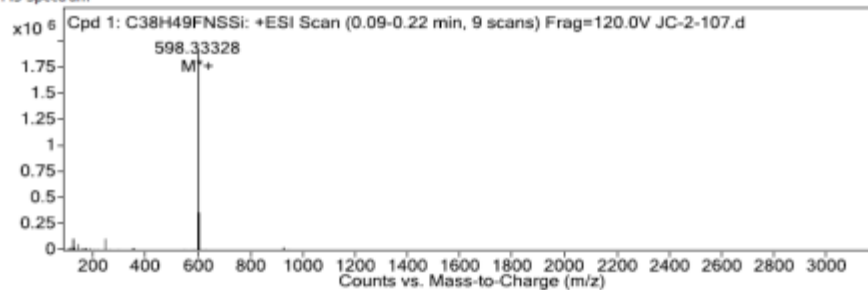
Rapport d'analyse

Data File JC-2-107.d Sample Name JC-2-107
 Sample Type Sample Position P1-C8
 Analysis Date 11/10/2010 6:13:23 PM User Name Marie-Christine

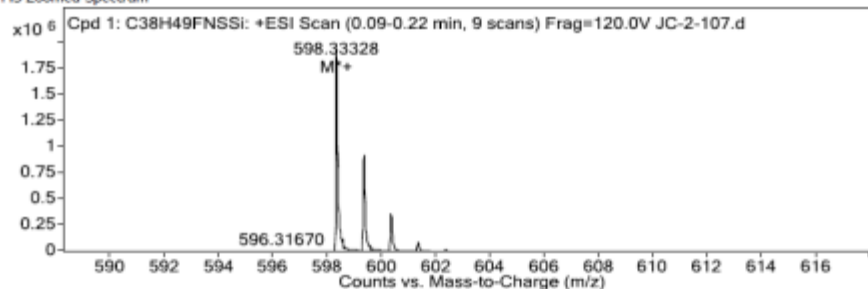
Acq Method ESI_POS_DI.m DA Method ESI_POS_DI.m

Comment

MS Spectrum

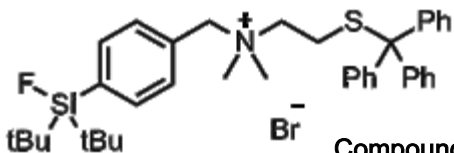


MS Zoomed Spectrum



MS Spectrum Peak List

Ion	Ion Formula	Abund	Expe. m/z	Calc. m/z	Diff(ppm)
M ⁺	C38 H49 F N S Si	1928460	598.33328	598.33335	-0.13

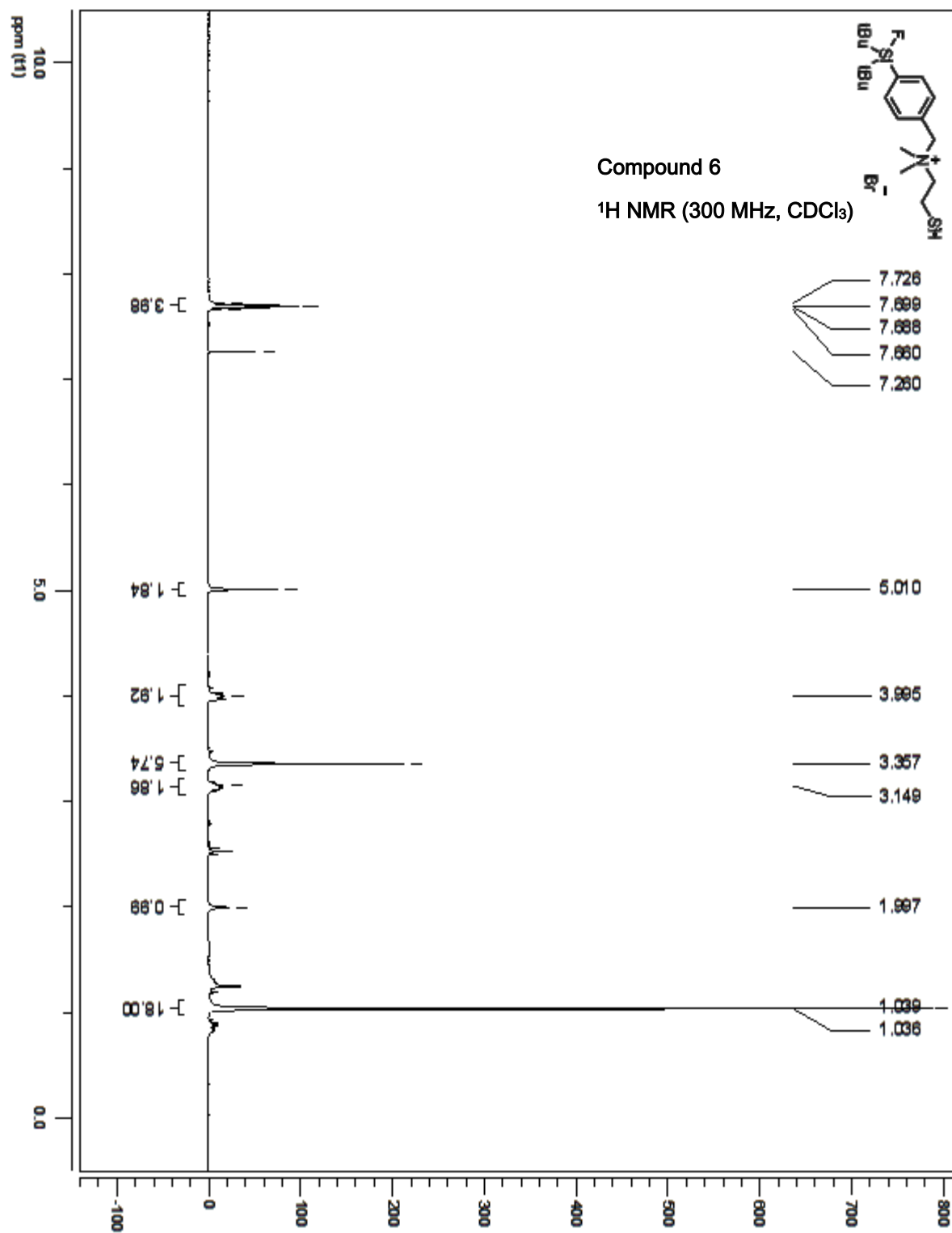


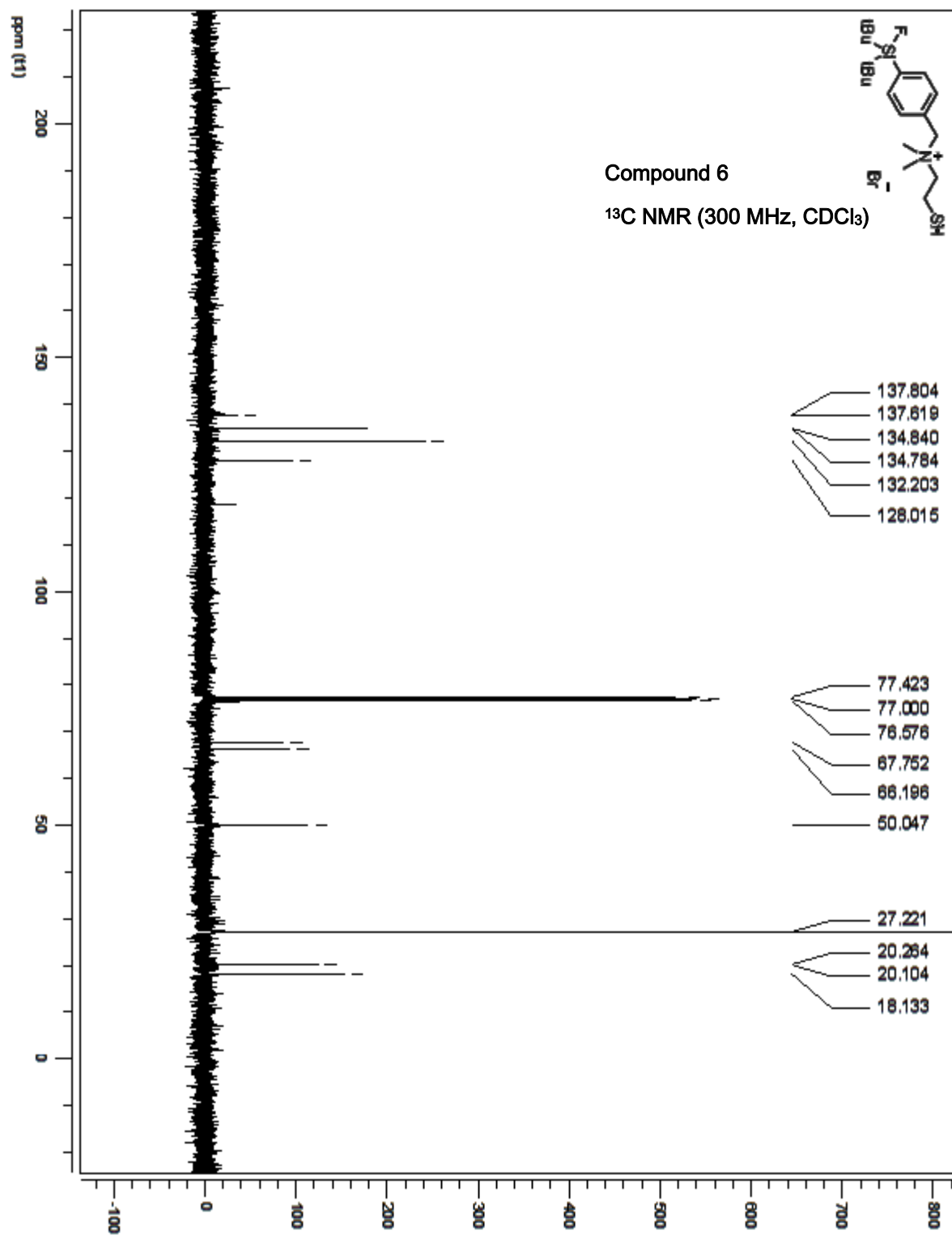
Compound 5

HRMS (ESI)



Centre Régional de Spectrométrie de Masse
 Université de Montréal





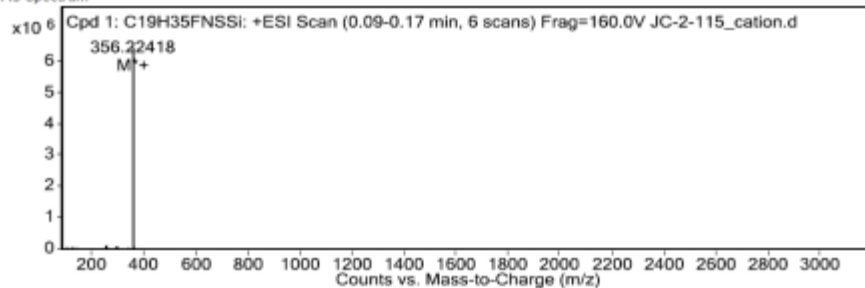
Rapport d'analyse

Data File JC-2-115_cation.d **Sample Name** JC-2-115
Sample Type Sample **Position** P1-C6
Analysis Date 11/24/2010 10:39:22 AM **User Name** Marie-Christine

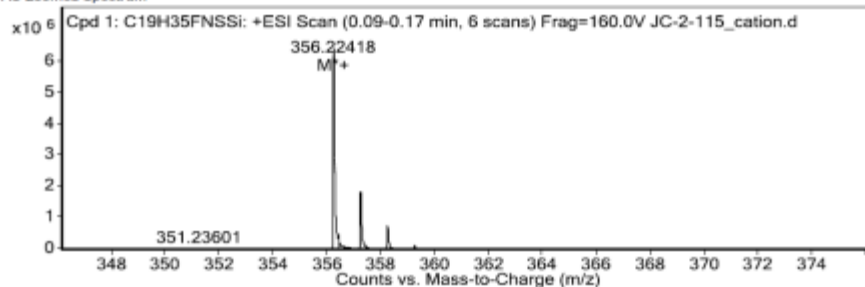
Acq Method ESI_POS_DL.m **DA Method** ESI_POS_DL.m

Comment

MS Spectrum

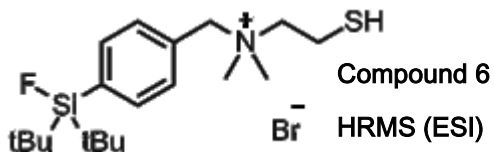


MS Zoomed Spectrum

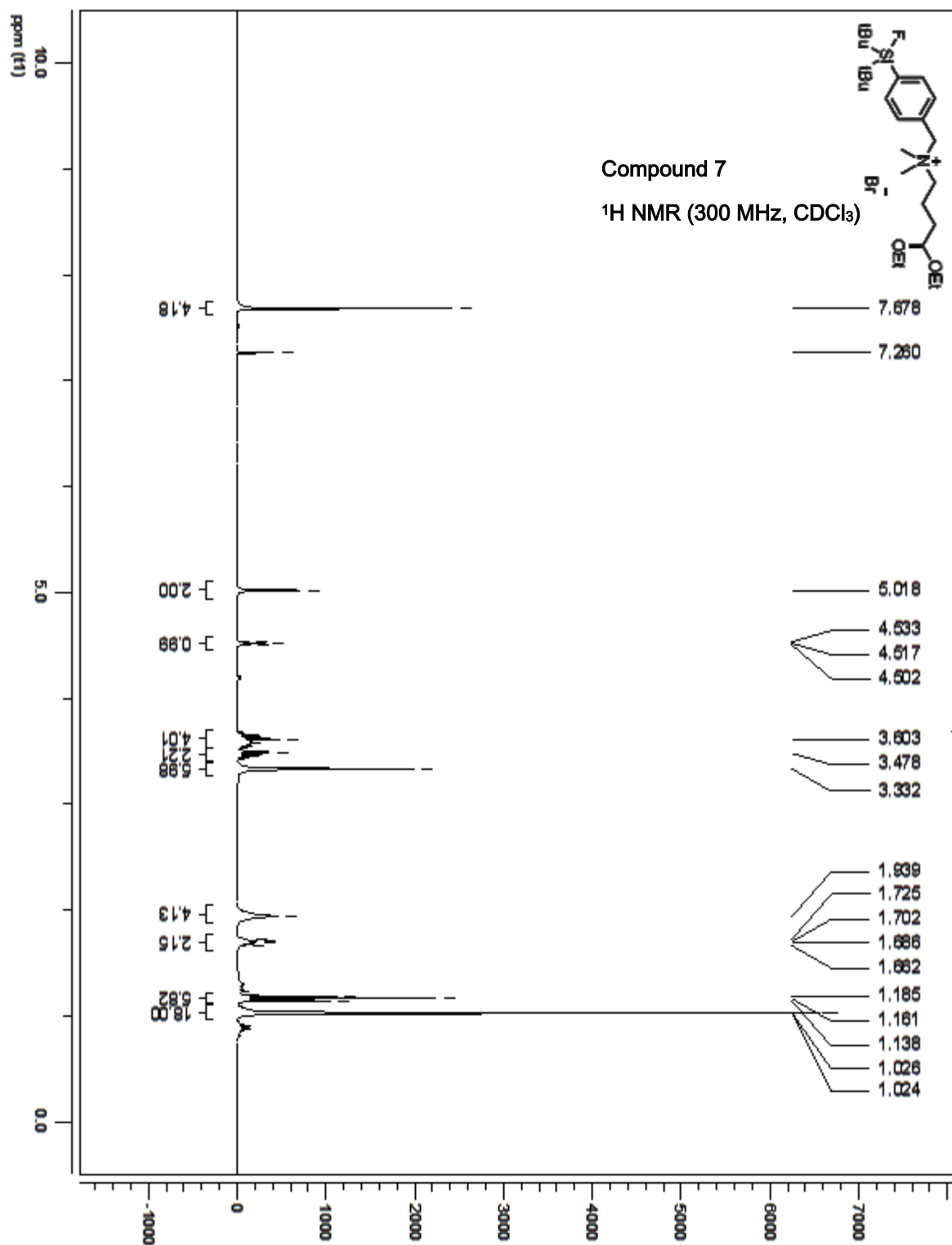


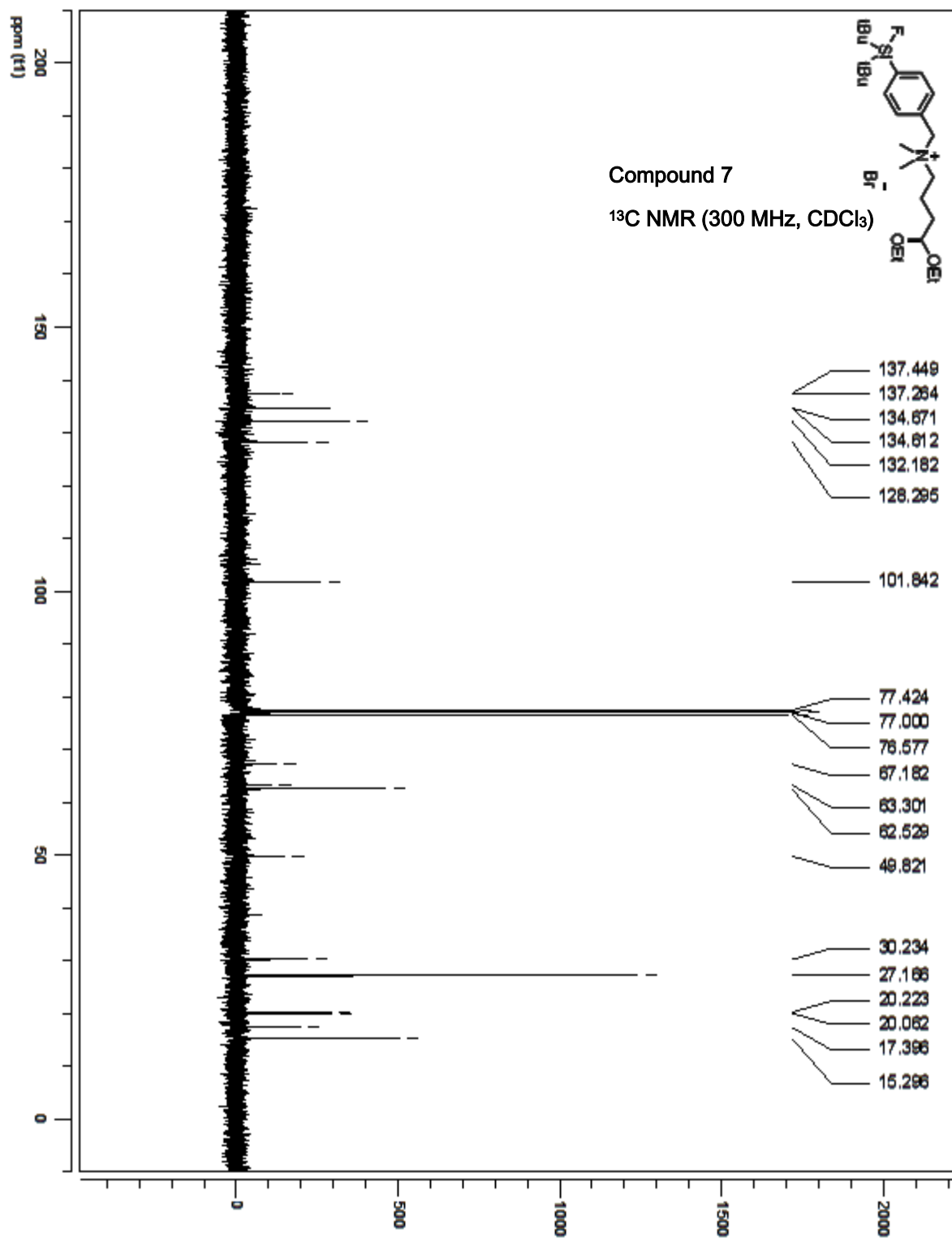
MS Spectrum Peak List

Ion	Ion Formula	Abund	Expe. m/z	Calc. m/z	Diff(ppm)
M ⁺	C19 H35 F N S Si	6426713	356.22418	356.2238	1.06



Centre Regional de Spectrometrie de Masse
Universite de Montreal

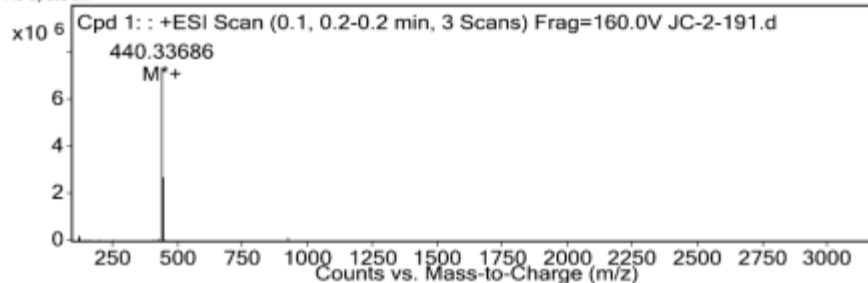




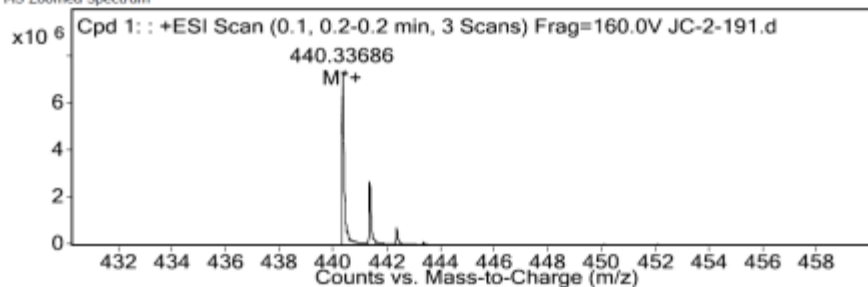
Rapport d'analyse

Data File JC-2-191.d **Sample Name** JC-2-191
Sample Type Sample **Position** P1-D9
Analysis Date 5/8/2012 1:37:02 PM **User Name** Marie-Christine
Acq Method ESI_POS_DLM **DA Method** ESI_POS_DLM
Comment

MS Spectrum

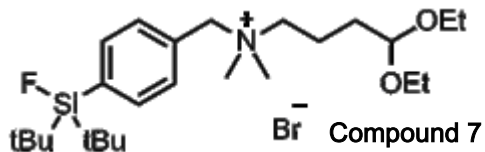


MS Zoomed Spectrum



MS Spectrum Peak List

Ion	Ion Formula	Abund	Expe. m/z	Calc. m/z	Diff(ppm)
M ⁺	C ₂₅ H ₄₇ FNO ₂ Si	7334945.2	440.33686	440.33546	-3.19

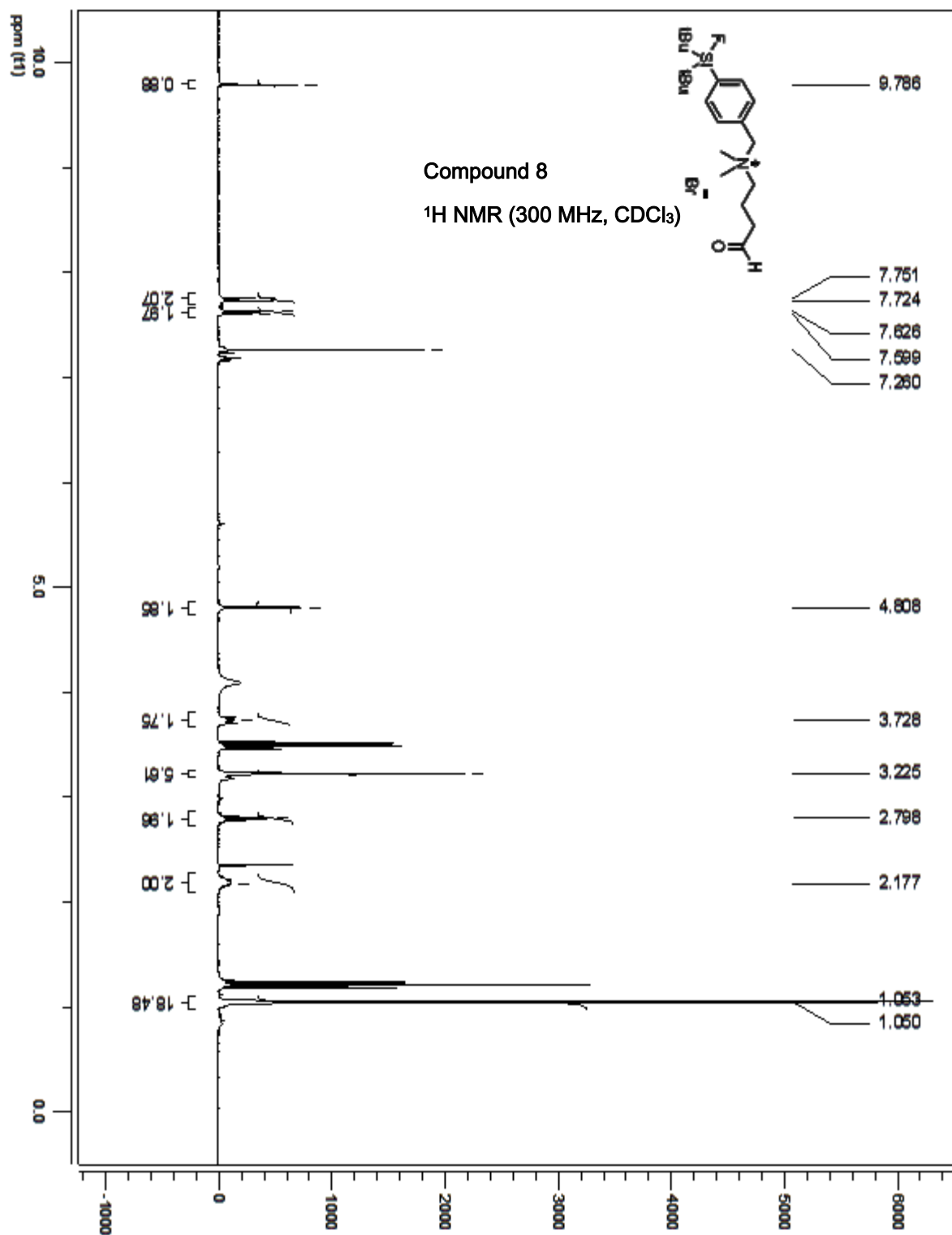


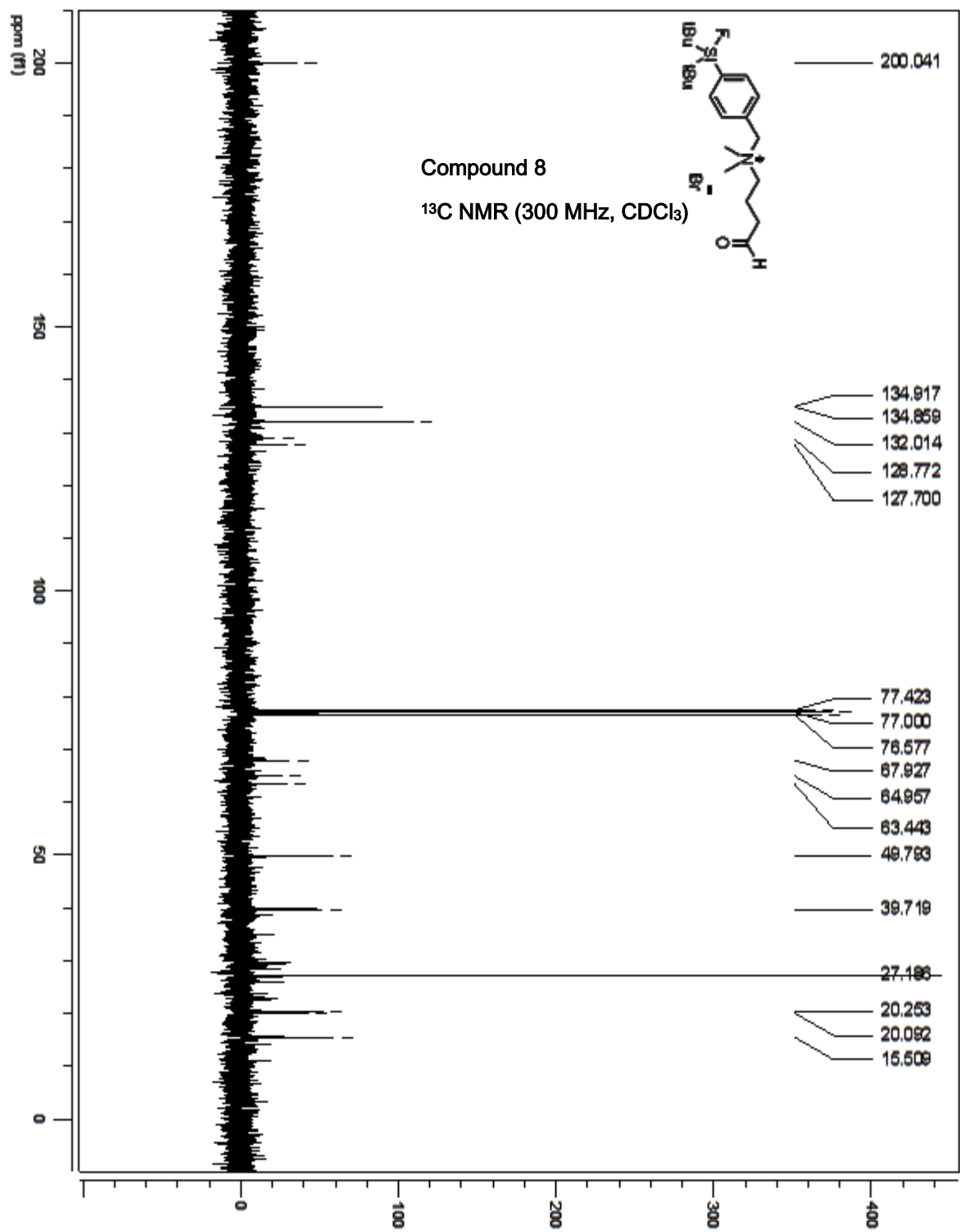
HRMS (ESI)



Centre Régional de Spectrométrie de Masse
Université de Montréal

Page 1 of 1

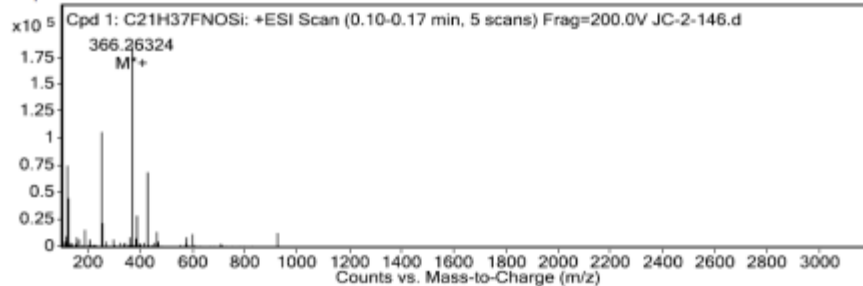




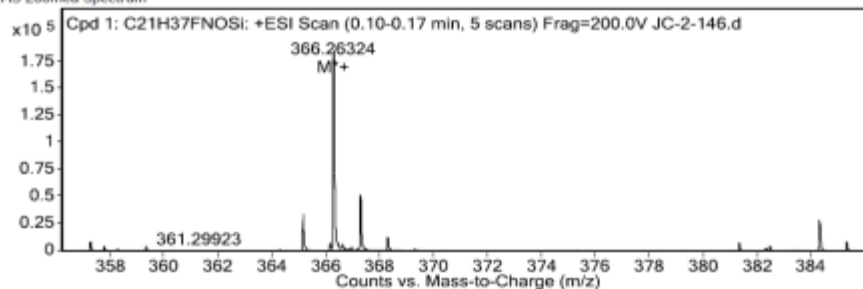
Rapport d'analyse

Data File JC-2-146.d **Sample Name** JC-2-146
Sample Type Sample **Position** P1-C7
Analysis Date 4/14/2011 3:18:54 PM **User Name** Marie-Christine
Acq Method ESI_POS_DLm **DA Method** ESI_POS_DLm
Comment

MS Spectrum

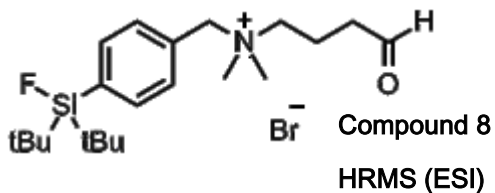


MS Zoomed Spectrum



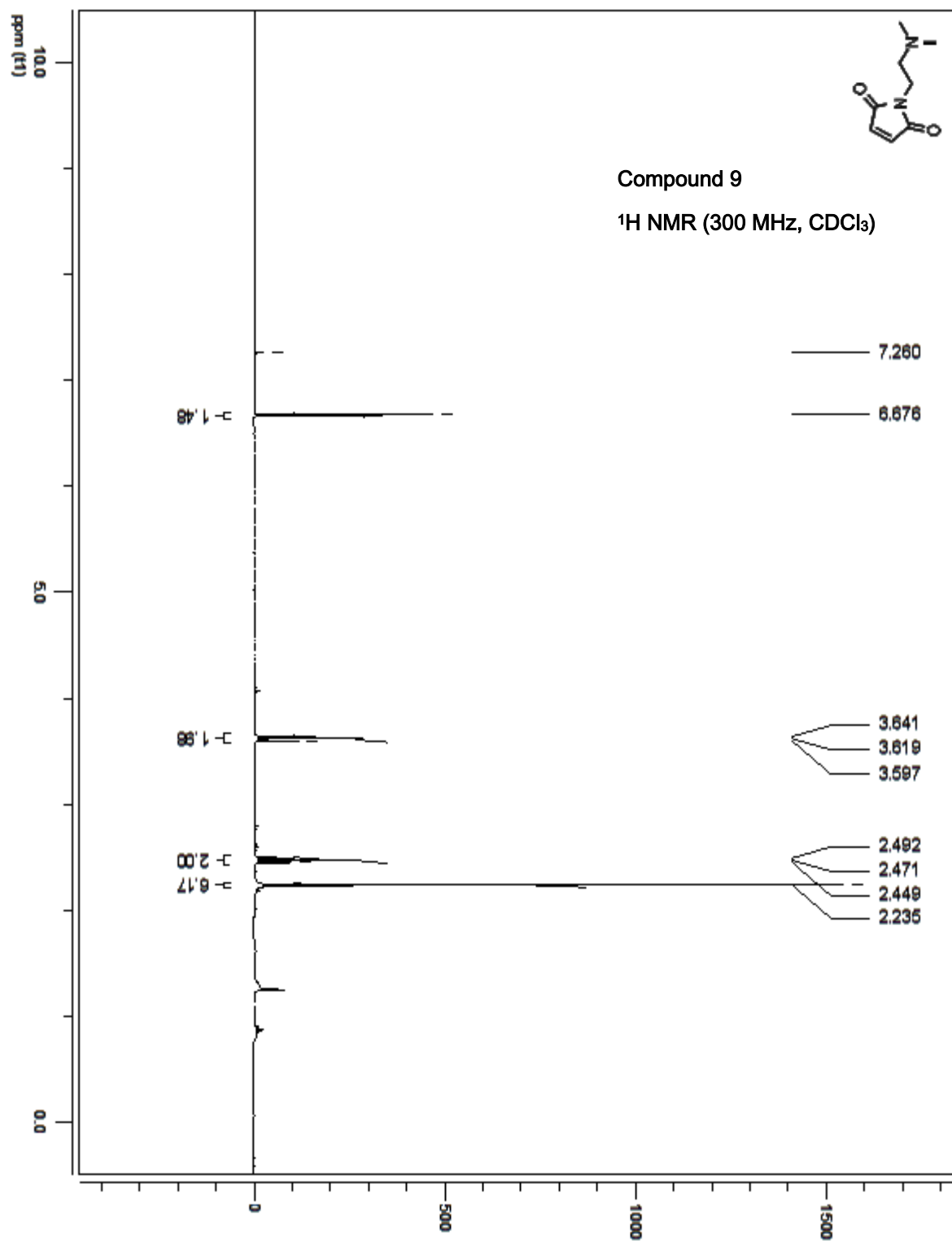
MS Spectrum Peak List

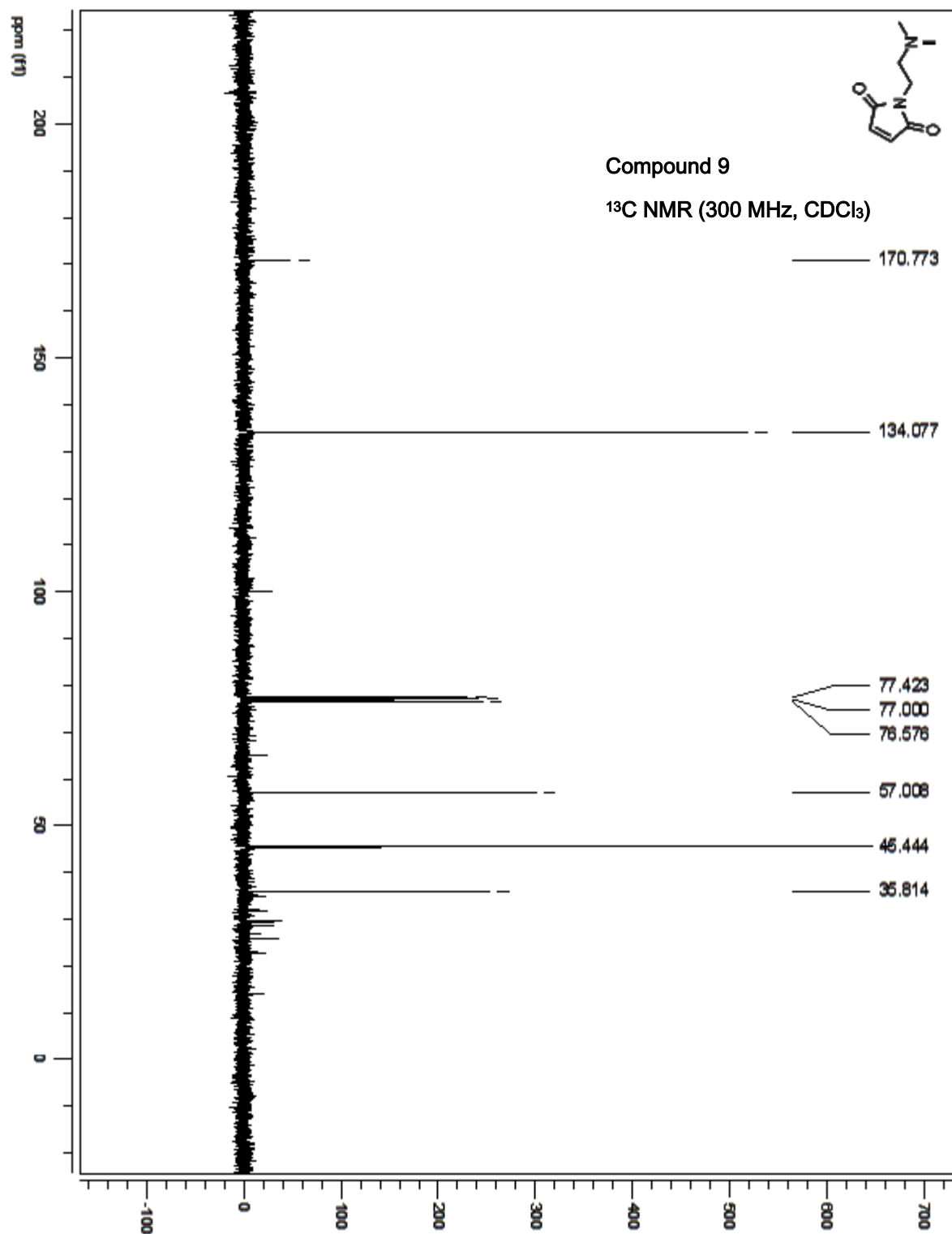
Ion	Ion Formula	Abund	Expe. m/z	Calc. m/z	Diff(ppm)
M ⁺	C ₂₁ H ₃₇ FNOSi	186696	366.26324	366.2623	2.57



Centre Regional de Spectrometrie de Masse
Universite de Montreal

Page 1 of 1

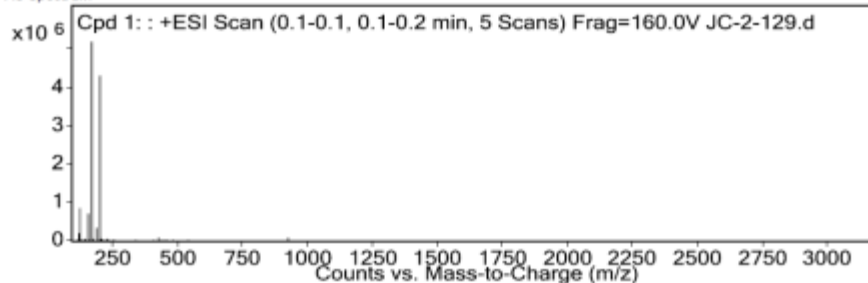




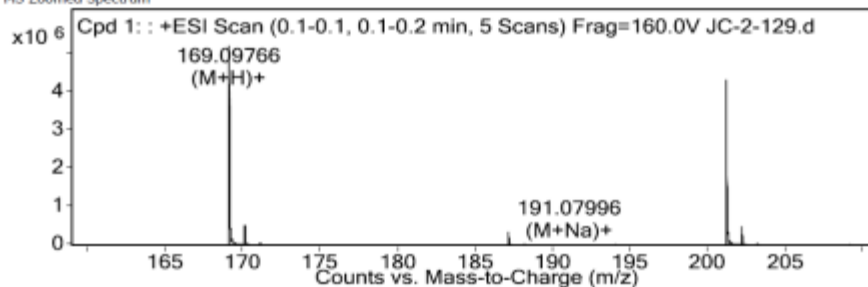
Rapport d'analyse

Data File JC-2-129.d **Sample Name** JC-2-129
Sample Type Sample **Position** P1-E1
Analysis Date 5/8/2012 1:38:59 PM **User Name** Marie-Christine
Acq Method ESI_POS_DLm **DA Method** ESI_POS_DLm
Comment

MS Spectrum

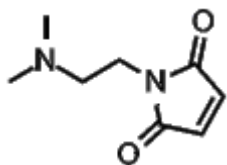


MS Zoomed Spectrum



MS Spectrum Peak List

Ion	Ion Formula	Abund	Expe. m/z	Calc. m/z	Diff(ppm)
(M+H)+	C8H13N2O2	5212050.6	169.09766	169.09715	2.97
(M+Na)+	C8H12N2NaO2	10966.7	191.07996	191.0791	4.51

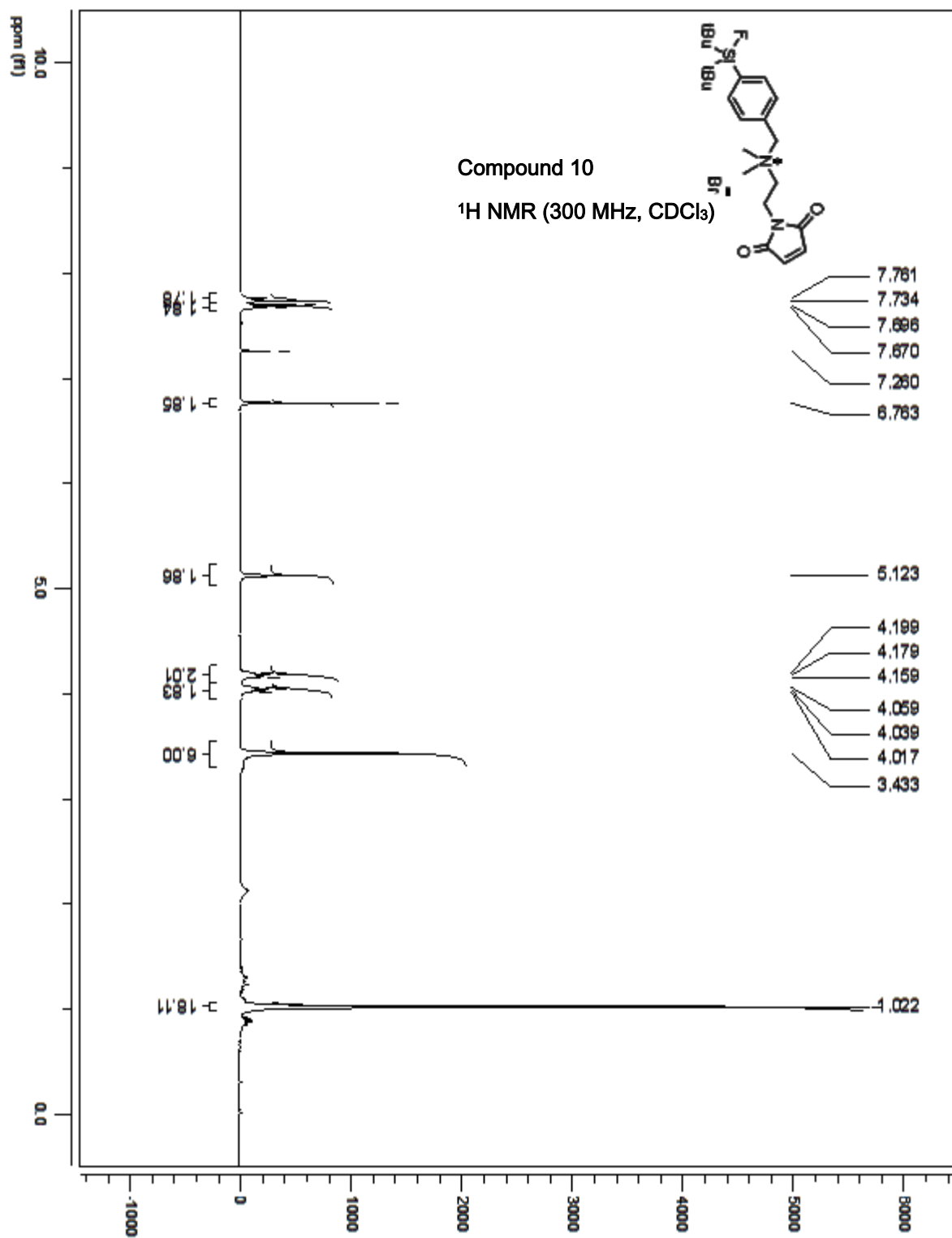


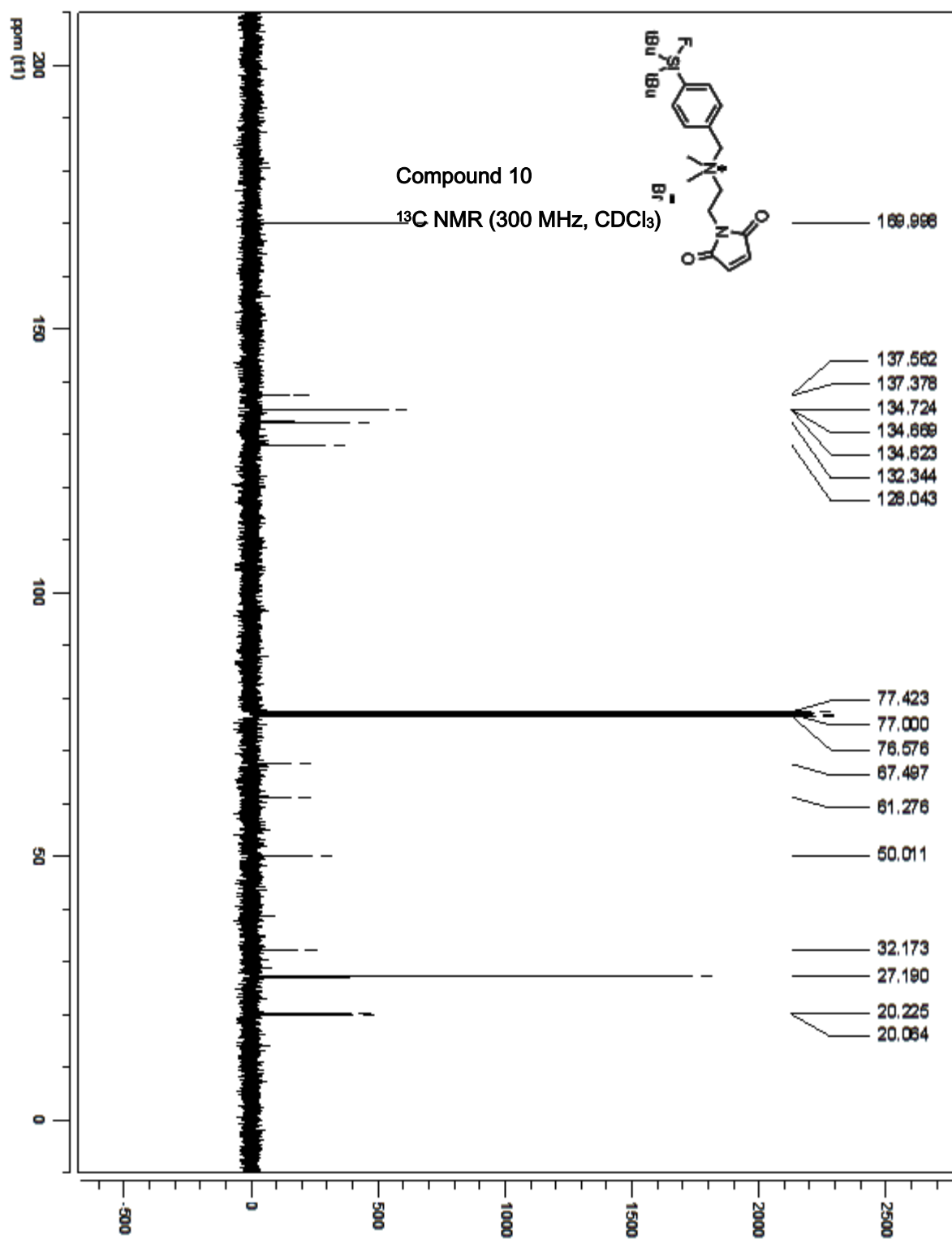
Compound 9

HRMS (ESI)



Centre Regional de Spectrometrie de Masse
Universite de Montreal

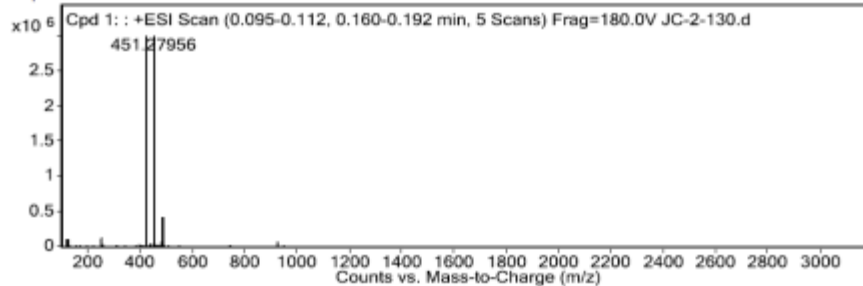




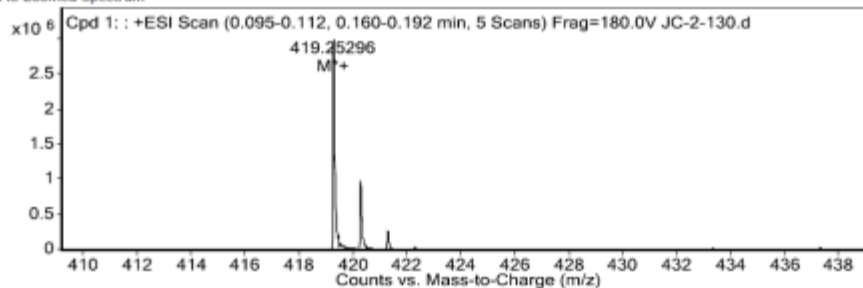
Rapport d'analyse

Data File JC-2-130.d
Sample Name JC-2-130
Sample Type Sample
Position P1-B3
Analysis Date 6/15/2011 5:04:27 PM
User Name Marie-Christine
Acq Method ESI_POS_DLm
DA Method ESI_POS_DLm
Comment

MS Spectrum

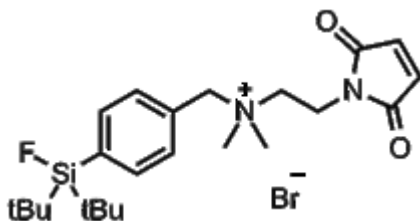


MS Zoomed Spectrum



MS Spectrum Peak List

Ion	Ion Formula	Abund	Expe. m/z	Calc. m/z	Diff(ppm)
M ⁺	C ₂₃ H ₃₆ N ₂ O ₂ Si	3046380.5	419.25296	419.25246	-1.2

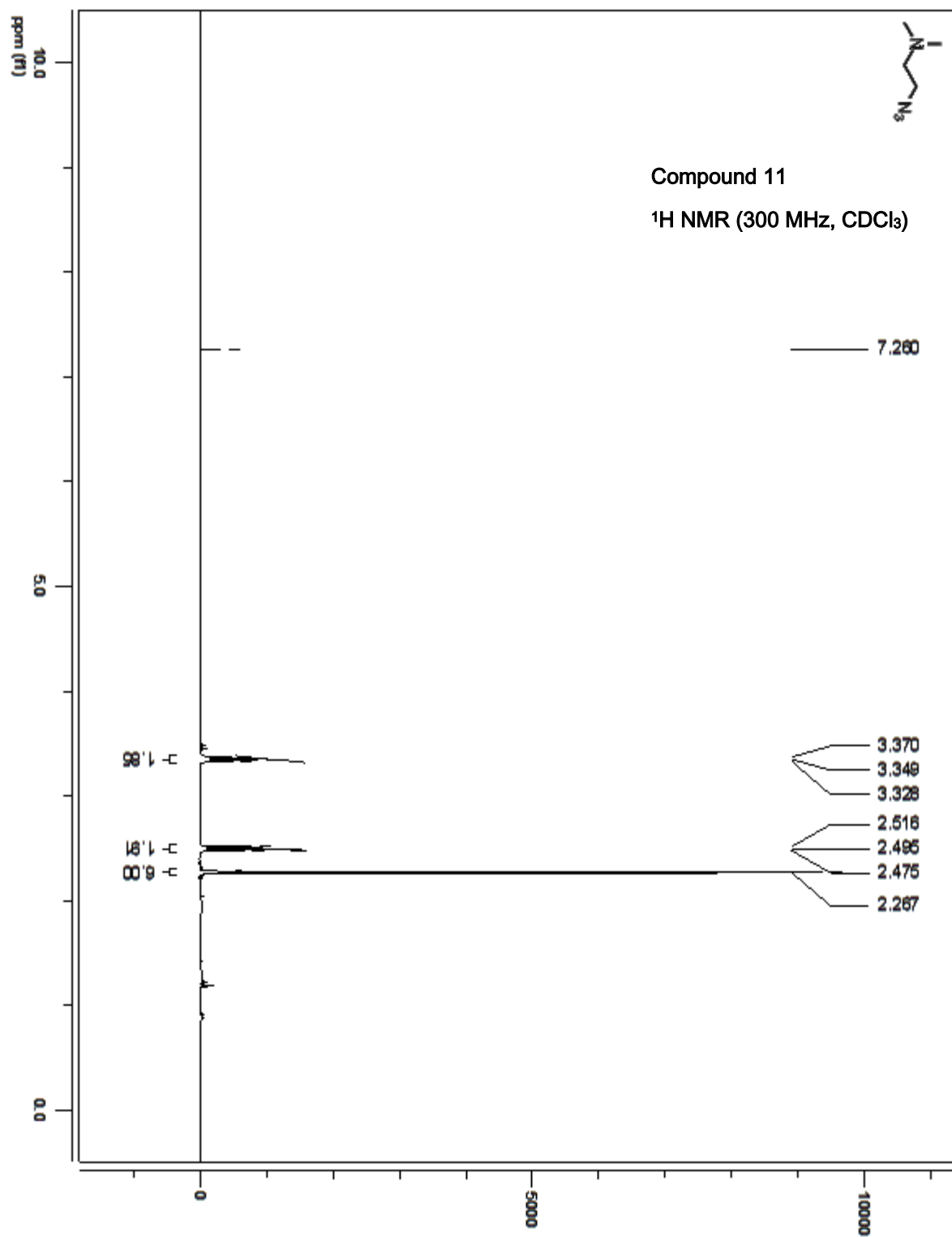


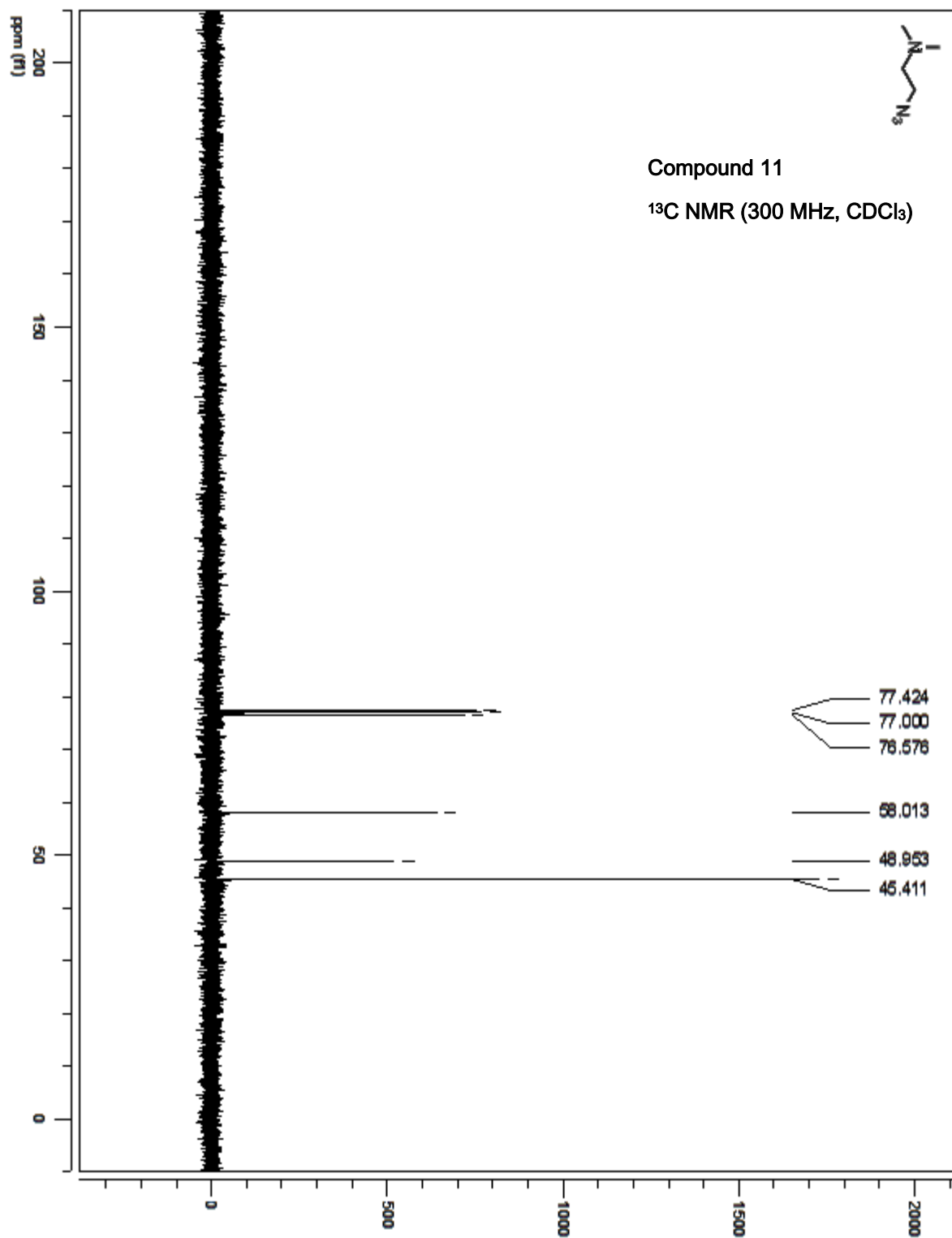
Compound 10

HRMS (ESI)



Centre Regional de Spectrometrie de Masse
Universite de Montreal

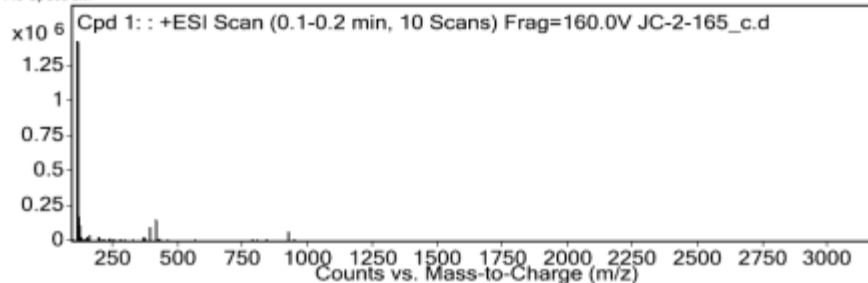




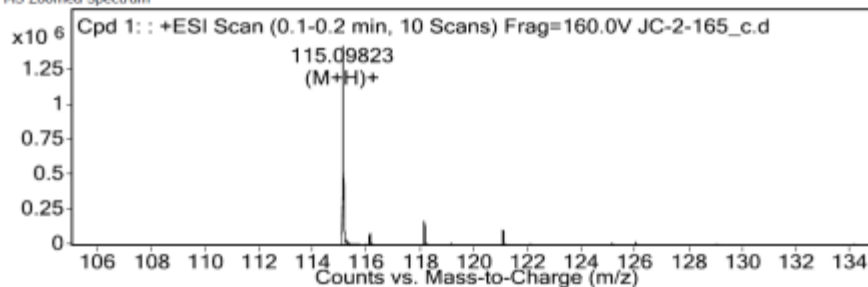
Rapport d'analyse

Data File JC-2-165_c.d **Sample Name** JC-2-165
Sample Type Sample **Position** P1-E2
Analysis Date 5/8/2012 2:29:44 PM **User Name** Marie-Christine
Acq Method ESI_POS_DLM **DA Method** ESI_POS_DLM
Comment

MS Spectrum

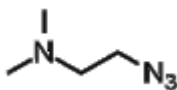


MS Zoomed Spectrum



MS Spectrum Peak List

Ion	Ion Formula	Abund	Expe. m/z	Calc. m/z	Diff(ppm)
(M+H)+	C4H11N4	1440590.5	115.09823	115.09782	3.55

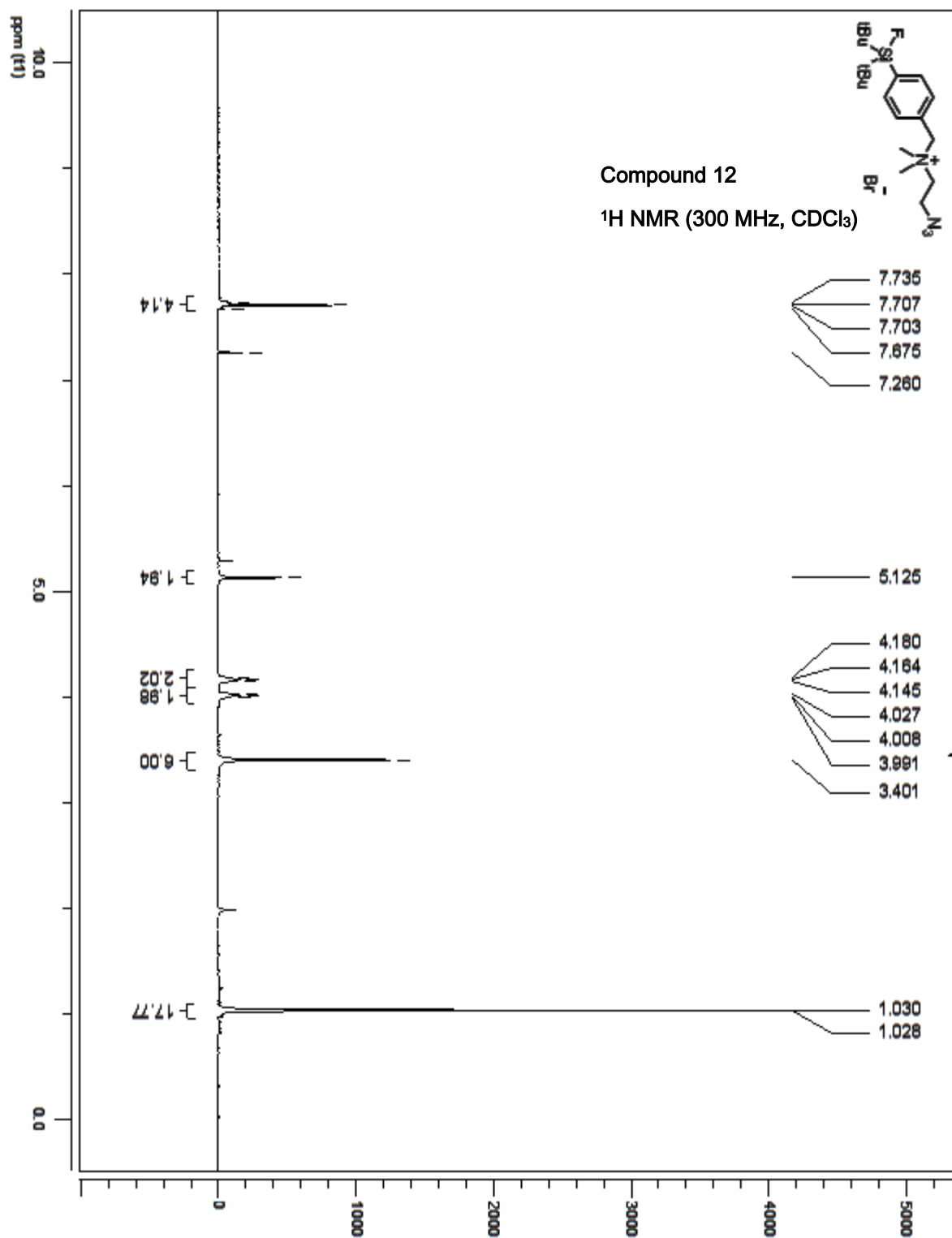


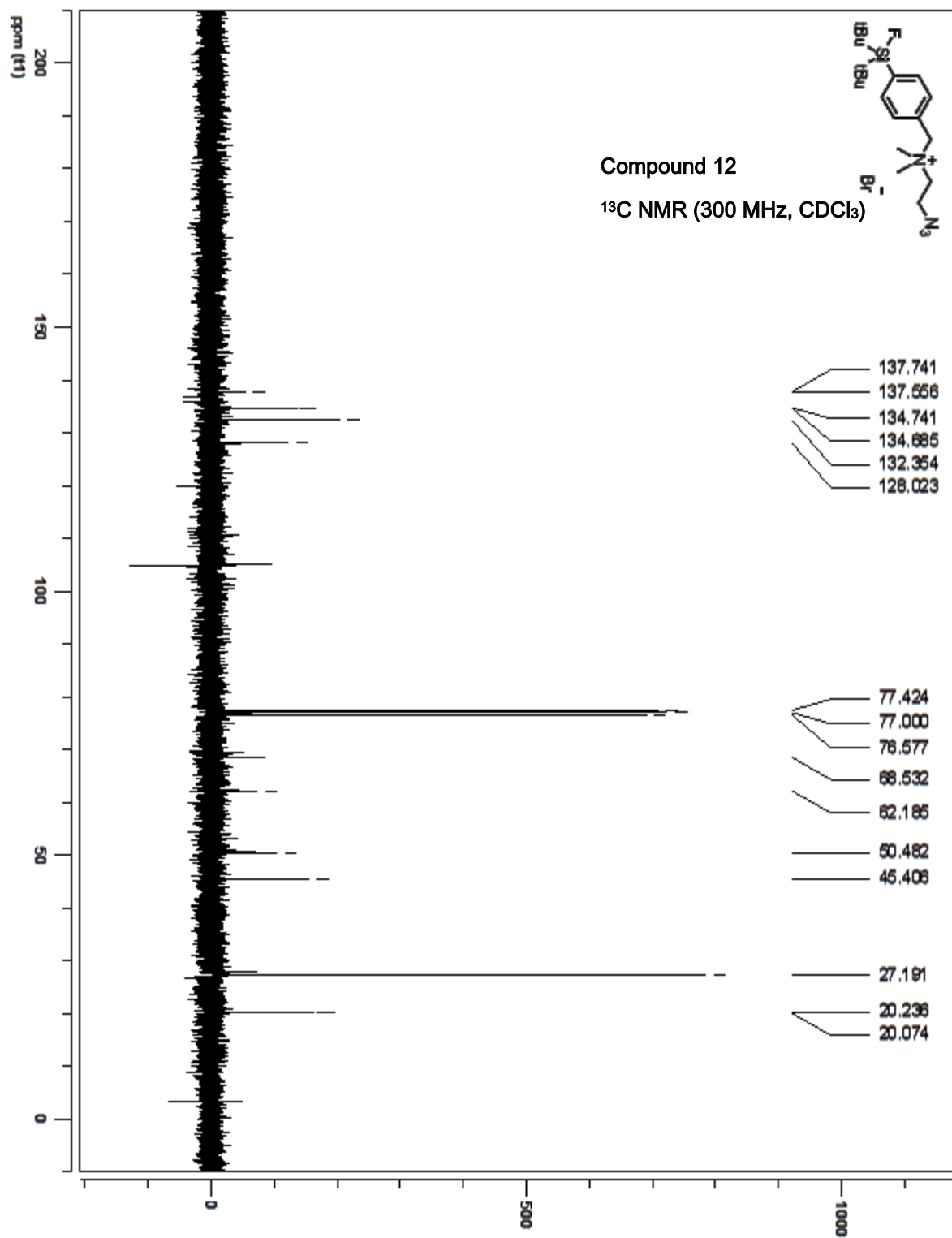
Compound 11

HRMS (ESI)



Centre Regional de Spectrometrie de Masse
Universite de Montreal

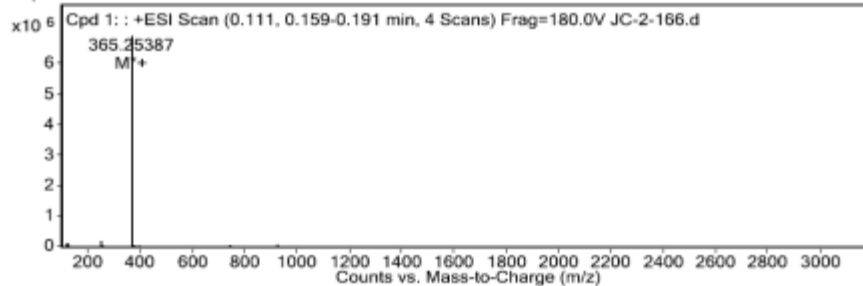




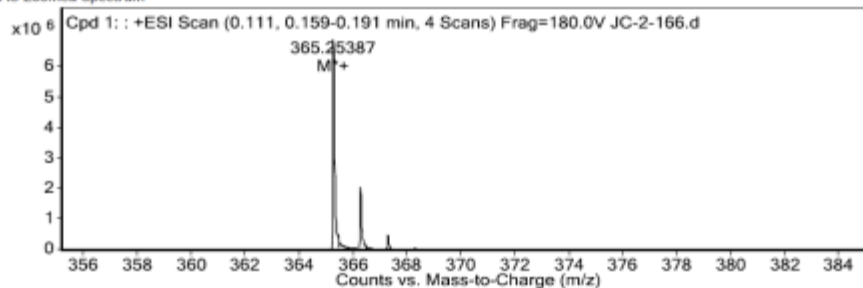
Rapport d'analyse

Data File JC-2-166.d **Sample Name** JC-2-166
Sample Type Sample **Position** P1-B5
Analysis Date 6/15/2011 5:08:33 PM **User Name** Marie-Christine
Acq Method ESI_POS_DLM **DA Method** ESI_POS_DLM
Comment

MS Spectrum

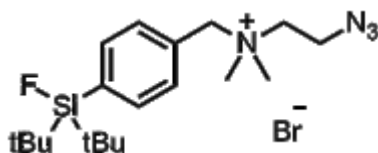


MS Zoomed Spectrum



MS Spectrum Peak List

Ion	Ion Formula	Abund	Expe. m/z	Calc. m/z	Diff(ppm)
[M] ⁺	C ₁₉ H ₃₄ FN ₃ Si	7006179.6	365.25387	365.25313	-2.04

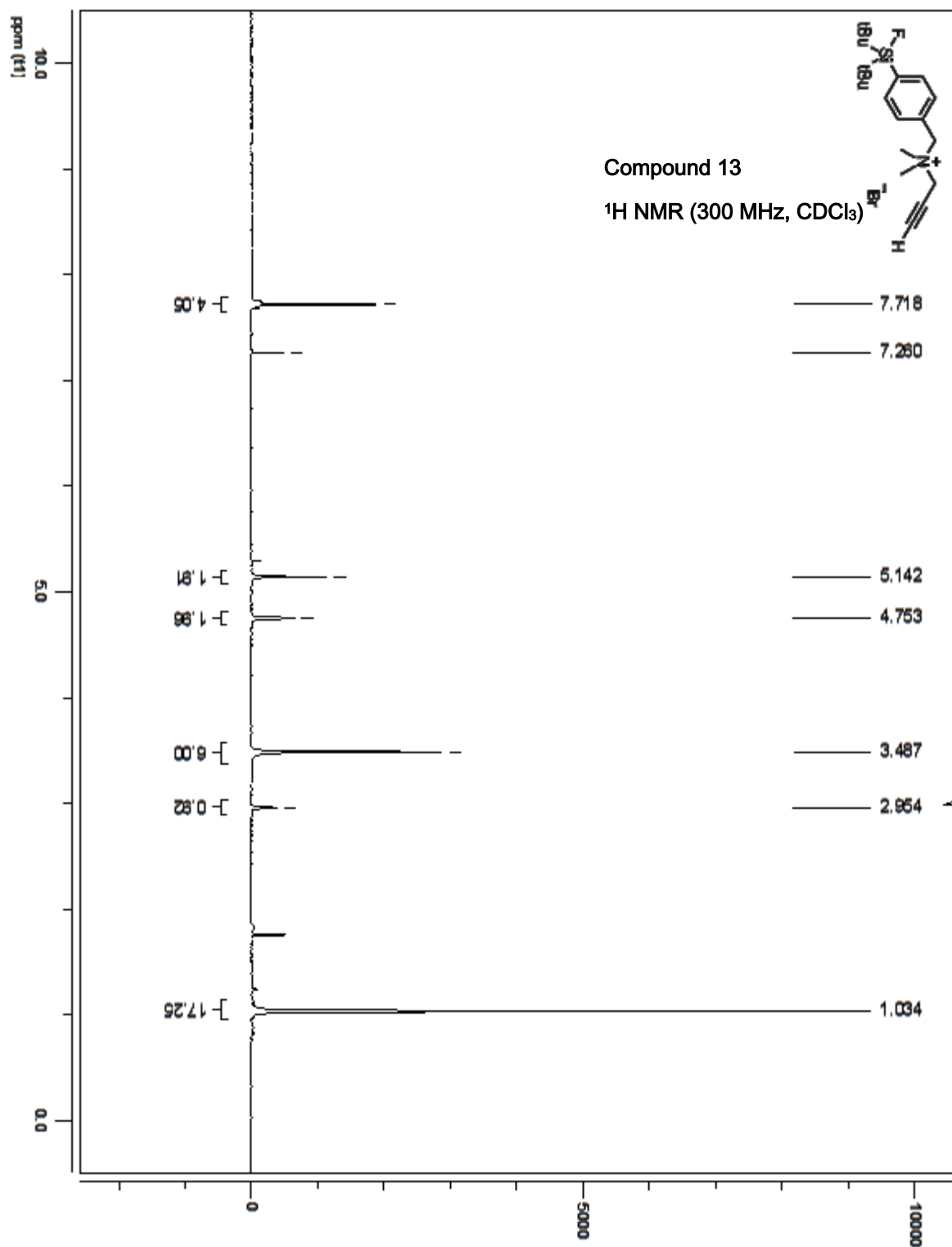


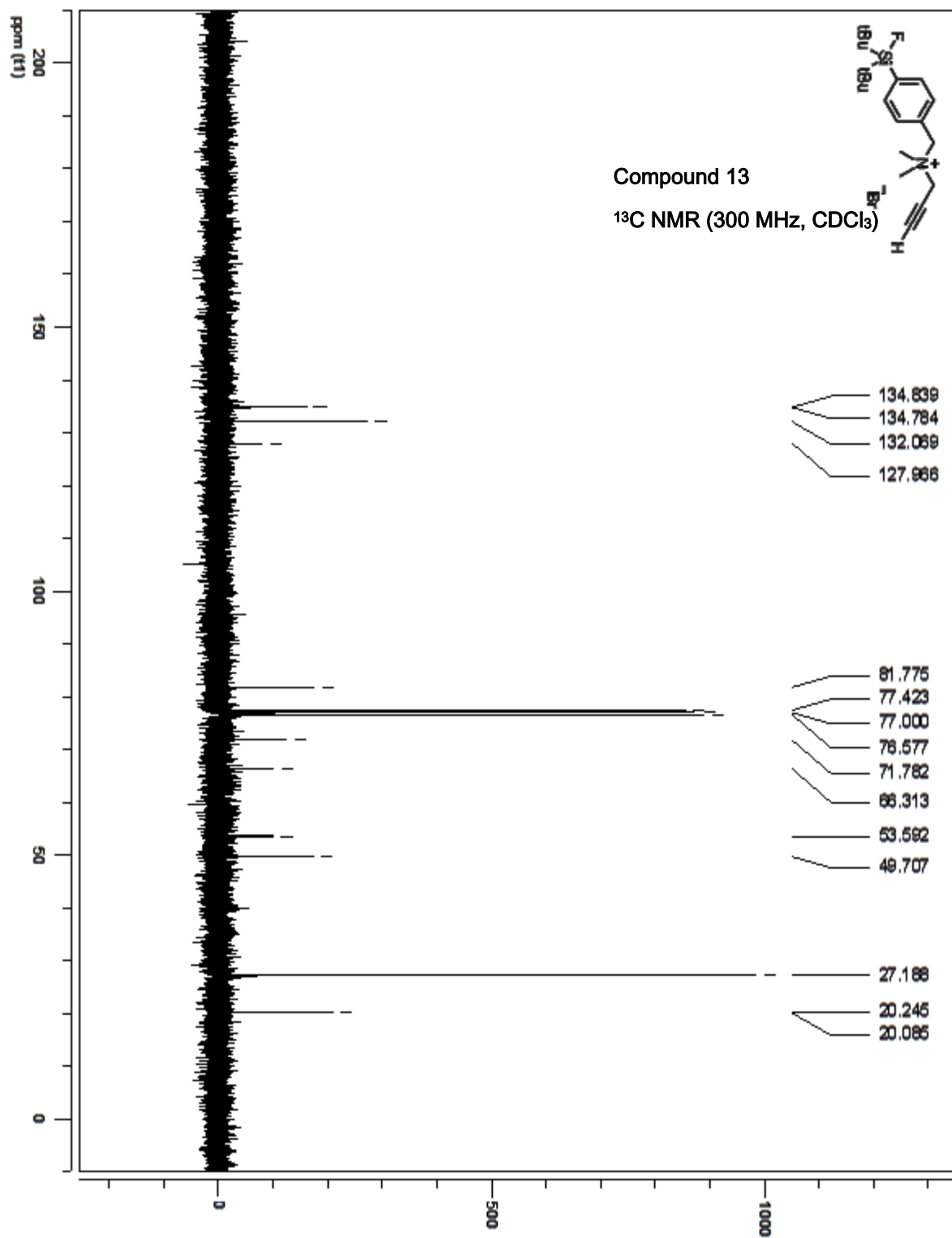
Compound 12

HRMS (ESI)



Centre Régional de Spectrométrie de Masse
Université de Montréal

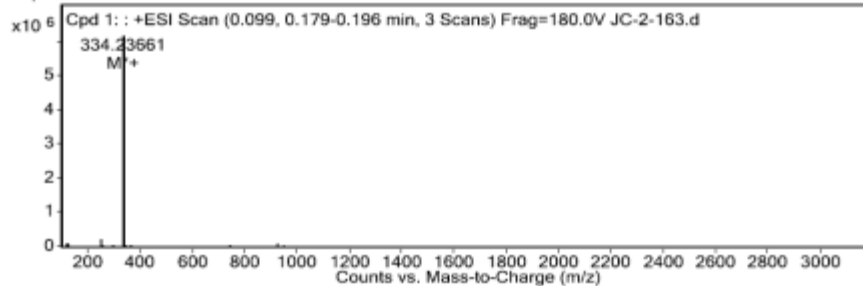




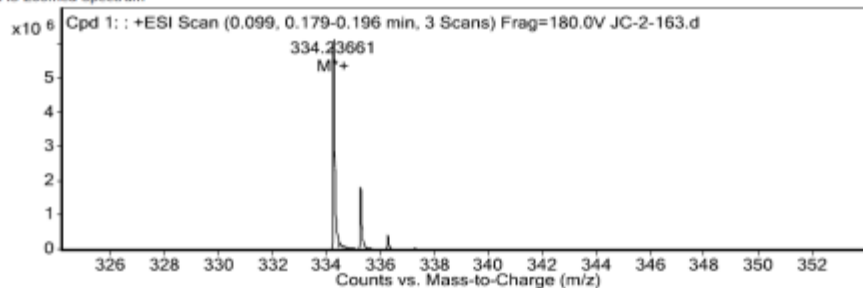
Rapport d'analyse

Data File JC-2-163.d **Sample Name** JC-2-163
Sample Type Sample **Position** P1-B4
Analysis Date 6/15/2011 5:06:31 PM **User Name** Marie-Christine
Acq Method ESI_POS_DLM **DA Method** ESI_POS_DLM
Comment

MS Spectrum

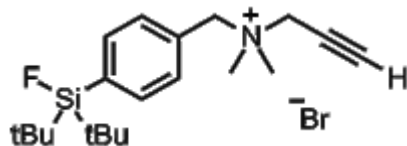


MS Zoomed Spectrum



MS Spectrum Peak List

Ion	Ion Formula	Abund	Expe. m/z	Calc. m/z	Diff(ppm)
M ⁺⁺	C ₂₀ H ₃₃ FNSi	6213516.9	334.23661	334.23608	-1.58

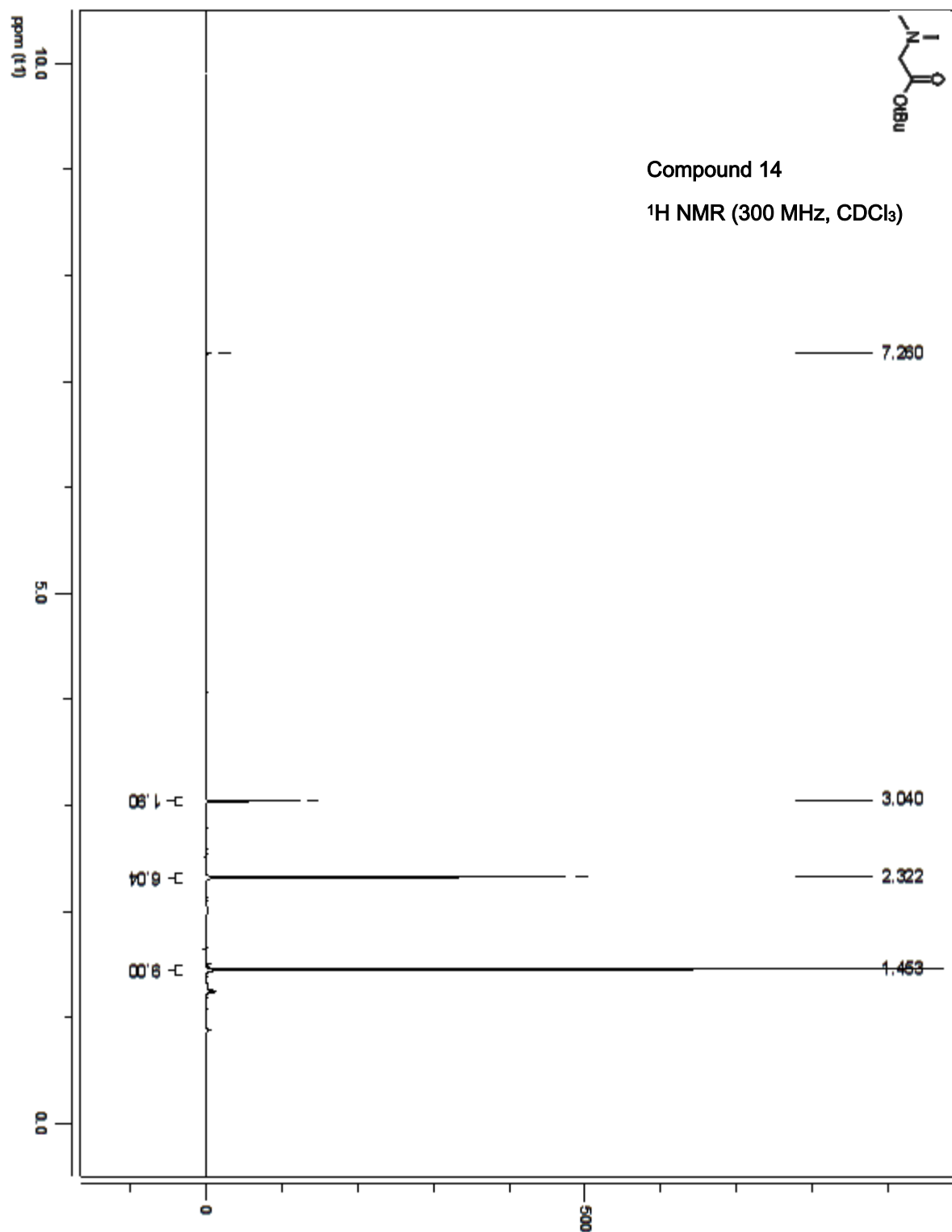


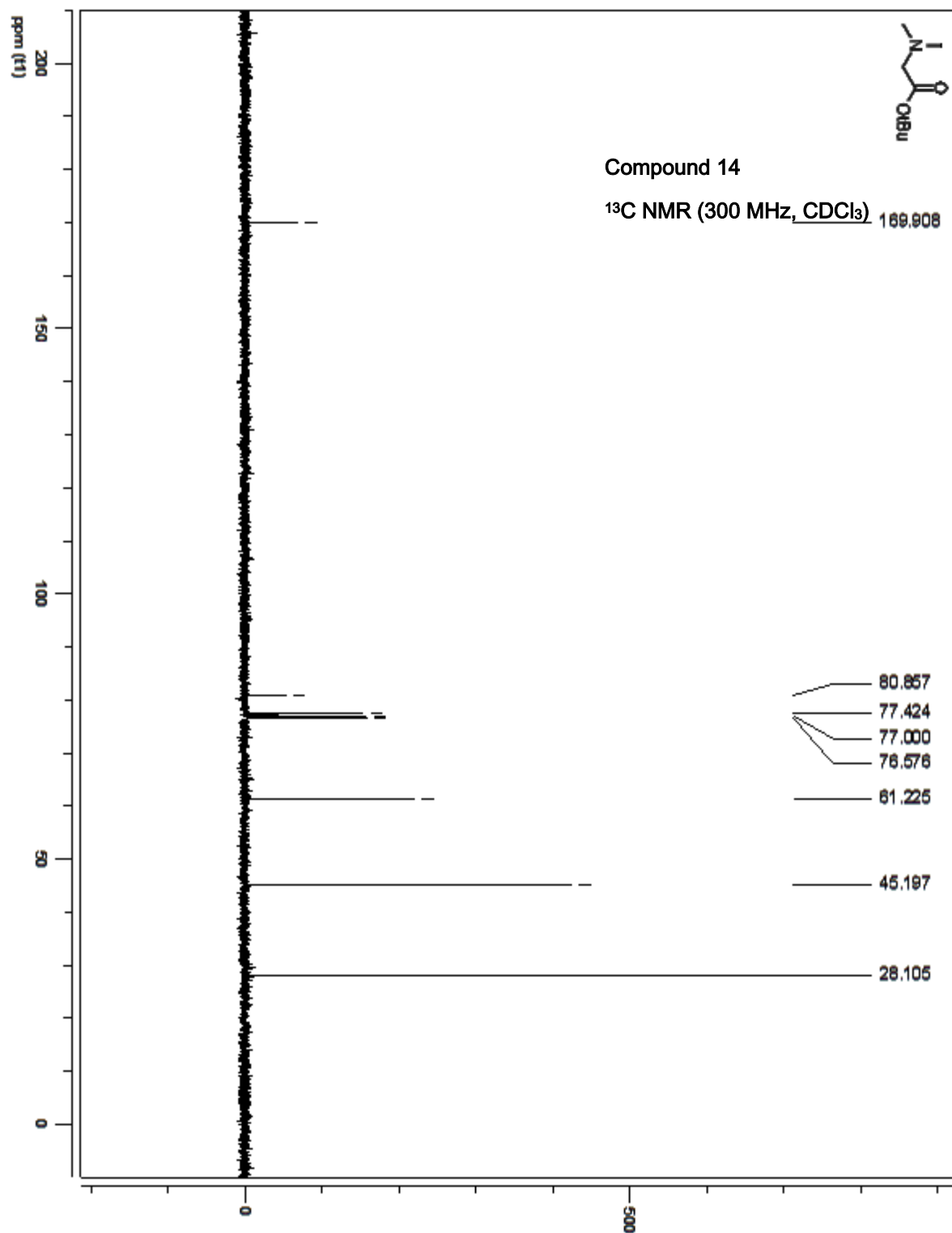
Compound 13

HRMS (ESI)



Centre Regional de Spectrometrie de Masse
Universite de Montreal

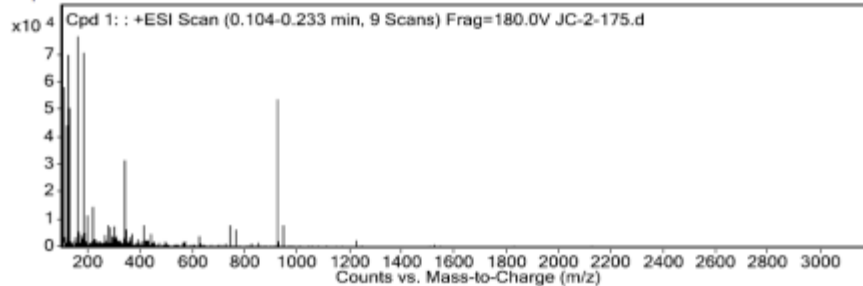




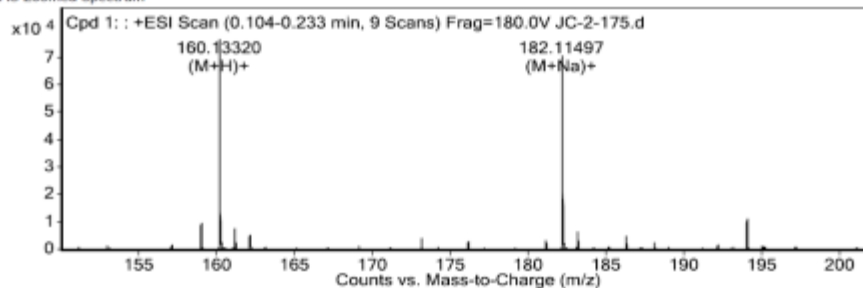
Rapport d'analyse

Data File JC-2-175.d **Sample Name** JC-2-175
Sample Type Sample **Position** P1-B6
Analysis Date 6/15/2011 5:10:41 PM **User Name** Marie-Christine
Acq Method ESI_POS_DLm **DA Method** ESI_POS_DLm
Comment

MS Spectrum

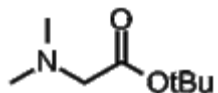


MS Zoomed Spectrum



MS Spectrum Peak List

Ion	Ion Formula	Abund	Expe. m/z	Calc. m/z	Diff(ppm)
(M+H)+	C8H18NO2	78675.1	160.1332	160.13321	-0.06
(M+Na)+	C8H17NNaO2	71094.9	182.11497	182.11515	-1

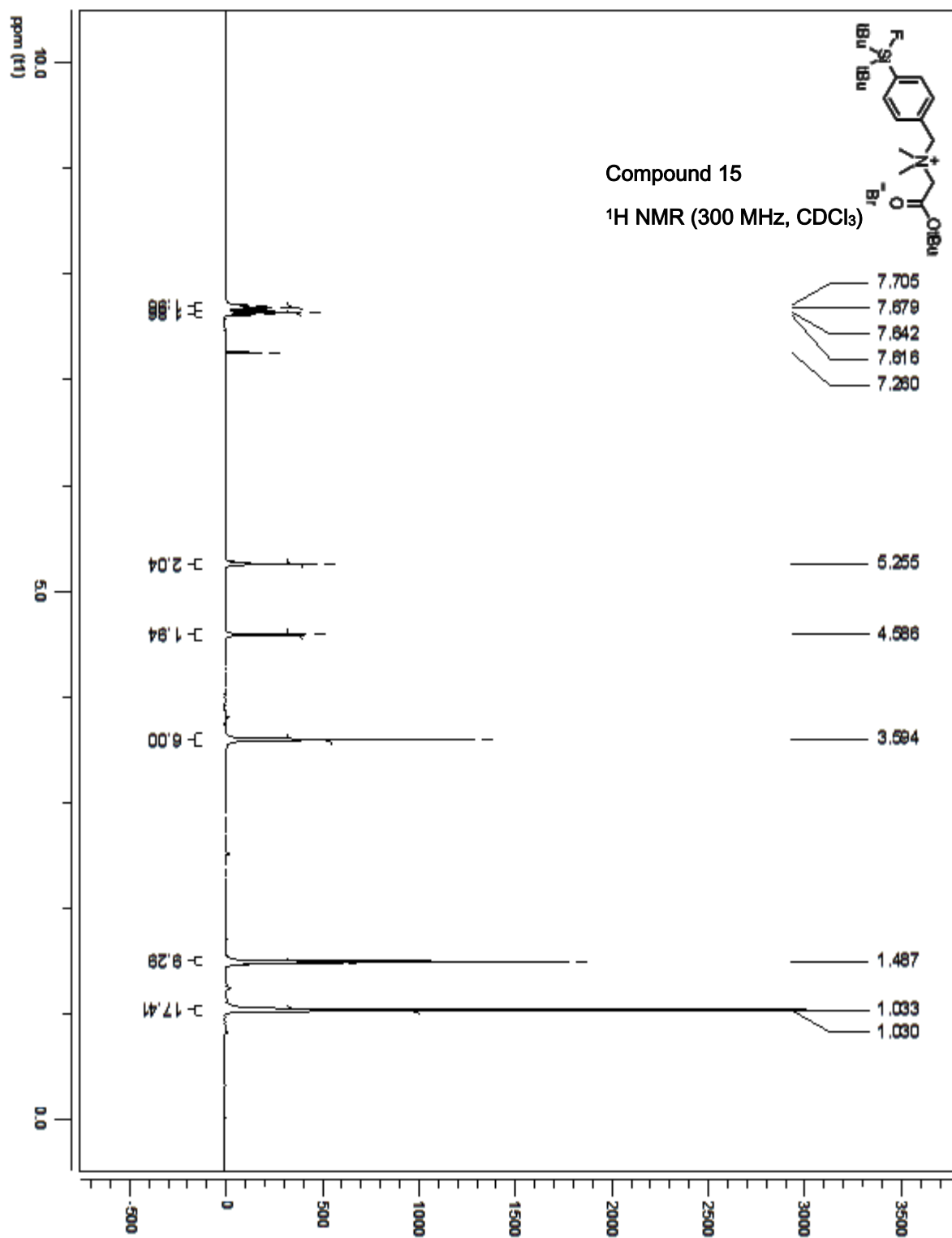


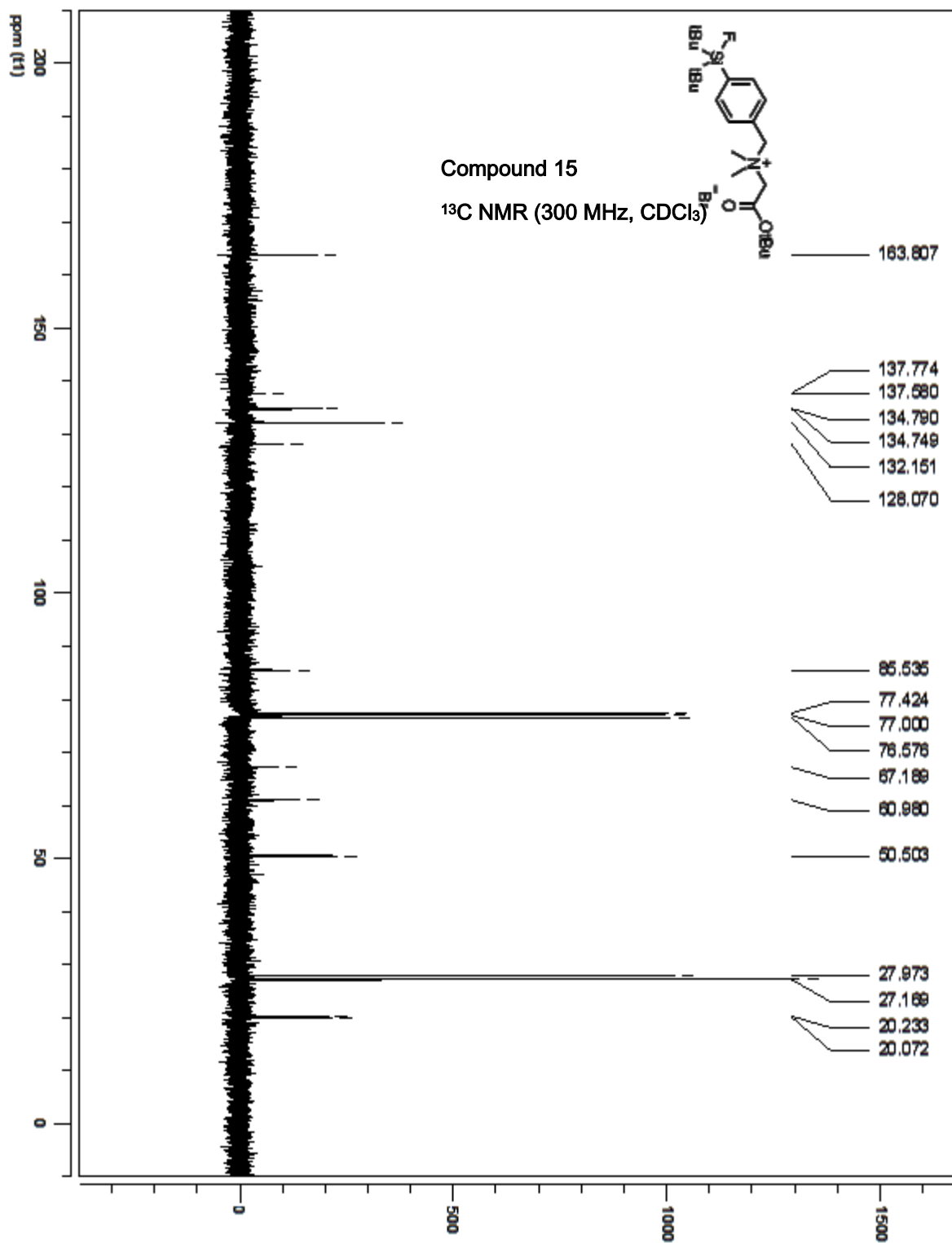
Compound 14

HRMS (ESI)



Centre Regional de Spectrometrie de Masse
Universite de Montreal

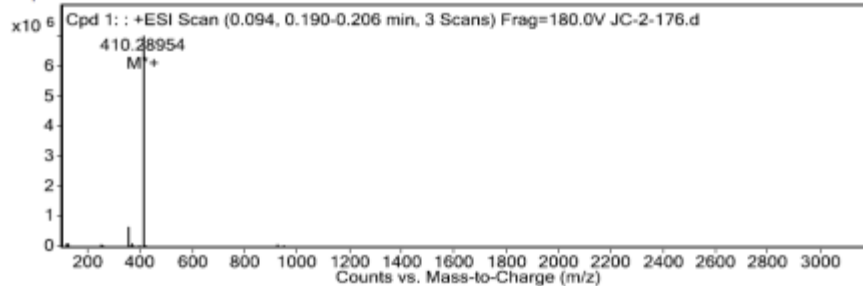




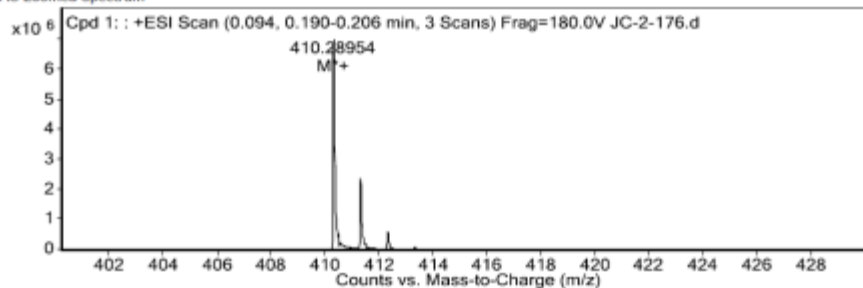
Rapport d'analyse

Data File JC-2-176.d **Sample Name** JC-2-176
Sample Type Sample **Position** P1-B7
Analysis Date 6/15/2011 5:12:53 PM **User Name** Marie-Christine
Acq Method ESI_POS_DLm **DA Method** ESI_POS_DLm
Comment

MS Spectrum

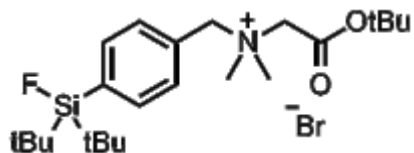


MS Zoomed Spectrum



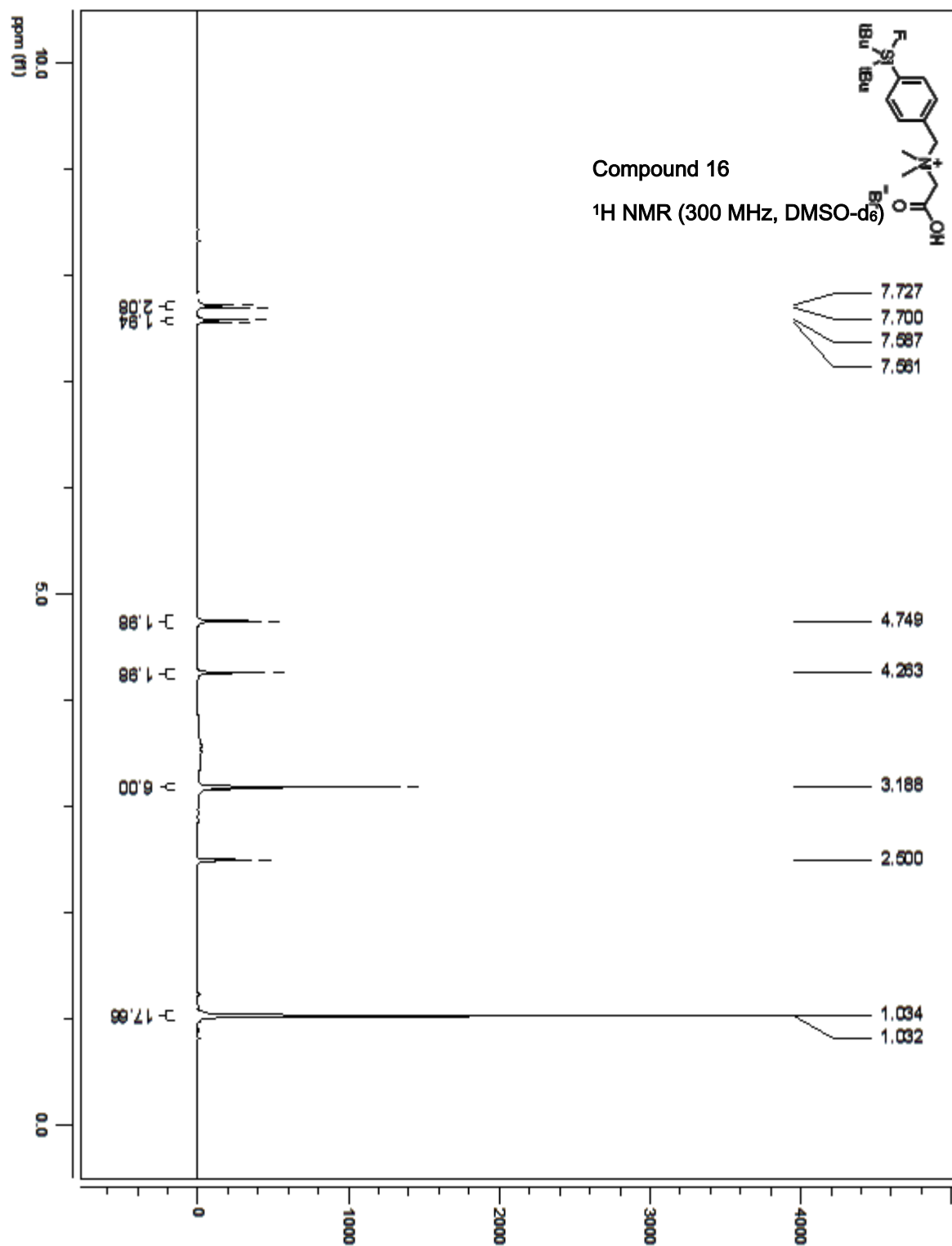
MS Spectrum Peak List

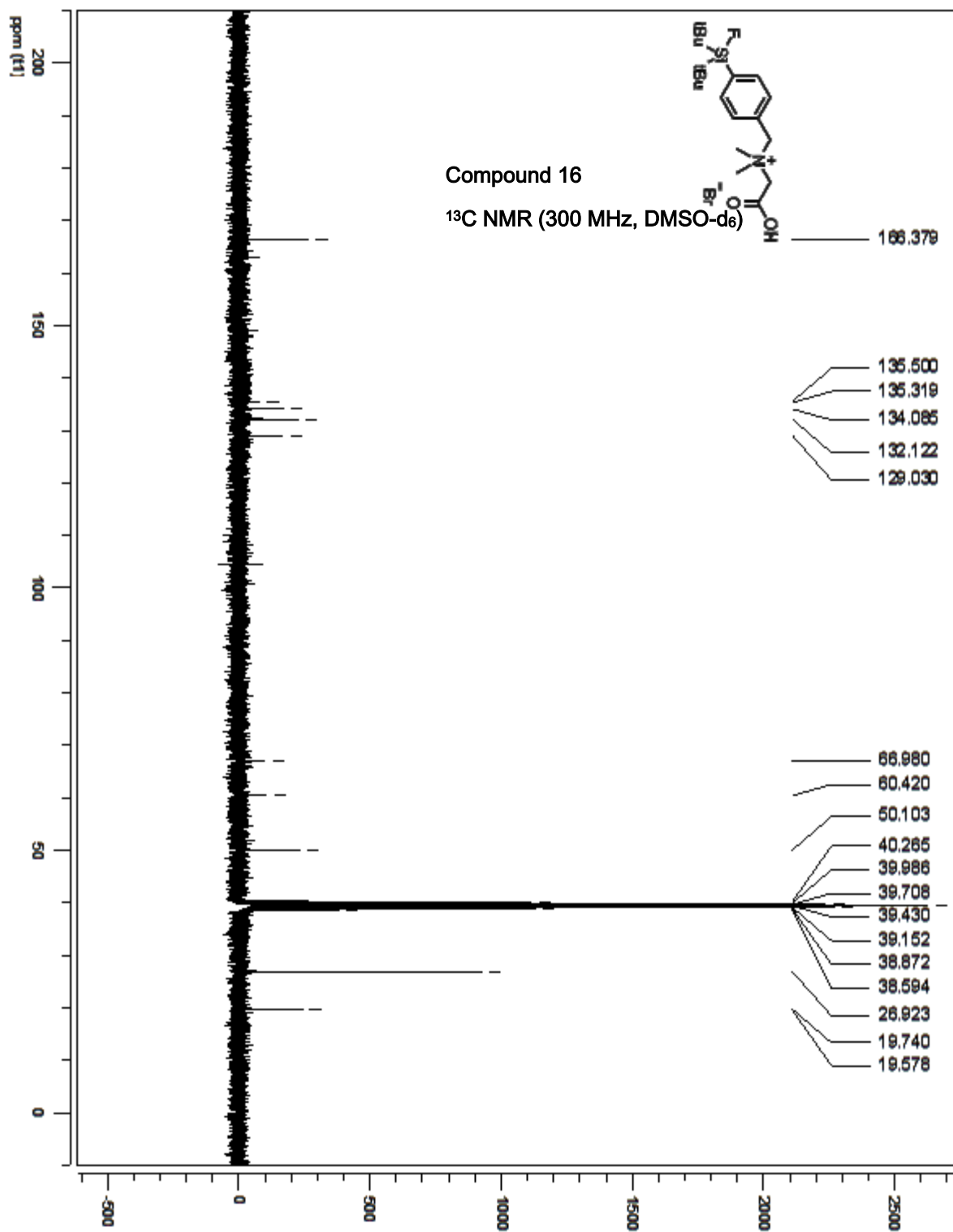
Ion	Ion Formula	Abund	Expe. m/z	Calc. m/z	Diff(ppm)
[M] ⁺	C ₂₃ H ₄₁ FN ₂ Si	7039386.5	410.28954	410.28851	-2.52



Compound 15

HRMS (ESI)

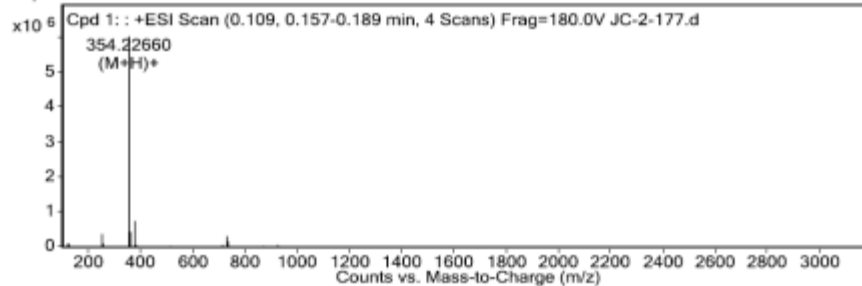




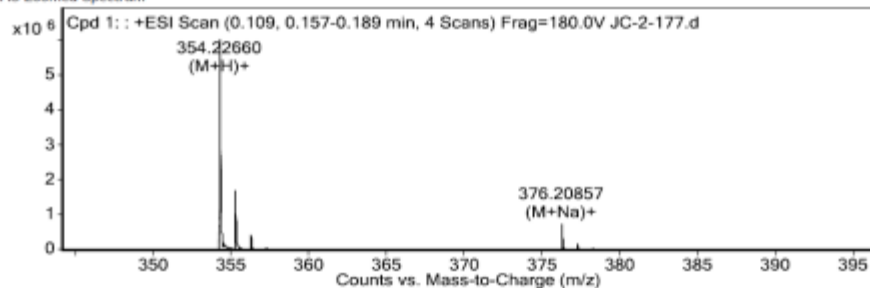
Rapport d'analyse

Data File JC-2-177.d
Sample Name JC-2-177
Sample Type Sample
Position P1-B8
Analysis Date 6/15/2011 5:14:53 PM
User Name Marie-Christine
Acq Method ESI_POS_D1.m
DA Method ESI_POS_D1.m
Comment

MS Spectrum

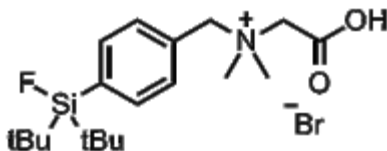


MS Zoomed Spectrum



MS Spectrum Peak List

Ion	Ion Formula	Abund	Expe. m/z	Calc. m/z	Diff(ppm)
(M+H)+	C19H33FNO2Si	6060797.1	354.2266	354.22591	1.94
(M+Na)+	C19H32FNNaO2Si	757188.4	376.20857	376.20786	1.89

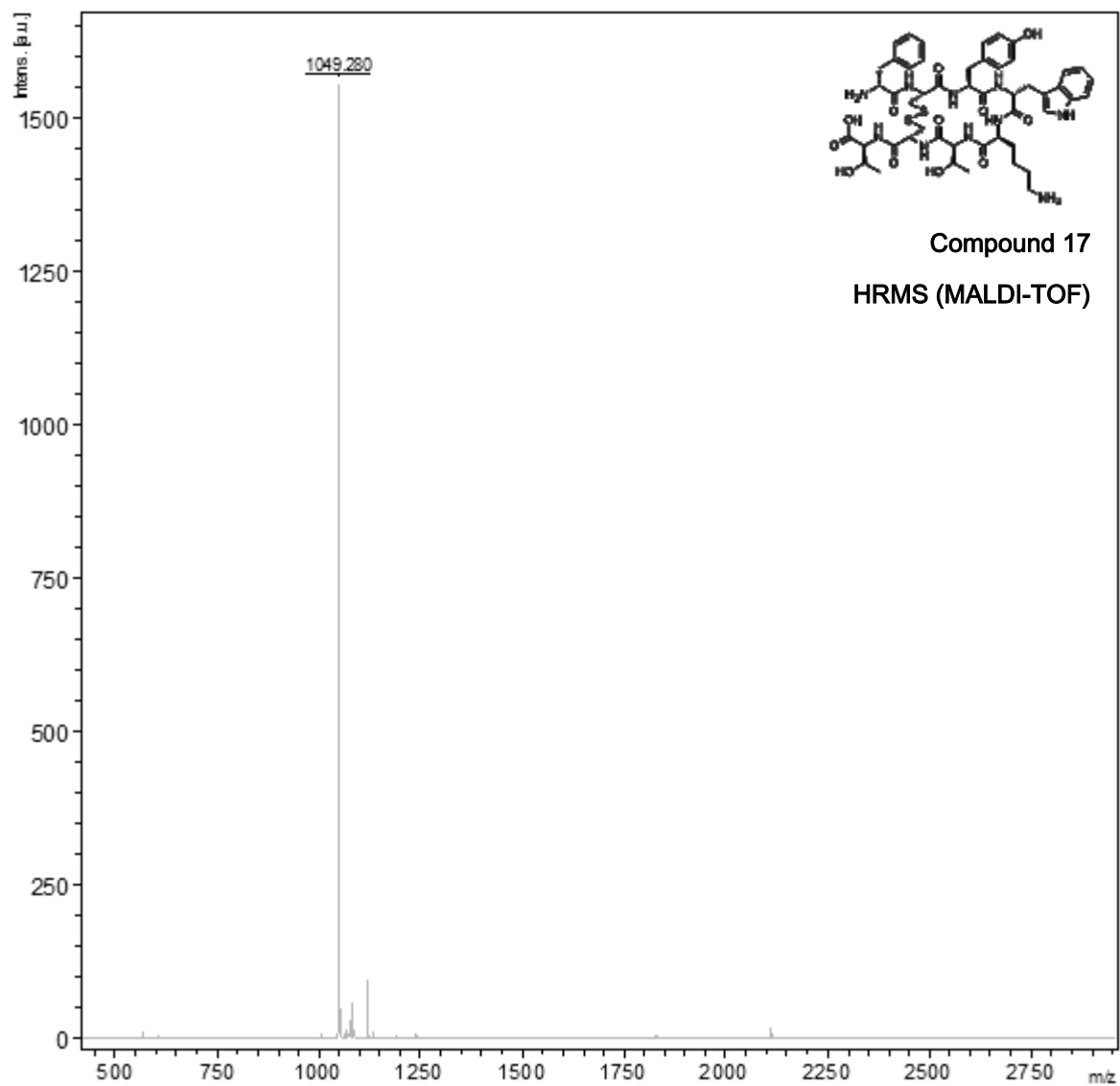


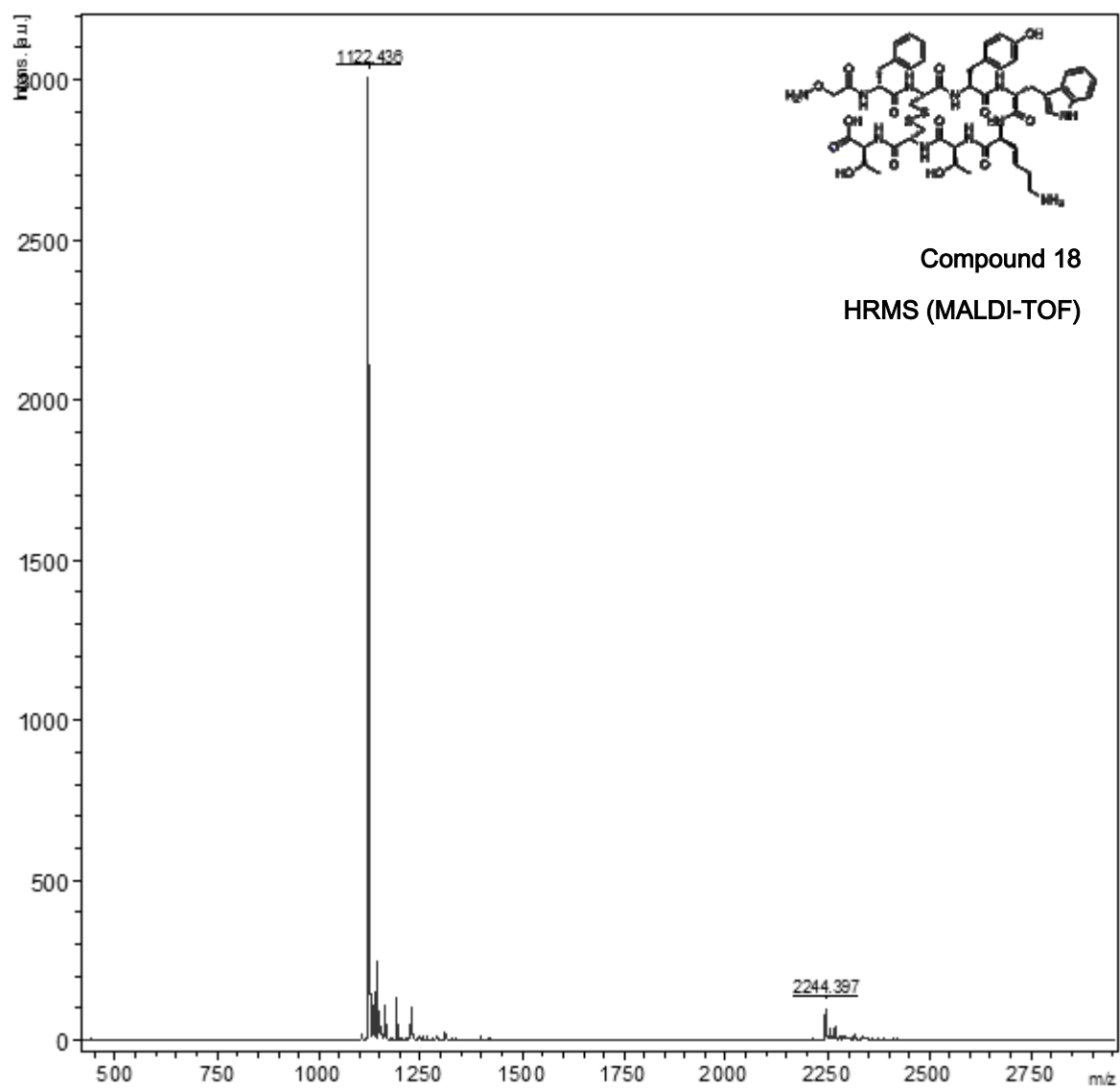
Compound 16

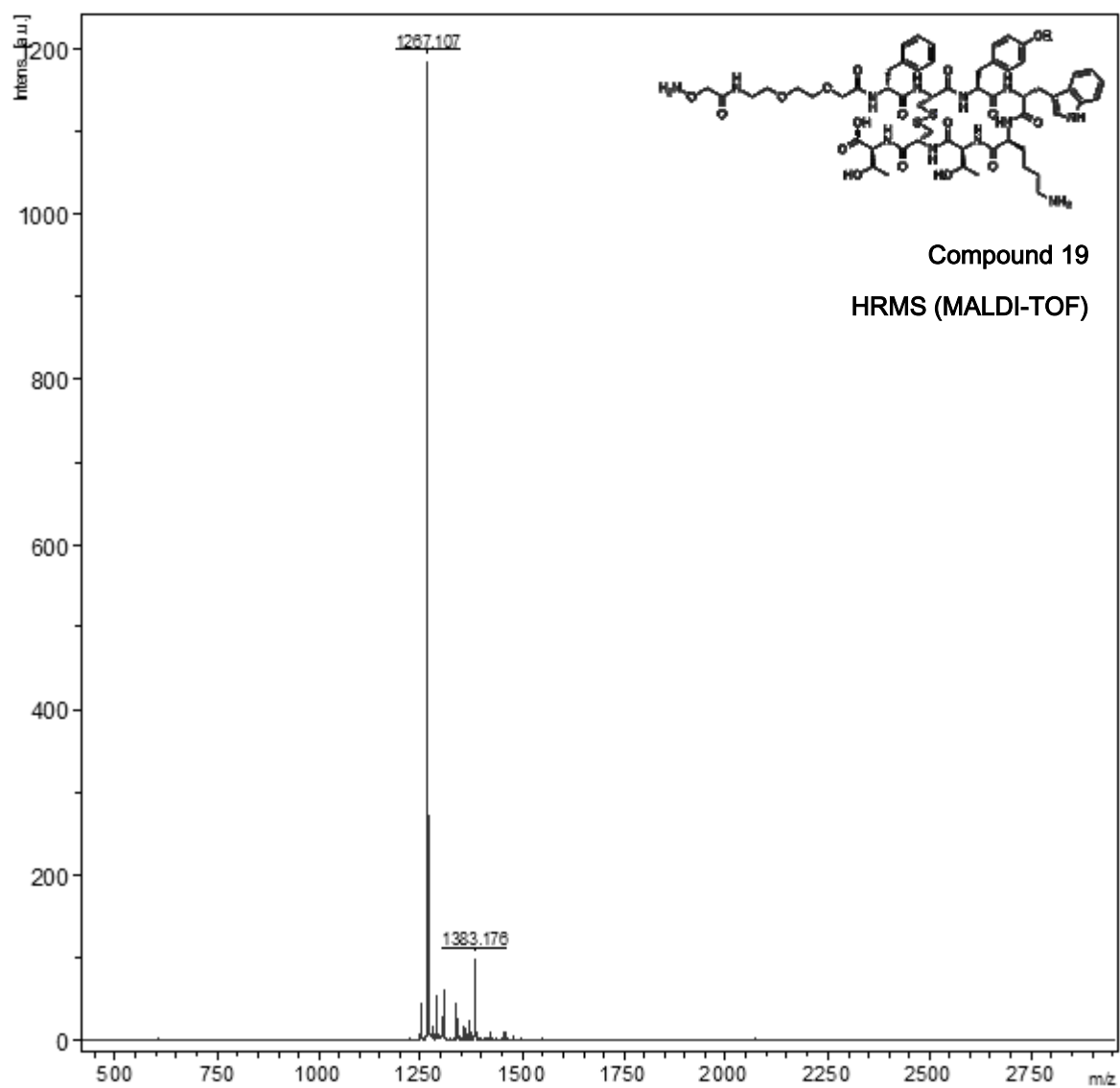
HRMS (ESI)

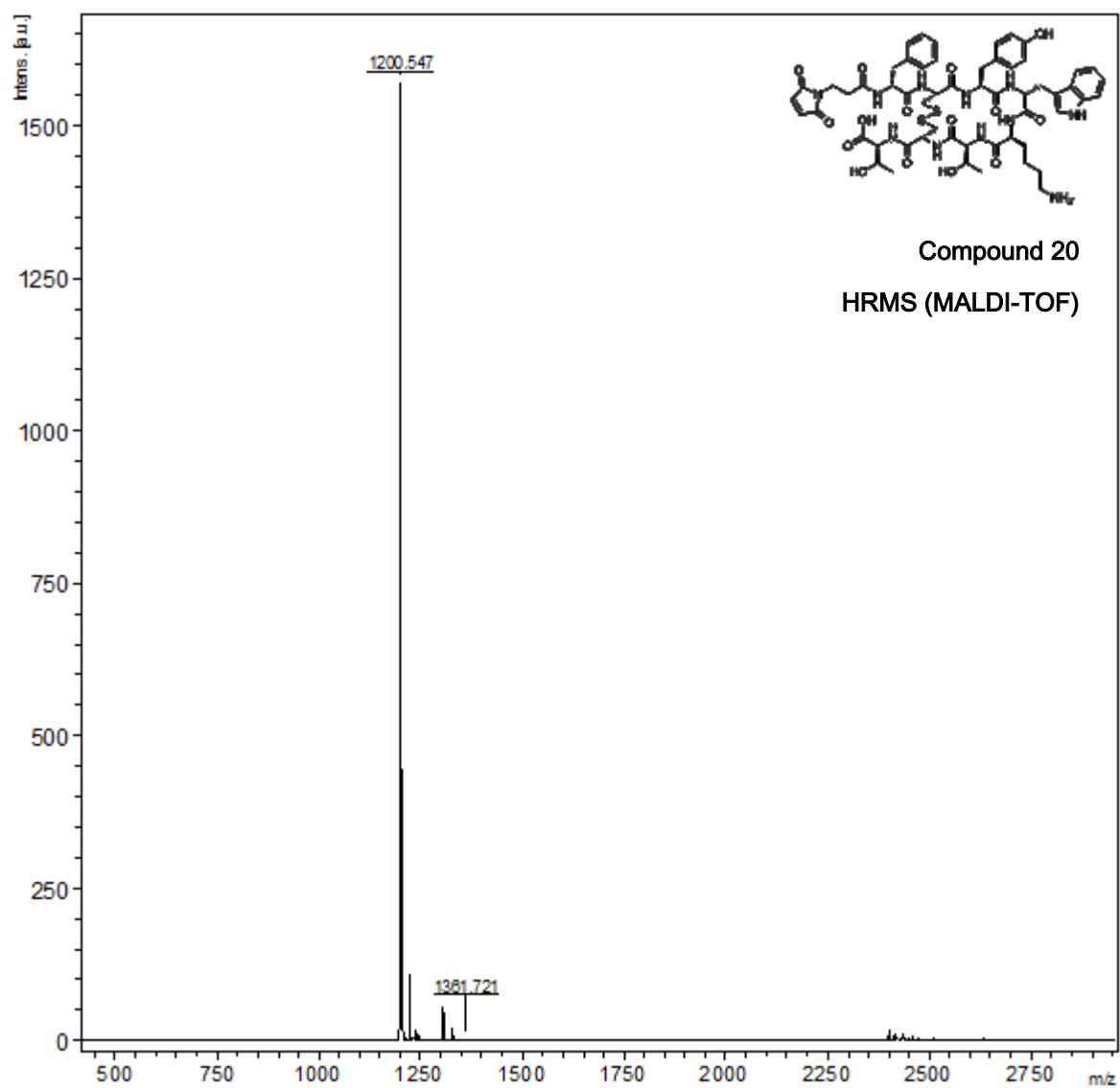
7.3 Peptide characterization data

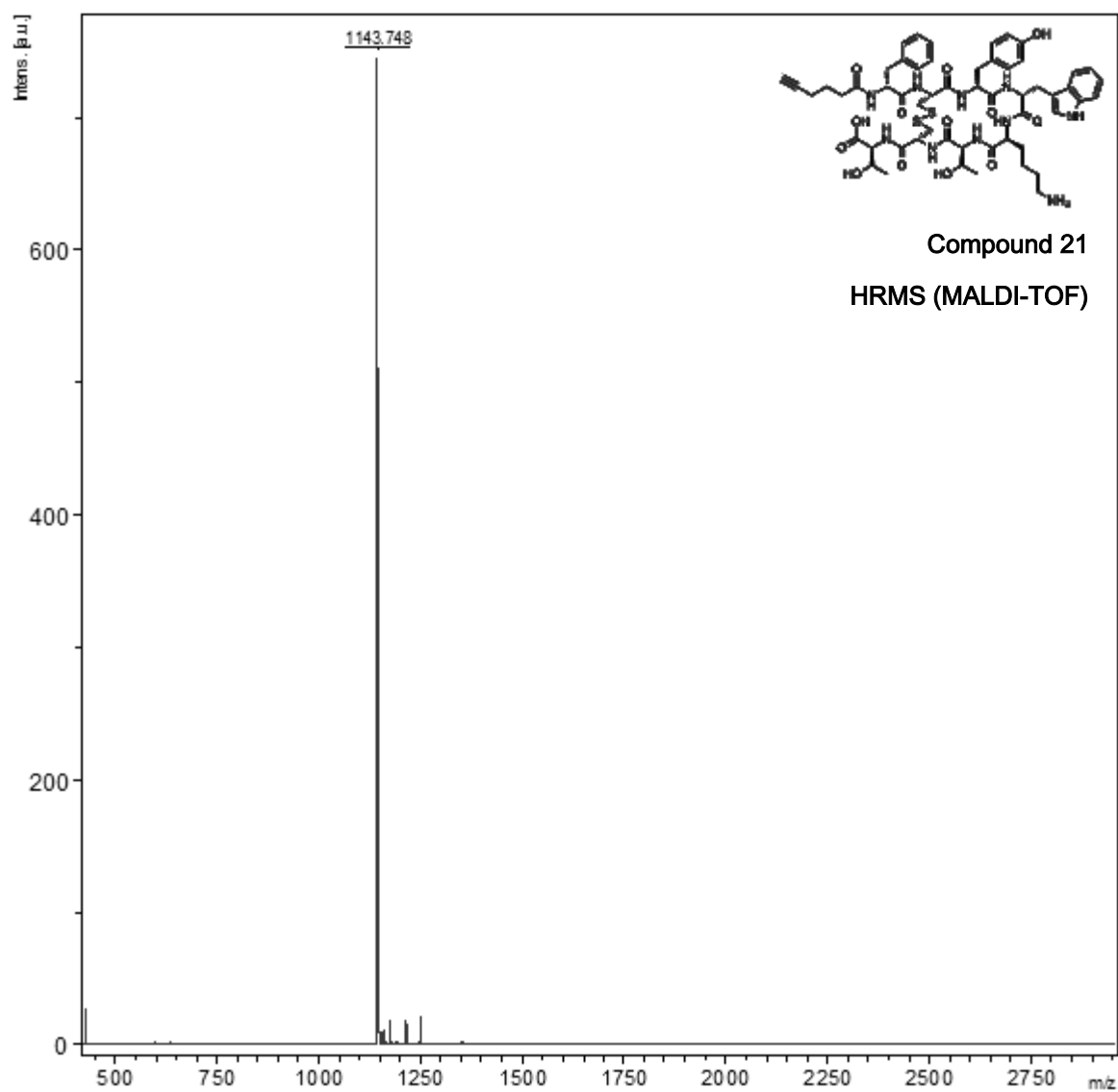
Mass spectrometry of peptides was performed using a Bruker Microflex LT MALDI-TOF MS (Bruker Daltonics, Billerica, MA, USA).

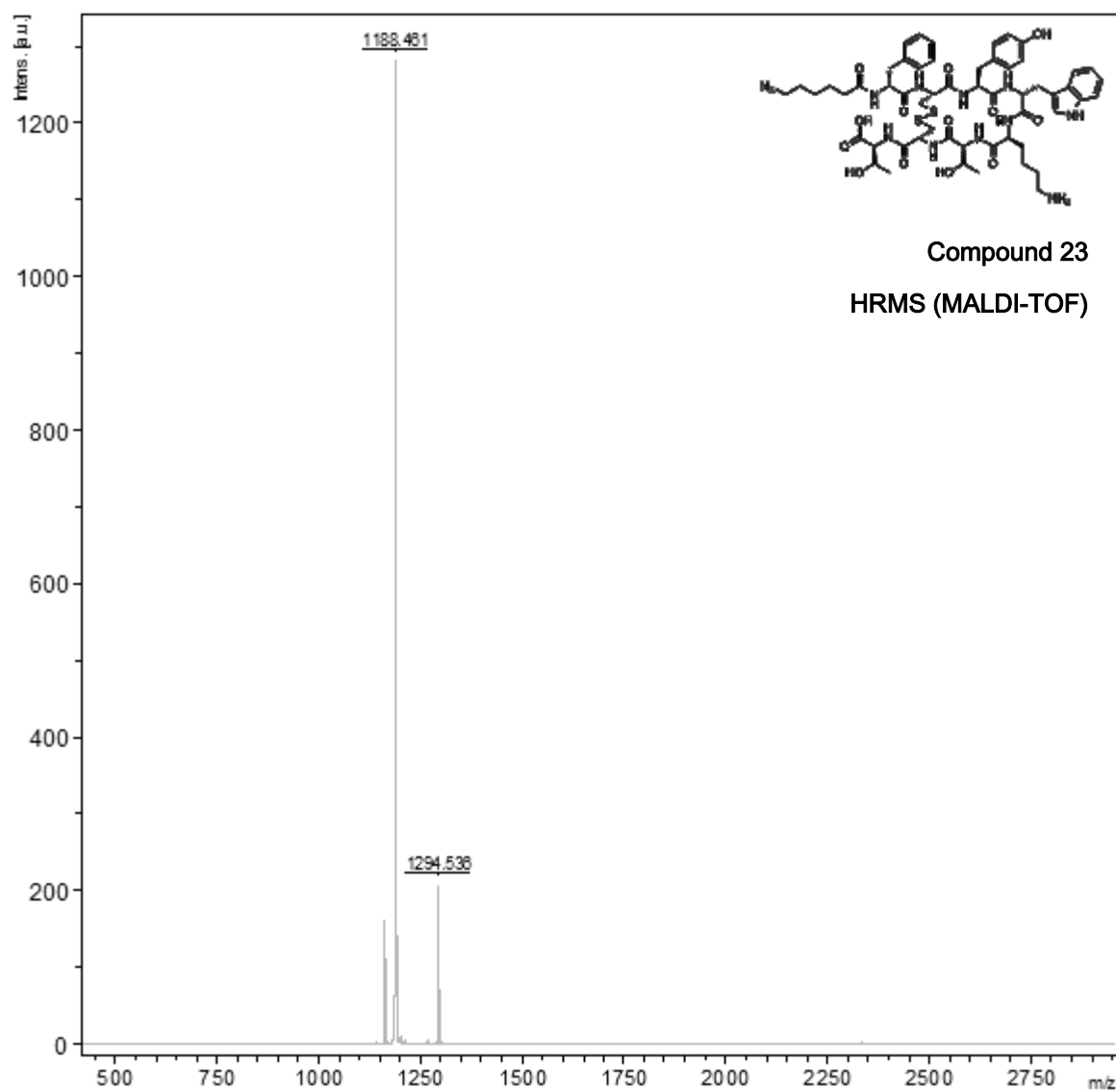


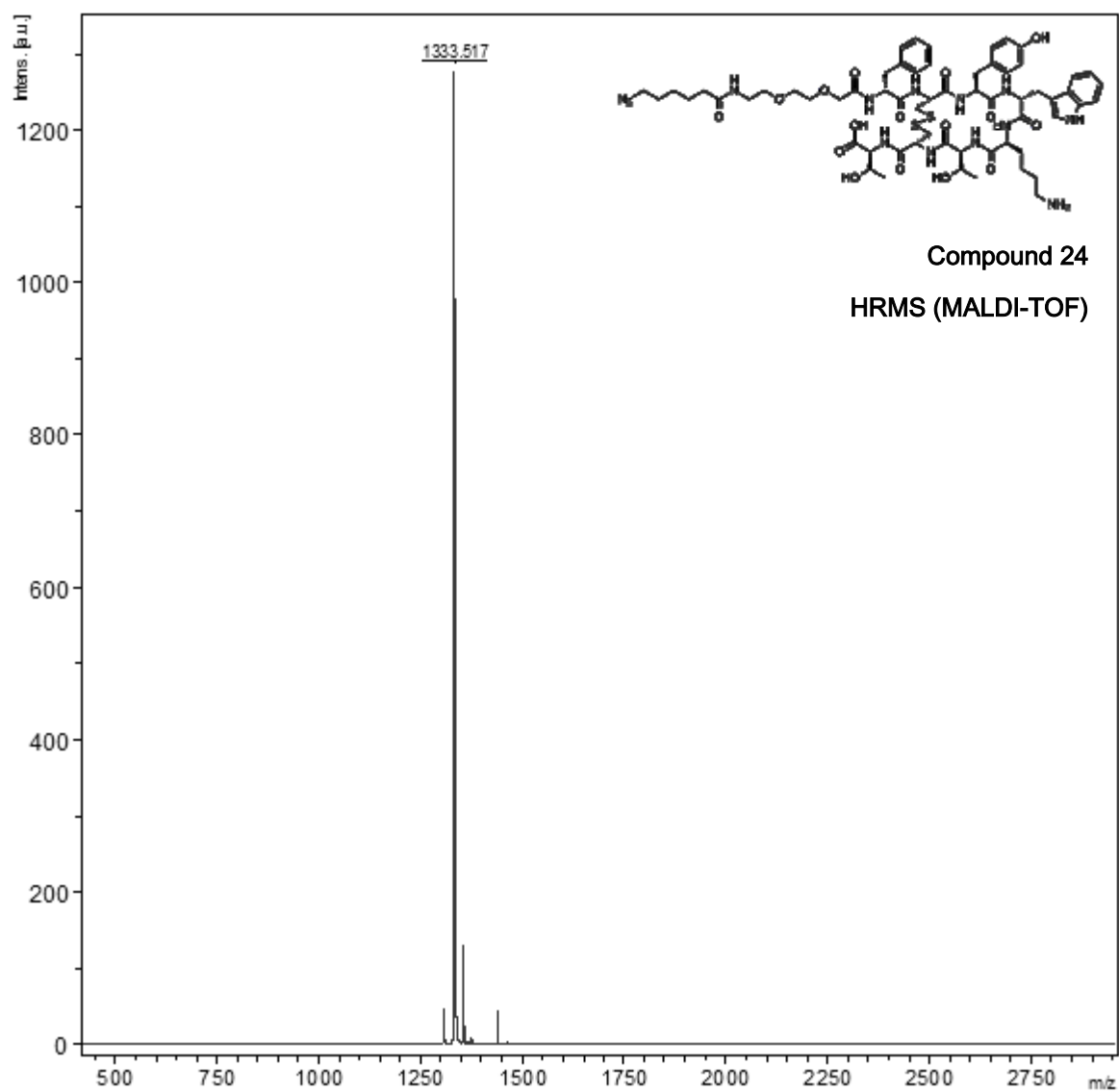


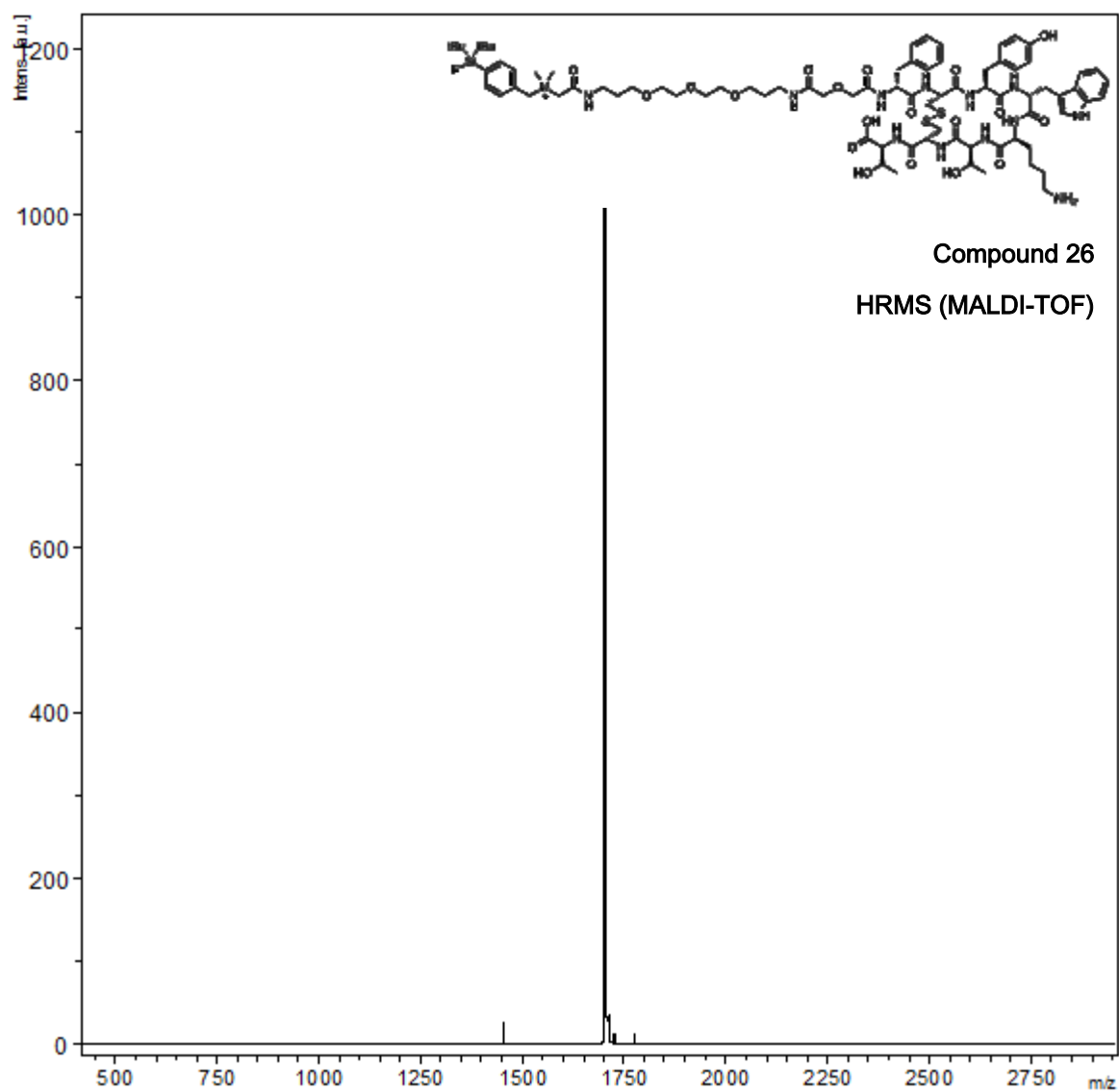


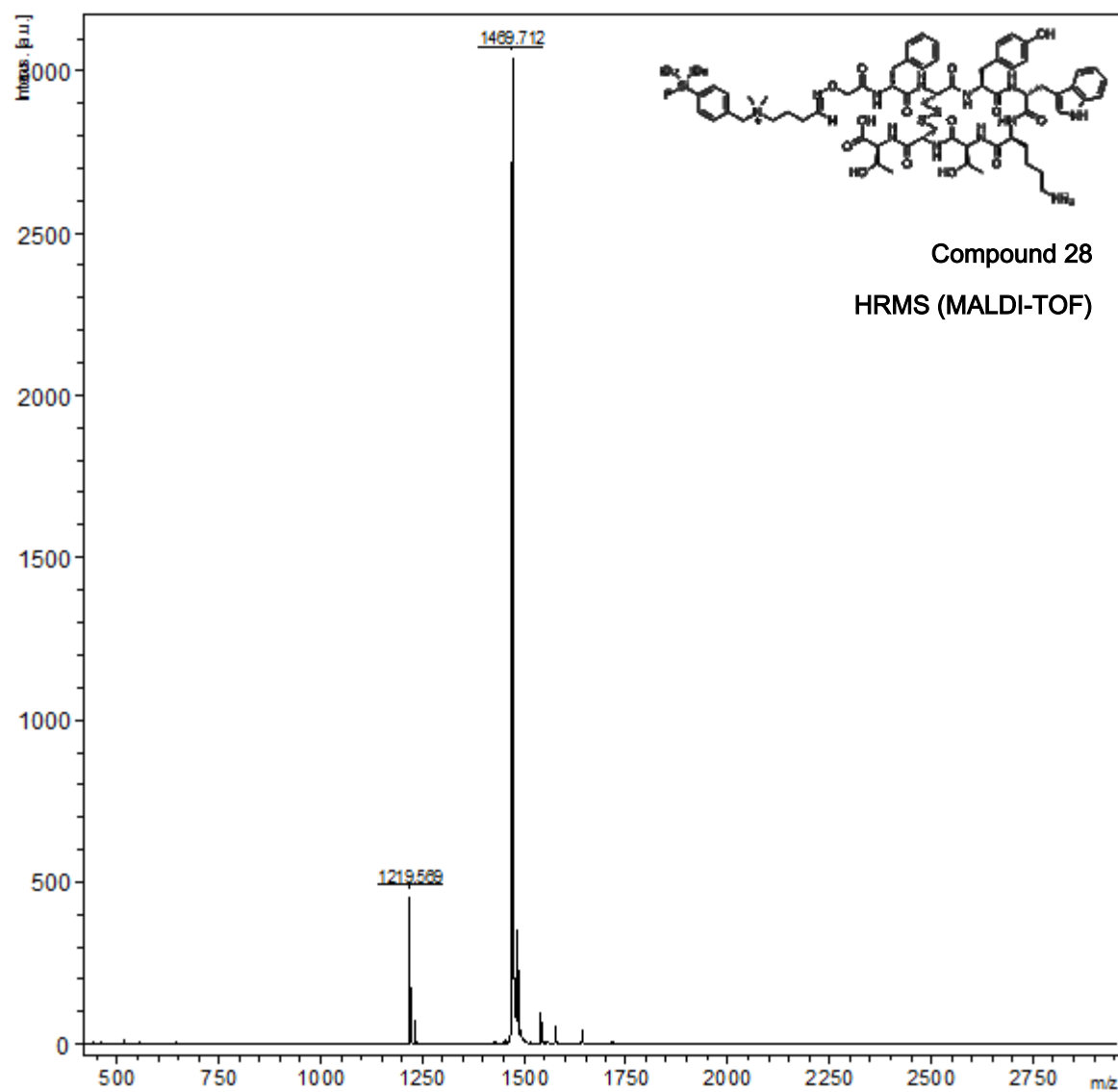


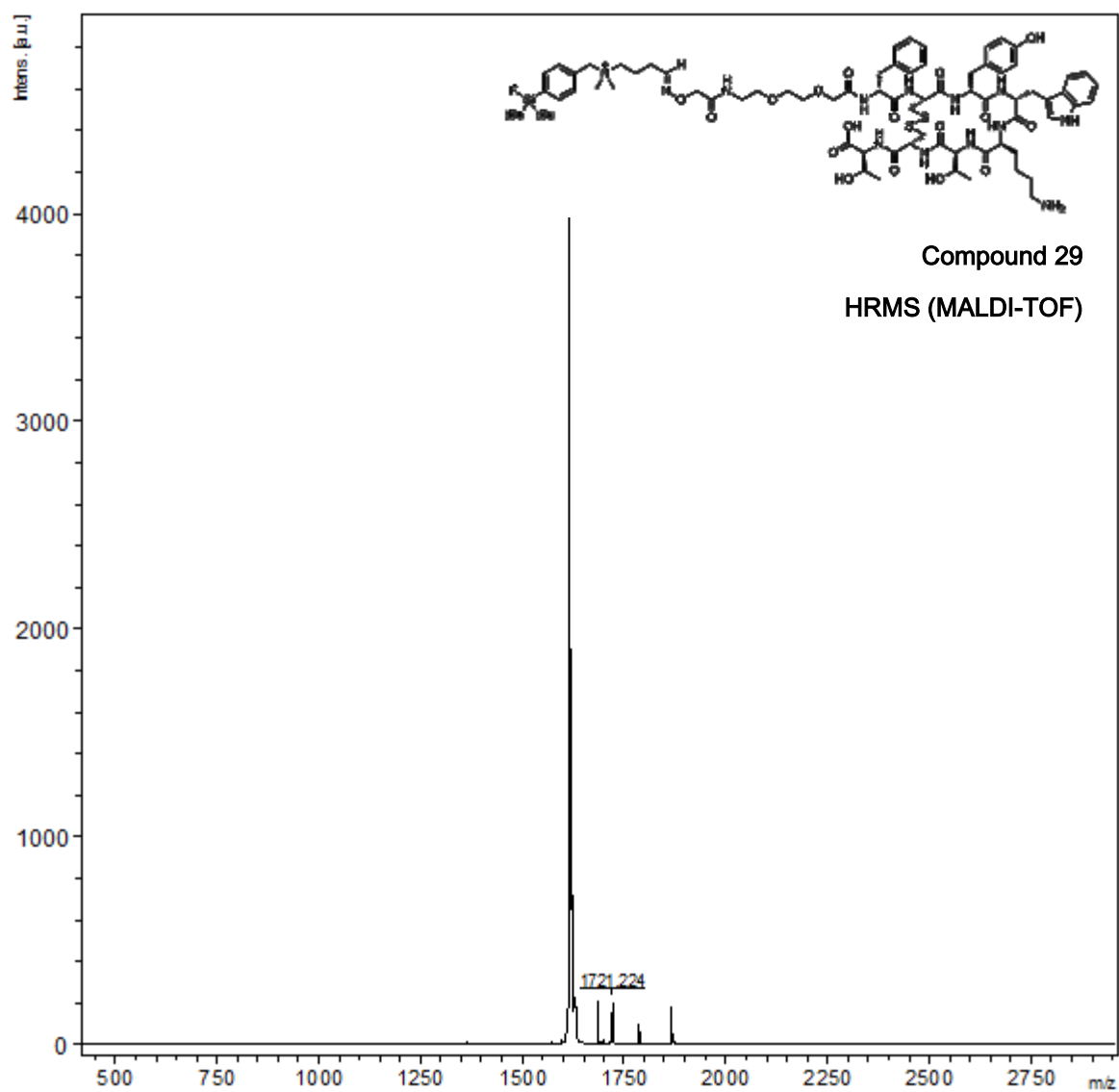


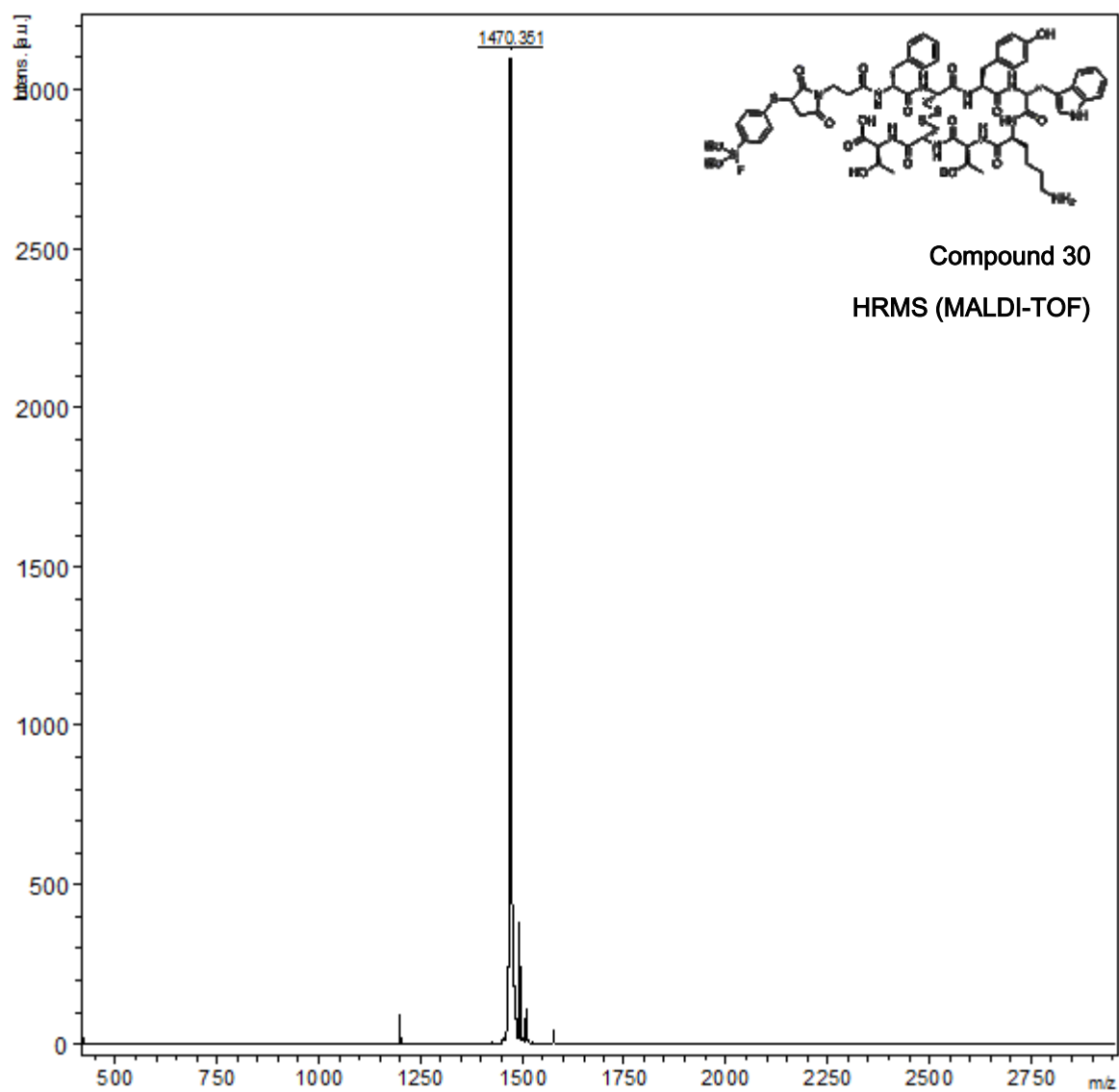












Compound 30
HRMS (MALDI-TOF)

